NOTICES

When Government drawings, specifications, or other data are used for any purpose other than in connection with a definitely related Government procurement operation, the United States Government thereby incurs no responsibility nor any obligation whatsoever; and the fact that the Government may have formulated, furnished, or in any way supplied the said drawings, specifications, or other data, is not to be regarded by implication or otherwise as in any manner licensing the holder or any other person or corporation, or conveying any rights or permission to manufacture, use or sell any patented invention that may in any way be related thereto.

This document is subject to special export controls and each transmittal to foreign governments or foreign nationals may be made only with prior approval of AFAL (AVWE), Wright-Patterson AFB, Ohio.

The distribution of this report is restricted in accordance with the United States Export Act of 1949 as amended (DOD Directive 203.4 AFR 400-10).

Copies of this report should not be returned unless return is required by security considerations, contractual obligations, or notice on a specific document.

THE INTERDIGITAL ARRAY AS A BOUNDARY VALUE PROBLEM

William W. Parker

FOREWORD

This report, 1770-3-T, was prepared by the Radiation Laboratory of the University of Michigan, Department of Electrical Engineering, 201 East Catherine Street, Ann Arbor, Michigan 48108, under the direction of Professors Ralph E. Hiatt and John A. M. Lyon on Air Force Contract F33615-68-C-1381, Task 627801 of Project 6278, "Study and Investigation of UHF-VHF Antennas." The work was administered under the direction of the Air Force Avionics Laboratory, Wright-Patterson Air Force Base, Ohio 45433. The Task Engineer was Mr. Olin E. Horton and the Project Engineer, Mr. Edwin M. Turner, AVWE. This report was submitted by the authors in March 1970.

Acknowledgments

The author wishes to express his gratitude to all the members of his Doctoral Committee for their helpful comments and criticisms. Special thanks are due to the Chairman, Professor John A. M. Lyon, for his valuable help and encouragement. The author is also indebted to Mr. Peter H. Wilcox for help with many of the computer programs, to Mr. Bruce F. Whitney for assistance in the experimental measurements, and especially to Mrs. Mary F. Wright for typing the manuscript. Finally, the author wishes to express his appreciation to his wife, Bev, for her support and encouragement throughout this investigation.

This technical report has been reviewed and is approved.

for Maurice A. Hill

RONALD G. STIMMEL
Act'g Chief
Electronic Warfare Division

ABSTRACT

In this report the center-fed interdigital array is analyzed as a boundary value problem. This antenna consists of an odd number of parallel conductors above a ground plane. Only the center element is driven and the other elements act as parasitics. Alternate ends of the parasitic elements are grounded, forming the interdigital boundary condition.

A system of integral equations is derived for the driven element of the array. The unknowns in these equations are the line currents on the driven element. The equations are solved numerically using a matrix method of solution. The input impedance, standing wave ratio, and the radiation patterns are calculated using the computed current distributions.

The theory is next extended to a three-element antenna consisting of the driven element and two parasitic elements. A system of integral equations is derived and solved for this case. Numerical data are obtained for four three-element arrays. The input impedance, standing-wave ratio, and the radiation patterns are calculated for each of the four antennas.

Models were constructed and tested to confirm the theoretical data. Experiments were performed to obtain the input impedances, standing-wave ratios, and the radiation patterns for all the models. The experimental data are compared with the theoretical results and the agreement is good. The driven element alone is not an effective antenna because the real part of the input impedance is too small. However, the addition of the two parasitic elements to the driven element markedly improves the antenna. A near optimum spacing of three elements is discovered.

Results are also reported for other experiments. In one experiment, the input impedance was measured as the number of parasitic elements was increased to a maximum of thirteen. It was found that the input impedance and standing-wave ratio is improved as each pair of parasitic elements is added.

Two thirteen-element antennas with different element spacings were tested experimentally. Data are presented for the input impedances, standing-wave ratios, and the radiation patterns. The better of these two antennas has a standing-wave ratio of less than three (with respect to a 50 Ω line) over a 25 per cent bandwidth.

TABLE OF CONTENTS

LIST OF ILLUSTRATIONS

LIST OF ILLUSTRATIONS

LIST OF ILLUSTRATIONS

LIST OF ILLUSTRATIONS

LIST OF ILLUSTRATIONS

Chapter I

INTRODUCTION

The interdigital circuit is a well-known slow wave structure. It was first proposed for use in a broadband traveling wave amplifier by Fletcher (1952). Later, the structure was developed into a microwave band pass filter (Bolljahn and Matthaei, 1962). All of these workers considered a closed structure, with the interdigital circuit between two ground planes.

The use of an open interdigital structure as a low-profile antenna was suggested by Wu (1967). The geometry of a five-element interdigital array antenna is shown in Fig. 1-1 . Basically the antenna consists of an odd number of parallel conductors above the ground plane. Only the center element (m=0) is driven. The other elements act as parasitics, and are connected directly to the ground plane at alternate ends . There may be a number of parasitic elements.

Wu's analysis of this antenna may be divided into two parts. In the first part, the dispersion characteristics were obtained for an infinite, source-free interdigital array. An unattenuated traveling wave was assumed on the infinite structure. Because of the periodic nature of the structure, Floquet's theorem (Walter, 1965) was used to relate the phase of the currents induced in each element. A sinusoidal distribution was assumed for the amplitude of the currents. The vertical z-directed segments of the elements were neglected in this analysis.

In the second part of Wu's analysis, the input impedance and radiation pattern were formulated for a finite, center-driven array. Again, the vertical, z-directed segments of the elements were neglected. The current distributions were assumed to be sinusoidal on all the elements but the driven element, where Hallén's (1938) first order distribution was used. A computer solution was obtained for the amplitudes of these currents to best match the boundary conditions of the problem.

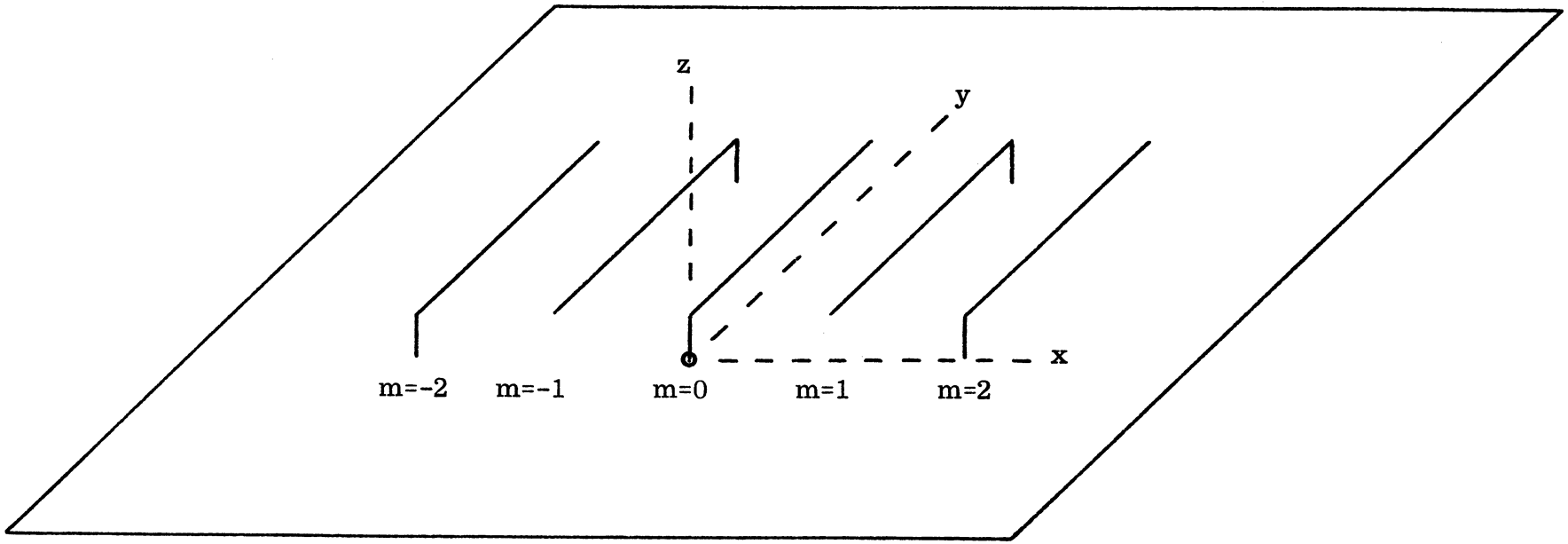

FIG. 1-1: FIVE-ELEMENT INTERDIGITAL ARRAY ANTENNA.

In this report , the finite center-fed interdigital array is analyzed as a boundary value problem. Both horizontal and vertical portions of the antenna elements are included in the analysis. A system of integral equations is derived in which the unknowns are the currents on the antenna elements. No assumptions are made on the element current distributions, other than requiring them to satisfy the boundary conditions of the problem. The complex current distributions are obtained using a matrix method of solution of the integral equations. The matrix approach is similar to the work of Mei (1965), of Richmond (1965), and of Harrington (1967, 1968).

The outline of this work is as follows. Chapter II solves the problem of the driven element. In Chapter III the solution is extended to include parasitic elements. Chapter IV presents experimental results, and the conclusions of this study are given in Chapter V.

Chapter II

THE DRIVEN ELEMENT

2.1 Introduction

The mathematical model of the driven element of the interdigital array is shown in Fig. 2-1. The element is made from wire having a circular cross section with a diameter of 2a. It is assumed to be perfectly conducting and very thin, so that the only currents of interest are line currents along the axis of the wire. This antenna is driven by a voltage source in an infinitesimally small gap of width 2δ.

Note that the ground plane of the physical model (assumed to be infinite and perfectly conducting) has been removed. This was achieved through the use of image theory (Ramo, Whinnery and Van Duzer, 1965). Consider a horizontal current-carrying wire a distance d above a ground plane. The ground plane may be removed if the image of the wire is placed a distance d below the ground plane with current in the opposite horizontal direction. In the case of a vertical wire, the image is placed with current in the same vertical direction. Because of the use of image theory, the theoretical input impedance must be divided by two in order to compare with experimental data obtained from physical models using a ground plane (Kraus, 1950).

Throughout this work the time dependence $e^{j\omega t}$ is assumed and suppressed. A standard right-hand x, y, z coordinate system is used with unit vectors $\hat{i}$, $\hat{j}$ and $\hat{k}$ pointing in the x, y, and z directions respectively.

2.2 Derivation of Integral Equations

Maxwell's equations state

$$\bar{E} = -\nabla\phi - \frac{\partial \bar{A}}{\partial t} \tag{2.1}$$

where $\bar{E}$ is the electric field and ϕ and $\bar{A}$ are the scalar and vector potentials respectively. Since the time dependence is $e^{j\omega t}$, this equation may be written

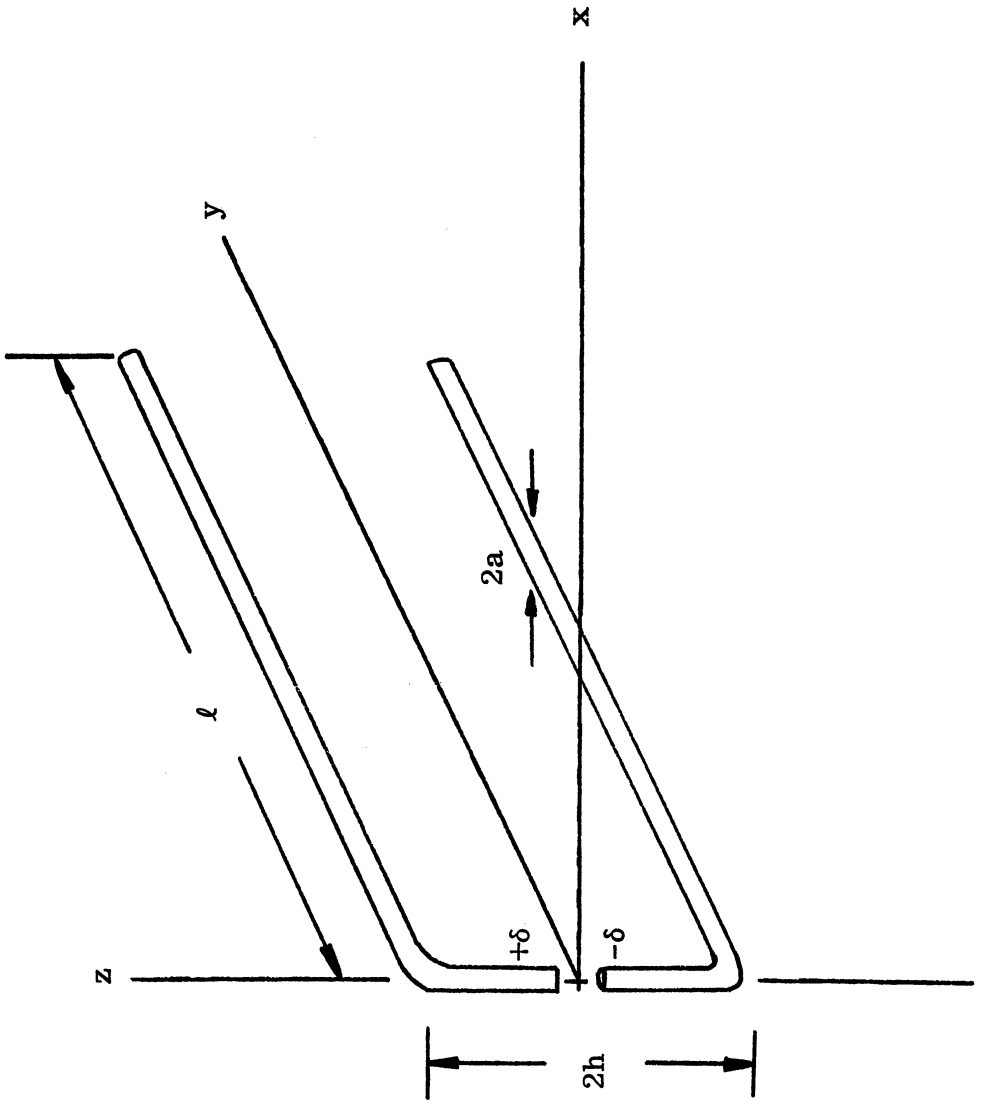

FIG. 2-1: THE DRIVEN ELEMENT OF THE ARRAY.

$$\bar{E} = -\nabla\phi - j\omega\bar{A} \quad . \tag{2.2}$$

ϕ and $\bar{A}$ are related by the Lorentz condition (Collin, 1960) which is

$$\phi = -\frac{1}{j\omega\mu\epsilon}\nabla\cdot\bar{A} \quad . \tag{2.3}$$

Substituting (2.3) into (2.2) one obtains

$$\bar{E} = -\frac{j\omega}{k^2}\left\{\nabla(\nabla\cdot\bar{A}) + k^2\bar{A}\right\} \tag{2.4}$$

where $k^2 = \omega^2\mu\epsilon$. Now specialize to the case of free space. k becomes k_o, defined by:

$$k_o^2 = \omega^2\mu_o\epsilon_o = \frac{\omega^2}{c^2} \quad , \tag{2.5}$$

where c is the velocity of light in free space. Then (2.4) becomes

$$\bar{E} = -\frac{j\omega}{k_o^2}\left\{\nabla(\nabla\cdot\bar{A}) + k_o^2\bar{A}\right\}. \tag{2.6}$$

Consider the current as being given by a vector density $\bar{J}$ in amperes per unit area spread over a volume V. Then the vector potential $\bar{A}$ is defined in free space by

$$\bar{A} = \frac{\mu_o}{4\pi}\iiint_V \frac{\bar{J}\, e^{-jk_oR}}{R}\, dV \tag{2.7}$$

where R is the distance from a current element of the integration to the point where $\bar{A}$ is being evaluated. Because of the geometry of the driven element and the assumption of line currents, there are no x-directed currents. Thus, from (2.7) there can be no x-component of $\bar{A}$. The vector potential $\bar{A}$ can be written

$$\bar{A} = A_y\hat{j} + A_z\hat{k} \quad . \tag{2.8}$$

Now substitute (2.8) into (2.6) to obtain:

$$\bar{E} = -\frac{j\omega}{k_o^2}\left\{\frac{\partial}{\partial x}\left(\frac{\partial A_y}{\partial y}+\frac{\partial A_z}{\partial z}\right)\hat{i}+\frac{\partial}{\partial y}\left(\frac{\partial A_y}{\partial y}+\frac{\partial A_z}{\partial z}\right)\hat{j}+\right.$$

$$\left.+\frac{\partial}{\partial z}\left(\frac{\partial A_y}{\partial y}+\frac{\partial A_z}{\partial z}\right)\hat{k}+k_o^2\left(A_y\hat{j}+A_z\hat{k}\right)\right\} . \qquad (2.9)$$

Next apply boundary conditions to the problem. Since the element is assumed to be a perfect conductor, the tangential $\bar{E}$ must be zero everywhere along the surface of the wire. Because the wire is assumed to be very thin with a line current distribution, the only tangential $\bar{E}$ components of importance are longitudinal ones. Thus, along the two y-directed segments the tangential field is E_y, while along the z-directed segment, the tangential field is E_z (see Fig. 2-1). For convenience, the boundary conditions are applied along the surface where $x=a$. For a thin wire this introduces negligible error. Thus for the upper y-directed segment

$$E_y = -\frac{j\omega}{k_o^2}\left\{\frac{\partial}{\partial y}\left(\frac{\partial A_y}{\partial y}+\frac{\partial A_z}{\partial z}\right)+k_o^2 A_y\right\} = 0 , \quad x=a, \quad 0\le y\le \ell , \quad z = h . \qquad (2.10)$$

For the lower y-directed segment one obtains

$$E_y = -\frac{j\omega}{k_o^2}\left\{\frac{\partial}{\partial y}\left(\frac{\partial A_y}{\partial y}+\frac{\partial A_z}{\partial z}\right)+k_o^2 A_y\right\} = 0 , \quad x=a, \quad 0\le y\le \ell , \quad z=-h . \qquad (2.11)$$

Finally for the z-directed segment

$$E_z = -\frac{j\omega}{k_o^2}\left\{\frac{\partial}{\partial z}\left(\frac{\partial A_y}{\partial y}+\frac{\partial A_z}{\partial z}\right)+k_o^2 A_z\right\} = 0 , \quad \begin{array}{l} x = a, \quad y = 0, \\ -h\le z\le -\delta, \quad \delta\le z\le h. \end{array} \qquad (2.12)$$

The application of boundary conditions has produced three differential equations in the vector potentials A_y and A_z. From (2.7) the vector potential $\bar{A}$ is known in terms of unknown current distributions along the antenna. The

problem is to determine these current distributions. By image theory, the current distributions along the upper and lower y-directed segments are equal and opposite. Thus it is only necessary to solve for one of these distributions. Equation (2. 11) is not needed to do this.

From (2. 10) and (2. 12) the two differential equations which must be solved are obtained:

$$\frac{\partial}{\partial y}\left(\frac{\partial A_y}{\partial y}+\frac{\partial A_z}{\partial z}\right)+k_o^2 A_y = 0,\ x=a,\ 0 \le y \le \ell\ ,\ z = h \tag{2.13}$$

$$\frac{\partial}{\partial z}\left(\frac{\partial A_y}{\partial y}+\frac{\partial A_z}{\partial z}\right)+k_o^2 A_z=0\ ,\ x=a,\ y=0,\ -h \le z \le -\delta,\ \delta \le z \le h\ . \tag{2.14}$$

The components of the vector potential are next related to the unknown current distributions using (2. 7) with line currents:

$$A_z(x, y, z)= \frac{\mu_o}{4\pi}\int_{-h}^{h} I_z(z')\,\frac{e^{-jk_oR_o}}{R_o}\,dz' \tag{2.15}$$

where

$$R_o=\sqrt{x^2+y^2+(z-z')^2}$$

and

$$A_y(x, y, z)= \frac{\mu_o}{4\pi}\int_{0}^{\ell} I_y(y')\left\{\frac{e^{-jk_oR_1}}{R_1}-\frac{e^{-jk_oR_2}}{R_2}\right\}dy' \tag{2.16}$$

where

$$R_1=\sqrt{x^2+(y-y')^2+(z-h)^2}$$

and

$$R_2=\sqrt{x^2+(y-y')^2+(z+h)^2}$$

Equation (2. 13) will now be solved. Rewriting, the equation becomes

$$\frac{\partial^2 A_y}{\partial y^2} + k_o^2 A_y = -\frac{\partial}{\partial y}\left(\frac{\partial A_z}{\partial z}\right) \quad . \tag{2.17}$$

From the Lorentz condition given in (2.3)

$$\phi = \frac{-1}{j\omega\mu_o\epsilon_o} \nabla \cdot \bar{A} = \frac{-1}{j\omega\mu_o\epsilon_o}\left(\frac{\partial A_y}{\partial y} + \frac{\partial A_z}{\partial z}\right) = \phi_y + \phi_z \tag{2.18}$$

where

$$\phi_y = \frac{-1}{j\omega\mu_o\epsilon_o}\frac{\partial A_y}{\partial y} \quad \text{and} \quad \phi_z = \frac{-1}{j\omega\mu_o\epsilon_o}\frac{\partial A_z}{\partial z} \quad .$$

Then (2.17) becomes:

$$\frac{\partial^2 A_y}{\partial y^2} + k_o^2 A_y = j\frac{k_o^2}{\omega}\frac{\partial \phi_z}{\partial y} \quad . \tag{2.19}$$

Equation (2.19) is a standard form and has a solution given by

$$A_y(y) = \frac{-j}{c}\left[C_1 \cos k_o y + C_2 \sin k_o y - \int_{y_o}^{y} \frac{\partial \phi_z(s)}{\partial s} \sin k_o(y-s)\,ds\right] . \tag{2.20}$$

There is no loss of generality if y_o is set equal to zero because there are still two arbitrary constants left in the solution of a second order equation. Integrating by parts in (2.20) the solution becomes

$$A_y(y) = -\frac{j}{c}\left[C_1 \cos k_o y + C_2 \sin k_o y + \phi_z(0)\sin k_o y - k_o \int_0^y \phi_z(s)\cos k_o(y-s)\,ds\right] . \tag{2.21}$$

The two terms involving $\sin k_o y$ may be combined to get:

$$A_y(y) = -\frac{j}{c}\left[C_1 \cos k_o y + C_3 \sin k_o y - k_o \int_0^y \phi_z(s)\cos k_o(y-s)\,ds\right] . \tag{2.22}$$

The expression for $\phi_z(s)$ is needed .

$$\phi_z = -\frac{1}{j\omega\mu_o\epsilon_o}\frac{\partial A_z}{\partial z} = \frac{-1}{j\omega\mu_o\epsilon_o}\frac{\partial}{\partial z}\left\{\frac{\mu_o}{4\pi}\int_{-h}^{h} I_z(z')\frac{e^{-jk_oR_o}}{R_o}dz'\right\} =$$

$$= \frac{-1}{j\omega\mu_o\epsilon_o}\frac{\mu_o}{4\pi}\int_{-h}^{h} I_z(z')\frac{e^{-jk_oR_o}}{R_o^3}(z-z')(-jk_oR_o-1)dz' \qquad (2.23)$$

Equation (2.13), which is being solved, is valid for $x=a, 0\leq y\leq \ell$, $z = h$.

$$R_o\Big|_{\substack{x=a\\0\leq y\leq \ell\\z=h}} = R_{o,1} = \sqrt{a^2+y^2+(h-z')^2} \qquad (2.24)$$

Then (2.23) becomes

$$\phi_z(y) = \frac{-1}{j\omega\mu_o\epsilon_o}\frac{\mu_o}{4\pi}\int_{-h}^{h} I_z(z')\frac{e^{-jk_oR_{o,1}}}{R_{o,1}^3}(h-z')(-jk_oR_{o,1}-1)dz'. \qquad (2.25)$$

To get $\phi_z(s)$, a simple change of variable from y to s is used. Now substitute (2.25) into (2.22) and interchange the order of integration of dz' and ds:

$$A_y(y) = -\frac{jC_1}{c}\cos k_oy - \frac{jC_3}{c}\sin k_oy - \frac{\mu_o}{4\pi}\int_{-h}^{h} I_z(z')F(y,z')dz' \qquad (2.26)$$

valid for $0\leq y\leq \ell$ where

$$F(y,z') = (h-z')\int_0^y \frac{e^{-jk_oR_s}}{R_s^3}(-jk_oR_s-1)\cos k_o(y-s)ds$$

$$R_s = \sqrt{a^2+s^2+(h-z')^2} \qquad (2.27)$$

The first integral equation may now be derived by equating $A_y(y)$ in (2.26) with $A_y(x, y, z)$ in (2.16) evaluated at $x = a$, $0 \leq y \leq \ell$, $z = h$. The result is:

$$-\frac{jC_1}{c}\cos k_o y - \frac{jC_3}{c}\sin k_o y - \frac{\mu_o}{4\pi}\int_{-h}^{h} I_z(z')\, F(y, z')\, dz' =$$

$$= \frac{\mu_o}{4\pi}\int_0^{\ell} I_y(y')\left\{\frac{e^{-jk_o R_{1,1}}}{R_{1,1}} - \frac{e^{-jk_o R_{2,1}}}{R_{2,1}}\right\} dy' \qquad (2.28)$$

where

$$R_{1,1} = \sqrt{a^2+(y-y')^2} = R_1 \Big|_{\substack{x=a \\ o\leq y\leq \ell \\ z=h}}$$

and

$$R_{2,1} = \sqrt{a^2+(y-y')^2+4h^2} = R_2 \Big|_{\substack{x=a \\ o\leq y\leq \ell \\ z=h}}$$

This equation can be simplified somewhat:

$$\int_{-h}^{h} I_z(z')F(y, z')dz' + \int_0^{\ell} I_y(y')\left\{\frac{e^{-jk_o R_{1,1}}}{R_{1,1}} - \frac{e^{-jk_o R_{2,1}}}{R_{2,1}}\right\}dy' +$$

$$+B_1 \cos k_o y + B_2 \sin k_o y = 0 \qquad (2.29)$$

valid for $0 \leq y \leq \ell$, where $B_1 = \frac{j4\pi}{\mu_o c} C_1$ and $B_2 = \frac{j4\pi}{\mu_o c} C_3$.

Equation (2.14) will now be solved. Rewriting, the equation becomes

$$\frac{\partial^2 A_z}{\partial z^2} + k_o^2 A_z = -\frac{\partial}{\partial z}\left(\frac{\partial A_y}{\partial y}\right). \qquad (2.30)$$

Using the Lorentz condition as expressed in (2.18), equation (2.30) becomes

$$\frac{\partial^2 A_z}{\partial z^2} + k_o^2 A_z = j\frac{k_o^2}{\omega}\frac{\partial \phi_y}{\partial z}. \qquad (2.31)$$

This equation is a standard form. The solution for $z > 0$ may be written as

$$A_z(z) = -\frac{j}{c}\left[D_1 \cos k_o z + D_2 \sin k_o z - \int_{\delta}^{z} \frac{\partial \phi_y(s)}{\partial s} \sin k_o(z-s)\,ds\right] \qquad (2.32)$$

valid for x=a, y=0, $\delta \leq z \leq h$. For $z < 0$, the solution is

$$A_z(z) = -\frac{j}{c}\left[D_3 \cos k_o z + D_4 \sin k_o z - \int_{-\delta}^{z} \frac{\partial \phi_y(s)}{\partial s} \sin k_o(z-s)\,ds\right] \qquad (2.33)$$

valid for x= a, y=0, $-h \leq z \leq -\delta$.

Consider next the potential function $\phi(z)$ evaluated on the surface of the z-directed segment of the driven element (x=a, y=0, $-h \leq z \leq -\delta$, $\delta \leq z \leq h$). This segment contains a voltage source of strength V volts in an infinitesimal gap of width 2δ. Note that

$$\phi(\delta) = V/2 \qquad (2.34)$$

$$\phi(-\delta) = -V/2 \qquad (2.35)$$

and $\phi(z)$ is an odd function of z. From (2.18) $\phi(z)$ is given by

$$\phi(z) = -\frac{1}{j\omega\mu_o\epsilon_o}\left(\frac{\partial A_y}{\partial y} + \frac{\partial A_z}{\partial z}\right)\Bigg|_{\substack{x=a \\ y=0}} \qquad (2.36)$$

It may be shown that

$$\frac{\partial A_y}{\partial y}\Bigg|_{\substack{x=a \\ y=0}}$$

is an odd function of z. Then

$$\frac{\partial A_z}{\partial z}\Bigg|_{\substack{x=a \\ y=0}}$$

must also be an odd function of z. This means that $A_z(z)$ has to be an even function of z. Looking at the two solutions given by (2.32) and (2.33), it may be observed that $A_z(z)$ will be an even function of z if $D_1 = D_3$ and $D_2 = -D_4$.

Consider the case where $z > 0$. From (2.18) the potential function $\phi(z)$ may be written

$$\phi(z)=\phi_y(z)+ j\omega/k_o^2 \frac{\partial A_z}{\partial z} \quad . \tag{2.37}$$

To get $\partial A_z/\partial z$ differentiate the solution given in (2.32). The result is

$$\phi(z)=\phi_y(z) -D_1 \sin k_o z+D_2 \cos k_o z- \int_\delta^z \frac{\partial \phi_y(s)}{\partial s} \cos k_o (z-s)\, ds \quad . \tag{2.38}$$

Now $\phi(\delta) = V/2$. Using this with (2.38) one finds that:

$$\phi(\delta)=V/2=\phi_y(\delta) -D_1 \sin k_o \delta+D_2 \cos k_o \delta \quad . \tag{2.39}$$

Solving (2.39) for D_2, the result is

$$D_2 = \frac{V/2-\phi_y(\delta)+D_1 \sin k_o \delta}{\cos k_o \delta} \quad . \tag{2.40}$$

Then D_2 is substituted back into (2.32)

$$A_z(z) = -\frac{j}{c} \left\{ D_1 \cos k_o z+\left[\frac{V/2-\phi_y(\delta)+D_1 \sin k_o \delta}{\cos k_o \delta}\right] \sin k_o z - \right.$$
$$\left. - \int_\delta^z \frac{\partial \phi_y(s)}{\partial s} \sin k_o (z-s) ds \right\} \tag{2.41}$$

valid for $x=a$, $y=0$, $\delta \leq z \leq h$.

Consider the case where $z < 0$. From (2.18) the potential function $\phi(z)$ may be written

$$\phi(z)=\phi_y(z) + \frac{j\omega}{k_o^2} \frac{\partial A_z}{\partial z} \quad . \tag{2.42}$$

To get $\partial A_z/\partial z$, differentiate the solution given in (2.33). The result is

$$\phi(z)=\phi_y(z)-D_1\sin k_o z-D_2\cos k_o z-\int_{-\delta}^{z}\frac{\partial\phi_y(s)}{\partial s}\cos k_o(z-s)ds \quad . \quad (2.43)$$

Now $\phi(-\delta) = -V/2$. Using this with (2.43) one finds that:

$$\phi(-\delta)= -\frac{V}{2} = \phi_y(-\delta)-D_1\sin k_o(-\delta)-D_2\cos k_o(-\delta) \quad . \quad (2.44)$$

Solving (2.44) for D_2, the result is

$$D_2 = \frac{-V/2-\phi_y(-\delta)+D_1\sin k_o(-\delta)}{-\cos k_o(-\delta)} \quad . \quad (2.45)$$

Next substitute D_2 back into (2.33)

$$A_z(z)= -\frac{j}{c}\left\{D_1\cos k_o z-\left[\frac{V/2+\phi_y(-\delta)-D_1\sin k_o(-\delta)}{\cos k_o(-\delta)}\right]\sin k_o z - \right.$$
$$\left. -\int_{-\delta}^{z}\frac{\partial\phi_y(s)}{\partial s}\sin k_o(z-s)ds\right\} \quad (2.46)$$

valid for $x = a$, $y = 0$, $-h \le z \le -\delta$. Now let δ approach zero. From (2.41) the result is

$$A_z(z)= -\frac{j}{c}\left\{D_1\cos k_o z+\left[\frac{V}{2}-\phi_y(0)\right]\sin k_o z-\int_0^z\frac{\partial\phi_y(s)}{\partial s}\sin k_o(z-s)ds\right\} \quad (2.47)$$

valid for $x = a$, $y = 0$, $0 \le z \le h$. From (2.46) the result is

$$A_z(z)= -\frac{j}{c}\left\{D_1\cos k_o z-\left[\frac{V}{2}+\phi_y(0)\right]\sin k_o z-\int_0^z\frac{\partial\phi_y(s)}{\partial s}\sin k_o(z-s)ds\right\} \quad (2.48)$$

valid for $x = a$, $y = 0$, $-h \le z \le 0$.

Next investigate $\phi_y(0)$. From (2.18)

$$\phi_y(0) = \frac{-1}{j\omega\mu_o\epsilon_o} \frac{\partial A_y}{\partial y} \Bigg|_{\substack{x=a \\ y=0 \\ z=0}} \tag{2.49}$$

From (2.16) $R_1=R_2$ at z=0. Therefore $\phi_y(0)=0$. With this information the solutions in (2.47) and (2.48) can be combined.

$$A_z(z) = -\frac{j}{c}\left[D_1 \cos k_o z + \frac{V}{2}\sin k_o |z| - \int_0^z \frac{\partial \phi_y(s)}{\partial s} \sin k_o(z-s)ds\right] \tag{2.50}$$

valid for x=a, y=0, $-h \leq z \leq h$. Integrating by parts in (2.50) the solution becomes

$$A_z(z) = -\frac{j}{c}\left[D_1 \cos k_o z + \frac{V}{2}\sin k_o |z| - k_o \int_0^z \phi_y(s)\cos k_o(z-s)ds\right] . \tag{2.51}$$

The expression for $\phi_y(s)$ is needed.

$$\phi_y = \frac{-1}{j\omega\mu_o\epsilon_o} \frac{\partial A_y}{\partial y} =$$

$$= \frac{-1}{j\omega\mu_o\epsilon_o} \frac{\partial}{\partial y}\left[\frac{\mu_o}{4\pi}\int_0^{\ell} I_y(y')\left\{\frac{e^{-jk_oR_1}}{R_1} - \frac{e^{-jk_oR_2}}{R_2}\right\}dy'\right] =$$

$$= \frac{-1}{j\omega\mu_o\epsilon_o} \frac{\mu_o}{4\pi}\int_0^{\ell} I_y(y')\left\{\frac{e^{-jk_oR_1}(y-y')(-jk_oR_1-1)}{R_1^3} - \right.$$

$$\left. - \frac{e^{-jk_oR_2}(y-y')(-jk_oR_2-1)}{R_2^3}\right\} dy' . \tag{2.52}$$

Equation (2.14), which is being solved, is valid for x = a, y=0, $-h \leq z \leq h$.

$$R_{1,2} = R_1\Big|_{\substack{x=a\\y=0\\-h\le z\le h}} = \sqrt{a^2+y'^2+(z-h)^2}$$

$$R_{2,2} = R_2\Big|_{\substack{x=a\\y=0\\-h\le z\le h}} = \sqrt{a^2+y'^2+(z+h)^2} \qquad (2.53)$$

Then (2.52) becomes

$$\phi_y(z) = \frac{-1}{j\omega\mu_o\epsilon_o}\,\frac{\mu_o}{4\pi}\int_0^{\ell} I_y(y')\left\{\frac{e^{-jk_oR_{1,2}(y')}(jk_oR_{1,2}+1)}{R_{1,2}^3} - \right.$$

$$\left. - \frac{e^{-jk_oR_{2,2}(y')}(jk_oR_{2,2}+1)}{R_{2,2}^3}\right\} dy' \ . \qquad (2.54)$$

To get $\phi_y(s)$ a simple change of variable from z to s is used. Now substitute (2.54) into (2.51) and interchange order of integration of dy' and ds:

$$A_z(z) = -\frac{j}{c}D_1\cos k_o z - \frac{j}{c}\,\frac{V}{2}\sin k_o|z| - \frac{\mu_o}{4\pi}\int_0^{\ell} I_y(y')G(z,y')dy' \ , \qquad (2.55)$$

valid for $-h \le z \le h$ where

$$G(z,y') = y'\int_0^z \left\{\frac{e^{-jk_oR_{1s}}(jk_oR_{1s}+1)}{R_{1s}^3} - \frac{e^{-jk_oR_{2s}}(jk_oR_{2s}+1)}{R_{2s}^3}\right\}\cos k_o(z-s)ds$$

$$R_{1s} = \sqrt{a^2+y'^2+(s-h)^2} \quad , \quad R_{2s} = \sqrt{a^2+y'^2+(s+h)^2} \ . \qquad (2.56)$$

The second integral equation may now be derived by equating $A_z(z)$ in (2.55) with $A_z(x,y,z)$ in (2.15) evaluated at x=a, y=0, $-h \le z \le h$. The result is:

$$-\frac{j}{c} D_1 \cos k_o z - \frac{j}{c}\frac{V}{2} \sin k_o |z| - \frac{\mu_o}{4\pi} \int_0^{\ell} I_y(y')G(z,y')dy' =$$

$$= \frac{\mu_o}{4\pi} \int_{-h}^{h} I_z(z') \frac{e^{-jk_o R_{o,2}}}{R_{o,2}} dz' \qquad (2.57)$$

where

$$R_{o,2} = \sqrt{a^2+(z-z')^2} = R_o \Big|_{\substack{x=a \\ y=0 \\ -h\leq z\leq h}} .$$

This equation may be simplified somewhat

$$\int_{-h}^{h} I_z(z') \frac{e^{-jk_o R_{o,2}}}{R_{o,2}} dz' + \int_0^{\ell} I_y(y')G(z,y')dy' + B_3 \cos k_o z + j\frac{2\pi V}{\eta_o} \sin k_o |z| = 0, \qquad (2.58)$$

valid for $-h\leq z\leq h$, where

$$\eta_o = \sqrt{\frac{\mu_o}{\epsilon_o}} \approx 377 \text{ ohms and } B_3 = \frac{j4\pi}{\mu_o c} D_1 . \qquad (2.59)$$

Two integral equations have now been derived from the boundary conditions on the tangential electric field. The unknown functions in these equations are the line current distributions $I_y(y')$ and $I_z(z')$ on the driven element. Observe that there are also three unknown constants B_1, B_2, and B_3.

Three assumed conditions are used with these two equations. The first is that the line currents are continuous across the junctions of the two wire segments. In equation form

$$I_y(0) = I_z(h) . \qquad (2.60)$$

The second condition is that the current goes to zero at the end of the wire.

$$I_y(\ell) = 0 . \qquad (2.61)$$

The third condition is that the scalar potential is continuous across the junction of the wire segments:

$$\phi(z)\Big|_{z=h} = \phi(y)\Big|_{y=0} \quad . \tag{2.62}$$

Now equation (2.62) will be investigated more carefully. From (2.36)

$$\phi(z) = \frac{-1}{j\omega\mu_o \epsilon_o} \left(\frac{\partial Ay}{\partial y} + \frac{\partial Az}{\partial z} \right) \Bigg|_{\substack{x=a \\ y=0}} =$$

$$= \phi_y(z) + j\omega/k_o^2 \quad \frac{\partial Az}{\partial z} \Bigg|_{\substack{x=a \\ y=0}} \tag{2.63}$$

The expression for $A_z(z)$ is given by (2.51). Since $\phi(z)$ will be evaluated in (2.62) at $z = h$, the absolute value sign may be removed from (2.51). The result is

$$A_z(z) = \frac{-j}{c} \left[D_1 \cos k_o z + \frac{V}{2} \sin k_o z - \right.$$

$$\left. - k_o \int_0^z \phi_y(s) \cos k_o (z-s)\, ds \right] \quad . \tag{2.64}$$

Then differentiating

$$\frac{\partial Az(z)}{\partial z} = j \frac{D_1 k_o}{c} \sin k_o z \frac{-jVk_o}{2c} \cos k_o z -$$

$$- \frac{j k_o^2}{c} \int_0^z \phi_y(s) \sin k_o (z-s)\, ds + \frac{jk_o}{c} \phi_y(z) \quad . \tag{2.65}$$

Substituting (2.65) into (2.63)

$$\phi(z) = \phi_y(z) - D_1 \sin k_o z + \frac{V}{2} \cos k_o z +$$

$$+ k_o \int_0^z \phi_y(s) \sin k_o (z-s)\, ds - \phi_y(z) \quad . \tag{2.66}$$

Simplifying, the result is:

$$\phi(z) = -D_1 \sin k_o z + \frac{V}{2} \cos k_o z + k_o \int_0^z \phi_y(s) \sin k_o (z-s)\, ds. \tag{2.67}$$

Similarly for $\phi(y)$,

$$\phi(y) = \frac{-1}{j\omega \mu_o \epsilon_o} \left(\frac{\partial Ay}{\partial y} + \frac{\partial Az}{\partial z} \right) \Bigg|_{\substack{x=a \\ z=h}} = \frac{j\omega}{k_o^2} \frac{\partial Ay}{\partial y} \Bigg|_{\substack{x=a \\ z=h}} + \phi_z(y) \quad . \tag{2.68}$$

The expression for $A_y(y)$ is given by (2.22). Differentiating (2.22),

$$\frac{\partial Ay(y)}{\partial y} = \frac{jk_o C_1}{c} \sin k_o y - \frac{jk_o C_3}{c} \cos k_o y -$$

$$- \frac{jk_o^2}{c} \int_0^y \phi_z(s) \sin k_o (y-s)\, ds + \frac{jk_o}{c} \phi_z(y). \tag{2.69}$$

Substituting (2.69) into (2.68)

$$\phi(y) = \phi_z(y) - C_1 \sin k_o y + C_3 \cos k_o y - \phi_z(y) +$$

$$+ k_o \int_0^y \phi_z(s) \sin k_o (y-s)\, ds. \tag{2.70}$$

Simplifying (2.70), the result is

$$\phi(y) = -C_1 \sin k_o y + C_3 \cos k_o y + k_o \int_0^y \phi_z(s) \sin k_o (y-s)\, ds. \tag{2.71}$$

Now applying (2.62) to (2.67) and (2.71), the third condition becomes

$$C_3 = -D_1 \sin k_o h + \frac{V}{2} \cos k_o h + k_o \int_0^h \phi_y(s) \sin k_o (h-s)\, ds. \tag{2.72}$$

The expression for $\phi_y(s)$ is needed. $\phi_y(z)$ is given by (2.54). To get $\phi_y(s)$ a simple change of variable from z to s is used. Now substitute (2.54) into (2.72)

and interchange the order of integration of dy' and ds:

$$C_3 = -D_1 \sin k_o h + \frac{V}{2} \cos k_o h + \frac{j\mu_o c}{4\pi} \int_0^{\ell} I_y(y') H(y') \, dy' \tag{2.73}$$

where

$$H(y') = y' \int_0^h \left\{ \frac{e^{-jk_o R_{1s}}}{R_{1s}^3} (jk_o R_{1s} + 1) - \frac{e^{-jk_o R_{2s}} (jk_o R_{2s} + 1)}{R_{2s}^3} \right\} \cdot$$

$$\cdot \sin k_o (h-s) \, ds$$

and

$$R_{1s} = \sqrt{a^2 + y'^2 + (s-h)^2},$$

$$R_{2s} = \sqrt{a^2 + y'^2 + (s+h)^2} \quad . \tag{2.74}$$

Equation (2.73) may be simplified somewhat:

$$\int_0^{\ell} I_y(y') H(y') \, dy' + B_2 + B_3 \sin k_o h - \frac{j2\pi V}{\eta_o} \cos k_o h = 0. \tag{2.75}$$

2.3 Solution of Integral Equations

For convenience, the system of equations governing the driven element is repeated below. The voltage source V has been normalized to one volt. η_o has been replaced by its approximate value of 377 ohms.

$$\int_{-h}^{h} I_z(z') F(y, z') dz' + \int_0^{\ell} I_y(y') \left\{ \frac{e^{-jk_o R_{1,1}}}{R_{1,1}} - \frac{e^{-jk_o R_{2,1}}}{R_{2,1}} \right\} dy' +$$

$$+ B_1 \cos k_o y + B_2 \sin k_o y = 0,$$

valid for $0 \leq y \leq \ell$. (2.76)

$$\int_{-h}^{h} I_z(z') \frac{e^{-jk_o R_{o,2}}}{R_{o,2}} dz' + \int_0^{\ell} I_y(y') G(z,y') dy' + B_3 \cos k_o z +$$

$$+ j\frac{2\pi}{377} \sin k_o |z| = 0$$

valid for $-h \leq z \leq h$. (2.77)

Then as assumed before:

$$I_y(0) = I_z(h), \tag{2.78}$$

$$I_y(\ell) = 0 , \tag{2.79}$$

and

$$\int_0^{\ell} I_y(y') H(y') dy' + B_2 + B_3 \sin k_o h - j\frac{2\pi}{377} \cos k_o h = 0. \tag{2.80}$$

Now a matrix method of solution similar to work of Mei (1965) and of Harrington (1967) is used. Basically, the procedure is to replace an integration by a summation.

The interval in z' from -h to +h is divided into N segments. The center of each ith segment is denoted by z_i', and an unknown value of current I_{zi} is assigned to each ith segment. The currents are assumed to be constant over each segment. The continuous function $I_z(z')$ is thus replaced by the segmented function $I_{z1}, I_{z2}, \ldots I_{zN}$ with N values.

Likewise, the interval in y' from 0 to ℓ is divided into M segments. The center of each ith segment is denoted by y_i' and an unknown value of current I_{yi} is assigned to each ith segment. Again the currents are assumed to be constant over each segment. The continuous function $I_y(y')$ is thus replaced by the segmented function $I_{y1}, I_{y2}, \ldots I_{yM}$ with M values.

The modified problem now has M + N + 3 unknowns with apparently only 5 equations. However, equation (2.76) is valid for $0 \leq y \leq \ell$. Then M equations

can be derived from (2.76) by writing one equation for each $y_i = y_i'$. Likewise, equation (2.77) can yield N equations by writing one equation for each $z_i = z_i'$. The other 3 equations come from (2.78), (2.79), and (2.80). Then a compatible system of M + N + 3 unknowns with M + N + 3 equations can be written.

Now the change from integration to summation is completed by taking:

$$dz' \sim \Delta z' = \frac{2h}{N} \quad , \tag{2.81}$$

and

$$dy' \sim \Delta y' = \frac{\ell}{M} \quad .$$

Define the functions $P(y, y')$ and $Q(z, z')$ next:

$$P(y, y') = \frac{e^{-jk_o R_{1,1}}}{R_{1,1}} - \frac{e^{-jk_o R_{2,1}}}{R_{2,1}} \tag{2.82}$$

$$Q(z, z') = \frac{e^{-jk_o R_{o,2}}}{R_{o,2}} \quad .$$

Then the first M equations can be written:

$$\sum_{i=1}^{N} I_{zi} F(y_1, z_i') \frac{2h}{N} + \sum_{i=1}^{M} I_{yi} P(y_1, y_i') \frac{\ell}{M} + B_1 \cos k_o y_1 + B_2 \sin k_o y_1 = 0$$

$$\vdots \qquad\qquad \vdots$$

$$\sum_{i=1}^{N} I_{zi} F(y_M, z_i') \frac{2h}{N} + \sum_{i=1}^{M} I_{yi} P(y_M, y'_i) \frac{\ell}{M} + B_1 \cos k_o y_M + B_2 \sin k_o y_M = 0 \tag{2.83}$$

The next N equations are:

$$\sum_{i=1}^{N} I_{zi}\, Q(z_1, z_i')\, \frac{2h}{N} + \sum_{i=1}^{M} I_{yi} G(z_1, y_i')\, \frac{\ell}{M} + B_3 \cos k_o z_1 = -j\frac{2\pi}{377} \sin k_o |z_1| \ ,$$

$$\vdots \qquad\qquad \vdots$$

$$\sum_{i=1}^{N} I_{zi} Q(z_N, z_i')\, \frac{2h}{N} + \sum_{i=1}^{M} I_{yi} G(z_N, y_i')\, \frac{\ell}{M} + B_3 \cos k_o z_N = -j\frac{2\pi}{377} \sin k_o |z_N| \qquad (2.84)$$

The final 3 equations come from (2.78), (2.79), and (2.80)

Then consistent with previous assumptions the following can be written:

$$I_{y1} - I_{zN} = 0 \ , \qquad (2.85)$$

$$I_{yM} = 0 \ , \qquad (2.86)$$

and

$$\sum_{i=1}^{M} I_{yi} H(y_i')\, \frac{\ell}{M} + B_2 + B_3 \sin k_o h = +j\frac{2\pi}{377} \cos k_o h \ . \qquad (2.87)$$

In matrix form the equations are

$$\begin{bmatrix} & & \\ & \text{MATRIX} & \\ & & \end{bmatrix} \begin{bmatrix} I_{z1} \\ \vdots \\ I_{zN} \\ I_{y1} \\ \vdots \\ I_{yM} \\ B_1 \\ B_2 \\ B_3 \end{bmatrix} = \begin{bmatrix} 0 \\ 0 \\ \vdots \\ 0 \end{bmatrix} M \\ -j\frac{2\pi}{377} \sin k_o |z_1| \\ \vdots \\ -j\frac{2\pi}{377} \sin k_o |z_N| \Big\} N \\ 0 \\ 0 \\ +j\frac{2\pi}{377} \cos k_o h \end{bmatrix} \qquad (2.88)$$

The solution of the matrix equation in (2.88) can be obtained from a high-speed digital computer. Of course, (2.88) only approximates the system of integral equations in (2.76) through (2.80). The accuracy of the matrix solution depends very heavily upon the fineness of the subdivisions used.

2.4 Numerical Results

The matrix equation (2.88) was programmed for the IBM 360 computer. This involved matrix inversion with complex algebra. The following physical parameters were used: ℓ = 8.0 cm, h = 1.0 cm, and a = 0.04 cm. The frequency was varied from 450 MHz to 950 MHz in 50 MHz steps.

Values of M and N were chosen in the same ratio as ℓ and 2h. This assured uniform segmentation along the wire element. To check the accuracy of the solutions for the currents, M and N were increased (corresponding to finer subdivisions) until the results converged. The final values were N = 11 and M = 44, corresponding to the inversion of a 58 x 58 matrix.

Normalized current distributions from the computer program are shown in Fig. 2-2 and Fig. 2-3 for three frequencies. The real part of the distribution is plotted in Fig. 2-2 and the imaginary part in Fig. 2-3. The horizontal axis contains both z and y so that I_z and I_y may be plotted on the same graph.

The dip shown in these curves at the junction of I_z and I_y is interesting. It is a direct result of equation (2.85). The original condition in (2.78) equated the two current distributions at the junction. However when segmentation was used to change from integration to summation, it was impossible to equate the two current distributions at the junction. Equation (2.85) does the next best thing by equating the currents on either side of the junction. Other conditions were tried in place of (2.85), but none solved the problem of the dip.

The input impedance of the driven element may be easily calculated. The voltage source has been normalized to unity and the current is known at the feed point (z = 0).

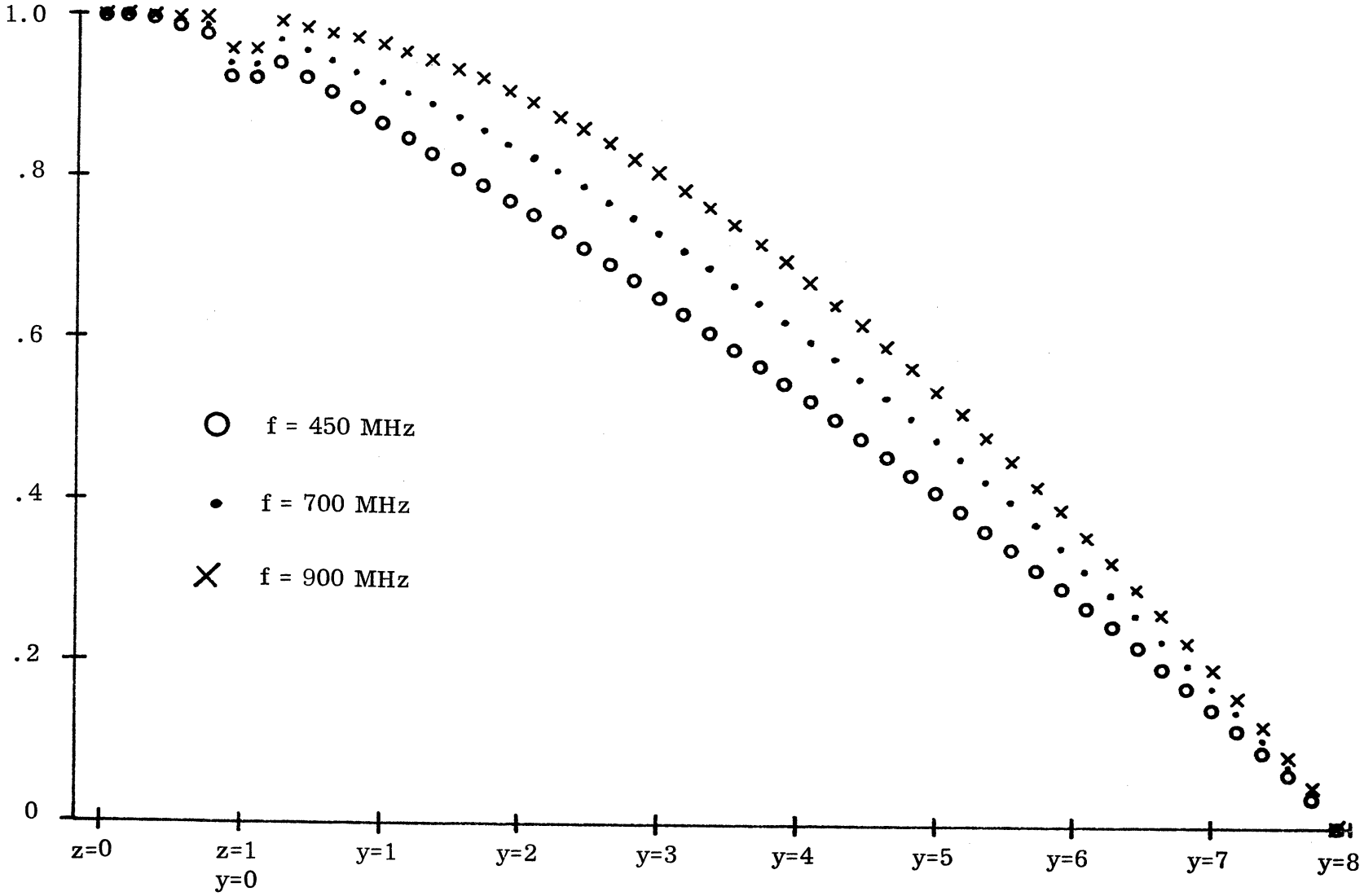

FIG. 2-2: NORMALIZED CURRENT DISTRIBUTIONS (Real Part).

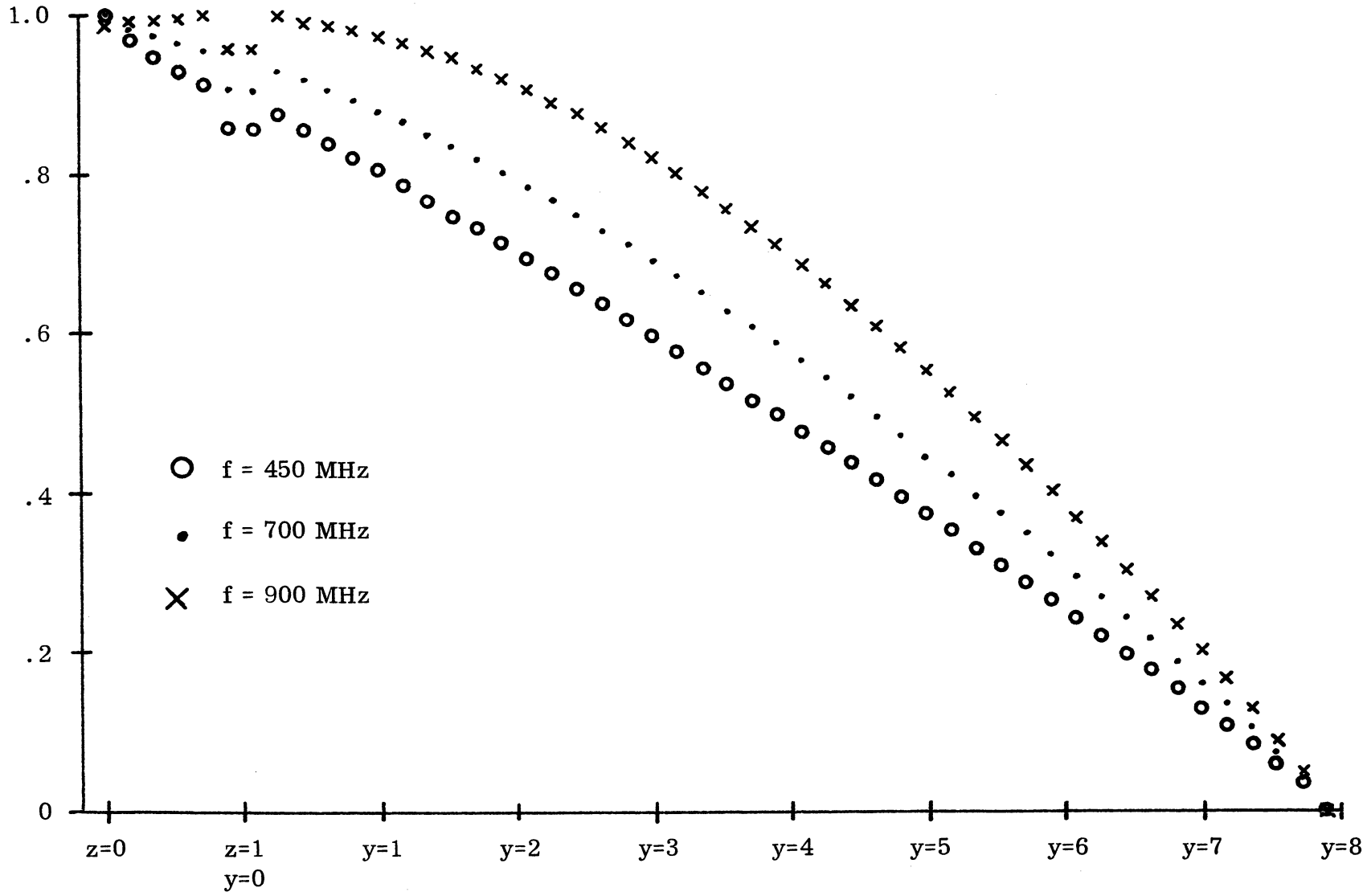

FIG. 2-3: NORMALIZED CURRENT DISTRIBUTIONS (Imaginary Part).

$$Z_{in} = \frac{1.0}{I_z \Big|_{z=0}} \quad . \tag{2.89}$$

The real part and the imaginary part of the input impedance are plotted in Figs. 2-4 and 2-5 respectively. As mentioned earlier, these values must be divided by two in order to compare with experimental data obtained from a model using a ground plane.

2.5 The Radiation Pattern

Once the current distribution is known on an antenna, it is relatively easy to calculate the far-zone electric field using the radiation vector $\bar{N}$ (Ramo, Whinnery and Van Duzer, 1965). The coordinate system is shown in Fig. 2-6. It is a standard spherical coordinate system.

Consider the current as being given by a vector density $\bar{J}$ in amperes per unit area spread throughout a volume V'. The radius vector from the origin to the volume source is $\bar{R}'$. Consider a field point in the far-zone. $\bar{R}$ is the radius vector from the origin to the field point. For the far-zone $|\bar{R}| >> |\bar{R}'|$. Then the radiation vector $\bar{N}$ is defined by

$$\bar{N}(\theta, \phi) = \iiint_{V'} \bar{J}(\bar{R}') \, e^{+jk_o \bar{R}' \cdot \hat{R}} \, dV'. \tag{2.90}$$

Define

$$\bar{N} = N_R \hat{R} + \bar{N}_t \quad . \tag{2.91}$$

where $\bar{N}_t$ contains the $\hat{\theta}$ and $\hat{\phi}$ components of $\bar{N}$. Then the electric field is related to $\bar{N}$ by

$$\bar{E} = -jk_o \eta_o \bar{N}_t \frac{e^{-jk_o R}}{4\pi R} \quad . \tag{2.92}$$

Equation (2.92) is valid only when there are no magnetic sources. This condition is satisfied for the driven element.

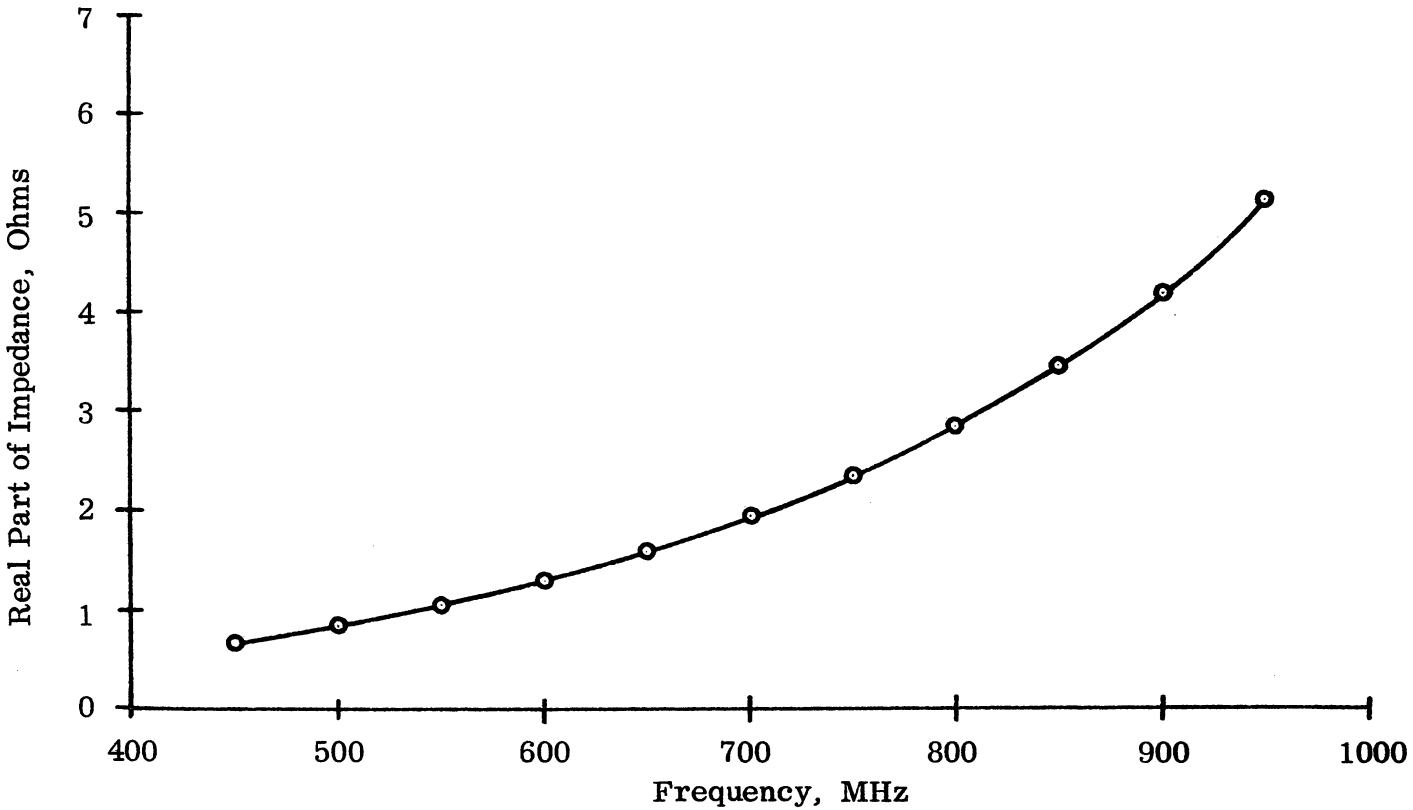

FIG. 2-4: INPUT IMPEDANCE OF DRIVEN ELEMENT (Real Part).

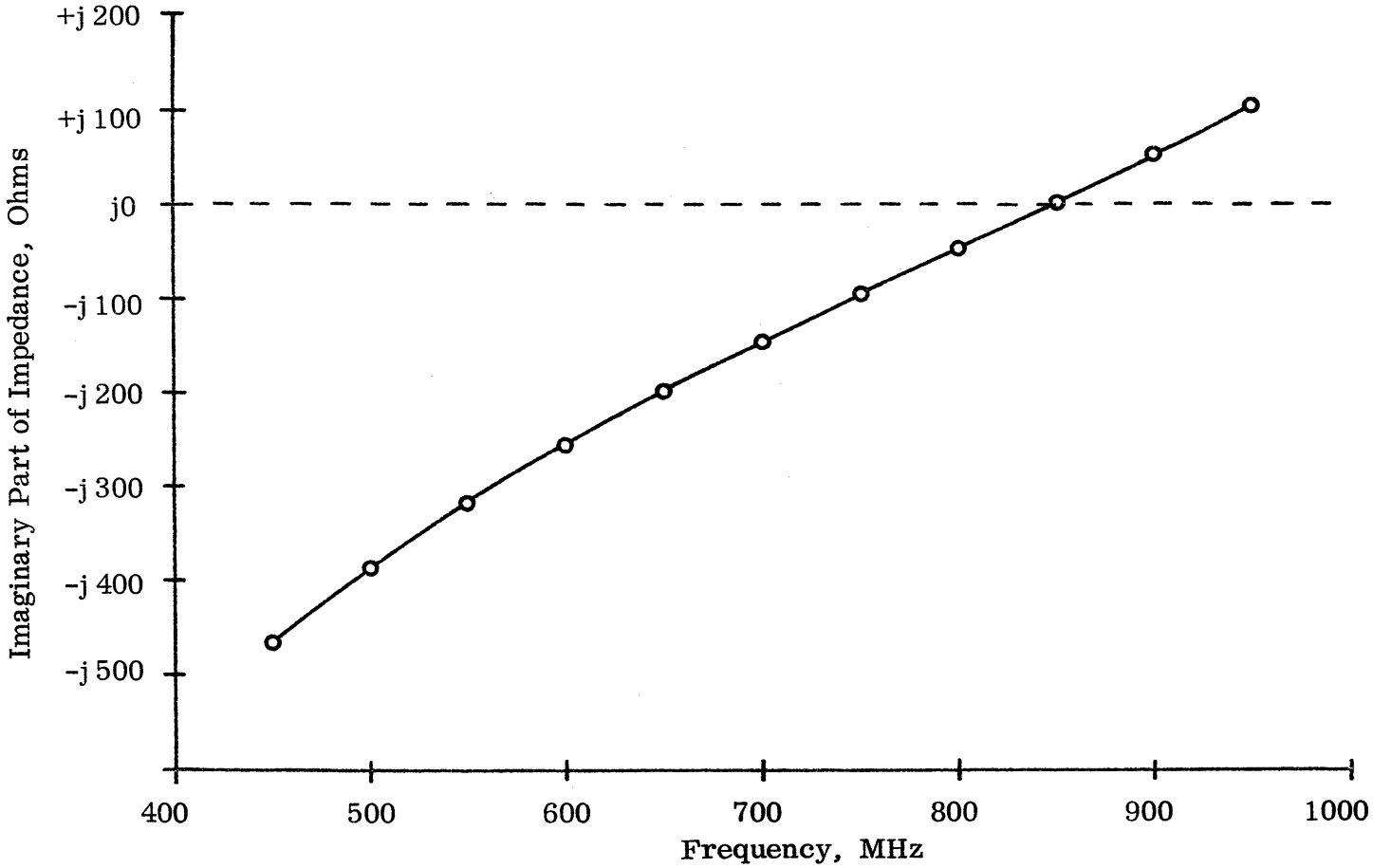

FIG. 2-5: INPUT IMPEDANCE OF DRIVEN ELEMENT (Imaginary Part).

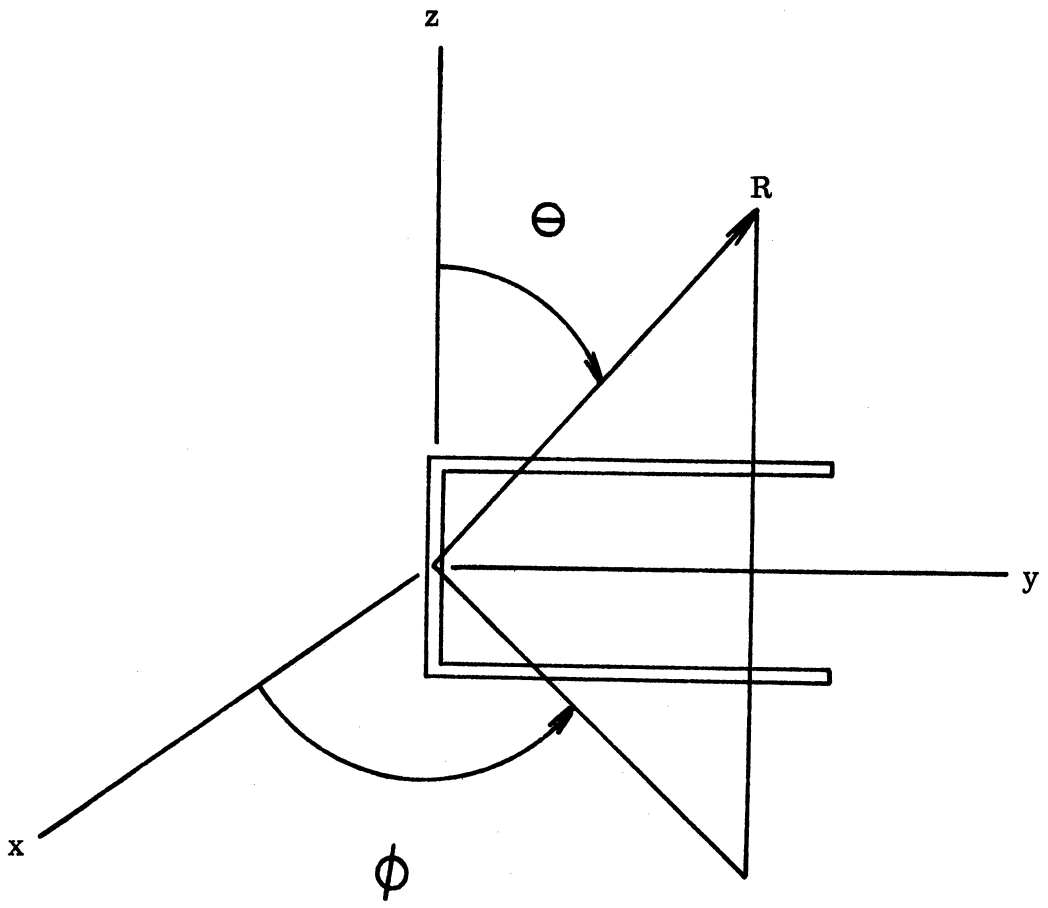

FIG. 2-6: SPHERICAL COORDINATE SYSTEM.

Now consider the driven element. There are two components of $\bar{N}$, N_y and N_z since current exists in the y and z directions. Using (2.90) and after some manipulations,

$$N_y = 2j \sin\left[k_o h \cos\theta\right] \int_0^{\ell} I_y(y') \, e^{+jk_o y' \sin\theta \sin\phi} \, dy' \tag{2.93}$$

and

$$N_z = \int_{-h}^{h} I_z(z') \, e^{+jk_o z' \cos\theta} \, dz' \quad . \tag{2.94}$$

Next the relationships between the rectangular and spherical coordinate systems are needed.

$$\begin{aligned}
\hat{X} &= \hat{R} \sin\theta \cos\phi + \hat{\theta} \cos\theta \cos\phi - \hat{\phi} \sin\phi \quad . \\
\hat{Y} &= \hat{R} \sin\theta \sin\phi + \hat{\theta} \cos\theta \sin\phi + \hat{\phi} \cos\phi \quad . \\
\hat{Z} &= \hat{R} \cos\theta - \hat{\theta} \sin\theta \quad .
\end{aligned} \tag{2.95}$$

Now using the definition of $\bar{N}_t$ in (2.91), and changing the expressions for N_y and N_z to the spherical coordinate system using the relations in (2.95), the result is

$$\begin{aligned}
\bar{N}_t = \hat{\theta} \Bigg\{ & 2j \cos\theta \sin\phi \sin\left[k_o h \cos\theta\right] \int_0^{\ell} I_y(y') e^{+jk_o y' \sin\theta \sin\phi} \, dy' - \\
& - \sin\theta \int_{-h}^{h} I_z(z') \, e^{+jk_o z' \cos\theta} \, dz' \Bigg\} + \\
& + \hat{\phi} \, 2j \cos\phi \sin\left[k_o h \cos\theta\right] \int_0^{\ell} I_y(y') \, e^{+jk_o y' \sin\theta \sin\phi} \, dy' \quad .
\end{aligned} \tag{2.96}$$

The electric field $\bar{E}$ is related to $\bar{N}_t$ by (2.92). For convenience, consider a normalized case where

$$-j\, k_o\, \eta_o\, \frac{e^{-jk_oR}}{4\pi R} = 1 \quad . \tag{2.97}$$

Then $\bar{E} = \bar{N}_t$. Next the magnitudes of E_θ and E_ϕ will be calculated in the upper half plane. Values will be obtained for the three principal planes, x-y, x-z, and y-z. Current distributions obtained in the previous section will be used, but they will be smoothed, with the dips at the junctions removed.

Consider first the x-y plane: $\theta = 90^o$ and $0^o \leq \phi \leq 360^o$. The expression for $\bar{N}_t$ in (2.96) becomes

$$N_\theta = -\int_{-h}^{h} I_z(z')\, dz' \quad ,$$

$$N_\phi = 0 \quad . \tag{2.98}$$

Next consider the x-z plane: $0^o \leq \theta \leq 90^o$ and $\phi = 0^o$ or 180^o. Then (2.96) becomes

$$N_\theta = -\sin\theta \int_{-h}^{h} I_z(z')\, e^{+jk_oz'\cos\theta}\, dz'$$

$$N_\phi = \pm 2j \sin\left[k_o h \cos\theta\right] \int_0^{\ell} I_y(y')\, dy' \quad . \tag{2.99}$$

Finally consider the y-z plane: $0^o \leq \theta \leq 90^o$ and $\phi = 90^o$ or 270^o. Then (2.96) becomes

$$\text{RHP:}\quad N_\theta = 2j\cos\theta \sin\left[k_o h \cos\theta\right] \int_0^{\ell} I_y(y')\, e^{+jk_oy'\sin\theta}\, dy' -$$

$$-\sin\theta \int_{-h}^{h} I_z(z')\, e^{+jk_oz'\cos\theta}\, dz';$$

$$\text{LHP: } N_\theta = -2j \cos\theta \sin\left[k_o h \cos\theta \int_0^{\ell} I_y(y') e^{-jk_o y' \sin\theta}\, dy' - \right.$$

$$\left. - \sin\theta \int_{-h}^{h} I_z(z') e^{+jk_o z' \cos\theta}\, dz' \right];$$

$$N_\phi = 0 ; \qquad (2.100)$$

where RHP denotes the right half of the y-z plane (y>0) and LHP denotes the left half of the y-z plane (y<0).

The radiation patterns were calculated in the three principal planes for five frequencies: 450 MHz, 700 MHz, 800 MHz, 850 MHz, and 900 MHz. Fig. 2-7 shows the pattern in the x-y plane. $E_\phi = 0$, and the E_θ pattern is a circle for all frequencies. Observe the resonance peak in the magnitude of E_θ at 850 MHz.

The radiation patterns in the x-z plane are given in Figs. 2-8 through 2-12. Observe that cross-polarization exists in this plane. At low frequencies E_θ is dominant, but at higher frequencies the two components become nearly equal. Notice that the scale has been changed in Fig. 2-11. This change was caused by the resonant peak at 850 MHz.

The radiation patterns in the y-z plane are given in Figs. 2-13 through 2-17. Again, $E_\phi = 0$. As frequency increases, the E_θ pattern becomes more nearly a circle. Although the expressions for N_θ in (2.100) were different in the RHP and LHP, when the calculations were performed this difference was negligible. Again notice the change of scale in Fig. 2-16 at 850 MHz.

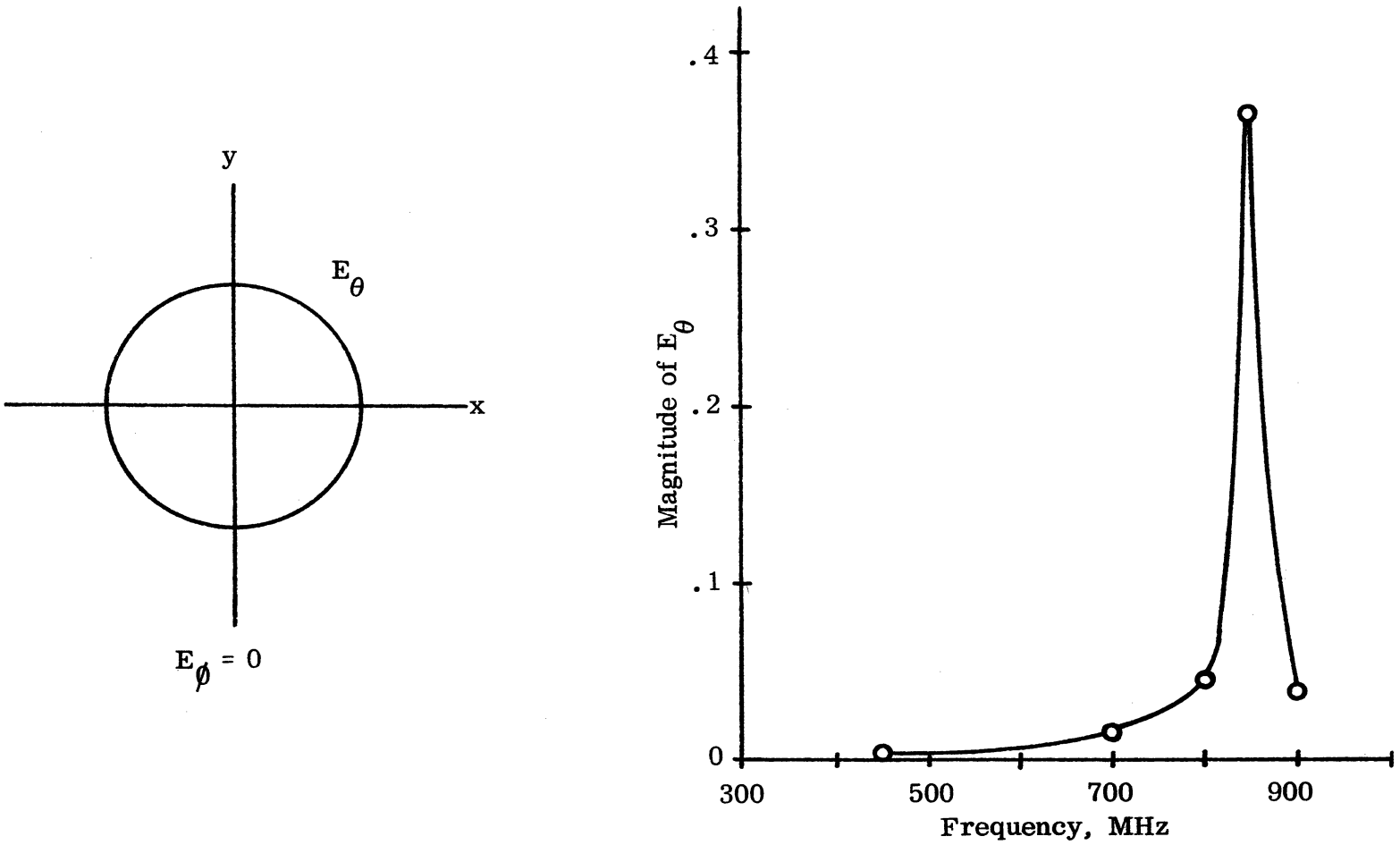

FIG. 2-7: RADIATION PATTERN IN x-y PLANE.

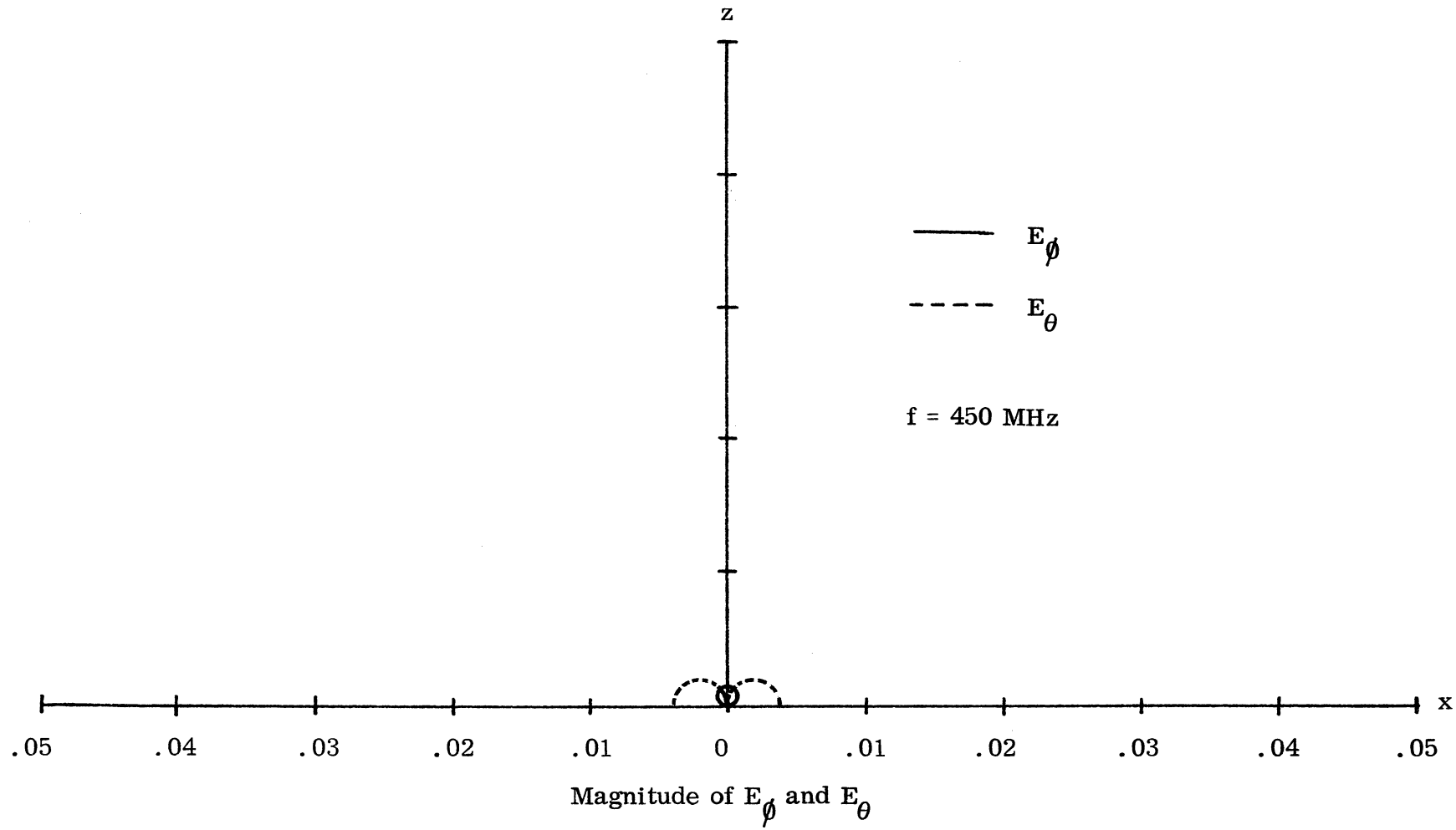

FIG. 2-8: RADIATION PATTERN IN x-z PLANE.

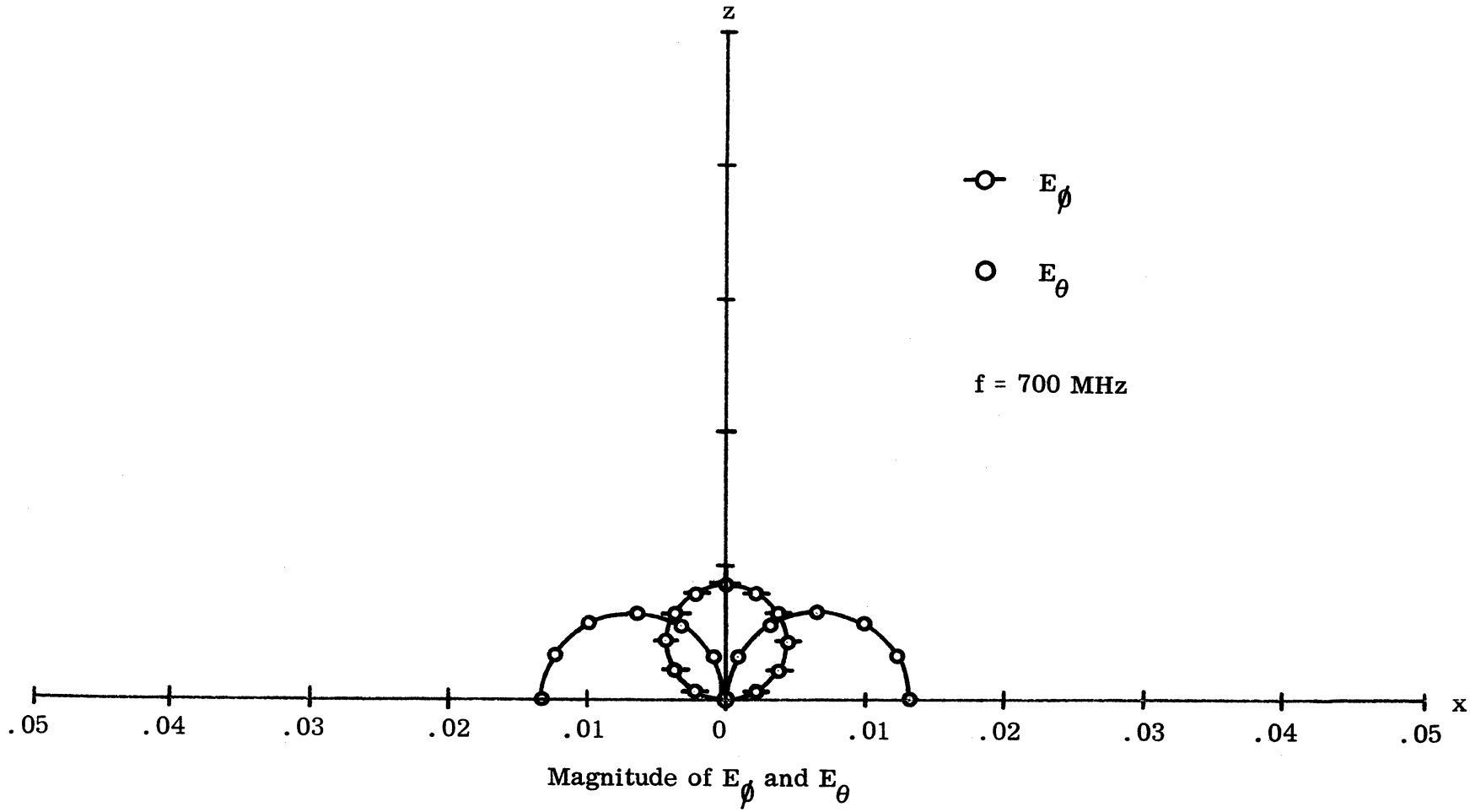

FIG. 2-9: RADIATION PATTERN IN x-z PLANE.

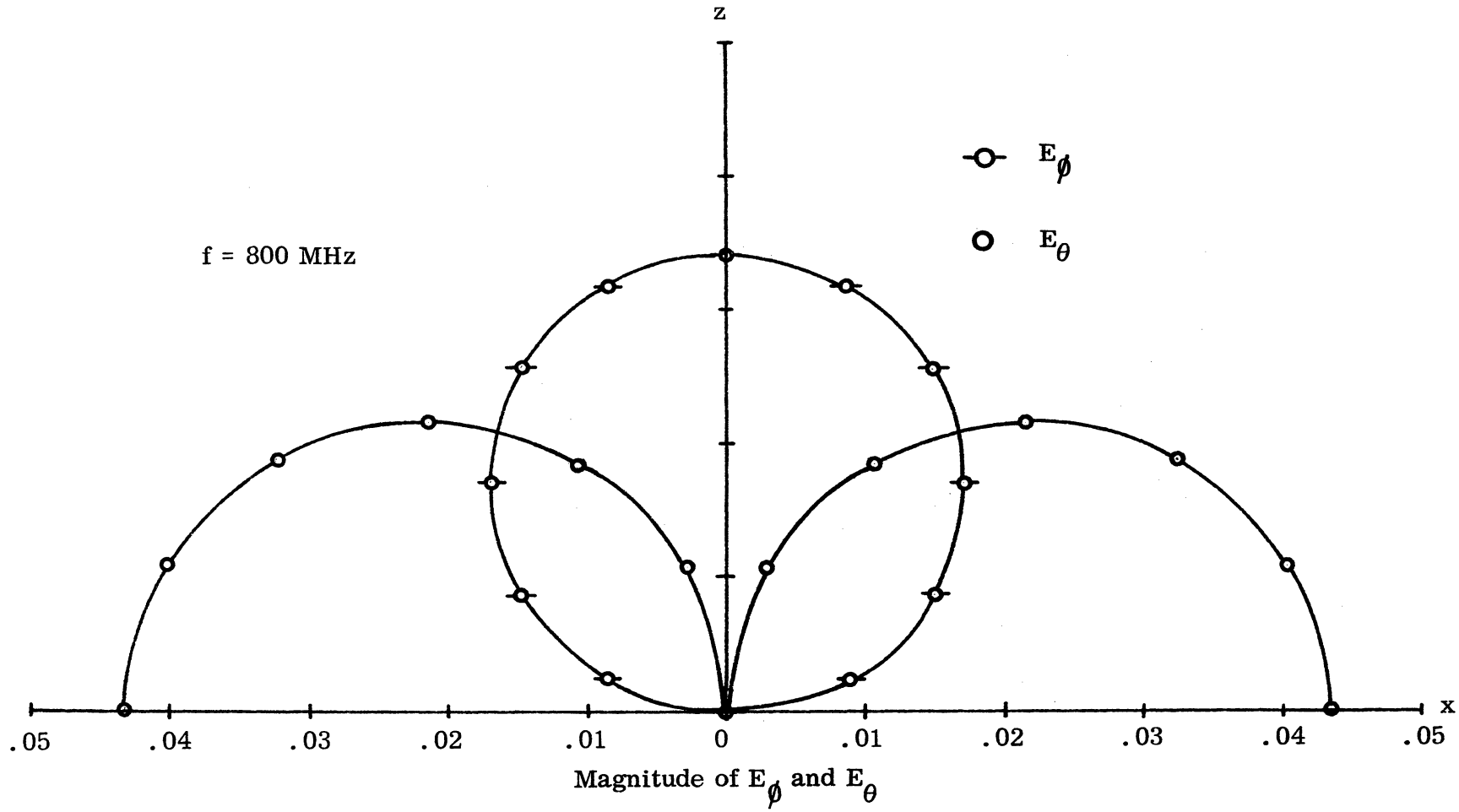

FIG. 2-10: RADIATION PATTERN IN x-z PLANE.

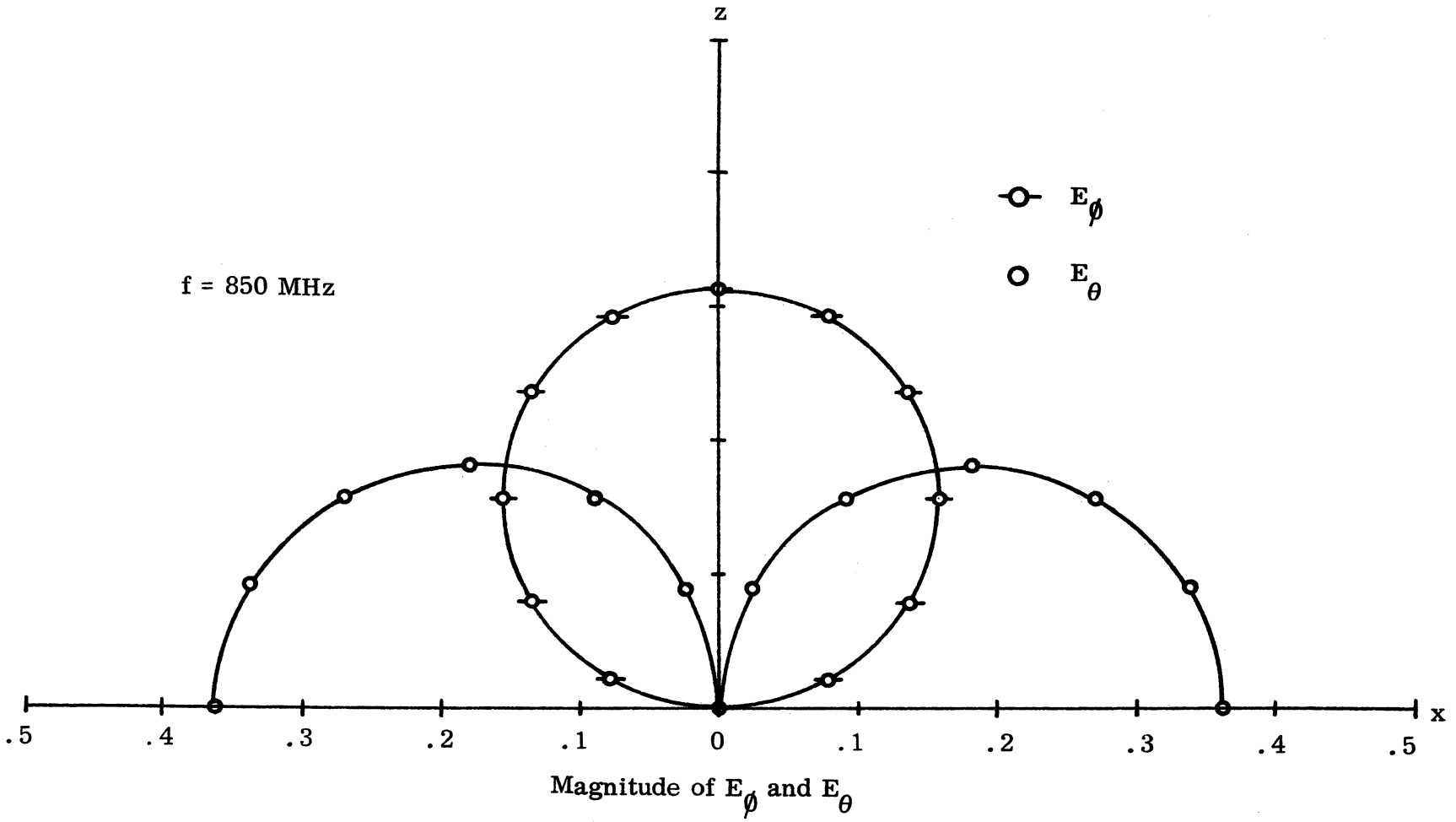

FIG. 2-11: RADIATION PATTERN IN x-z PLANE.

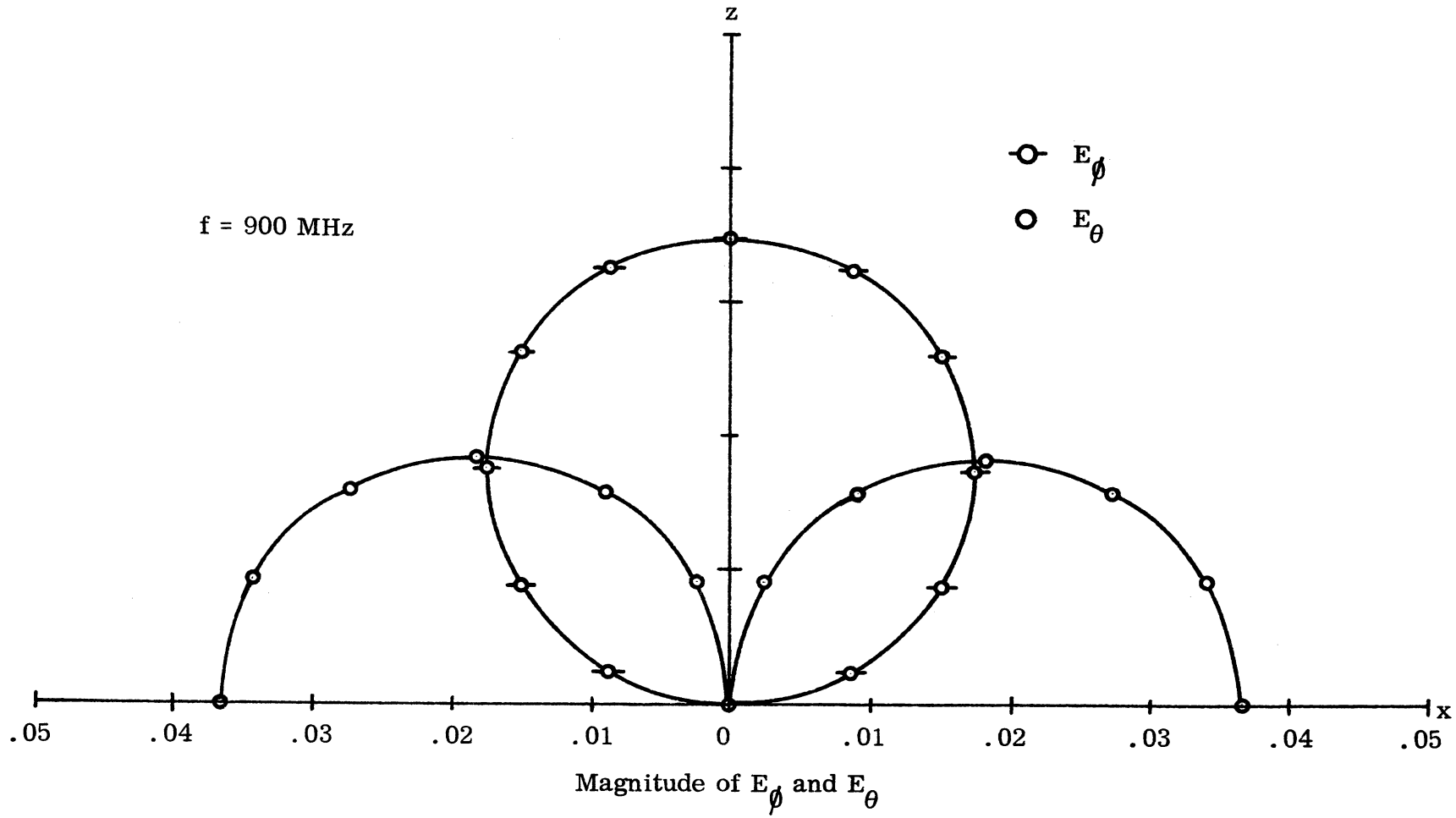

FIG. 2-12: RADIATION PATTERN IN x-z PLANE.

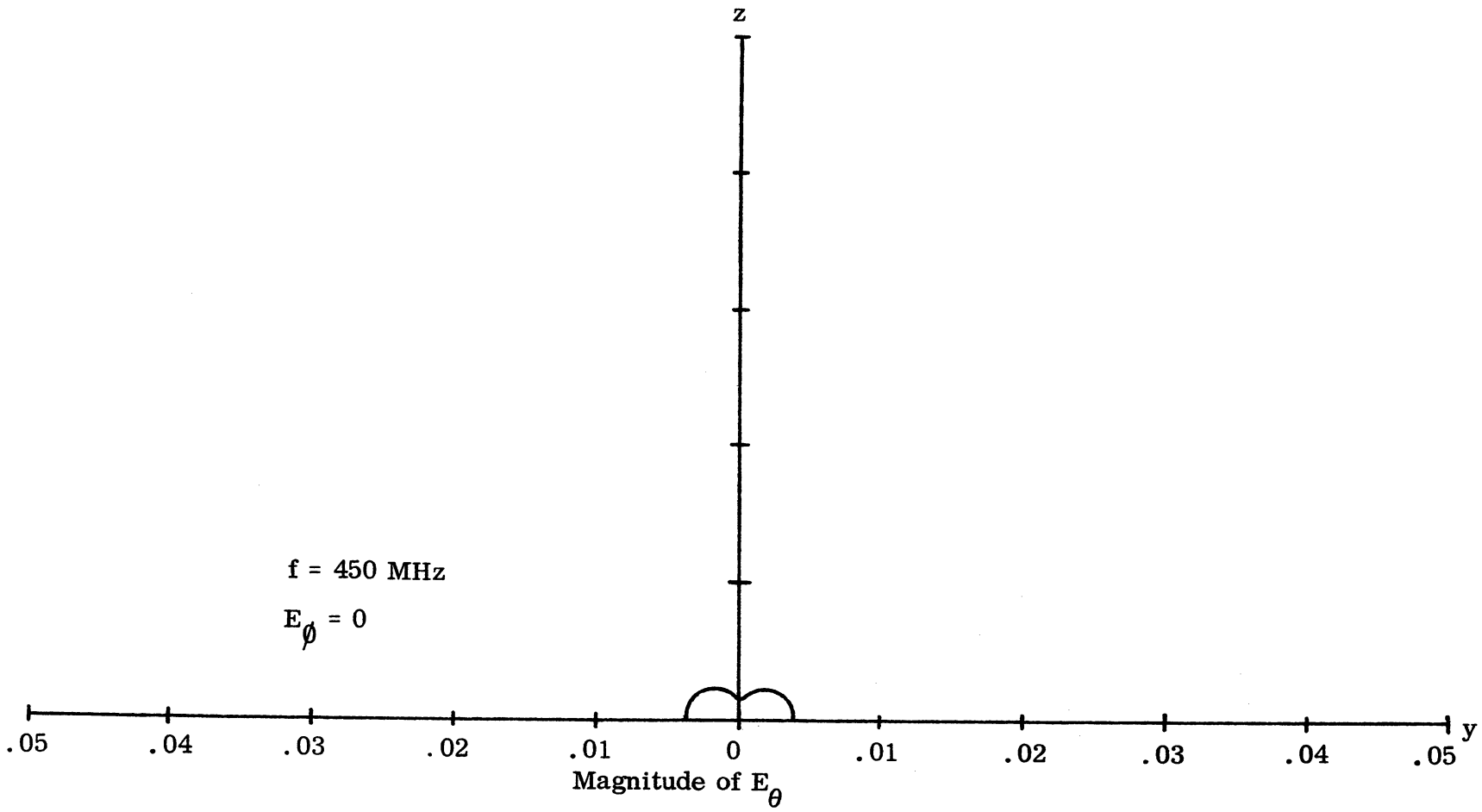

FIG. 2-13: RADIATION PATTERN IN y-z PLANE.

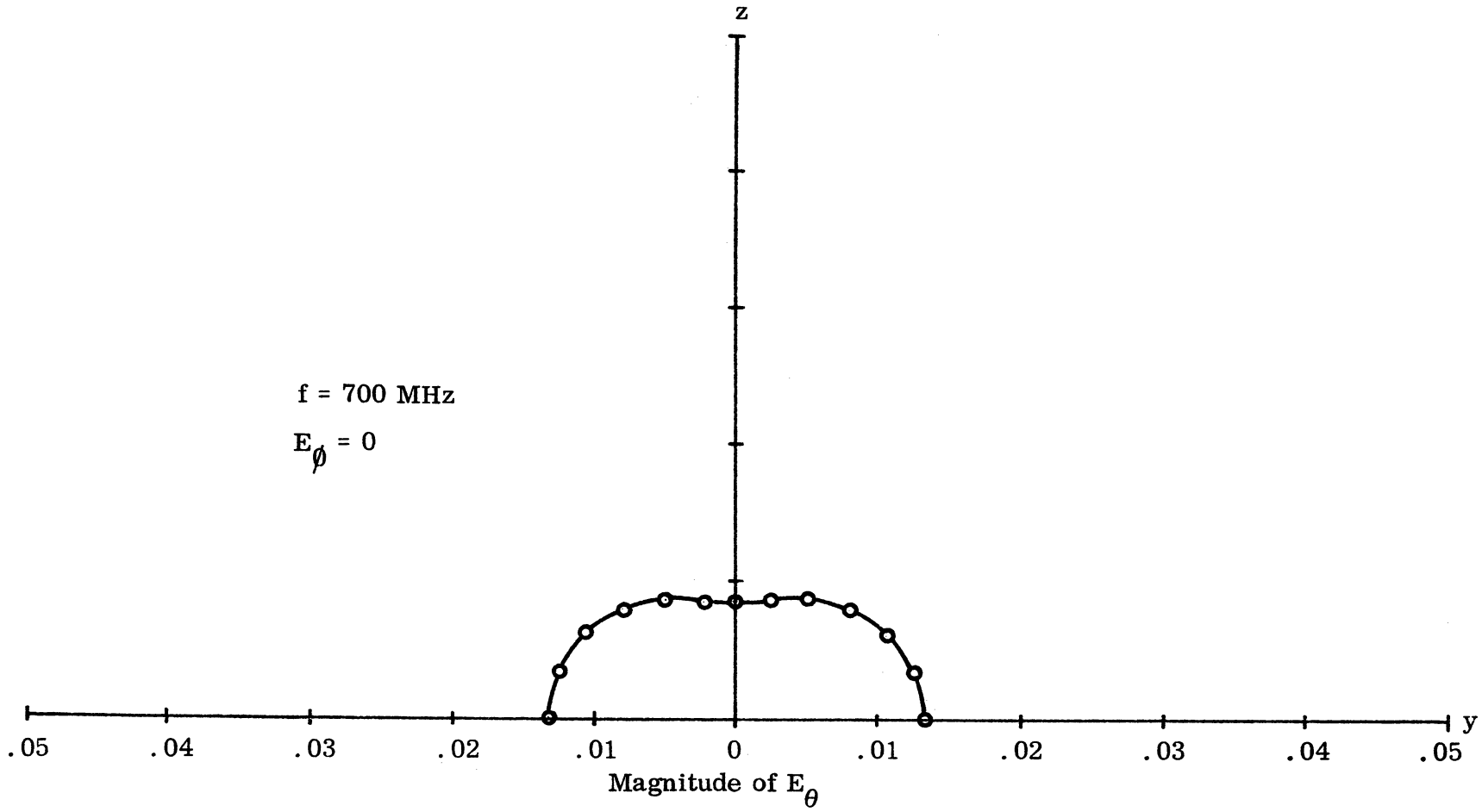

FIG. 2-14: RADIATION PATTERN IN y-z PLANE.

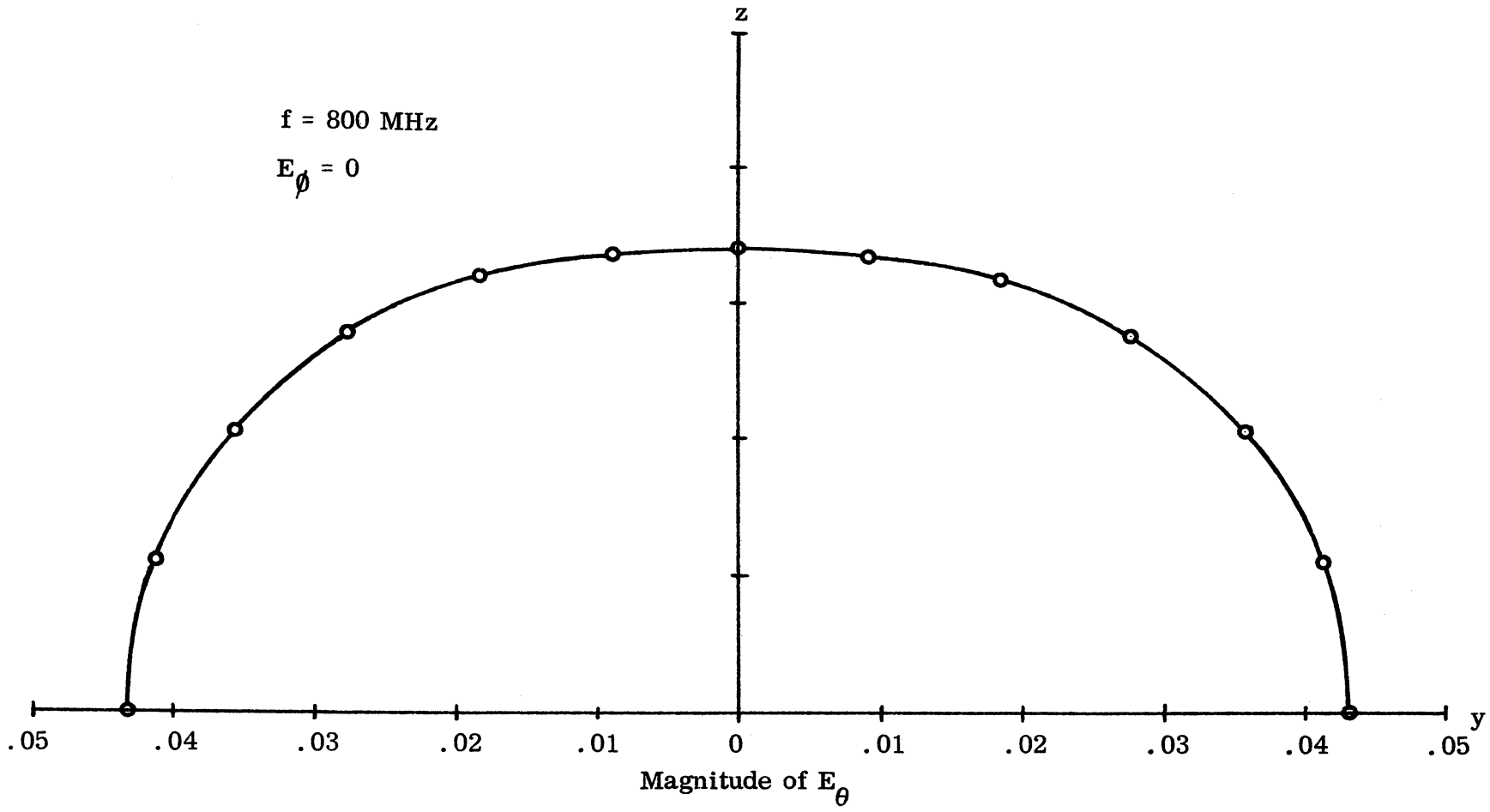

FIG. 2-15: RADIATION PATTERN IN y-z PLANE.

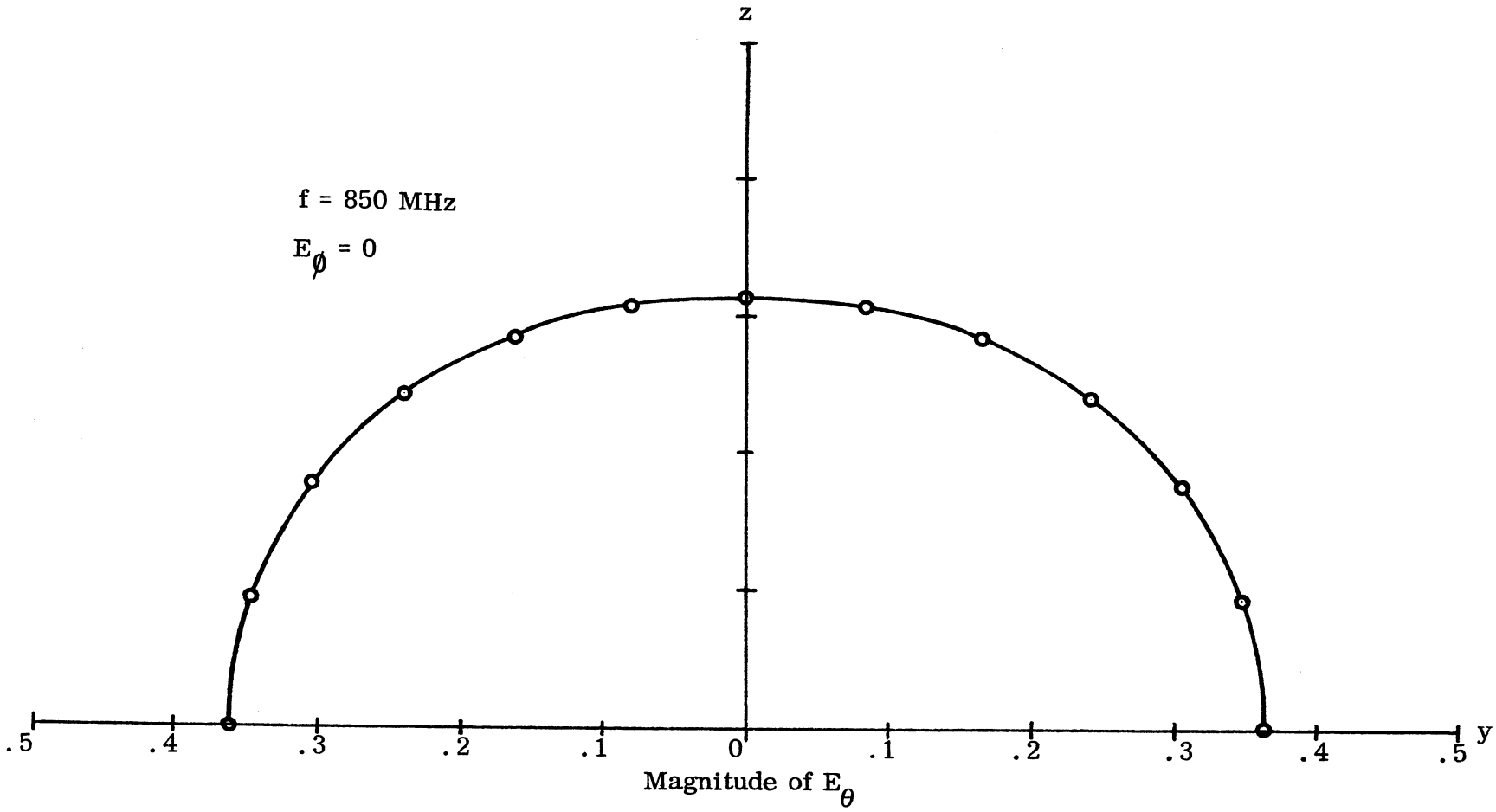

FIG. 2-16: RADIATION PATTERN IN y-z PLANE.

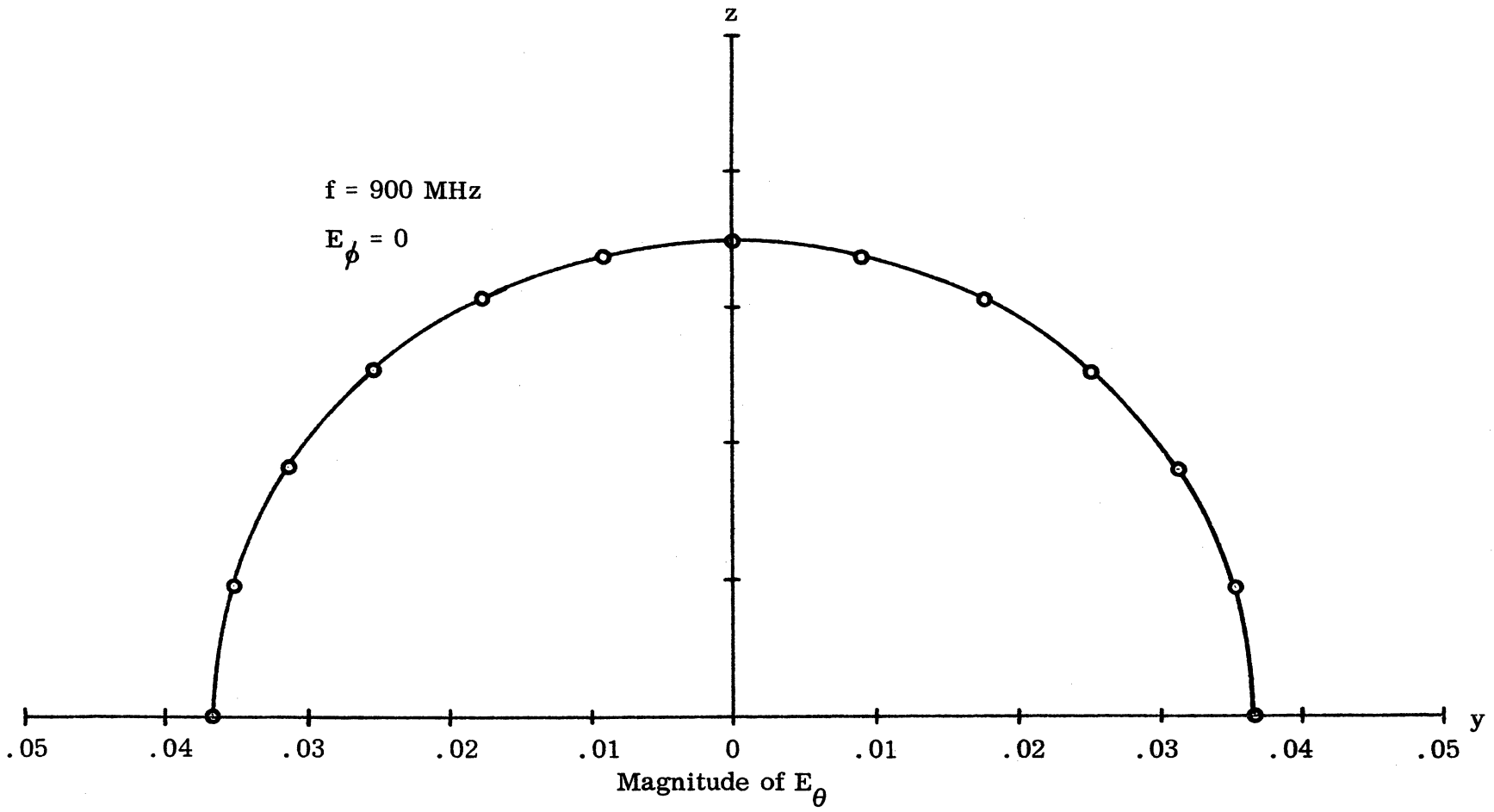

FIG. 2-17: RADIATION PATTERN IN y-z PLANE.

Chapter III

THE DRIVEN ELEMENT WITH PARASITIC ELEMENTS

3.1 Introduction

In this chapter the theory developed for the driven element in Chapter II is extended to include parasitic elements. The derivation of the integral equations is not inherently limited by the number of parasitic elements considered. However, the solution of the integral equations requires a matrix inversion to solve the system of simultaneous equations which approximates the integral equations. Although theoretically a matrix of any size may be inverted as long as it is non-singular, there are practical size limitations caused by excessive computer memory requirements and by cost. Since the driven element alone required a 58 x 58 matrix, it has been decided for reasons of economy to limit the analysis of the multielement interdigital array to an antenna with three elements.

The mathematical model of a three-element interdigital array is shown in Fig. 3-1. The elements are made from wire having a circular cross section with a diameter of 2a. They are assumed to be perfectly conducting and very thin, so that the only currents of interest are line currents along the axes of the wires. The center element of the antenna (m = 0) is driven by a voltage source in an infinitesimally small gap of width 2δ. The other two elements (m = 1 and m = -1) are parasitics. The ground plane of the physical model has again been removed by the use of image theory. Therefore, the theoretical input impedance must be divided by two in order to compare with experimental data.

3.2 Derivation of Integral Equations

Because of the geometry, the addition of the two parasitic elements to the problem does not produce any x-directed currents. Then as before there can be no x-component of $\bar{A}$, and the vector potential can be written

$$\bar{A} = A_y \hat{j} + A_z \hat{k} \quad . \tag{3.1}$$

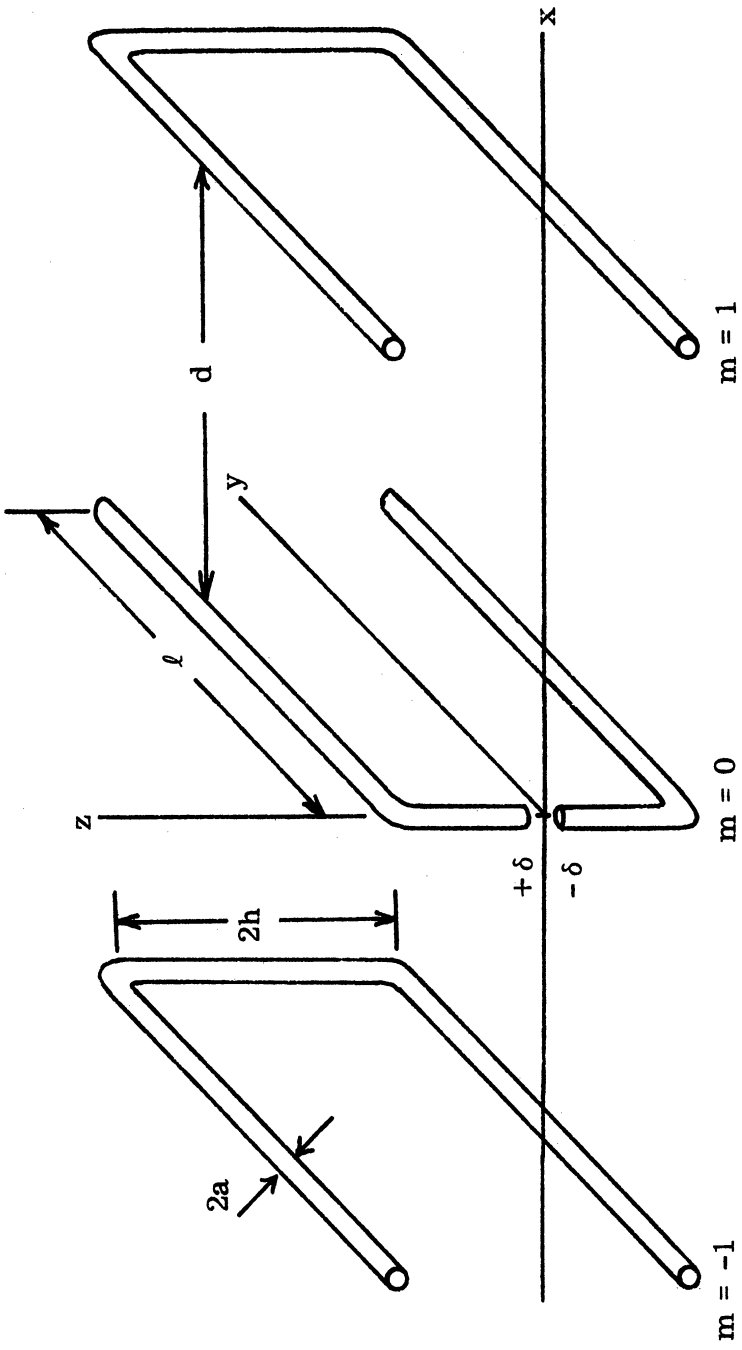

FIG. 3-1: THE DRIVEN ELEMENT WITH TWO PARASITIC ELEMENTS.

Then from (2.9) one obtains

$$\bar{E} = -\frac{j\omega}{k_o^2}\left\{\frac{\partial}{\partial x}\left(\frac{\partial A_y}{\partial y}+\frac{\partial A_z}{\partial z}\right)\hat{i} + \frac{\partial}{\partial y}\left(\frac{\partial A_y}{\partial y}+\frac{\partial A_z}{\partial z}\right)\hat{j} + \right.$$

$$\left. + \frac{\partial}{\partial z}\left(\frac{\partial A_y}{\partial y}+\frac{\partial A_z}{\partial z}\right)\hat{k} + k_o^2(A_y\hat{j}+A_z\hat{k})\right\} . \qquad (3.2)$$

Now the problem will be simplified. Because of symmetry, the two parasitic elements should have the same current distributions. In equation form

$$I_{1y}(y') = I_{-1y}(y') \qquad (3.3)$$

and

$$I_{1z}(z') = I_{-1z}(z') \ . \qquad (3.4)$$

Thus it is only necessary to solve for the currents on one parasitic element.

Next apply boundary conditions to the problem. Since the elements are assumed to be perfect conductors, the tangential $\bar{E}$ must be zero everywhere along the surface of the wires. For the driven element

$$E_y = -\frac{j\omega}{k_o^2}\left\{\frac{\partial}{\partial y}\left(\frac{\partial A_y}{\partial y}+\frac{\partial A_z}{\partial z}\right)+k_o^2\ A_y\right\} = 0$$

$$x = a, \quad 0 \le y \le \ell \ , \quad z = \pm h \qquad (3.5)$$

and

$$E_z = -\frac{j\omega}{k_o^2}\left\{\frac{\partial}{\partial z}\left(\frac{\partial A_y}{\partial y}+\frac{\partial A_z}{\partial z}\right)+k_o^2\ A_z\right\} = 0$$

$$x = a, \quad y = 0, \quad -h \le z \le -\delta, \quad \delta \le z \le h \ . \qquad (3.6)$$

For the $m = 1$ parasitic element

$$E_y = -\frac{j\omega}{k_o^2}\left\{\frac{\partial}{\partial y}\left(\frac{\partial A_y}{\partial y} + \frac{\partial A_z}{\partial z}\right) + k_o^2 A_y\right\} = 0$$

$$x = d + a, \quad 0 \le y \le \ell, \quad z = \pm h \tag{3.7}$$

and

$$E_z = -\frac{j\omega}{k_o^2}\left\{\frac{\partial}{\partial z}\left(\frac{\partial A_y}{\partial y} + \frac{\partial A_z}{\partial z}\right) + k_o^2 A_z\right\} = 0$$

$$x = d + a, \quad y = \ell, \quad -h \le z \le h \ . \tag{3.8}$$

The application of boundary conditions has produced six differential equations in the vector potentials A_y and A_z. From (2.7) the vector potential $\bar{A}$ is known in terms of unknown current distributions along the antenna. The problem is to determine these current distributions. By image theory, the current distributions along the upper and lower y-directed segments are equal and opposite. Thus it is only necessary to solve for one of these distributions on the driven element and one on the $m = 1$ parasitic element. Only one equation from (3.5) and one equation from (3.7) are needed to do this. Thus, four differential equations are obtained:

$$\frac{\partial}{\partial y}\left(\frac{\partial A_y}{\partial y} + \frac{\partial A_z}{\partial z}\right) + k_o^2 A_y = 0$$

$$x = a, \quad 0 \le y \le \ell, \quad z = h \tag{3.9}$$

$$\frac{\partial}{\partial z}\left(\frac{\partial A_y}{\partial y} + \frac{\partial A_z}{\partial z}\right) + k_o^2 A_z = 0$$

$$x = a, \quad y = 0, \quad -h \le z \le -\delta, \quad \delta \le z \le h \tag{3.10}$$

$$\frac{\partial}{\partial y}\left(\frac{\partial A_y}{\partial y}+\frac{\partial A_z}{\partial z}\right)+k_o^2 A_y = 0$$

$$x = d + a, \quad 0 \le y \le \ell, \quad z = h \tag{3.11}$$

$$\frac{\partial}{\partial z}\left(\frac{\partial A_y}{\partial y}+\frac{\partial A_z}{\partial z}\right)+k_o^2 A_z = 0$$

$$x = d + a, \quad y = \ell, \quad -h \le z \le h \tag{3.12}$$

The components of the vector potential $\bar{A}$ are next related to the unknown current distributions using (2.7) with line currents:

$$A_z(x,y,z) = \frac{\mu_o}{4\pi}\int_{-h}^{h}\left\{I_{oz}(z')\,\frac{e^{-jk_oR_o}}{R_o} - I_{1z}(z')\left(\frac{e^{-jk_oR_1}}{R_1}+\frac{e^{-jk_oR_{-1}}}{R_{-1}}\right)\right\}dz' \tag{3.13}$$

where

$$R_o = \sqrt{x^2+y^2+(z-z')^2},$$

$$R_1 = \sqrt{(x-d)^2+(y-\ell)^2+(z-z')^2},$$

and

$$R_{-1} = \sqrt{(x+d)^2+(y-\ell)^2+(z-z')^2}$$

and

$$A_y(x,y,z) = \frac{\mu_o}{4\pi}\int_0^{\ell}\left\{I_{oy}(y')\left(\frac{e^{-jk_oR_{o1}}}{R_{o1}} - \frac{e^{-jk_oR_{o2}}}{R_{o2}}\right) + \right.$$

$$\left. + I_{1y}(y')\left(\frac{e^{-jk_oR_{11}}}{R_{11}} - \frac{e^{-jk_oR_{12}}}{R_{12}} + \frac{e^{-jk_oR_{-11}}}{R_{-11}} - \frac{e^{-jk_oR_{-12}}}{R_{-12}}\right)\right\}dy' \qquad (3.14)$$

where

$$R_{o1} = \sqrt{x^2 + (y - y')^2 + (z - h)^2}\,,$$

$$R_{o2} = \sqrt{x^2 + (y - y')^2 + (z + h)^2}\,,$$

$$R_{11} = \sqrt{(x - d)^2 + (y - y')^2 + (z - h)^2}\,,$$

$$R_{12} = \sqrt{(x - d)^2 + (y - y')^2 + (z + h)^2}\,,$$

$$R_{-11} = \sqrt{(x + d)^2 + (y - y')^2 + (z - h)^2}\,,$$

and

$$R_{-12} = \sqrt{(x + d)^2 + (y - y')^2 + (z + h)^2}\,.$$

Equation (3.9) will now be solved. This equation may be rewritten using the Lorentz condition as expressed in (2.18). The result is:

$$\frac{\partial^2 A_y}{\partial y^2} + k_o^2 A_y = j\,\frac{k_o^2}{\omega}\,\frac{\partial \phi_z}{\partial y}\,. \qquad (3.15)$$

Equation (3.15) is a standard form and has a solution given by,

$$A_y(y) = -\frac{j}{c}\left[C_1 \cos k_o y + C_2 \sin k_o y - \int_{y_o}^{y} \frac{\partial \phi_z(s)}{\partial s} \sin k_o (y-s)\, ds\right] . \quad (3.16)$$

There is no loss of generality if y_o is set equal to zero because there are still two arbitrary constants left in the solution of a second order equation. Integrating by parts in (3.16) and combining terms involving $\sin k_o y$, the result is:

$$A_y(y) = -\frac{j}{c}\left[C_1 \cos k_o y + C_3 \sin k_o y - k_o \int_{o}^{y} \phi_z(s) \cos k_o (y-s)\, ds\right] \quad (3.17)$$

The expression for $\phi_z(s)$ is needed.

$$\phi_z = \frac{-1}{j\omega\mu_o \epsilon_o} \frac{\partial A_z}{\partial z} = \frac{j\omega}{k_o^2} \frac{\partial}{\partial z}\left[\frac{\mu_o}{4\pi} \int_{-h}^{h} \left\{ I_{oz}(z') \frac{e^{-jk_o R_o}}{R_o} - \right.\right.$$

$$\left.\left. - I_{1z}(z')\left(\frac{e^{-jk_o R_1}}{R_1} + \frac{e^{-jk_o R_{-1}}}{R_{-1}}\right)\right\} dz'\right] =$$

$$= \frac{j\omega}{k_o^2} \frac{\mu_o}{4\pi} \int_{-h}^{h} \left\{ I_{oz}(z') \frac{e^{-jk_o R_o}}{R_o^3} (z-z')(-jk_o R_o - 1) - \right.$$

$$\left. - I_{1z}(z')\left(\frac{e^{-jk_o R_1}}{R_1^3}(z-z')(-jk_o R_1 - 1) + \frac{e^{-jk_o R_{-1}}}{R_{-1}^3}(z-z')(-jk_o R_{-1} - 1)\right)\right\} dz' \quad (3.18)$$

Equation (3.9), which is being solved, is valid for $x = a$, $0 \leq y \leq \ell$, $z = h$.

$$R_o\Big|_{\substack{x=a\\0\le y\le \ell\\z=h}} = R_{o,a} = \sqrt{a^2 + y^2 + (h - z')^2}\ ,$$

$$R_1\Big|_{\substack{x=a\\0\le y\le \ell\\z=h}} = R_{1,a} = \sqrt{(a-d)^2 + (y-\ell)^2 + (h - z')^2}\ ,$$

and

$$R_{-1}\Big|_{\substack{x=a\\0\le y\le \ell\\z=h}} = R_{-1,a} = \sqrt{(a + d)^2 + (y - \ell)^2 + (h - z')^2} \qquad (3.19)$$

Then (3.18) becomes

$$\phi_z(y) = \frac{j\omega}{k_o^2}\frac{\mu_o}{4\pi}\int_{-h}^{h}\left\{I_{oz}(z')\,\frac{e^{-jk_oR_{o,a}}}{R_{o,a}^3}\,(h - z')\,(-jk_oR_{o,a} - 1) - \right.$$

$$\left. - I_{1z}(z')\left(\frac{e^{-jk_oR_{1,a}}}{R_{1,a}^3}\,(h - z')\,(-jk_oR_{1,a} - 1) + \frac{e^{-jk_oR_{-1,a}}}{R_{-1,a}^3}(h-z')(-jk_oR_{-1,a} - 1)\right)\right\}dz'$$

(3.20)

To get $\phi_z(s)$ a simple change of variable from y to s is used. Next define a function of $\gamma(\tau)$:

$$\gamma(\tau) = \frac{e^{-jk_o\tau}(-jk_o\tau - 1)}{\tau^3} \quad . \qquad (3.21)$$

Now substitute (3.20) back into (3.17) and interchange the order of integration of dz' and ds. The result is:

$$A_y(y) = -\frac{j}{c} C_1 \cos k_o y - \frac{j}{c} C_3 \sin k_o y - \frac{\mu_o}{4\pi}\int_{-h}^{h} I_{oz}(z')G_1(y,z')\,dz' +$$

$$+ \frac{\mu_o}{4\pi}\int_{-h}^{h} I_{1z}(z')\,G_2(y,z')\,dz' \qquad (3.22)$$

valid for $0 \le y \le \ell$ where

$$G_1(y,z') = (h-z')\int_o^y \gamma(R_{o,as}) \cdot \cos k_o (y-s)\,ds,$$

$$G_2(y,z') = (h-z')\int_o^y \left\{\gamma(R_{1,as}) + \gamma(R_{-1,as})\right\}\cos k_o (y-s)\,ds,$$

and

$$R_{o,as} = \sqrt{a^2 + s^2 + (h - z')^2},$$

$$R_{1,as} = \sqrt{(a - d)^2 + (s - \ell)^2 + (h - z')^2},$$

$$R_{-1,as} = \sqrt{(a + d)^2 + (s-\ell)^2 + (h-z')^2}\ . \qquad (3.23)$$

The first integral equation may now be derived by equating $A_y(y)$ in (3.22) with $A_y(x,y,z)$ in (3.14) evaluated at $x = a$, $0 \le y \le \ell$, $z = h$. The result is:

$$-\frac{j}{c} C_1 \cos k_o y - \frac{j}{c} C_3 \sin k_o y - \frac{\mu_o}{4\pi}\int_{-h}^{h} I_{oz}(z')\,G_1(y,z')\,dz' + \frac{\mu_o}{4\pi}\int_{-h}^{h} I_{1z}(z')G_2(y,z')dz' =$$

$$= \frac{\mu_o}{4\pi}\int_o^{\ell} I_{oy}(y')\,G_3(y,y')\,dy' + \frac{\mu_o}{4\pi}\int_o^{\ell} I_{1y}(y')\,G_4(y,y')\,dy' \qquad (3.24)$$

where

$$G_3(y,y') = \frac{e^{-jk_o R_{o1,a}}}{R_{o1,a}} - \frac{e^{-jk_o R_{o2,a}}}{R_{o2,a}} \quad ,$$

$$G_4(y,y') = \frac{e^{-jk_o R_{11,a}}}{R_{11,a}} - \frac{e^{-jk_o R_{12,a}}}{R_{12,a}} + \frac{e^{-jk_o R_{-11,a}}}{R_{-11,a}} - \frac{e^{-jk_o R_{-12,a}}}{R_{-12,a}} \quad ,$$

and

$$R_{o1,a} = \sqrt{a^2 + (y-y')^2} \quad ,$$

$$R_{o2,a} = \sqrt{a^2 + (y-y')^2 + 4h^2} \quad ,$$

$$R_{11,a} = \sqrt{(a-d)^2 + (y-y')^2} \quad ,$$

$$R_{12,a} = \sqrt{(a-d)^2 + (y-y')^2 + 4h^2} \quad ,$$

$$R_{-11,a} = \sqrt{(a+d)^2 + (y-y')^2} \quad ,$$

$$R_{-12,a} = \sqrt{(a+d)^2 + (y-y')^2 + 4h^2} \quad . \tag{3.25}$$

The integral equation in (3.24) may be simplified somewhat:

$$\int_{-h}^{h} I_{oz}(z')G_1(y,z')dz' - \int_{-h}^{h} I_{1z}(z')G_2(y,z')\,dz' + \int_{o}^{\ell} I_{oy}(y')G_3(y,y')dy' +$$

$$+ \int_{o}^{\ell} I_{1y}(y')G_4(y,y')dy' + B_1 \cos k_o y + B_2 \sin k_o y = 0 \tag{3.26}$$

valid for $0 \leq y \leq \ell$ where

$$B_1 = \frac{j4\pi}{\mu_o c} C_1 \quad \text{and} \quad B_2 = \frac{j4\pi}{\mu_o c} C_3 \ .$$

Equation (3.10) will now be solved. Using the Lorentz condition and rewriting:

$$\frac{\partial^2 A_z}{\partial z^2} + k_o^2 A_z = j \frac{k_o^2}{\omega} \frac{\partial \phi_y}{\partial z} \tag{3.27}$$

This equation is a standard form and the solution is identical with that of the driven element in Chapter II. The result is:

$$A_z(z) = -\frac{j}{c}\left[D_1 \cos k_o z + \frac{V}{2} \sin k_o |z| - \int_0^z \frac{\partial \phi_y(s)}{\partial s} \sin k_o (z-s)\, ds\right]$$

valid for $x = a, \ y = 0, \ -h \leq z \leq h$. (3.28)

Integrating by parts in (3.28) the solution becomes

$$A_z(z) = -\frac{j}{c}\left[D_1 \cos k_o z + \frac{V}{2} \sin k_o |z| - k_o \int_0^z \phi_y(s) \cos k_o (z-s)\, ds\right] \tag{3.29}$$

The expression for $\phi_y(s)$ is needed.

$$\phi_y = \frac{-1}{j\omega\mu_o\epsilon_o} \quad \frac{\partial A_y}{\partial y} = \frac{j\omega}{k_o^2} \quad \frac{\partial}{\partial y}\left[\frac{\mu_o}{4\pi}\int_0^{\ell}\left\{I_{oy}(y')\left(\frac{e^{-jk_oR_{o1}}}{R_{o1}} - \frac{e^{-jk_oR_{o2}}}{R_{o2}}\right) + \right.\right.$$

$$\left.\left. + I_{1y}(y')\left(\frac{e^{-jk_oR_{11}}}{R_{11}} - \frac{e^{-jk_oR_{12}}}{R_{12}} + \frac{e^{-jk_oR_{-11}}}{R_{-11}} - \frac{e^{-jk_oR_{-12}}}{R_{-12}}\right)\right\}dy'\right] =$$

$$= \frac{j\omega}{k_o^2}\frac{\mu_o}{4\pi}\int_0^{\ell}\left\{I_{oy}(y')\left(\frac{e^{-jk_oR_{o1}}}{R_{o1}^3}(y-y')\,(-jk_oR_{o1}-1) - \right.\right.$$

$$- \frac{e^{-jk_oR_{o2}}}{R_{o2}^3}(y-y')\,(-jk_oR_{o2}-1)\Big) + I_{1y}(y')\left(\frac{e^{-jk_oR_{11}}}{R_{11}^3}(y-y')\,(-jk_oR_{11}-1) - \right.$$

$$- \frac{e^{-jk_oR_{12}}}{R_{12}^3}(y-y')\,(-jk_oR_{12}-1) + \frac{e^{-jk_oR_{-11}}}{R_{-11}^3}(y-y')\,(-jk_oR_{-11}-1) -$$

$$\left.\left. - \frac{e^{-jk_oR_{-12}}}{R_{-12}^3}(y-y')\,(-jk_oR_{-12}-1)\right)\right\}dy' \qquad (3.30)$$

Equation (3.10) which is being solved is valid for $x = a$, $y = 0$, $-h \leq z \leq h$.

$$R_{o1}\Big|_{\substack{x=a\\y=0\\-h\le z\le h}} = R_{o1,b} = \sqrt{a^2 + (y')^2 + (z-h)^2}\ ,$$

$$R_{o2}\Big|_{\substack{x=a\\y=0\\-h\le z\le h}} = R_{o2,b} = \sqrt{a^2 + (y')^2 + (z+h)^2}\ ,$$

$$R_{11}\Big|_{\substack{x=a\\y=0\\-h\le z\le h}} = R_{11,b} = \sqrt{(a-d)^2 + (y')^2 + (z-h)^2}\ ,$$

$$R_{12}\Big|_{\substack{x=a\\y=0\\-h\le z\le h}} = R_{12,b} = \sqrt{(a-d)^2 + (y')^2 + (z+h)^2}\ ,$$

$$R_{-11}\Big|_{\substack{x=a\\y=0\\-h\le z\le h}} = R_{-11,b} = \sqrt{(a+d)^2 + (y')^2 + (z-h)^2}\ ,$$

and

$$R_{-12}\Big|_{\substack{x=a\\y=0\\-h\le z\le h}} = R_{-12,b} = \sqrt{(a+d)^2 + (y')^2 + (z+h)^2}\ . \qquad (3.31)$$

Then (3.30) becomes

$$\phi_y(z) = \frac{j\omega}{k_o^2}\,\frac{\mu_o}{4\pi}\int_0^{\ell}\Big\{I_{oy}(y')\Big(-y'\,\gamma(R_{o1,b}) + y'\,\gamma(R_{o2,b})\Big) + I_{1y}(y')\Big(-y'\,\gamma(R_{11,b}) +$$

$$+ y'\,\gamma(R_{12,b}) - y'\,\gamma(R_{-11,b}) + y'\,\gamma(R_{-12,b})\Big)\Big\}\,dy' \qquad (3.32)$$

To get $\phi_y(s)$ a simple change of variable from z to s is used. Now substitute (3.32) back into (3.29) and interchange the order of integration of dy' and ds. The result is:

$$A_z(z) = -\frac{j}{c} D_1 \cos k_o z - \frac{j}{c} \frac{V}{2} \sin k_o |z| -$$

$$-\frac{\mu_o}{4\pi}\int_0^{\ell} I_{oy}(y')\, H_1(z,y')\, dy' - \frac{\mu_o}{4\pi}\int_0^{\ell} I_{1y}(y')\, H_2(z,y')\, dy' \qquad (3.33)$$

valid for $-h \leq z \leq h$ where

$$H_1(z,y') = y'\int_0^z \left\{ \gamma(R_{o2,bs}) - \gamma(R_{o1,bs}) \right\} \cos k_o (z-s)\, ds,$$

$$H_2(z,y') = y'\int_0^z \left\{ \gamma(R_{12,bs}) - \gamma(R_{11,bs}) + \gamma(R_{-12,bs}) - \right.$$

$$\left. - \gamma(R_{-11,bs}) \right\} \cos k_o (z - s)\, ds \quad ,$$

and

$$R_{o1,bs} = \sqrt{a^2 + (y')^2 + (s-h)^2} \quad ,$$

$$R_{o2,bs} = \sqrt{a^2 + (y')^2 + (s+h)^2} \quad ,$$

$$R_{11,bs} = \sqrt{(a-d)^2 + (y')^2 + (s-h)^2} \quad ,$$

$$R_{12,bs} = \sqrt{(a-d)^2 + (y')^2 + (s+h)^2} \quad ,$$

$$R_{-11,bs} = \sqrt{(a+d)^2 + (y')^2 + (s-h)^2} \quad ,$$

and

$$R_{-12,bs} = \sqrt{(a+d)^2 + (y')^2 + (s+h)^2} \quad . \tag{3.34}$$

The second integral equation may now be derived by equating $A_z(z)$ in (3.33) with $A_z(x,y,z)$ in (3.13) evaluated at $x = a$, $y = 0$, $-h \leq z \leq h$. The result is:

$$-\frac{j}{c} D_1 \cos k_o z - \frac{j}{c}\frac{V}{2} \sin k_o |z| - \frac{\mu_o}{4\pi}\int_0^{\ell} I_{oy}(y')\, H_1(z,y')\, dy' -$$

$$-\frac{\mu_o}{4\pi}\int_0^{\ell} I_{1y}(y')\, H_2(z,y')dy' = \frac{\mu_o}{4\pi}\int_{-h}^{h} I_{oz}(z')\, H_3(z,z')\, dz' - \frac{\mu_o}{4\pi}\int_{-h}^{h} I_{1z}(z')H_4(z,z')dz' \tag{3.35}$$

where

$$H_3(z,z') = \frac{e^{-jk_o R_{o,b}}}{R_{o,b}}, \quad H_4(z,z') = \frac{e^{-jk_o R_{1,b}}}{R_{1,b}} + \frac{e^{-jk_o R_{-1,b}}}{R_{-1,b}},$$

$$R_{o,b} = \sqrt{a^2 + (z-z')^2},$$

$$R_{1,b} = \sqrt{(a-d)^2 + \ell^2 + (z-z')^2},$$

and

$$R_{-1,b} = \sqrt{(a+d)^2 + \ell^2 + (z-z')^2} \tag{3.36}$$

The integral equation in (3.35) may be simplified somewhat:

$$\int_{-h}^{h} I_{oz}(z')\, H_3(z,z')\, dz' - \int_{-h}^{h} I_{1z}(z')\, H_4(z,z')\, dz' + \int_0^{\ell} I_{oy}(y') H_1(z,y')\, dy' +$$

$$+ \int_0^{\ell} I_{1y}(y')\, H_2(z,y')\, dy' + B_3 \cos k_o z + j \frac{2\pi V}{\eta_o} \sin k_o |z| = 0 \qquad (3.37)$$

valid for $-h \leq z \leq h$ where

$$\eta_o \sqrt{\frac{\mu_o}{\epsilon_o}} \approx 377 \text{ ohms and } B_3 = \frac{j4\pi}{\mu_o c} D_1$$

Equation (3.11) will now be solved. Using the Lorentz condition and rewriting:

$$\frac{\partial^2 A_y}{\partial y^2} + k_o^2 A_y = j \frac{k_o^2}{\omega} \frac{\partial \phi_z}{\partial y} \qquad (3.38)$$

Equation (3.38) is a standard form and has a solution given by

$$A_y(y) = -\frac{j}{c}\left[E_1 \cos k_o y + E_2 \sin k_o y - \int_{y_o}^{y} \frac{\partial \phi_z(s)}{\partial s} \sin k_o (y-s)\, ds\right]. \qquad (3.39)$$

Again y_o is set equal to zero. Now integrating by parts in (3.39) and combining terms involving $\sin k_o y$, the result is:

$$A_y(y) = -\frac{j}{c}\left[E_1 \cos k_o y + E_3 \sin k_o y - \right.$$

$$\left. - k_o \int_0^{y} \phi_z(s) \cos k_o (y - s)\, ds\right] \qquad (3.40)$$

The expression for $\phi_z(s)$ is needed. Equation (3.18) gives ϕ_z. Equation (3.11), which is being solved, is valid for $x = d + a$, $0 \leq y \leq \ell$, $z = h$. Using this range for the variables in (3.18), the result is:

$$R_o\Big|_{\substack{x = d+a \\ 0 \leq y \leq \ell \\ z = h}} = R_{o,c} = \sqrt{(d+a)^2 + y^2 + (h - z')^2} \,,$$

$$R_1\Big|_{\substack{x = d+a \\ 0 \leq y \leq \ell \\ z = h}} = R_{1,c} = \sqrt{a^2 + (y - \ell)^2 + (h - z')^2} \,,$$

and

$$R_{-1}\Big|_{\substack{x = d+a \\ 0 \leq y \leq \ell \\ z = h}} = R_{-1,c} = \sqrt{(2d+a)^2 + (y - \ell)^2 + (h - z')^2} \qquad (3.41)$$

$$\phi_z(y) = \frac{j\omega}{k_o^2}\frac{\mu_o}{4\pi}\int_{-h}^{h}\Big\{ I_{oz}(z')(h-z')\,\gamma(R_{o,c}) - I_{1z}(z')(h-z')\Big(\gamma(R_{1,c}) +$$

$$+ \gamma(R_{-1,c})\Big)\Big\}\,dz' \qquad (3.42)$$

To get $\phi_z(s)$ a simple change of variable from y to s is used. Now substitute (3.42) back into (3.40) and interchange the order of integration of dz' and ds. The result is:

$$A_y(y) = -\frac{j}{c}E_1 \cos k_o y - \frac{j}{c}E_3 \sin k_o y - \frac{\mu_o}{4\pi}\int_{-h}^{h} I_{oz}(z')\,P_1(y,z')\,dz' +$$

$$+ \frac{\mu_o}{4\pi}\int_{-h}^{h} I_{1z}(z')\,P_2(y,z')\,dz' \qquad (3.43)$$

valid $0 \leq y \leq \ell$ where,

$$P_1(y,z') = (h - z')\int_0^y \gamma(R_{o,cs}) \cos k_o (y - s)\, ds \ ,$$

$$P_2(y,z') = (h - z')\int_0^y \left\{ \gamma(R_{1,cs}) + \gamma(R_{-1,cs}) \right\} \cos k_o (y - s)\, ds,$$

and

$$R_{o,cs} = \sqrt{(d + a)^2 + s^2 + (h - z')^2} \ ,$$

$$R_{1,cs} = \sqrt{a^2 + (s - \ell)^2 + (h - z')^2} \ ,$$

$$R_{-1,cs} = \sqrt{(2d + a)^2 + (s - \ell)^2 + (h - z')^2} \ . \qquad (3.44)$$

The third integral equation may now be derived by equating $A_y(y)$ in (3.43) with $A_y(x,y,z)$ in (3.14) evaluated at $x = d + a$, $0 \le y \le \ell$, $z = h$. The result is:

$$-\frac{j}{c} E_1 \cos k_o y - \frac{j}{c} E_3 \sin k_o y - \frac{\mu_o}{4\pi}\int_{-h}^{h} I_{oz}(z')\, P_1(y,z')\, dz' +$$

$$+ \frac{\mu_o}{4\pi}\int_{-h}^{h} I_{1z}(z')\, P_2(y,z')\, dz' = \frac{\mu_o}{4\pi}\int_0^{\ell} I_{oy}(y')\, P_3(y,y')\, dy' +$$

$$+ \frac{\mu_o}{4\pi}\int_0^{\ell} I_{1y}(y')\, P_4(y,y')\, dy' \qquad (3.45)$$

where

$$P_3(y,y') = \frac{e^{-jk_o R_{o1,c}}}{R_{o1,c}} - \frac{e^{-jk_o R_{o2,c}}}{R_{o2,c}} \ ,$$

$$P_4(y,y') = \frac{e^{-jk_o R_{11,c}}}{R_{11,c}} - \frac{e^{-jk_o R_{12,c}}}{R_{12,c}} + \frac{e^{-jk_o R_{-11,c}}}{R_{-11,c}} - \frac{e^{-jk_o R_{-12,c}}}{R_{-12,c}} \ ,$$

and

$$R_{o1,c} = \sqrt{(d+a)^2 + (y-y')^2}$$

$$R_{o2,c} = \sqrt{(d+a)^2 + (y-y')^2 + 4h^2}$$

$$R_{11,c} = \sqrt{a^2 + (y-y')^2}$$

$$R_{12,c} = \sqrt{a^2 + (y-y')^2 + 4h^2}$$

$$R_{-11,c} = \sqrt{(2d+a)^2 + (y-y')^2}$$

$$R_{-12,c} = \sqrt{(2d+a)^2 + (y-y') + 4h^2} \qquad (3.46)$$

The integral equation in (3.45) may be simplified somewhat:

$$\int_{-h}^{h} I_{oz}(z')\, P_1(y,z')\, dz' - \int_{-h}^{h} I_{1z}(z')\, P_2(y,z')\, dz' + \int_{0}^{\ell} I_{oy}(y')\, P_3(y,y')dy' +$$

$$+ \int_{0}^{\ell} I_{1y}(y')\, P_4(y,y')\, dy' + B_4 \cos k_o y + B_5 \sin k_o y = 0 \qquad (3.47)$$

valid for $0 \leq y \leq \ell$, where

$$B_4 = \frac{j4\pi}{\mu_o c} E_1 \quad \text{and} \quad B_5 = \frac{j4\pi}{\mu_o c} E_3 \ .$$

Finally, equation (3.12) will be solved. Using the Lorentz condition and rewriting:

$$\frac{\partial^2 A_z}{\partial z^2} + k_o^2 A_z = j \frac{k_o^2}{\omega} \frac{\partial \phi_y}{\partial z} \qquad (3.48)$$

This equation is a standard form and has a solution given by,

$$A_z(z) = -\frac{j}{c}\left[F_1 \cos k_o z + F_2 \sin k_o z - \int_{z_o}^{z} \frac{\partial \phi_y(s)}{\partial s} \sin k_o (z - s)\, ds\right] \tag{3.49}$$

Again z_o is set equal to zero. Now integrating by parts in (3.49) and combining terms in $\sin k_o z$, the result is:

$$A_z(z) = -\frac{j}{c}\left[F_1 \cos k_o z + F_3 \sin k_o z - k_o \int_0^z \phi_y(s) \cos k_o (z - s)\, ds\right] \tag{3.50}$$

Now from equation (2.18) we have

$$\phi(z) = \phi_y(z) + \phi_z(z) \tag{3.51}$$

Next solve for $\phi_z(z)$.

$$\phi_z(z) = \frac{j\omega}{k_o^2} \frac{\partial A_z}{\partial z}\bigg|_{\substack{x = d+a \\ y = \ell}} = \frac{1}{k_o}\frac{\partial}{\partial z}\left[F_1 \cos k_o z + F_3 \sin k_o z - k_o \int_0^z \phi_y(s) \cos k_o (z-s) ds\right] =$$

$$= \frac{1}{k_o}\left[-F_1 k_o \sin k_o z + F_3 k_o \cos k_o z + k_o^2 \int_0^z \phi_y(s) \sin k_o (z-s) ds - k_o \phi_y(z)\right] =$$

$$= -F_1 \sin k_o z + F_3 \cos k_o z + k_o \int_0^z \phi_y(s) \sin k_o (z-s)\, ds - \phi_y(z) \tag{3.52}$$

Then substitute (3.52) back into (3.51) to obtain:

$$\phi(z) = -F_1 \sin k_o z + F_3 \cos k_o z + k_o \int_0^z \phi_y(s) \sin k_o (z-s)\, ds \tag{3.53}$$

Equation (3.12), which is being solved, is for the $m = 1$ parasitic element. It has no source, and is grounded at $z = 0$. Then

$$\phi(z)\Big|_{z=0} = 0 \tag{3.54}$$

Looking at $\phi(0)$ in (3.53), the condition in (3.54) forces F_3 to be zero. Then for $A_z(z)$,

$$A_z(z) = -\frac{j}{c}\left[F_1 \cos k_o z - k_o \int_0^z \phi_y(s) \cos k_o (z - s)\, ds\right] \tag{3.55}$$

The expression for $\phi_y(s)$ is needed. Equation (3.30) gives ϕ_y. Equation (3.12) is valid for $x = d + a$, $y = \ell$, $-h \le z \le h$. Using this range for the variables in (3.30) the result is:

$$R_{o1}\Big|_{\substack{x=d+a\\y=\ell\\-h\le z\le h}} = R_{o1,d} = \sqrt{(d+a)^2 + (\ell - y')^2 + (z-h)^2}\ ,$$

$$R_{o2}\Big|_{\substack{x=d+a\\y=\ell\\-h\le z\le h}} = R_{o2,d} = \sqrt{(d+a)^2 + (\ell - y')^2 + (z+h)^2}\ ,$$

$$R_{11}\Big|_{\substack{x=d+a\\y=\ell\\-h\le z\le h}} = R_{11,d} = \sqrt{a^2 + (\ell - y')^2 + (z-h)^2}\ ,$$

$$R_{12}\Big|_{\substack{x=d+a\\y=\ell\\-h\le z\le h}} = R_{12,d} = \sqrt{a^2 + (\ell - y')^2 + (z+h)^2}\ ,$$

$$R_{-11}\Big|_{\substack{x=d+a\\y=\ell\\-h\le z\le h}} = R_{-11,d} = \sqrt{(2d+a)^2 + (\ell - y')^2 + (z-h)^2}\ ,$$

and

$$R_{-12}\Big|_{\substack{x=d+a\\y=\ell\\-h\le z\le h}} = R_{-12,d} = \sqrt{(2d+a)^2 + (\ell - y')^2 + (z+h)^2}\ . \tag{3.56}$$

$$\phi_y(z)=\frac{j\omega}{k_o^2}\frac{\mu_o}{4\pi}\int_0^{\ell}\Big\{I_{oy}(y')(\ell-y')\Big(\gamma(R_{o1,d})-\gamma(R_{o2,d})\Big)+I_{1y}(y')(\ell-y')\Big(\gamma(R_{11,d})-$$

$$-\gamma(R_{12,d})+\gamma(R_{-11,d})-\gamma(R_{-12,d})\Big)\Big\}dy' \qquad (3.57)$$

To get $\phi_y(s)$ a simple change of variable from z to s is used. Now substitute (3.57) into (3.55) and interchange the order of integration of dy' and ds. The result is:

$$A_z(z)=-\frac{j}{c}F_1\cos k_o z-\frac{\mu_o}{4\pi}\int_0^{\ell}I_{oy}(y')Q_1(z,y')dy'-\frac{\mu_o}{4\pi}\int_0^{\ell}I_{1y}(y')Q_2(z,y')\,dy' \qquad (3.58)$$

valid for $-h\le z\le h$ where

$$Q_1(z,y')=(\ell-y')\int_0^{z}\Big\{\gamma(R_{o1,ds})-\gamma(R_{o2,ds})\Big\}\cos k_o(z-s)\,ds,\quad ,$$

$$Q_2(z,\,y')=(\ell-y')\int_0^{z}\Big\{\gamma(R_{11,ds})-\gamma(R_{12,ds})+\gamma(R_{-11,ds})-$$

$$-\gamma(R_{-12,ds})\Big\}\cos k_o(z-s)\,ds\quad ,$$

and

$$R_{o1,ds}=\sqrt{(d+a)^2+(\ell-y')^2+(s-h)^2}\quad ,$$

$$R_{o2,ds}=\sqrt{(d+a)^2+(\ell-y')^2+(s+h)^2}\quad ,$$

$$R_{11,ds}=\sqrt{a^2+(\ell-y')^2+(s-h)^2}\quad ,$$

$$R_{12,ds}=\sqrt{a^2+(\ell-y')^2+(s+h)^2}\quad ,$$

$$R_{-11,ds} = \sqrt{(2d+a)^2 + (\ell - y')^2 + (s-h)^2} \quad ,$$

and

$$R_{-12,ds} = \sqrt{(2d+a)^2 + (\ell - y')^2 + (s+h)^2} \quad . \tag{3.59}$$

The fourth integral equation may now be derived by equating $A_z(z)$ in (3.58) with $A_z(x,y,z)$ in (3.13) evaluated at $x = d+a$, $y = \ell$, $-h \leq z \leq h$. The result is:

$$-\frac{j}{c} F_1 \cos k_o z - \frac{\mu_o}{4\pi}\int_0^{\ell} I_{oy}(y')Q_1(z,y')dy' - \frac{\mu_o}{4\pi}\int_0^{\ell} I_{1y}(y')Q_2(z,y')dy' =$$

$$= \frac{\mu_o}{4\pi}\int_{-h}^{h} I_{oz}(z')Q_3(z,z')dz' - \frac{\mu_o}{4\pi}\int_{-h}^{h} I_{1z}(z')Q_4(z,z')dz' \tag{3.60}$$

where

$$Q_3(z,z') = \frac{e^{-jk_o R_{o,d}}}{R_{o,d}} \quad , \quad Q_4(z,z') = \frac{e^{-jk_o R_{1,d}}}{R_{1,d}} + \frac{e^{-jk_o R_{-1,d}}}{R_{-1,d}} \quad ,$$

$$R_{o,d} = \sqrt{(d+a)^2 + \ell^2 + (z-z')^2} \quad ,$$

$$R_{1,d} = \sqrt{a^2 + (z-z')^2} \quad ,$$

and

$$R_{-1,d} = \sqrt{(2d+a)^2 + (z-z')^2} \quad . \tag{3.61}$$

The integral equation in (3.60) may be simplified somewhat:

$$\int_{-h}^{h} I_{oz}(z')Q_3(z,z')dz' - \int_{-h}^{h} I_{1z}(z')\,Q_4(z,z')dz' + \int_{0}^{\ell} I_{oy}(y')Q_1(z,y')dy' +$$

$$+\int_{0}^{\ell} I_{1y}(y')Q_2(z,y')dy' + B_6 \cos k_o z = 0 \qquad (3.62)$$

valid for $-h \leq z \leq h$ where $B_6 = \frac{j4\pi}{\mu_o c} F_1$.

Four integral equations have now been derived from the boundary conditions on the tangential electric field. The unknown functions in these equations are the line current distributions $I_{oz}(z')$ and $I_{oy}(y')$ on the driven element, and the line current distributions $I_{1z}(z')$ and $I_{1y}(y')$ on the $m = 1$ parasitic element. Observe that there are six unknown constants, $B_1, \ldots, B_6$.

Six assumed conditions are used with these four equations. The first is that the line currents are continuous across the junctions of the wire segments. For the driven element

$$I_{oz}(h) = I_{oy}(0) \quad . \qquad (3.63)$$

For the parasitic element

$$I_{1z}(h) = I_{1y}(\ell) \quad . \qquad (3.64)$$

The second condition is that the current goes to zero at the end of the wire. For the driven element

$$I_{oy}(\ell) = 0 \quad . \qquad (3.65)$$

For the parasitic element

$$I_{1y}(0) = 0 \quad . \qquad (3.66)$$

The third condition is that the scalar potential is continuous across the junction of the wire segments. For the driven element

$$\phi(z)\Big|_{z=h} = \phi(y)\Big|_{y=0} . \tag{3.67}$$

For the parasitic element

$$\phi(z)\Big|_{z=h} = \phi(y)\Big|_{y=\ell} . \tag{3.68}$$

Equation (3.67) will now be investigated more carefully. From the Lorentz condition, for the driven element one obtains

$$\phi(z) = \frac{j\omega}{k_o^2}\left(\frac{\partial A_y}{\partial y} + \frac{\partial A_z}{\partial z}\right)\Bigg|_{\substack{x=a\\y=0}} = \phi_y(z) + \frac{j\omega}{k_o^2}\left.\frac{\partial A_z}{\partial z}\right|_{\substack{x=a\\y=0}} . \tag{3.69}$$

The expression for $A_z(z)$ is given in (3.29). Since $\phi(z)$ will be evaluated at $z = h$ in (3.67), the absolute value sign may be removed from (3.29). Differentiating (3.29), the result is

$$\frac{\partial A_z}{\partial z} = +\frac{j}{c}k_o D_1 \sin k_o z - \frac{j}{c}k_o \frac{V}{2}\cos k_o z - \frac{jk_o^2}{c}\int_0^z \phi_y(s)\sin k_o(z-s)ds + \phi_y(z)\frac{jk_o}{c} \tag{3.70}$$

Substituting (3.70) into (3.69), the result is

$$\phi(z) = -D_1 \sin k_o z + \frac{V}{2}\cos k_o z + k_o\int_0^z \phi_y(s)\sin k_o(z-s)\,ds \tag{3.71}$$

Similarly for $\phi(y)$,

$$\phi(y) = \frac{j\omega}{k_o^2}\left(\frac{\partial A_y}{\partial y} + \frac{\partial A_z}{\partial z}\right)\Bigg|_{\substack{x=a\\z=h}} = \frac{j\omega}{k_o^2}\left.\frac{\partial A_y}{\partial y}\right|_{\substack{x=a\\z=h}} + \phi_z(y) \tag{3.72}$$

The expression for $A_y(y)$ is given by (3.17). Differentiating (3.17), one obtains

$$\frac{\partial A_y}{\partial y} = +\frac{jk_o}{c} C_1 \sin k_o y - \frac{jk_o}{c} C_3 \cos k_o y - \frac{jk_o^2}{c}\int_0^y \phi_z(s) \sin k_o(y-s)\, ds + \frac{jk_o}{c}\phi_z(y) \tag{3.73}$$

Substituting (3.73) into (3.72), the result is

$$\phi(y) = - C_1 \sin k_o y + C_3 \cos k_o y + k_o \int_0^y \phi_z(s) \sin k_o (y - s)\, ds \tag{3.74}$$

Now apply (3.67) to (3.71) and (3.74).

$$C_3 = - D_1 \sin k_o h + \frac{V}{2} \cos k_o h + k_o \int_0^h \phi_y(s) \sin k_o (h - s)\, ds \tag{3.75}$$

The expression for $\phi_y(s)$ is needed. $\phi_y(z)$ is given in (3.32). To get $\phi_y(s)$, a simple change of variable from z to s is used. Now substitute (3.32) into (3.75) and interchange the order of integration of dy' and ds. The result is:

$$\int_0^\ell I_{oy}(y')\, T_1(h, y')\, dy' + \int_0^\ell I_{1y}(y')\, T_2(h, y') dy' + B_2 + B_3 \sin k_o h - j\frac{2\pi V}{\eta_o} \cos k_o h = (\tag{3.76}$$

where

$$T_1(h, y') = y' \int_0^h \left\{ \gamma(R_{o2, bs}) - \gamma(R_{o1, bs}) \right\} \sin k_o (h - s)\, ds$$

$$T_2(h, y') = y' \int_0^h \left\{ \gamma(R_{12, bs}) - \gamma(R_{11, bs}) + \gamma(R_{-12, bs}) - \gamma(R_{-11, bs}) \right\} \sin k_o (h - s)\, ds \tag{3.77}$$

Finally, equation (3.68) will be studied. For the parasitic element, the expression for $\phi(z)$ is given by equation (3.53). Noting that F_3 is zero, the result is

$$\phi(z) = - F_1 \sin k_o z + k_o \int_0^z \phi_y(s) \sin k_o (z - s)\, ds \tag{3.78}$$

For $\phi(y)$, using the Lorentz condition for the parasitic element,

$$\phi(y) = \frac{j\omega}{k_o^2} \left(\frac{\partial A_y}{\partial y} + \frac{\partial A_z}{\partial z} \right) \Bigg|_{\substack{x = d + a \\ z = h}} = \frac{j\omega}{k_o^2} \frac{\partial A_y}{\partial y} \Bigg|_{\substack{x = d + a \\ z = h}} + \phi_z(y). \tag{3.79}$$

The expression for $A_y(y)$ is given in (3.40). Differentiating (3.40), one obtains

$$\frac{\partial A_y}{\partial y} = \frac{jk_o}{c} E_1 \sin k_o y - \frac{jk_o}{c} E_3 \cos k_o y - \frac{jk_o^2}{c} \int_0^y \phi_z(s) \sin k_o (y - s)\, ds + \frac{jk_o}{c} \phi_z(y) . \tag{3.80}$$

Substituting (3.80) into (3.79), the result is

$$\phi(y) = - E_1 \sin k_o y + E_3 \cos k_o y + k_o \int_0^y \phi_z(s) \sin k_o (y - s)\, ds . \tag{3.81}$$

Now apply (3.68) to (3.78) and (3.81). The result is:

$$-F_1 \sin k_o h + k_o \int_0^h \phi_y(s) \sin k_o (h - s)\, ds =$$

$$= - E_1 \sin k_o \ell + E_3 \cos k_o \ell + k_o \int_0^\ell \phi_z(s) \sin k_o (\ell - s)\, ds . \tag{3.82}$$

The expressions for $\phi_y(s)$ and $\phi_z(s)$ are needed. $\phi_y(z)$ is given in (3.57). To get $\phi_y(s)$, a simple change of variable from z to s is used. $\phi_z(y)$ is

given by (3.42). To get $\phi_z(s)$, a simple change of variable from y to s is used. Now equations (3.57) and (3.42) are substituted into (3.82) and the order of integration is interchanged in both integrals. The result is:

$$\int_{-h}^{h} I_{oz}(z')\, V_1(\ell, z')\, dz' - \int_{-h}^{h} I_{1z}(z')\, V_2(\ell, z')\, dz' - \int_0^{\ell} I_{oy}(y') U_1(h, y')\, dy' -$$

$$- \int_0^{\ell} I_{1y}(y')\, U_2(h, y') dy' + B_4 \sin k_o \ell - B_5 \cos k_o \ell - B_6 \sin k_o h = 0 \qquad (3.83)$$

where

$$V_1(\ell, z') = (h - z') \int_0^{\ell} \gamma(R_{o,cs}) \cdot \sin k_o (\ell - s)\, ds \quad ,$$

$$V_2(\ell, z') = (h - z') \int_0^{\ell} \left\{ \gamma(R_{1,cs}) + \gamma(R_{-1,cs}) \right\} \sin k_o (\ell - s)\, ds \quad ,$$

$$U_1(h, y') = (\ell - y') \int_0^{h} \left\{ \gamma(R_{o1,ds}) - \gamma(R_{o2,ds}) \right\} \sin k_o (h - s)\, ds,$$

and

$$U_2(h, y') = (\ell - y') \int_0^{h} \left\{ \gamma(R_{11,ds}) - \gamma(R_{12,ds}) + \gamma(R_{-11,ds}) - \right.$$

$$\left. - \gamma(R_{-12,ds}) \right\} \sin k_o (h - s)\, ds \qquad (3.84)$$

3.3 Solution of Integral Equations

For convenience, the system of equations governing the three-element interdigital array is repeated below. The voltage source V has been normalized to one volt. η_o has been replaced by its approximate value of 377 ohms.

$$\int_{-h}^{h} I_{oz}(z')\, G_1(y,z')\, dz' - \int_{-h}^{h} I_{1z}(z')\, G_2(y,z')\, dz' + \int_{0}^{\ell} I_{oy}(y')\, G_3(y,y')\, dy' +$$

$$+ \int_{0}^{\ell} I_{1y}(y')\, G_4(y,y')\, dy' + B_1 \cos k_o y + B_2 \sin k_o y = 0 \qquad (3.85)$$

valid for $0 \leq y \leq \ell$

$$\int_{-h}^{h} I_{oz}(z')\, H_3(z,z')\, dz' - \int_{-h}^{h} I_{1z}(z')\, H_4(z,z')\, dz' + \int_{0}^{\ell} I_{oy}(y')\, H_1(z,y')\, dy' +$$

$$+ \int_{0}^{\ell} I_{1y}(y')\, H_2(z,y')\, dy' + B_3 \cos k_o z + j\frac{2\pi}{377} \sin k_o |z| = 0 \qquad (3.86)$$

valid for $-h \leq z \leq h$

$$\int_{-h}^{h} I_{oz}(z')P_1(y,z')dz' - \int_{-h}^{h} I_{1z}(z')P_2(y,z')dz' + \int_{0}^{\ell} I_{oy}(y')\, P_3(y,y')\, dy' +$$

$$+ \int_{0}^{\ell} I_{1y}(y')\, P_4(y,y')\, dy' + B_4 \cos k_o y + B_5 \sin k_o y = 0 \qquad (3.87)$$

valid for $0 \leq y \leq \ell$

$$\int_{-h}^{h} I_{oz}(z')\, Q_3(z,z')dz' - \int_{-h}^{h} I_{1z}(z')Q_4(z,z')\, dz' + \int_{0}^{\ell} I_{oy}(y')Q_1(z,y')dy' +$$

$$+ \int_{0}^{\ell} I_{1y}(y')Q_2(z,y')\, dy' + B_6 \cos k_o z = 0 \qquad (3.88)$$

valid for $-h \leq z \leq h$

Then as assumed before

$$I_{oz}(h) = I_{oy}(0) \tag{3.89}$$

$$I_{1z}(h) = I_{1y}(\ell) \tag{3.90}$$

$$I_{oy}(\ell) = 0 \tag{3.91}$$

$$I_{1y}(0) = 0 \tag{3.92}$$

and

$$\int_0^{\ell} I_{oy}(y')T_1(h,y')dy' + \int_0^{\ell} I_{1y}(y')T_2(h,y')dy' + B_2 + B_3 \sin k_o h - j\frac{2\pi}{377}\cos k_o h = 0 \tag{3.93}$$

$$\int_{-h}^{h} I_{oz}(z')V_1(\ell,z')dz' - \int_{-h}^{h} I_{1z}(z')V_2(\ell,z')dz' - \int_0^{\ell} I_{oy}(y')\, U_1(h,y')\, dy' -$$

$$- \int_0^{\ell} I_{1y}(y')\, U_2(h,y')\, dy' + B_4 \sin k_o \ell - B_5 \cos k_o \ell - B_6 \sin k_o h = 0 \tag{3.94}$$

Again, a matrix method of solution is used. Basically the solution involves replacing an integration by a summation. Segmentation is used as in Chapter II. The interval in z' from -h to +h is divided into N segments. The interval in y' from 0 to ℓ is divided into M segments. In the three-element interdigital array, there are 2M + 2N + 6 unknowns. M equations can be derived from both (3.85) and (3.87). N equations can be obtained from both (3.86) and (3.88). Finally, there are six equations in (3.89) through (3.94). Then a compatible system of 2M + 2N + 6 unknowns with 2M + 2N + 6 equations exists.

The change from integration to summation is completed by taking:

$$dz' \sim \Delta z' = \frac{2h}{N} \quad \text{and} \quad dy' \sim \Delta y' = \frac{\ell}{M} \tag{3.95}$$

Then the first M equations can be written:

$$\sum_{i=1}^{N} I_{ozi} G_1(y_1, z_i') \frac{2h}{N} - \sum_{i=1}^{N} I_{1zi} G_2(y_1, z_i') \frac{2h}{N} + \sum_{i=1}^{M} I_{oyi} G_3(y_1, y_i') \frac{\ell}{M} + \sum_{i=1}^{M} I_{1yi} G_4(y_1, y_i') \frac{\ell}{M} + B_1 \cos k_o y_1 + B_2 \sin k_o y_1 = 0$$

$$\vdots \qquad \vdots \qquad \vdots \qquad \vdots \qquad \vdots \qquad \vdots$$

$$\sum_{i=1}^{N} I_{ozi} G_1(y_M, z_i') \frac{2h}{N} - \sum_{i=1}^{N} I_{1zi} G_2(y_M, z_i') \frac{2h}{N} + \sum_{i=1}^{M} I_{oyi} G_3(y_M, y_i') \frac{\ell}{M} + \sum_{i=1}^{M} I_{1yi} G_4(y_M, y_i') \frac{\ell}{M} + B_1 \cos k_o y_M + B_2 \sin k_o y_M = 0$$

(3.96)

The next N equations are:

$$\sum_{i=1}^{N} I_{ozi} H_3(z_1, z_i') \frac{2h}{N} - \sum_{i=1}^{N} I_{1zi} H_4(z_1, z_i') \frac{2h}{N} + \sum_{i=1}^{M} I_{oyi} H_1(z_1, y_i') \frac{\ell}{M} + \sum_{i=1}^{M} I_{1yi} H_2(z_1, y_i') \frac{\ell}{M} + B_3 \cos k_o z_1 = \frac{j2\pi}{377} \sin k_o |z_1|$$

$$\vdots \qquad \vdots \qquad \vdots \qquad \vdots \qquad \vdots$$

$$\sum_{i=1}^{N} I_{ozi} H_3(z_N, z_i') \frac{2h}{N} - \sum_{i=1}^{N} I_{1zi} H_4(z_N, z_i') \frac{2h}{N} + \sum_{i=1}^{M} I_{oyi} H_1(z_N, y_i') \frac{\ell}{M} + \sum_{i=1}^{M} I_{1yi} H_2(z_N, y_i') \frac{\ell}{M} + B_3 \cos k_o z_N = \frac{j2\pi}{377} \sin k_o |z_N|$$

(3.97)

The next M equations are:

$$\sum_{i=1}^{N} I_{ozi} P_1(y_1, z_i') \frac{2h}{N} - \sum_{i=1}^{N} I_{1zi} P_2(y_1, z_i') \frac{2h}{N} + \sum_{i=1}^{M} I_{oyi} P_3(y_1, y_i') \frac{\ell}{M} + \sum_{i=1}^{M} I_{1yi} P_4(y_1, y_i') \frac{\ell}{M} + B_4 \cos k_o y_1 + B_5 \sin k_o y_1 = 0$$

$$\vdots \qquad \vdots \qquad \vdots \qquad \vdots \qquad \vdots \qquad \vdots \qquad \vdots$$

$$\sum_{i=1}^{N} I_{ozi} P_1(y_M, z_i') \frac{2h}{N} - \sum_{i=1}^{N} I_{1zi} P_2(y_M, z_i') \frac{2h}{N} + \sum_{i=1}^{M} I_{oyi} P_3(y_M, y_i') \frac{\ell}{M} + \sum_{i=1}^{M} I_{1yi} P_4(y_M, y_i') \frac{\ell}{M} + B_4 \cos k_o y_M + B_5 \sin k_o y_M = 0$$

(3.98)

The next N equations are:

$$\sum_{i=1}^{N} I_{ozi} Q_3(z_1, z_i') \frac{2h}{N} - \sum_{i=1}^{N} I_{1zi} Q_4(z_1, z_i') \frac{2h}{N} + \sum_{i=1}^{M} I_{oyi} Q_1(z_1, y_i') \frac{\ell}{M} + \sum_{i=1}^{M} I_{1yi} Q_2(z_1, y_i') \frac{\ell}{M} + B_6 \cos k_o z_1 = 0$$

$$\vdots \qquad \vdots \qquad \vdots \qquad \vdots \qquad \vdots$$

$$\sum_{i=1}^{N} I_{ozi} Q_3(z_N, z_i') \frac{2h}{N} - \sum_{i=1}^{N} I_{1zi} Q_4(z_N, z_i') \frac{2h}{N} + \sum_{i=1}^{M} I_{oyi} Q_1(z_N, y_i') \frac{\ell}{M} + \sum_{i=1}^{M} I_{1yi} Q_2(z_N, y_i') \frac{\ell}{M} + B_6 \cos k_o z_N = 0$$

(3.99)

Then consistent with previous assumptions the following can be written:

$$I_{ozN} - I_{oy1} = 0 \tag{3.100}$$

$$I_{1zN} - I_{1yM} = 0 \tag{3.101}$$

$$I_{oyM} = 0 \tag{3.102}$$

$$I_{1y1} = 0 \tag{3.103}$$

and finally

$$\sum_{i=1}^{M} I_{oyi}\, T_1(h, y_i')\, \frac{\ell}{M} + \sum_{i=1}^{M} I_{1yi}\, T_2(h, y_i')\, \frac{\ell}{M} + $$

$$+ B_2 + B_3 \sin k_o h = \frac{j2\pi}{377} \cos k_o h \tag{3.104}$$

$$\sum_{i=1}^{N} I_{ozi} V_1(\ell, z_i')\, \frac{2h}{N} - \sum_{i=1}^{N} I_{1zi}\, V_2(\ell, z_i')\, \frac{2h}{N} - \sum_{i=1}^{M} I_{oyi} U_1(h, y_i')\, \frac{\ell}{M} -$$

$$- \sum_{i=1}^{M} I_{1yi} U_2(h, y_i')\, \frac{\ell}{M} + B_4 \sin k_o \ell - B_5 \cos k_o \ell - B_6 \sin k_o h = 0 \tag{3.105}$$

In matrix form the equations are:

$$\begin{bmatrix} \\ \\ \\ \text{MATRIX} \\ \\ \\ \\ \end{bmatrix} \begin{bmatrix} I_{oz1} \\ \vdots \\ I_{ozN} \\ I_{1z1} \\ \vdots \\ I_{1zN} \\ I_{oy1} \\ \vdots \\ I_{oyM} \\ I_{1y1} \\ \vdots \\ I_{1yM} \\ B_1 \\ B_2 \\ B_3 \\ B_4 \\ B_5 \\ B_6 \end{bmatrix} = \left[\begin{array}{c} \left.\begin{array}{c} 0 \\ \vdots \\ 0 \end{array}\right\} M \\ \left.\begin{array}{c} -\frac{j2\pi}{377} \sin k_o \left| z_1 \right| \\ \vdots \\ -\frac{j2\pi}{377} \sin k_o \left| z_N \right| \end{array}\right\} N \\ \left.\begin{array}{c} 0 \\ \vdots \\ 0 \end{array}\right\} M \\ \left.\begin{array}{c} 0 \\ \vdots \\ 0 \end{array}\right\} N \\ \left.\begin{array}{c} 0 \\ 0 \\ 0 \\ 0 \end{array}\right\} 4 \\ +\frac{j2\pi}{377} \cos k_o h \\ 0 \end{array} \right] \tag{3.106}$$

The solution of the matrix equation in (3.106) can be obtained from a high-speed digital computer. Of course, (3.106) only approximates the system of equations in (3.85) through (3.94). The accuracy of the matrix solution depends heavily upon the fineness of the subdivisions used.

3.4 Numerical Results

The matrix equation (3.106) was programmed for the IBM 360 computer. The solution of this equation involved matrix inversion with complex algebra. Four different three-element antennas were studied. The following physical parameters were common in all four cases: ℓ = 8.0 cm, h = 1.0 cm, and a = 0.04 cm. The spacing, d, between the elements was varied (see Fig. 3-1). Values of d used were 0.6 cm, 1.2 cm, 2.4 cm, and 3.6 cm. As d becomes very large, the results should reduce to those of the driven element. The program was checked in this limit case by choosing d = 100,000 cm. As expected, the driven element data were obtained.

Values of M and N were chosen in the same ratio as ℓ and 2h to obtain uniform segmentation along the wire elements. To check the accuracy of the solutions for the currents, M and N were increased (corresponding to finer subdivisions) until the results converged. The final values were N = 9 and M = 36, corresponding to the inversion of a 96 x 96 matrix. The convergence obtained with this choice of M and N was not quite as good as that of the driven element in Chapter II. However, because the price of a computer run was already $9.90 for each frequency, it was decided not to increase M and N any further. This choice was considered a good compromise between convergence and cost.

Data were obtained for the four antennas in the frequency range from 450 MHz to 900 MHz. Usually the frequency was varied in 50 MHz steps, but occasionally a finer frequency division was necessary.

Normalized current distributions from the computer program are shown in Figs. 3-2 through 3-11. This selection includes unusual as well as typical distributions. The horizontal axis contains both z and y so that I_z and I_y may be plotted on the same graph.

For the real part of the current on the driven element and the imaginary part of the current on the parasitic element, the current distributions were almost identical for all four values of d. Figure 3-2 gives the real part of the current on the driven element for three frequencies. Figure 3-11 gives the imaginary part of the current on the parasitic element for three frequencies. While these figures were actually for d = 0.6 cm, they serve all four cases.

The imaginary part of the current on the driven element is plotted in Figs. 3-3 through 3-6. The real part of the current on the parasitic element is plotted in Figs. 3-7 through 3-10. Each figure contains current distributions at four selected frequencies for a single value of d.

The discontinuity or dip in the current distributions at the junction of I_z and I_y is again present. This phenomenon may be traced directly to equations (3.100) and (3.101). These equations equate the currents on either side of the junctions for the driven element and for the parasitic element respectively. This discontinuity is a direct result of using segmentation to change from integration to summation.

The input impedance may be easily calculated using equation (2.89). The voltage source has been normalized to unity and the current is known at the feed point (z = 0) of the driven element. The real part of the impedance is plotted in Figs. 3-12 and 3-13, and the imaginary part is plotted in Figs. 3-14 and 3-15. The real part of the impedance is very small except for the peaks near 850 MHz. In Fig. 3-12 the peak of the curve for d = 0.6 cm is off-scale. It actually occurs at 9800 Ω. The height of the peaks decreases as the spacing d increases. The imaginary part of the impedance also exhibits interesting behavior near 850 MHz. As the frequency increases, the

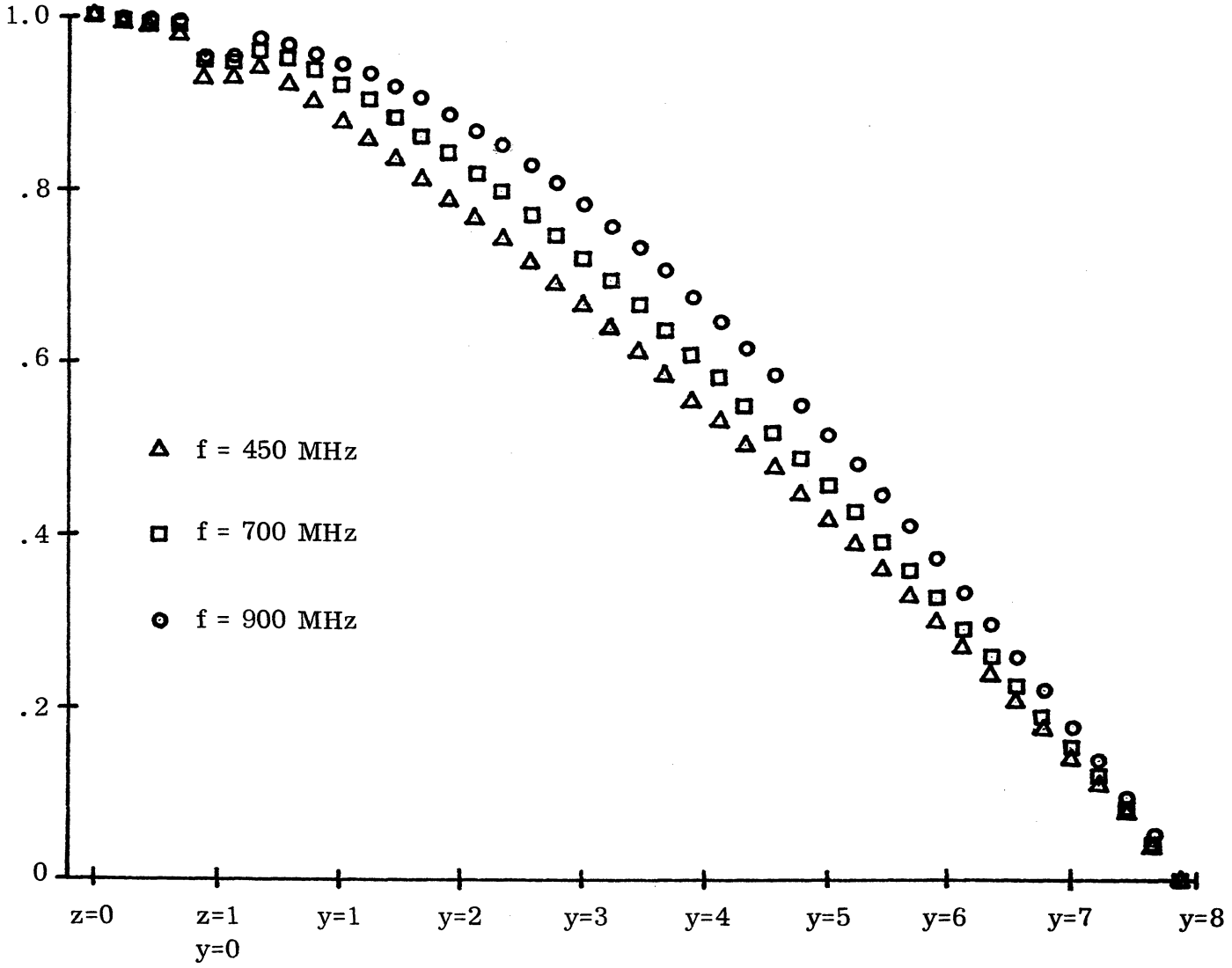

FIG. 3-2: NORMALIZED CURRENT DISTRIBUTIONS (Driven Element, Real Part).

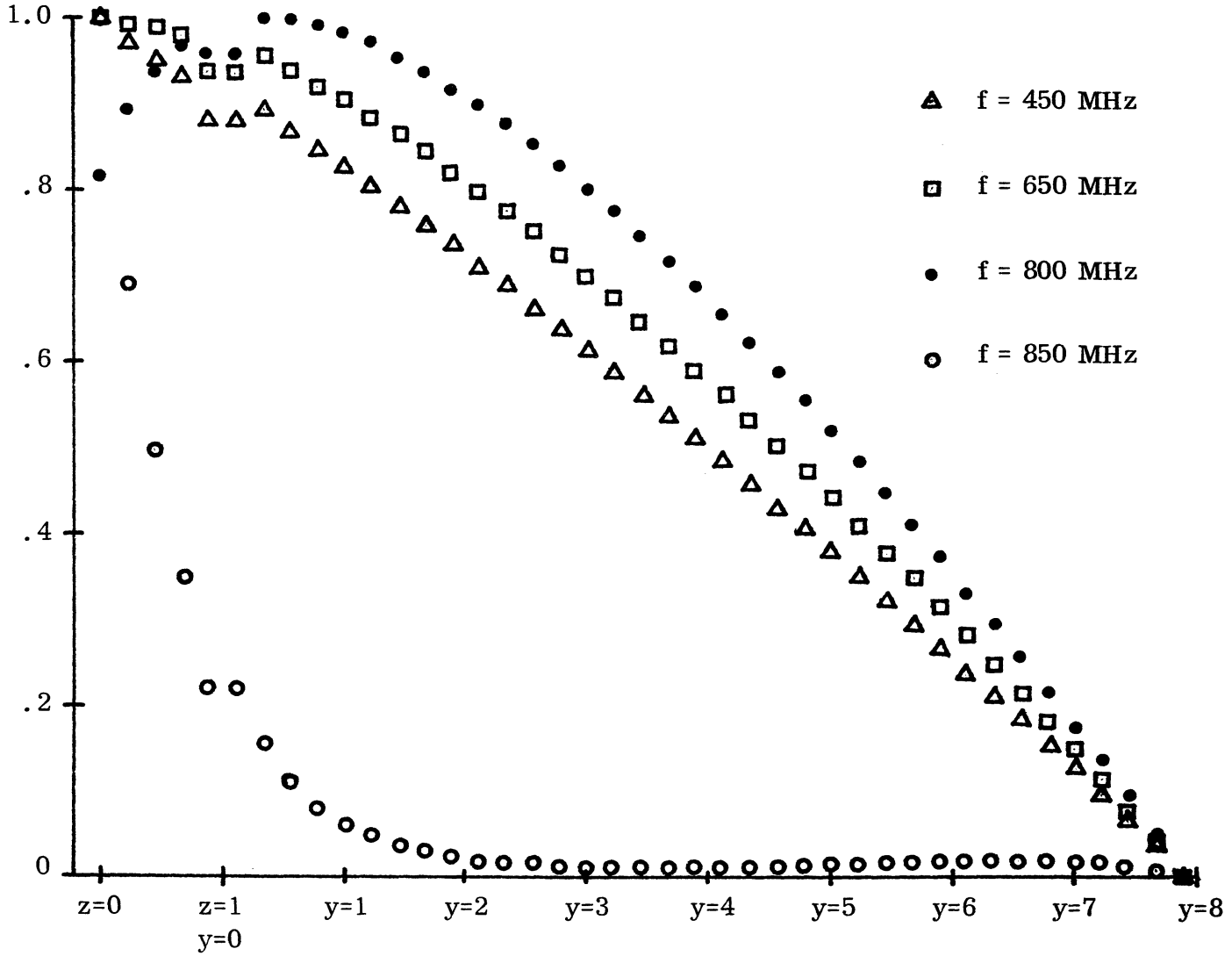

FIG. 3-3: NORMALIZED CURRENT DISTRIBUTIONS (Driven Element, Imaginary Part, d=0.6 cm).

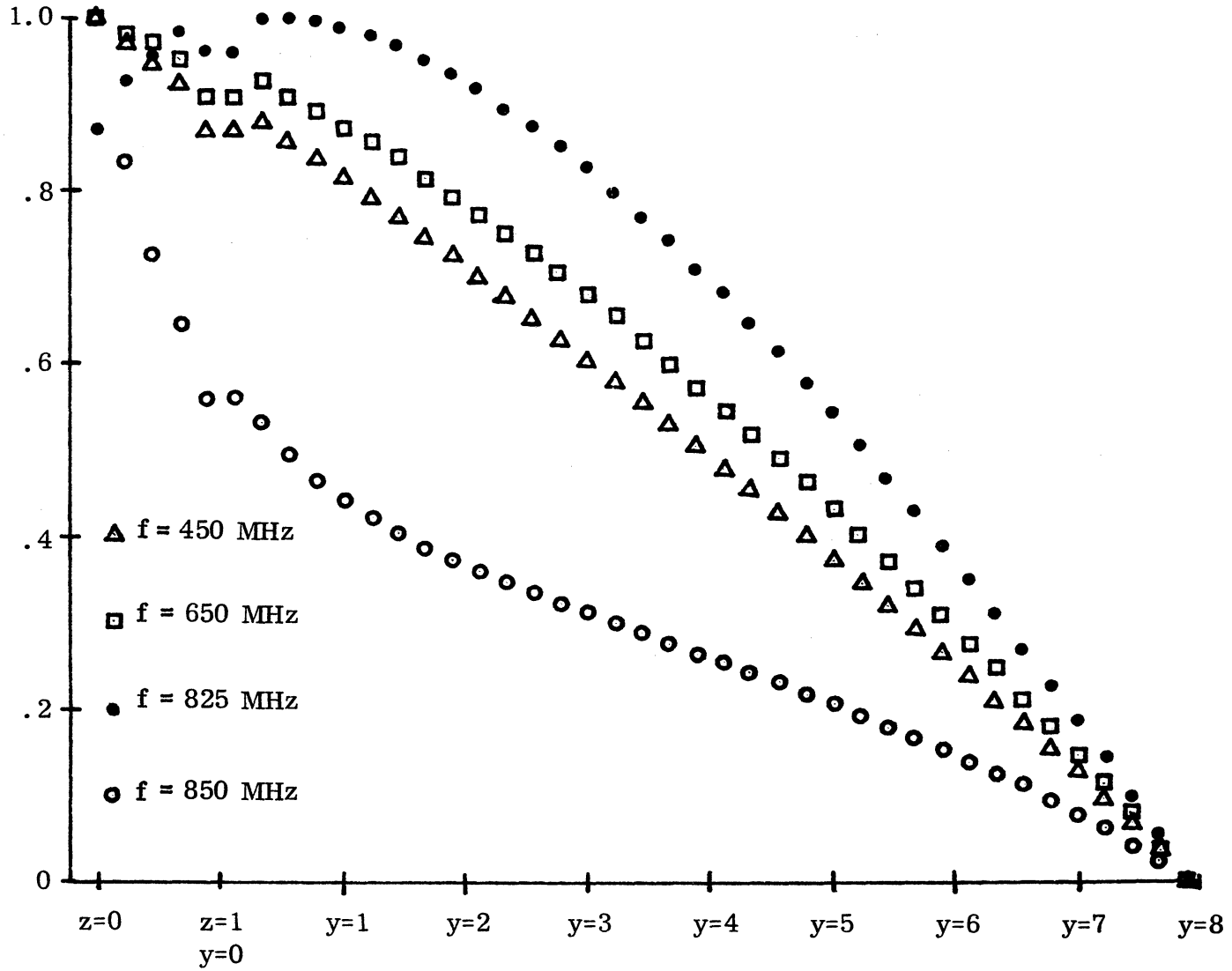

FIG. 3-4: NORMALIZED CURRENT DISTRIBUTIONS (Driven Element, Imaginary Part, d=1.2 cm).

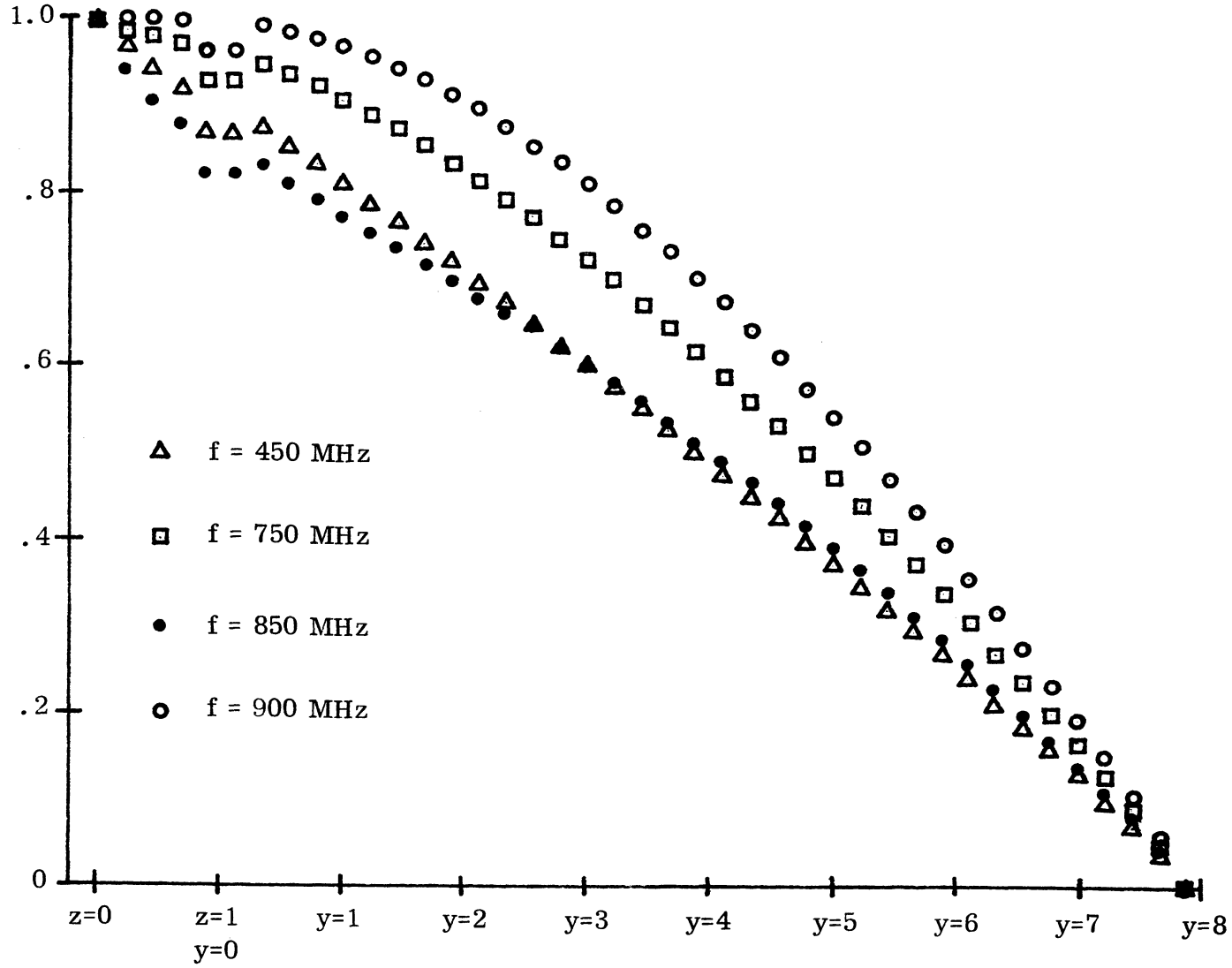

FIG. 3-5: NORMALIZED CURRENT DISTRIBUTIONS(Driven Element, Imaginary Part, d=2.4cm).

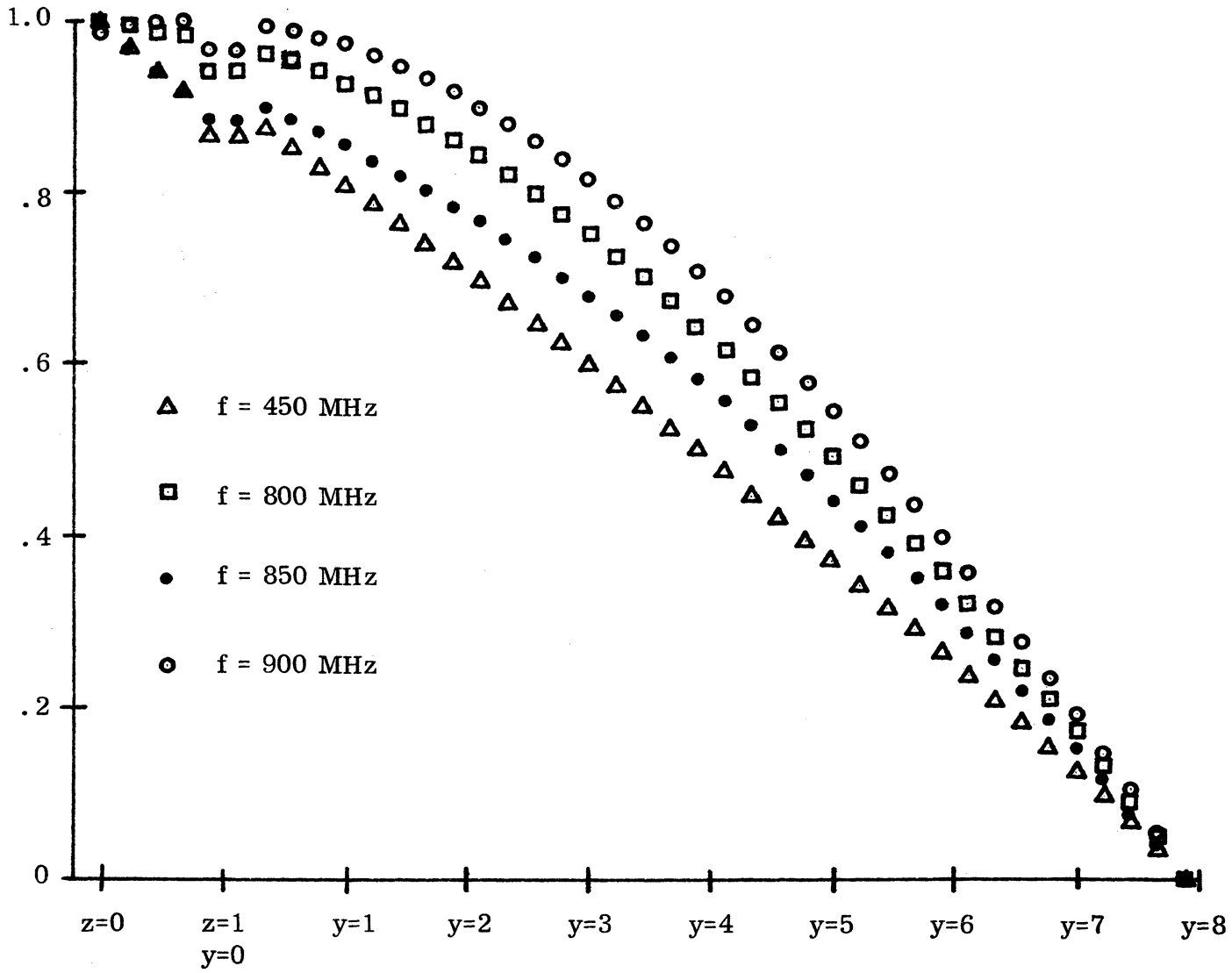

FIG. 3-6: NORMALIZED CURRENT DISTRIBUTIONS (Driven Element, Imaginary Part, d=3.6 cm).

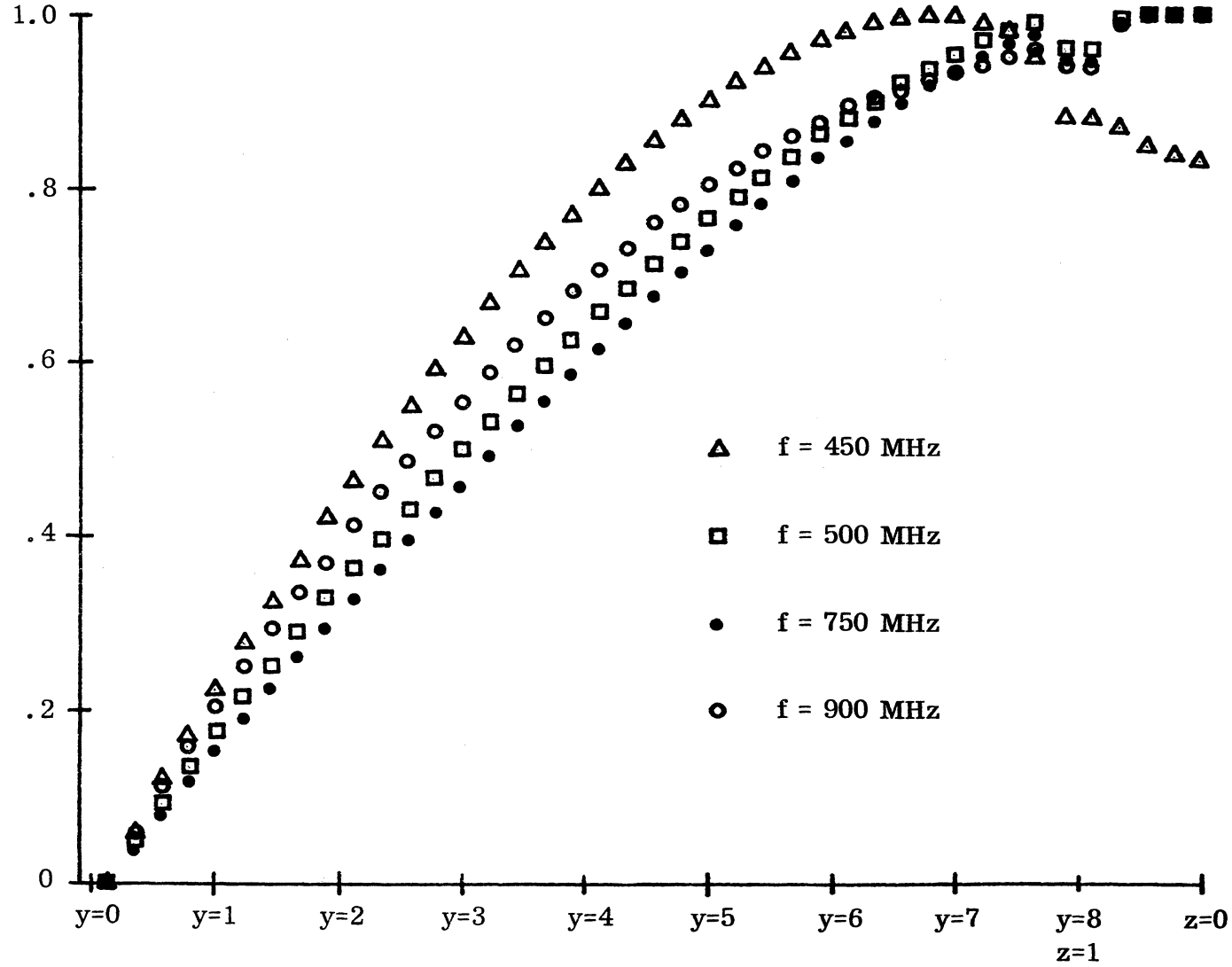

FIG. 3-7: NORMALIZED CURRENT DISTRIBUTIONS (Parasitic Element, Real Part, d=0.6 cm).

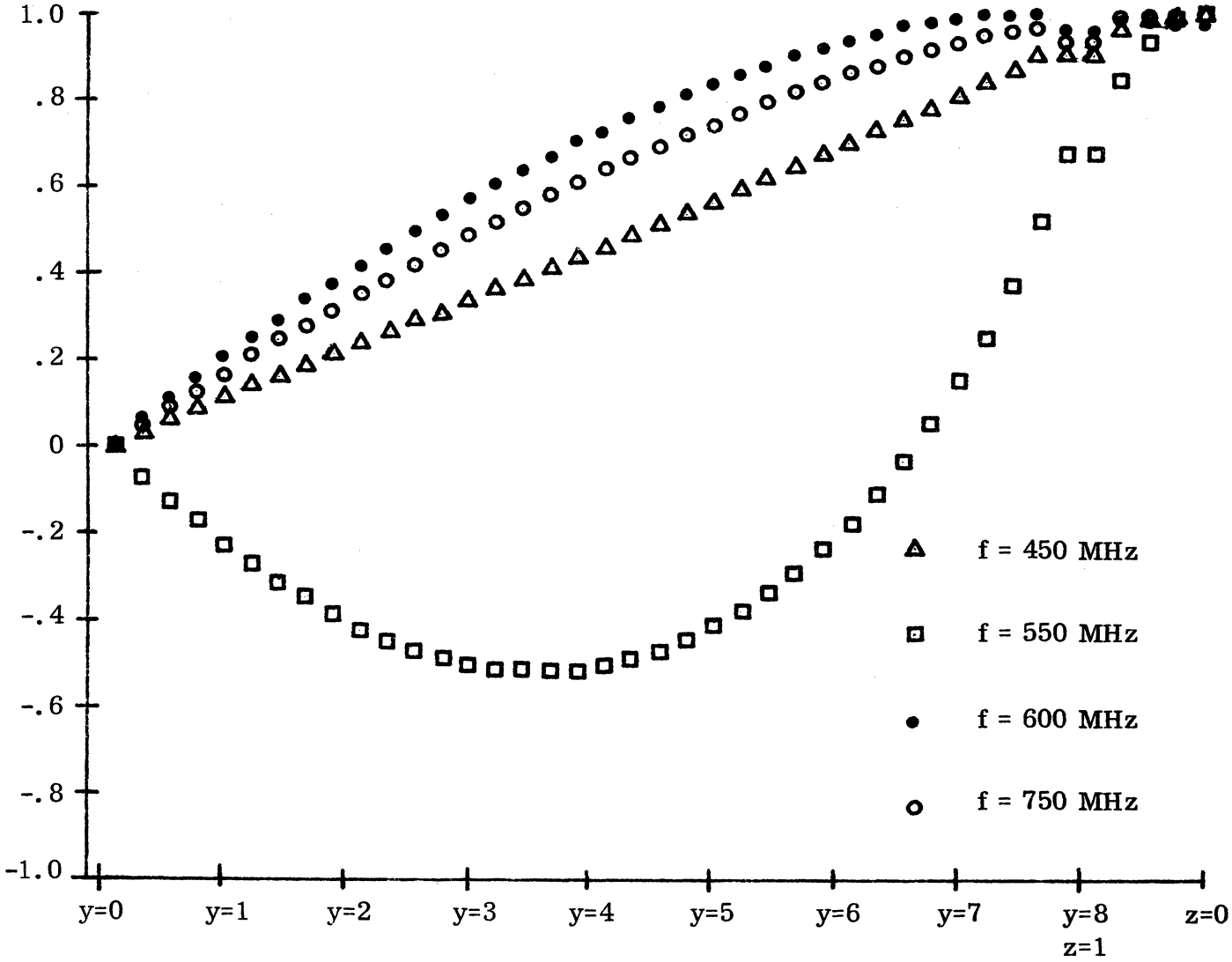

FIG. 3-8: NORMALIZED CURRENT DISTRIBUTIONS (Parasitic Element, Real Part, d=1.2 cm).

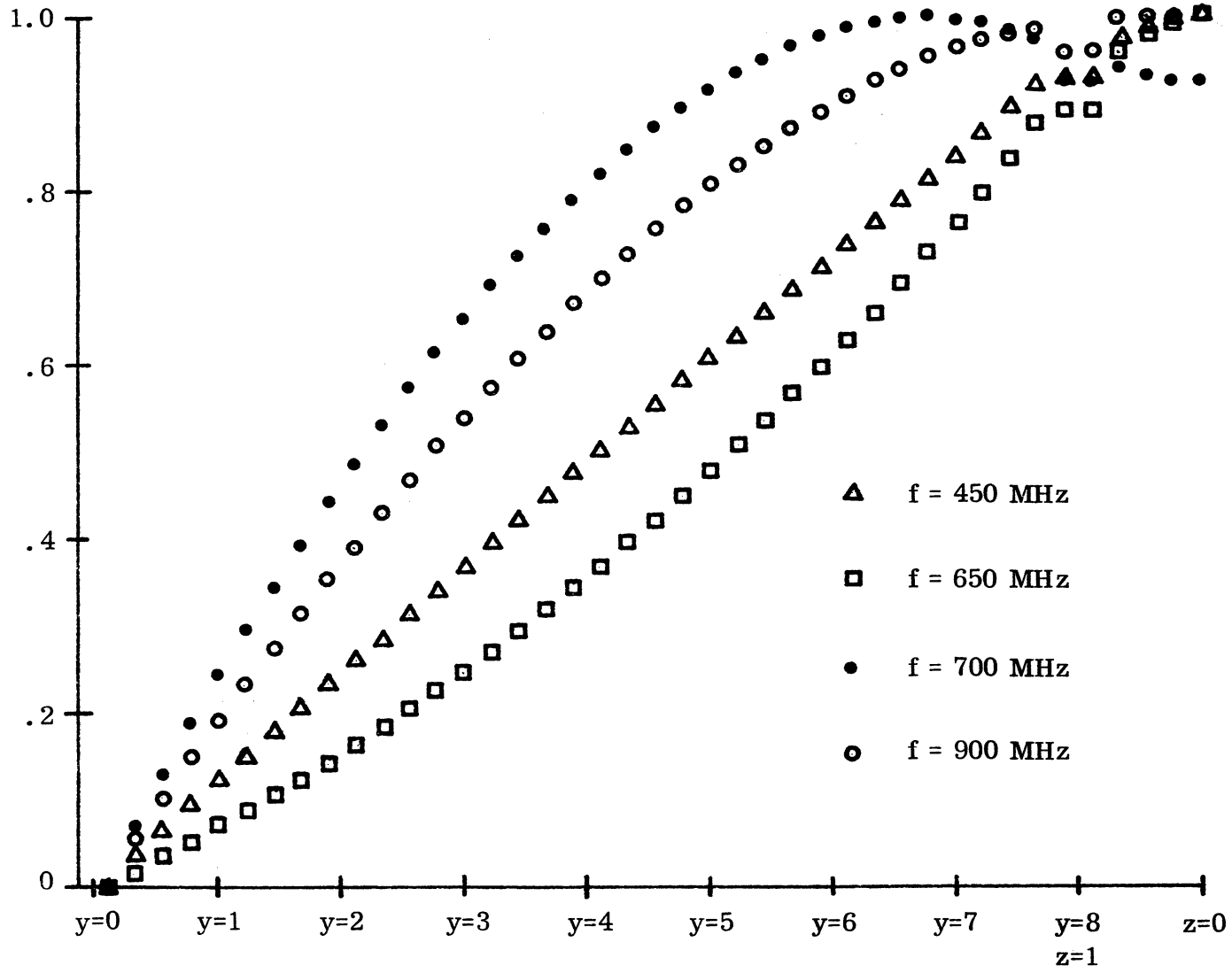

FIG. 3-9: NORMALIZED CURRENT DISTRIBUTIONS(Parasitic Element, Real Part, d=2.4 cm).

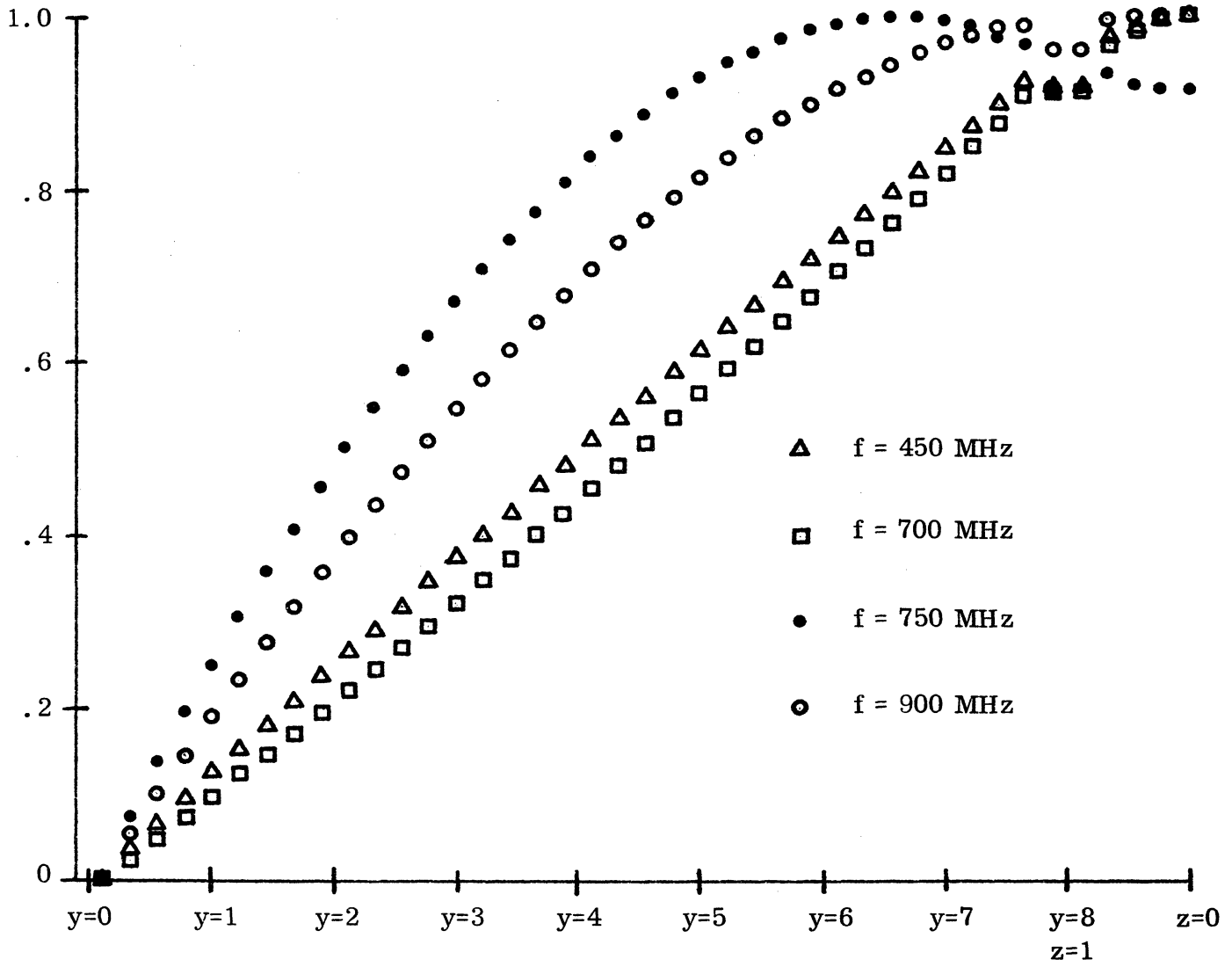

FIG. 3-10: NORMALIZED CURRENT DISTRIBUTIONS (Parasitic Element, Real Part, d=3.6 cm).

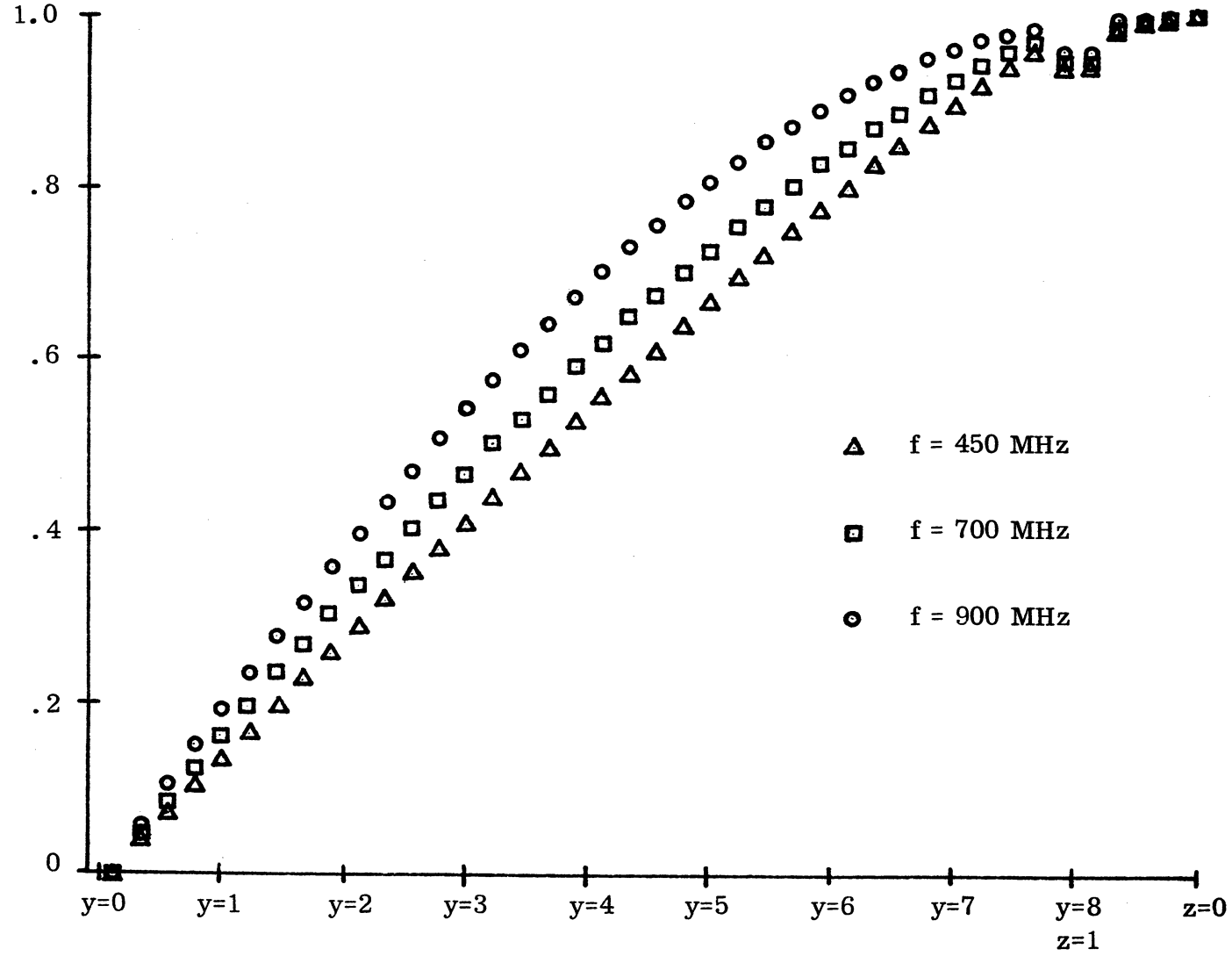

FIG. 3-11: NORMALIZED CURRENT DISTRIBUTIONS (Parasitic Element, Imaginary Part).

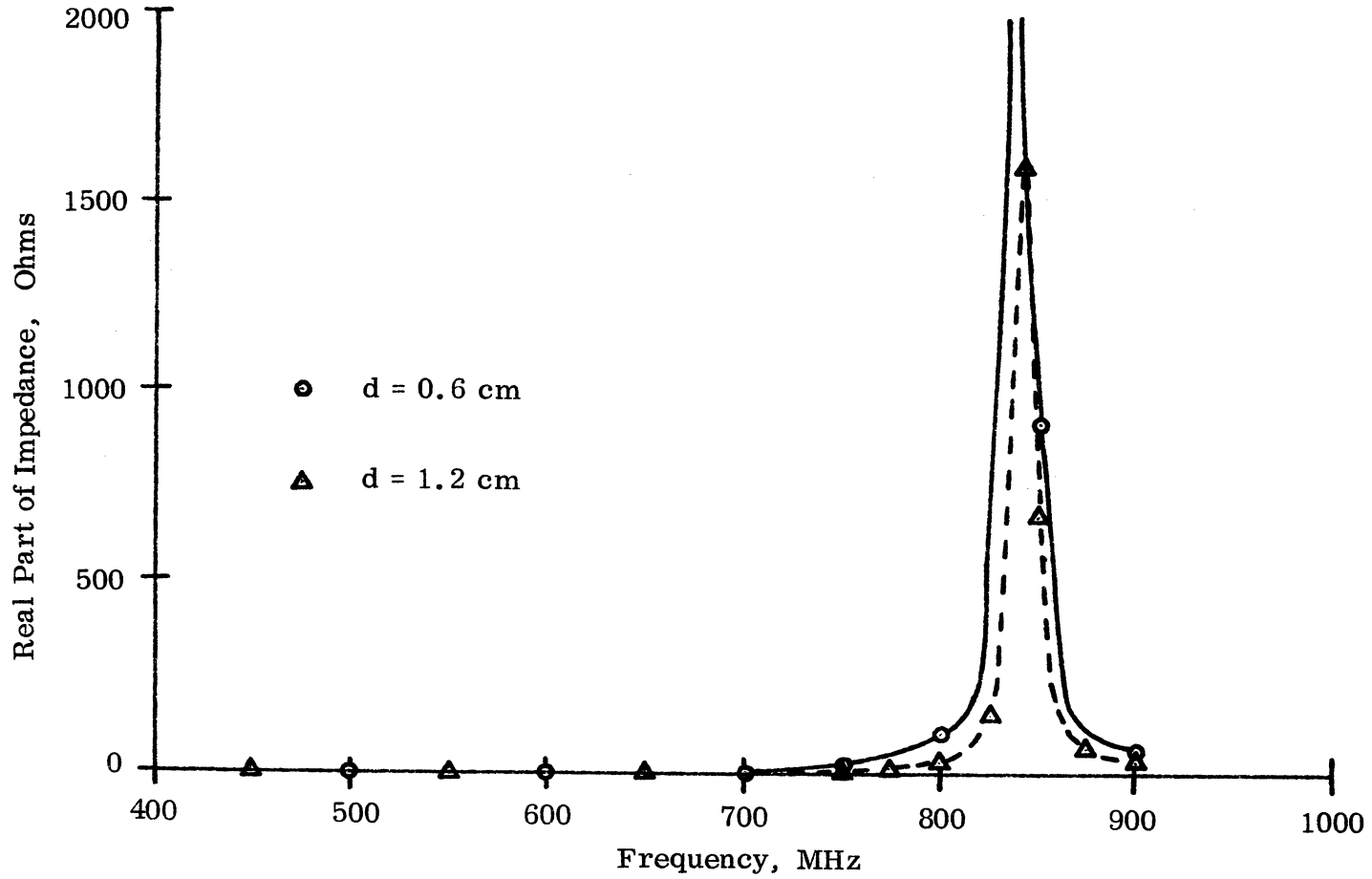

FIG. 3-12: INPUT IMPEDANCE WITH 3 ELEMENTS (Real Part).

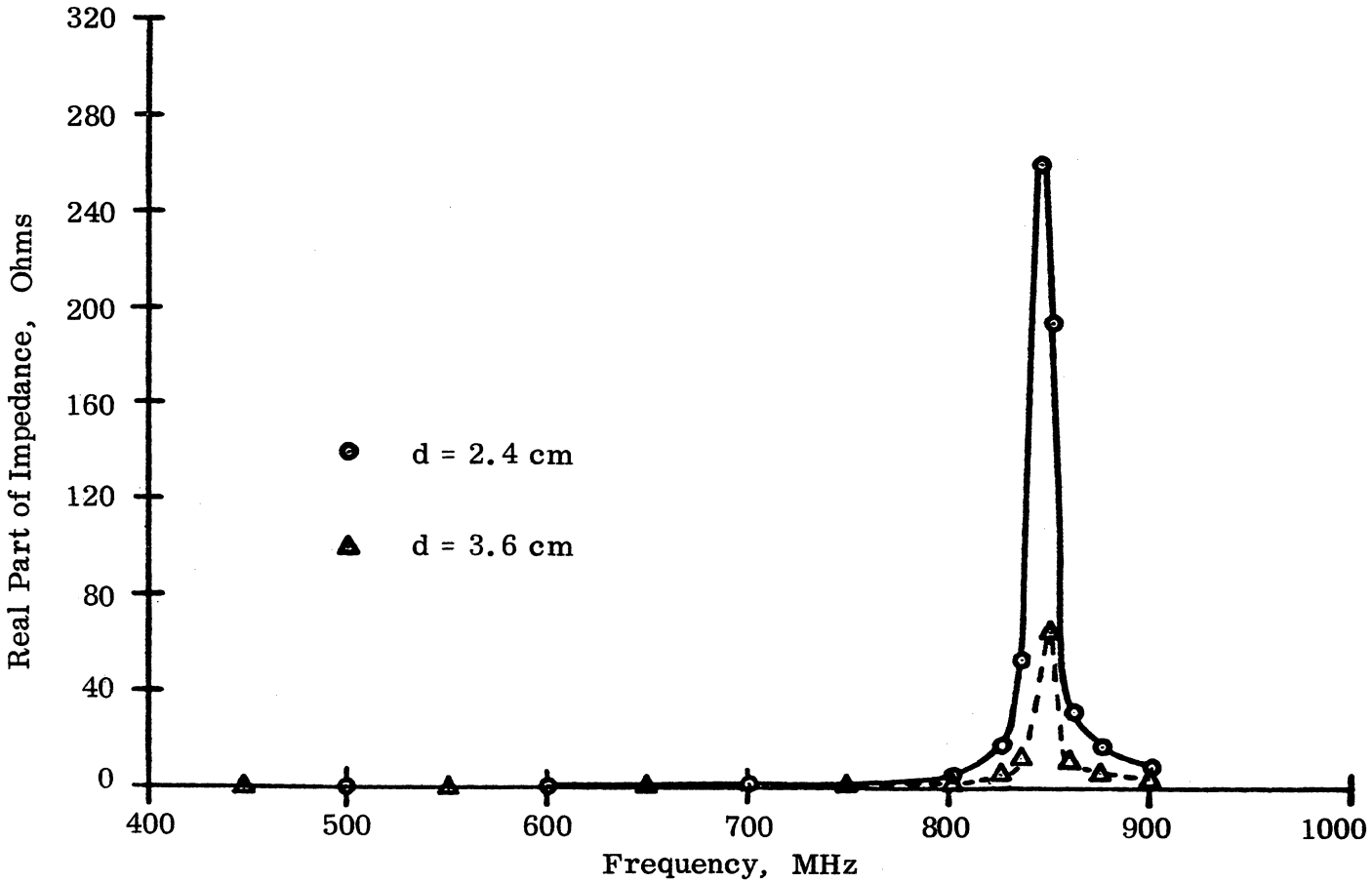

FIG. 3-13: INPUT IMPEDANCE WITH 3 ELEMENTS (Real Part).

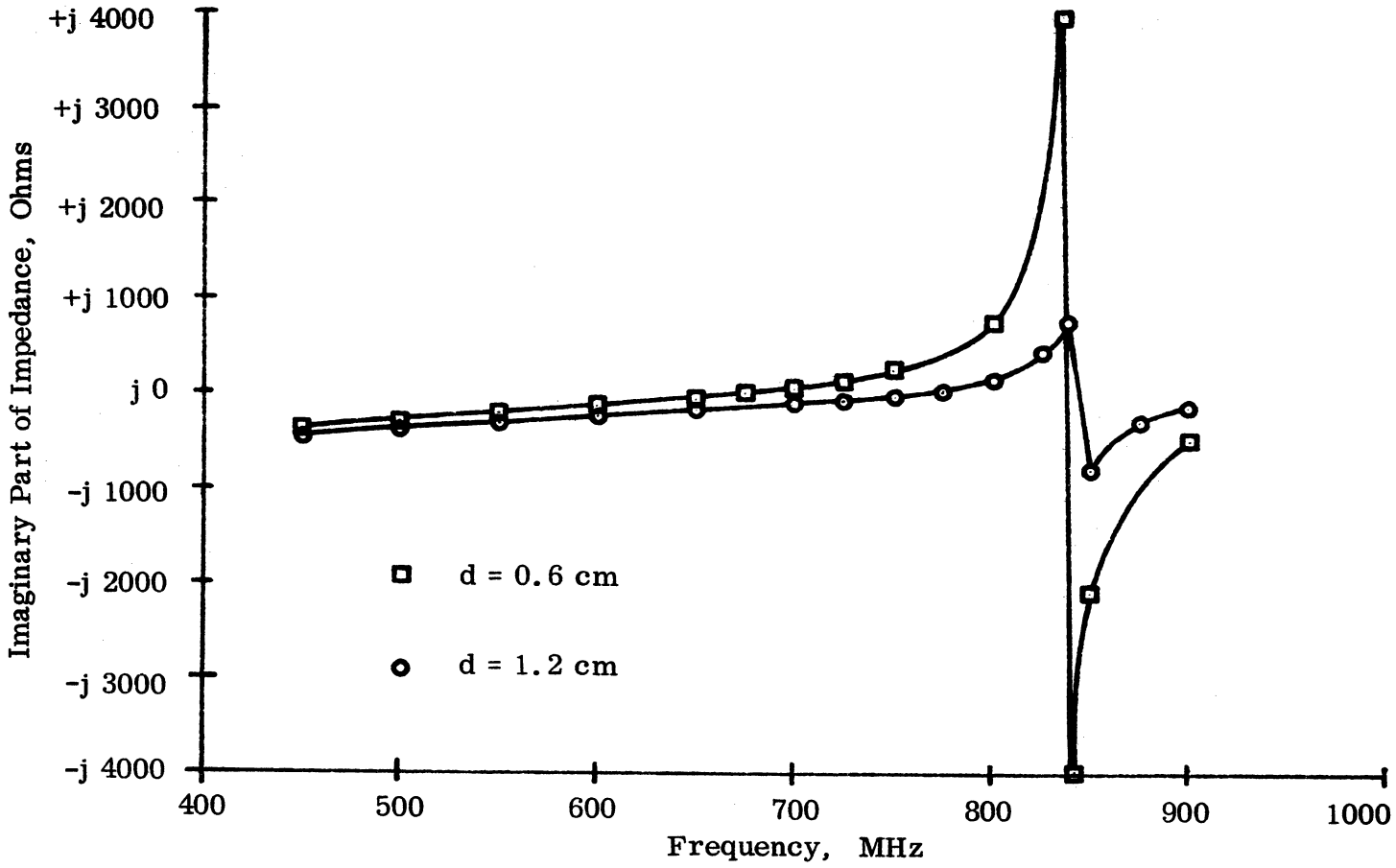

FIG. 3-14: INPUT IMPEDANCE WITH 3 ELEMENTS (Imaginary Part).

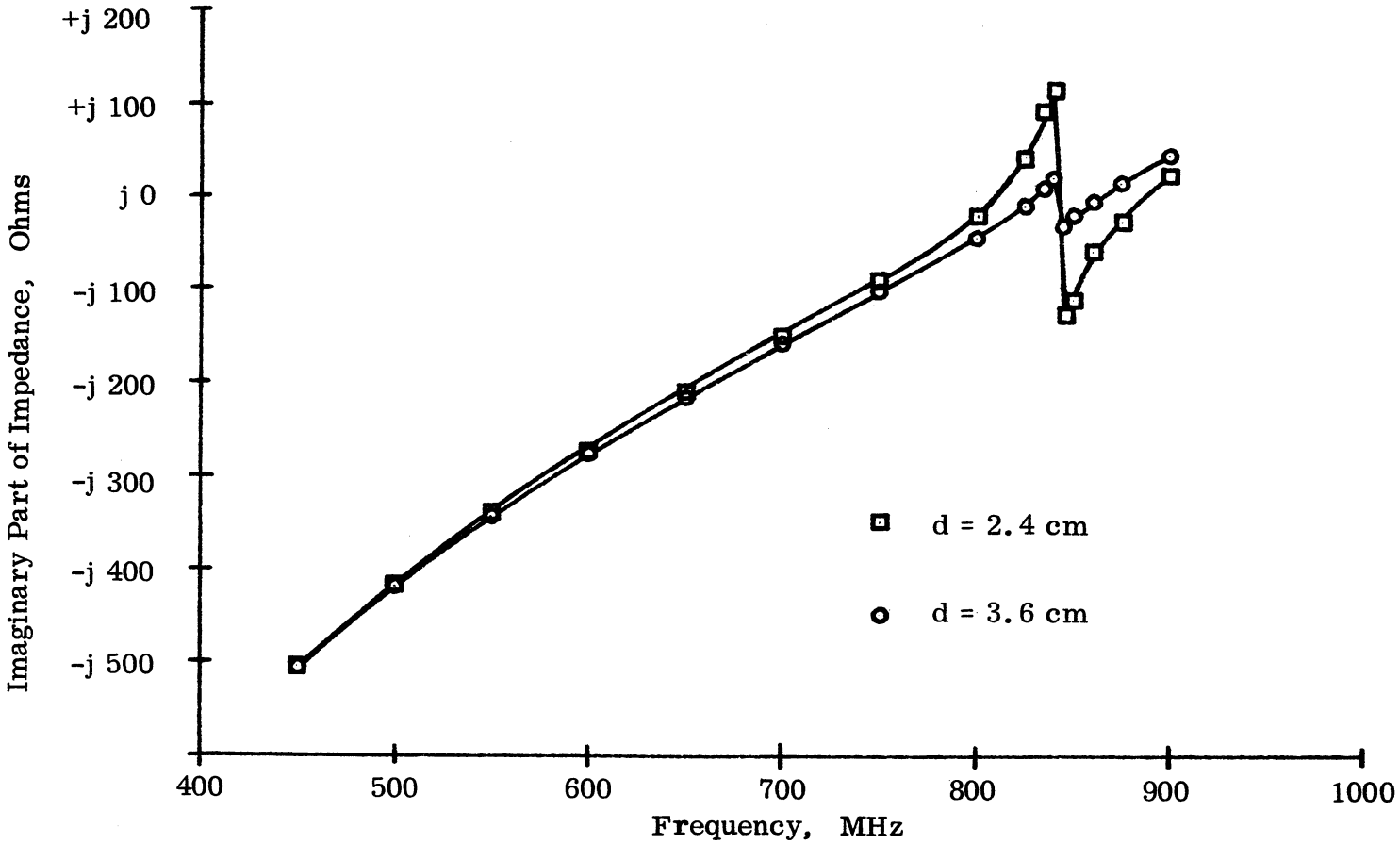

FIG. 3-15: INPUT IMPEDANCE WITH 3 ELEMENTS (Imaginary Part).

reactance becomes large and inductive, goes through zero, and then becomes large and capacitive. The magnitude of the swing decreases as the spacing increases. The changes in both the real part and in the imaginary part of the impedance as d increases are as expected, for the impedance has to reduce to that of the driven element alone when d becomes large.

3.5 The Radiation Pattern

The radiation vector, $\bar{N}$, was used to calculate the far-zone electric fields of the four three-element interdigital arrays studied in this chapter. The rectangular coordinate system is shown in Fig. 3-1, and the relationship between the spherical coordinate system and the x, y, and z axes is shown in Fig. 2-6.

The far-zone radiation vector is defined by equation (2.90), and the relationship between $\bar{N}$ and the electric field, $\bar{E}$, is given by equations (2.91) and (2.92). For convenience, a normalized case is obtained by applying the condition in equation (2.97). This sets $\bar{E} = \bar{N}_t$.

Consider the three-element interdigital array. There are two components of $\bar{N}$, N_y and N_z, since current exists in the y and z directions. Using (2.90) and after some manipulations,

$$N_y = 2j \sin\left[k_o h \cos\theta\right] \int_0^{\ell} I_{oy}(y') \, e^{+jk_o y' \sin\theta \sin\phi} \, dy' +$$

$$+ 4j \sin\left[k_o h \cos\theta\right] \cos\left[k_o d \sin\theta \cos\phi\right] \int_0^{\ell} I_{1y}(y') \, e^{+jk_o y' \sin\theta \sin\phi} \, dy' \qquad (3.107)$$

and

$$N_z = \int_{-h}^{h} I_{oz}(z')\, e^{+jk_o z' \cos\theta}\, dz' \; -$$

$$-2\cos\left[k_o d \sin\theta\cos\phi\right] e^{+jk_o \ell \sin\theta\sin\phi} \int_{-h}^{h} I_{1z}(z')\, e^{+jk_o z' \cos\theta}\, dz' \,. \tag{3.108}$$

Now using the definition of $\bar{N}_t$ in (2.91), and changing the expressions for N_y and N_z to the spherical coordinate system using the relations in (2.95), the result is

$$\bar{N}_t = \hat{\theta}\Big\{2j\cos\theta\sin\phi\sin\left[k_o h\cos\theta\right]\int_0^{\ell} I_{oy}(y')\, e^{+k_o y' \sin\theta\sin\phi}\, dy' \; +$$

$$+4j\cos\theta\sin\phi\sin\left[k_o h\cos\theta\right]\cos\left[k_o d\sin\theta\cos\phi\right]\int_0^{\ell} I_{1y}(y')\, e^{+jk_o y' \sin\theta\sin\phi}\, dy' -$$

$$-\sin\theta\int_{-h}^{h} I_{oz}(z')\, e^{+jk_o z' \cos\theta}\, dz' \; +$$

$$+2\sin\theta\cos\left[k_o d\sin\theta\cos\phi\right] e^{+jk_o \ell \sin\theta\sin\phi}\int_{-h}^{h} I_{1z}(z')\, e^{+jk_o z'\cos\theta}\, dz' \Big\} +$$

$$+\hat{\phi}\Big\{2j\cos\phi\sin\left[k_o h\cos\theta\right]\int_0^{\ell} I_{oy}(y')\, e^{+jk_o y' \sin\theta\sin\phi}\, dy' \; +$$

$$+4j\cos\phi\sin\left[k_o h\cos\theta\right]\cos\left[k_o d\sin\theta\cos\phi\right]\int_0^{\ell} I_{1y}(y')\, e^{+jk_o y' \sin\theta\sin\phi}\, dy'\Big\} \tag{3.109}$$

The magnitudes of E_θ and E_ϕ were calculated in the upper half plane. Values were obtained in the three principal planes x-y, x-z, and y-z. The current distributions obtained from the computer program were used in the integrals of (3.109).

Consider first the x-y plane: $\theta = 90^\circ$ and $0^\circ \leq \phi \leq 360^\circ$. The expression for $\bar{N}_t$ in (3.109) becomes

$$N_\theta = -\int_{-h}^{h} I_{oz}(z')\,dz' \quad +$$

$$+ 2\cos\left[k_o d\cos\phi\right] e^{+jk_o \ell \sin\phi} \int_{-h}^{h} I_{1z}(z')\,dz' \quad ,$$

$$N_\phi = 0 \quad . \tag{3.110}$$

Next consider the x-z plane: $0^\circ \leq \theta \leq 90^\circ$ and $\phi = 0^\circ$ or 180°. Then (3.109) becomes

$$N_\theta = -\sin\theta \int_{-h}^{h} I_{oz}(z')\, e^{+jk_o z' \cos\theta}\, dz' \quad +$$

$$+ 2\sin\theta\cos\left[k_o d\sin\theta\right] \int_{-h}^{h} I_{1z}(z')\, e^{+jk_o z' \cos\theta}\, dz' \quad ,$$

$$N_\phi = \pm\left\{2j\sin\left[k_o h\cos\theta\right] \int_{0}^{\ell} I_{oy}(y')\,dy' \quad +\right.$$

$$\left. + 4j\sin\left[k_o h\cos\theta\right]\cos\left[k_o d\sin\theta\right] \int_{0}^{\ell} I_{1y}(y')\,dy' \right\} \quad . \tag{3.111}$$

Finally consider the y-z plane: $0^o \leq \theta \leq 90^o$ and $\phi = 90^o$ or 270^o. Then (3.109) becomes

$$\text{RHP: } N_\theta = 2j \cos\theta \sin\left[k_o h \cos\theta\right] \int_0^{\ell} I_{oy}(y') e^{+jk_o y' \sin\theta} dy' +$$

$$+ 4j \cos\theta \sin\left[k_o h \cos\theta\right] \int_0^{\ell} I_{1y}(y') e^{+jk_o y' \sin\theta} dy' -$$

$$- \sin\theta \int_{-h}^{h} I_{oz}(z') e^{+jk_o z' \cos\theta} dz' +$$

$$+ 2 \sin\theta \, e^{+jk_o \ell \sin\theta} \int_{-h}^{h} I_{1z}(z') e^{+jk_o z' \cos\theta} dz'$$

$$\text{LHP: } N_\theta = -2j \cos\theta \sin\left[k_o h \cos\theta\right] \int_0^{\ell} I_{oy}(y') e^{-jk_o y' \sin\theta} dy'$$

$$-4j \cos\theta \sin\left[k_o h \cos\theta\right] \int_0^{\ell} I_{1y}(y') e^{-jk_o y' \sin\theta} dy'$$

$$- \sin\theta \int_{-h}^{h} I_{oz}(z') e^{+jk_o z' \cos\theta} dz'$$

$$+ 2 \sin\theta \, e^{-jk_o \ell \sin\theta} \int_{-h}^{h} I_{1z}(z') e^{+jk_o z' \cos\theta} dz'$$

$$N_\phi = 0 \qquad (3.112)$$

where RHP denotes the right half of the y-z plane ($y > 0$) and LHP denotes the left half of the y-z plane ($y < 0$).

The theoretical radiation patterns are presented in Figs. 3-16 through 3-27. Each figure contains twelve patterns in a given plane for one of the four antennas.

The patterns in the x-y plane are shown in Figs. 3-16 through 3-19. Only E_θ exists, as E_ϕ equals zero. This plane contains the ground plane of the physical model. With the driven element alone, the theoretical patterns in this plane were circles. The addition of the two parasitic elements has modified the circular shape. In all four cases, as the frequency is increased, the radiation patterns are first gradually pinched in along the x-axis and then are returned to a more circular shape. The pinching effect starts at a higher frequency and lasts over a narrower bandwidth as the spacing, d, is increased.

The radiation patterns in the x-z plane are given in Figs. 3-20 through 3-23. Cross-polarization exists in this plane. E_ϕ has its maximum along the z-axis and E_θ has its maximum along the x-axis. For the driven element alone, the ratio of E_ϕ / E_θ was approximately between 0.4 and 1.0 as the frequency was varied. With the three-element arrays, however, much higher ratios can occur. In all four cases, the ratio of E_ϕ/E_θ first increases and then decreases as the frequency is increased. At the peak of the ratio, E_ϕ completely overshadows E_θ. As the spacing, d, is increased, the peak of the ratio occurs at a higher frequency, but the bandwidth over which E_ϕ is dominant is narrower.

The radiation patterns in the y-z plane are given in Figs. 3-24 through 3-27. Only E_θ exists, as E_ϕ equals zero. This is the plane of the driven element. The patterns are roughly semicircular with perturbations which seem to increase as the spacing, d, increases.

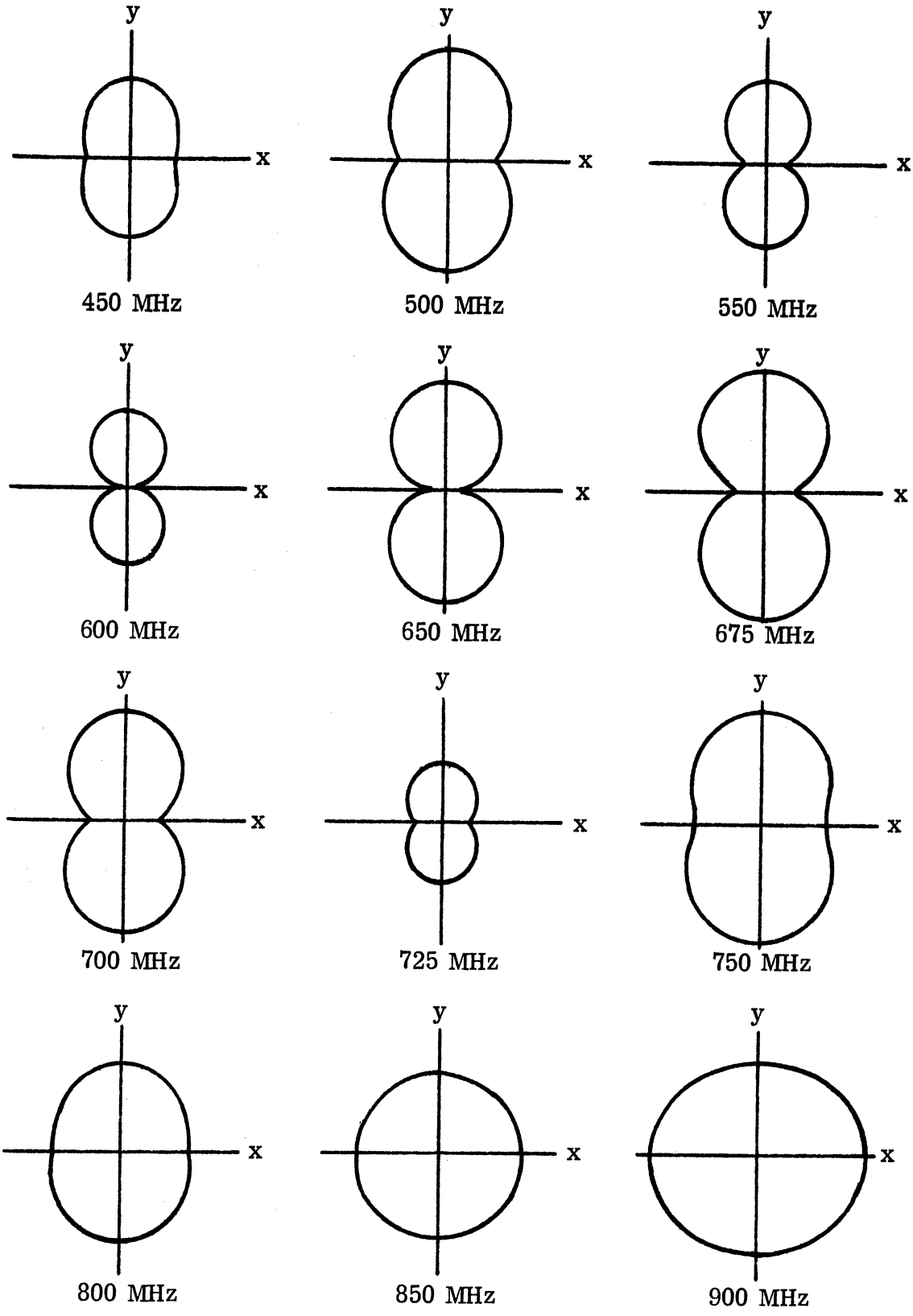

FIG. 3-16: E_θ PATTERNS IN x-y PLANE (d = 0.6 cm).

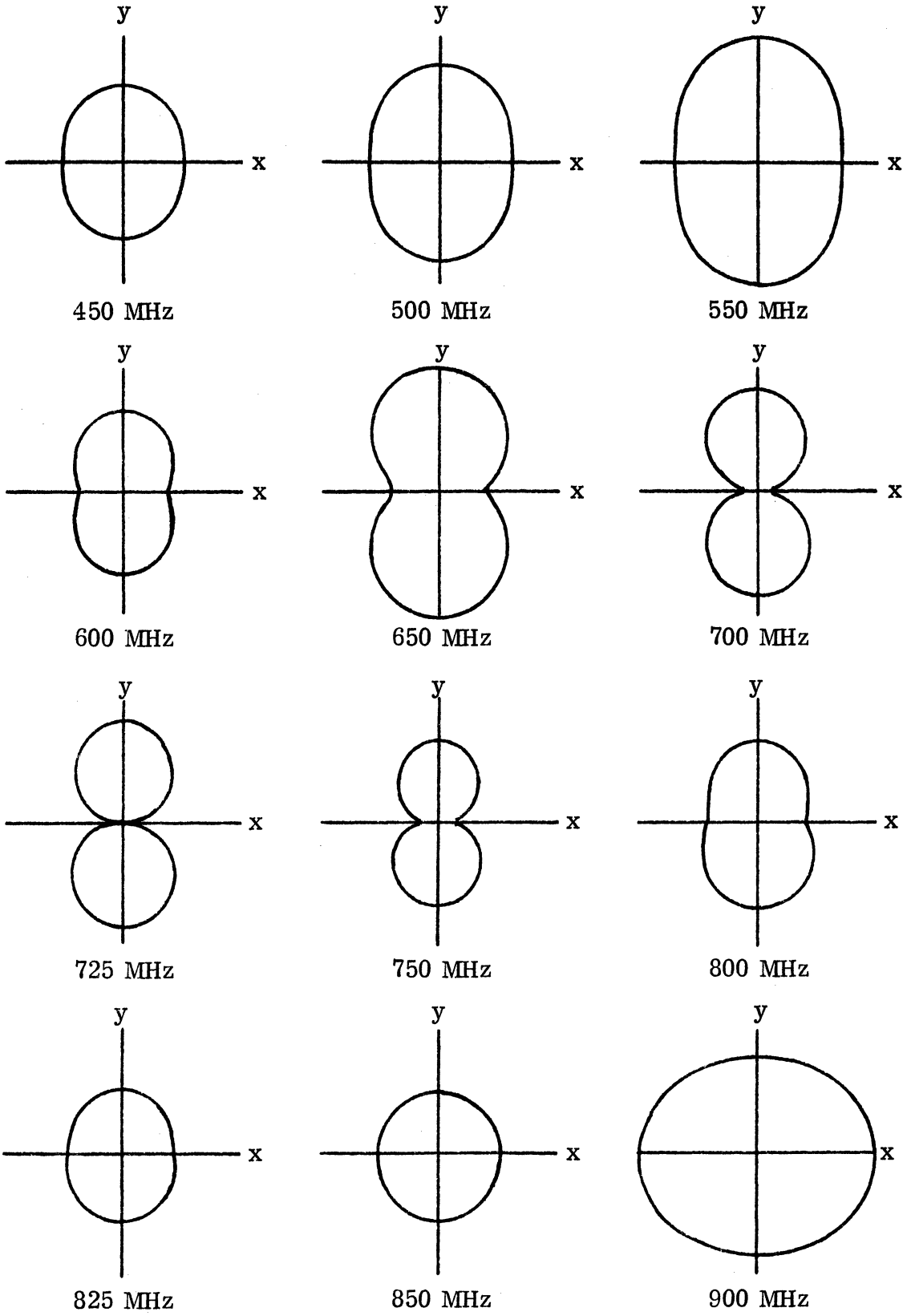

FIG. 3-17: E_θ PATTERNS IN x-y PLANE (d = 1.2 cm).

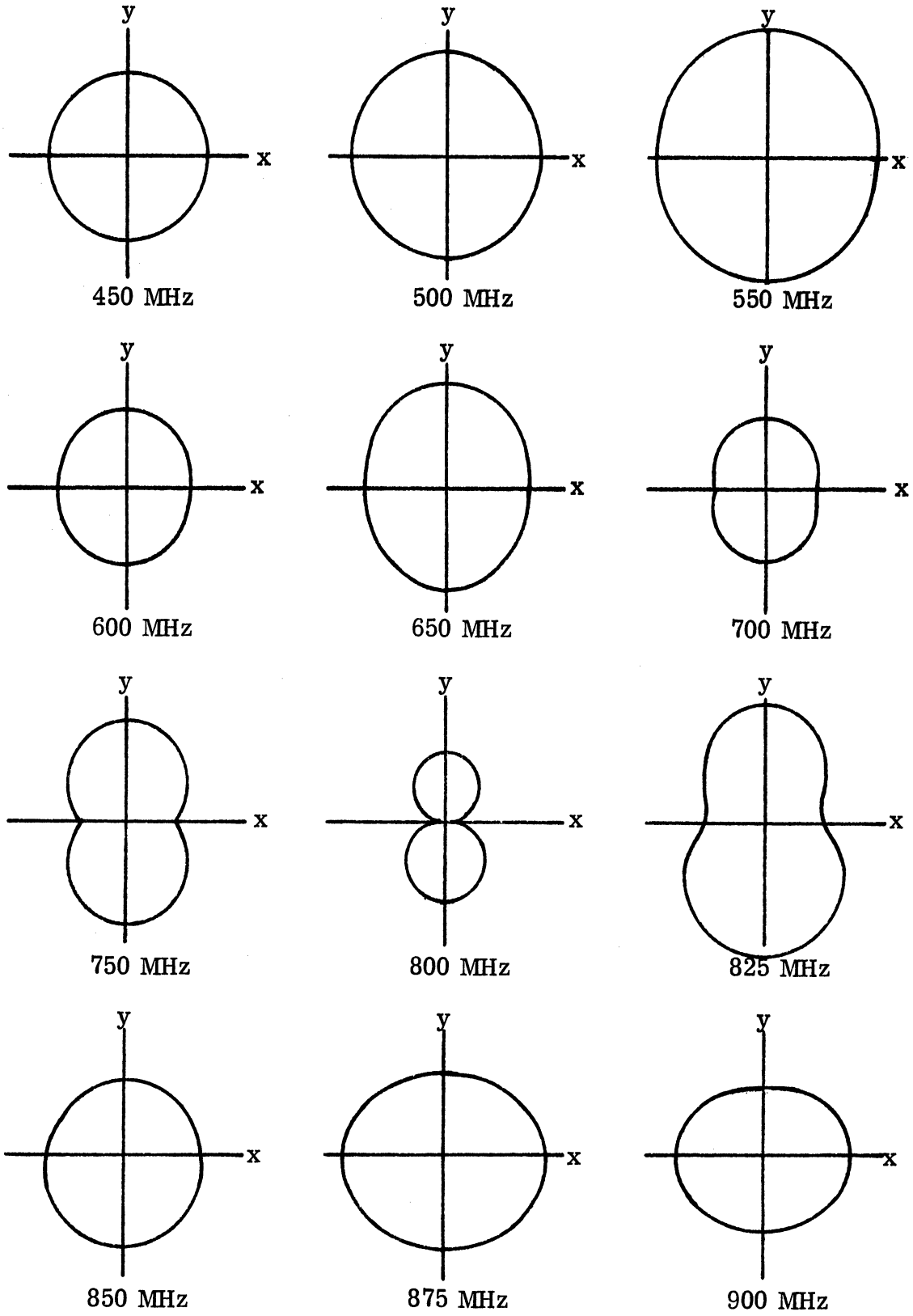

FIG. 3-18: E_θ PATTERNS IN x-y PLANE (d = 2.4 cm).

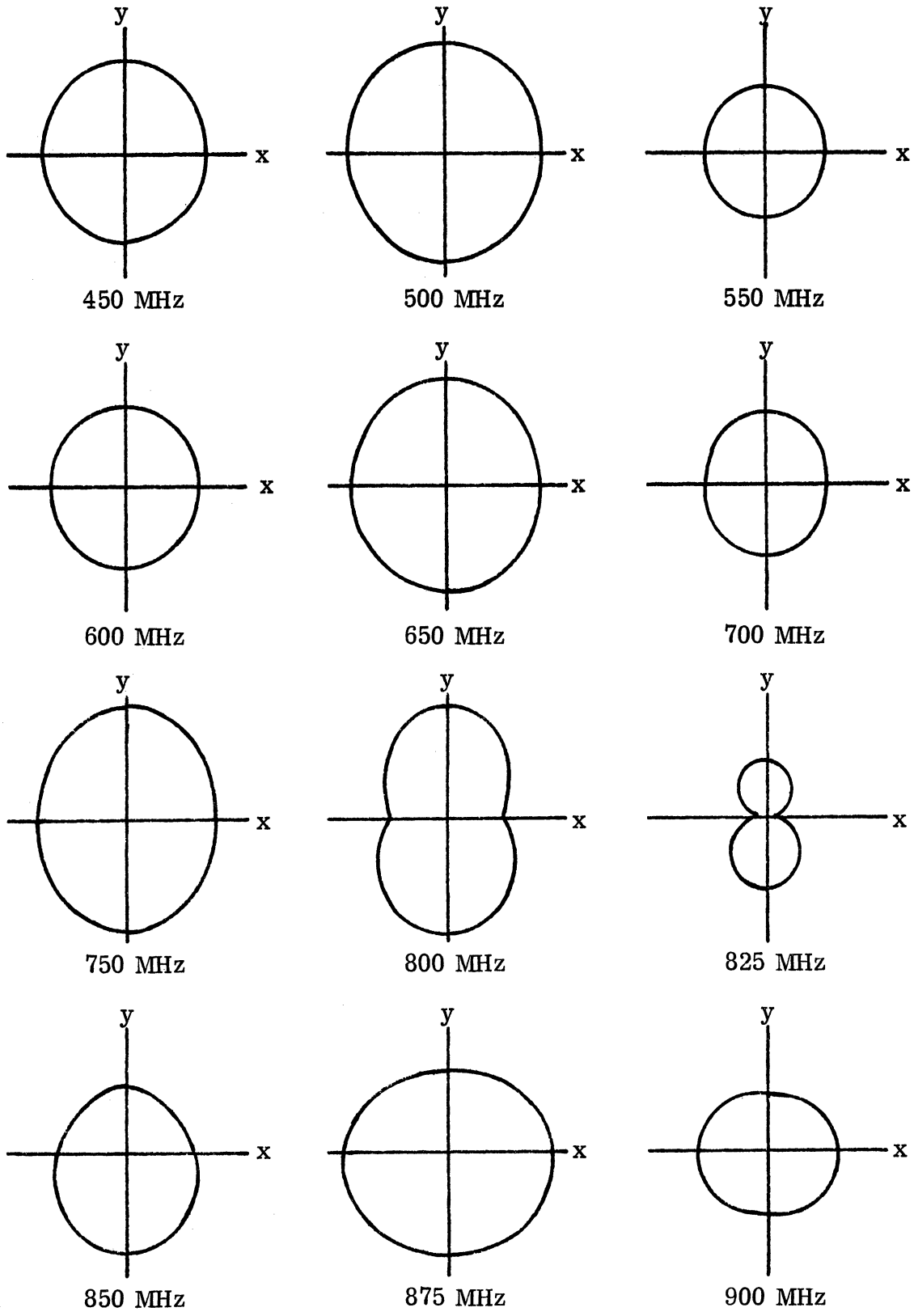

FIG. 3-19: E_θ PATTERNS IN x-y PLANE (d = 3.6 cm).

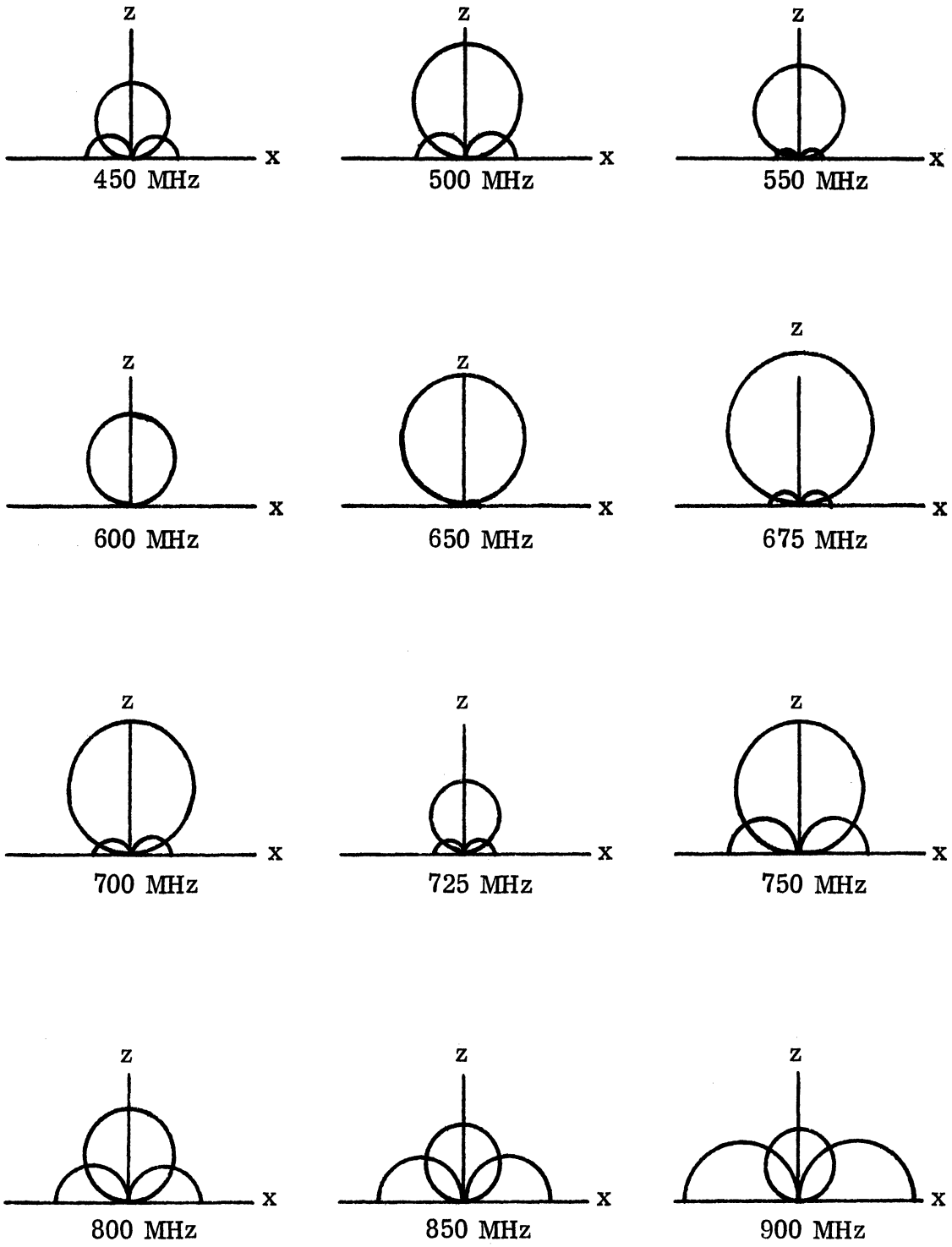

FIG. 3-20: E_ϕ AND E_θ PATTERNS IN x-z PLANE (d = 0.6 cm). The E_θ Pattern Has a Null Along the z-Axis.

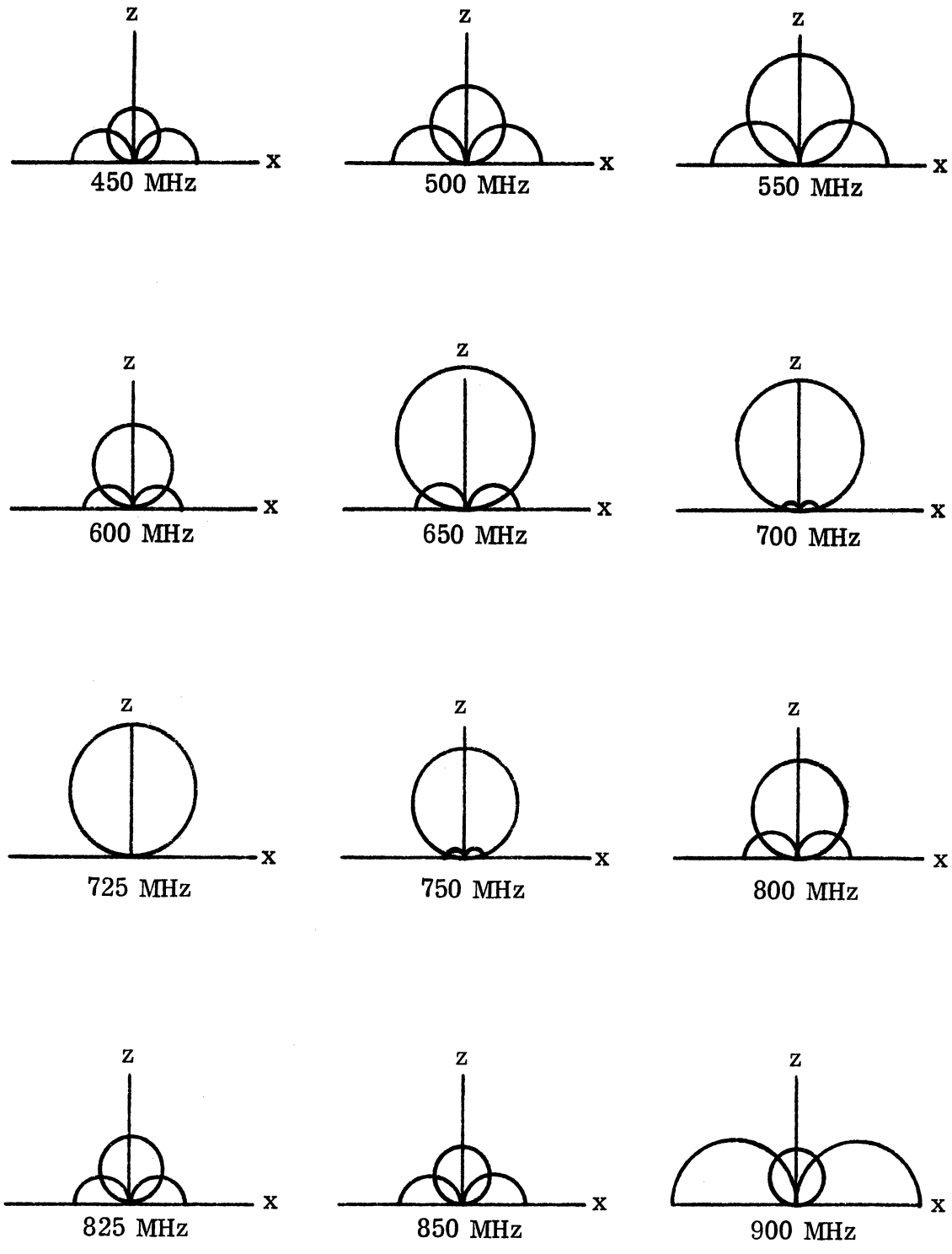

FIG. 3-21: E_{ϕ} AND E_{θ} PATTERNS IN x-z PLANE (d = 1.2 cm). The E_{θ} Pattern Has a Null Along the z-Axis.

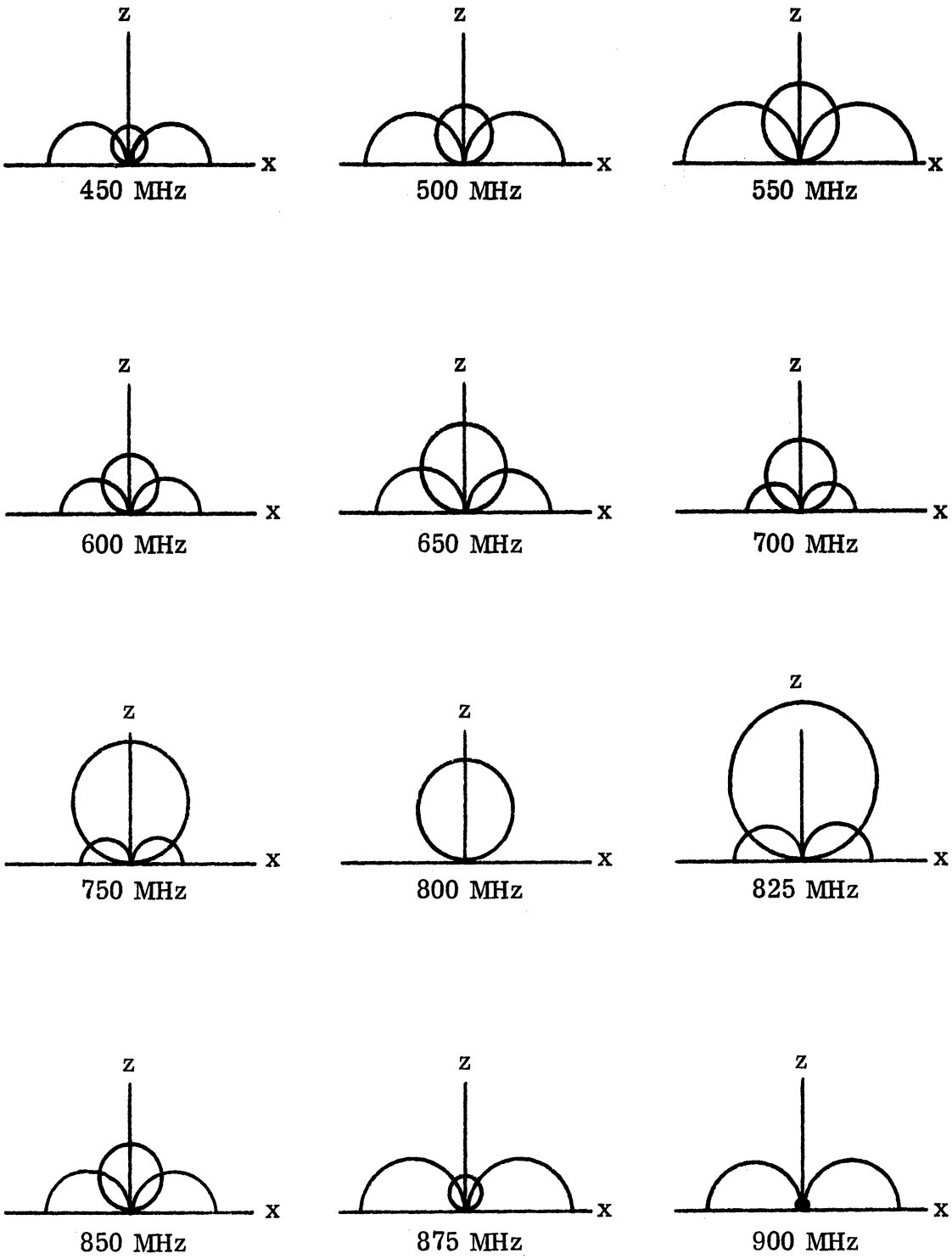

FIG. 3-22: E_ϕ AND E_θ PATTERNS IN x-z PLANE (d = 2.4 cm). The E_θ Pattern Has a Null Along the z-Axis.

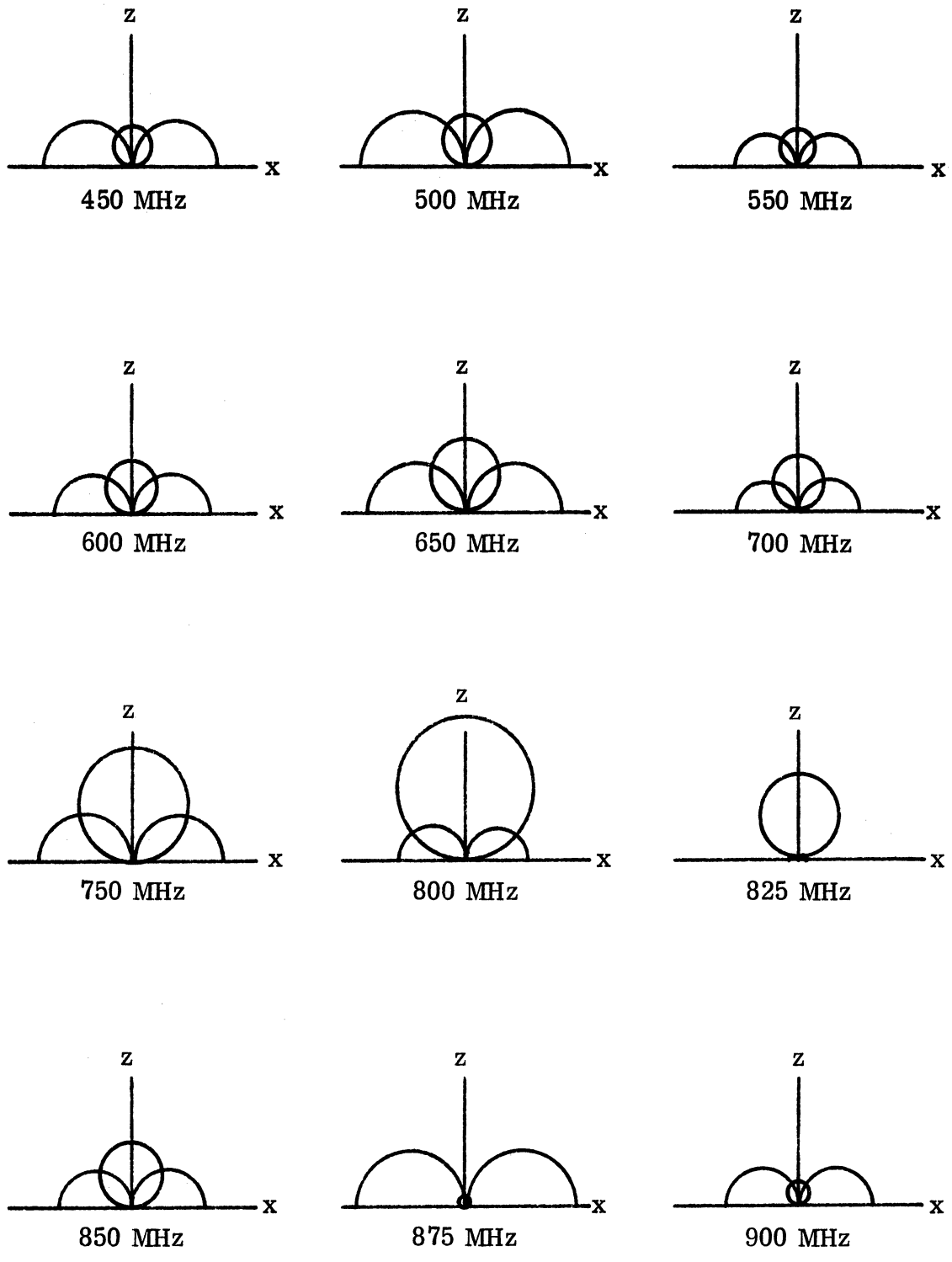

FIG. 3-23: E_ϕ AND E_θ PATTERNS IN x-z PLANE (d = 3.6 cm). The E_θ Pattern Has a Null Along the z-Axis.

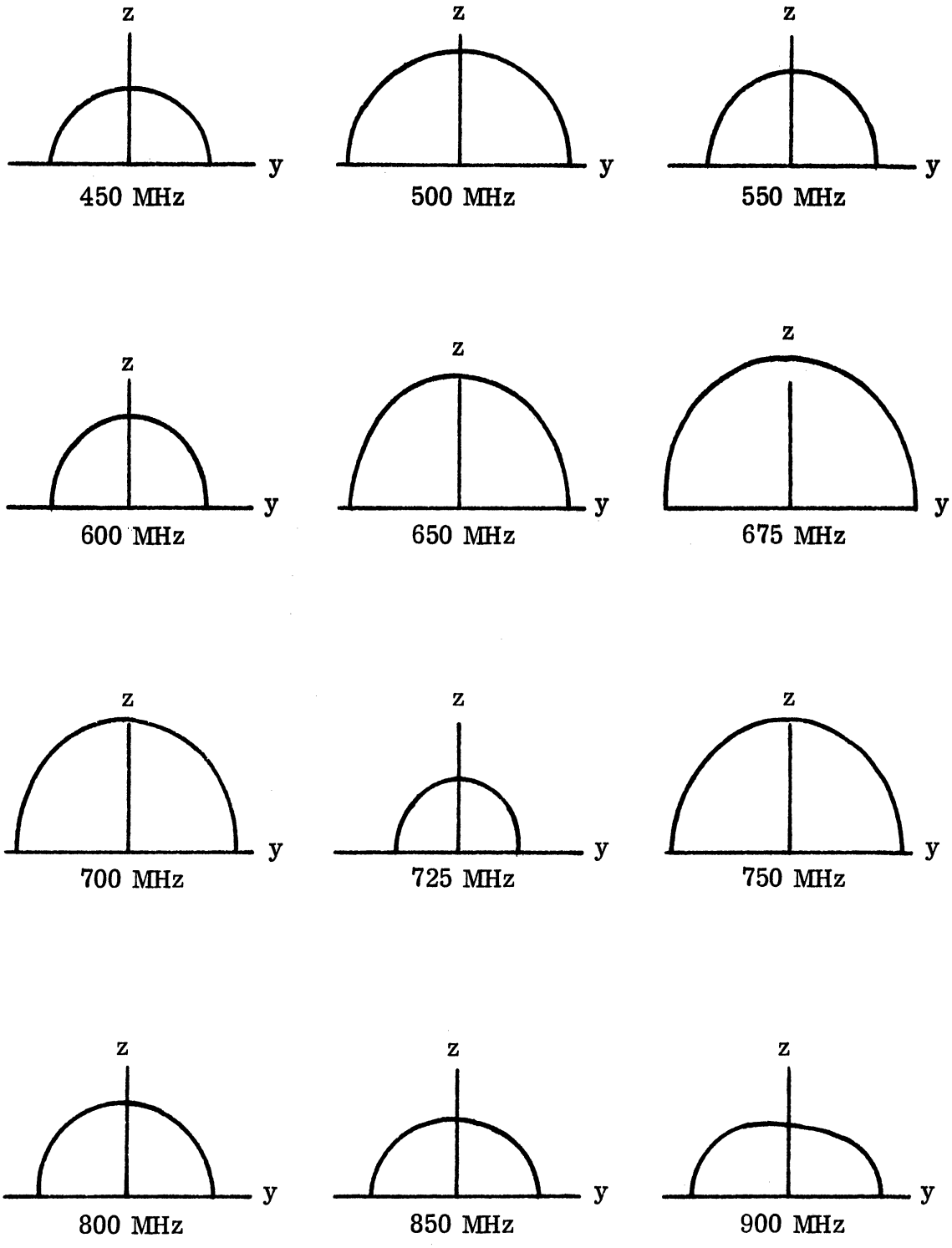

FIG. 3-24: E_θ PATTERNS IN y-z PLANE (d = 0.6 cm).

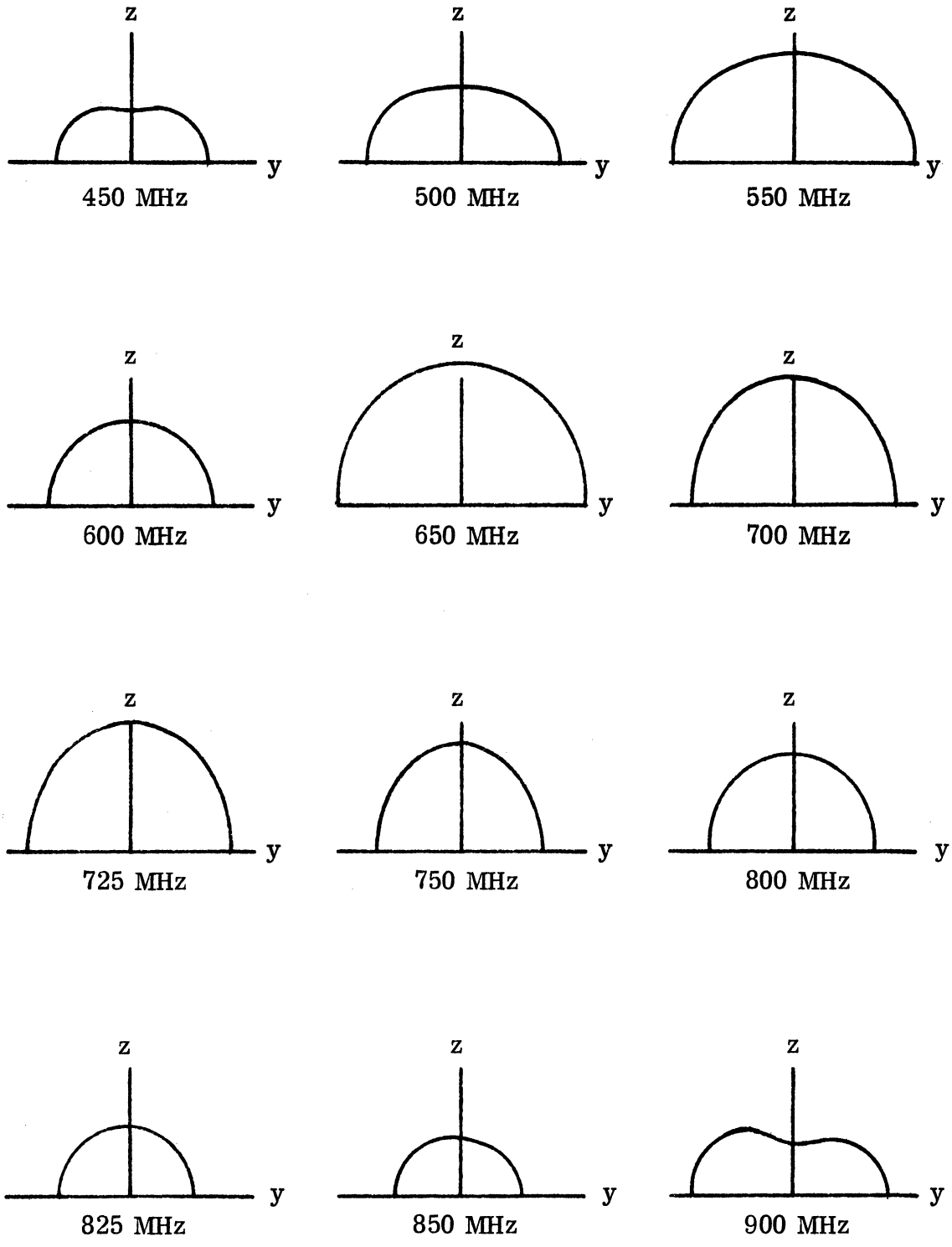

FIG. 3-25: E_θ PATTERNS IN y-z PLANE (d = 1.2 cm).

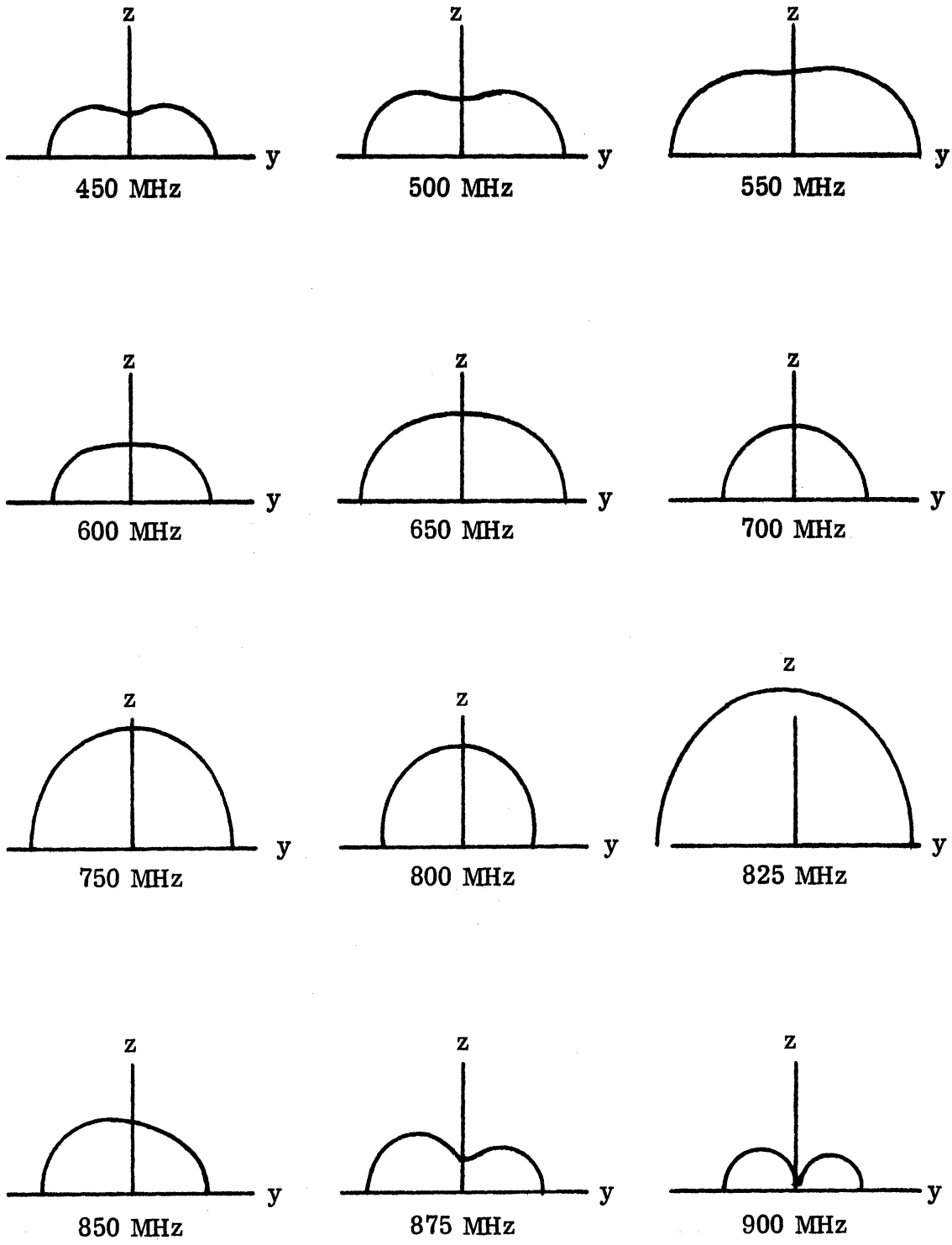

FIG. 3-26: E_θ PATTERNS IN y-z PLANE (d = 2.4 cm).

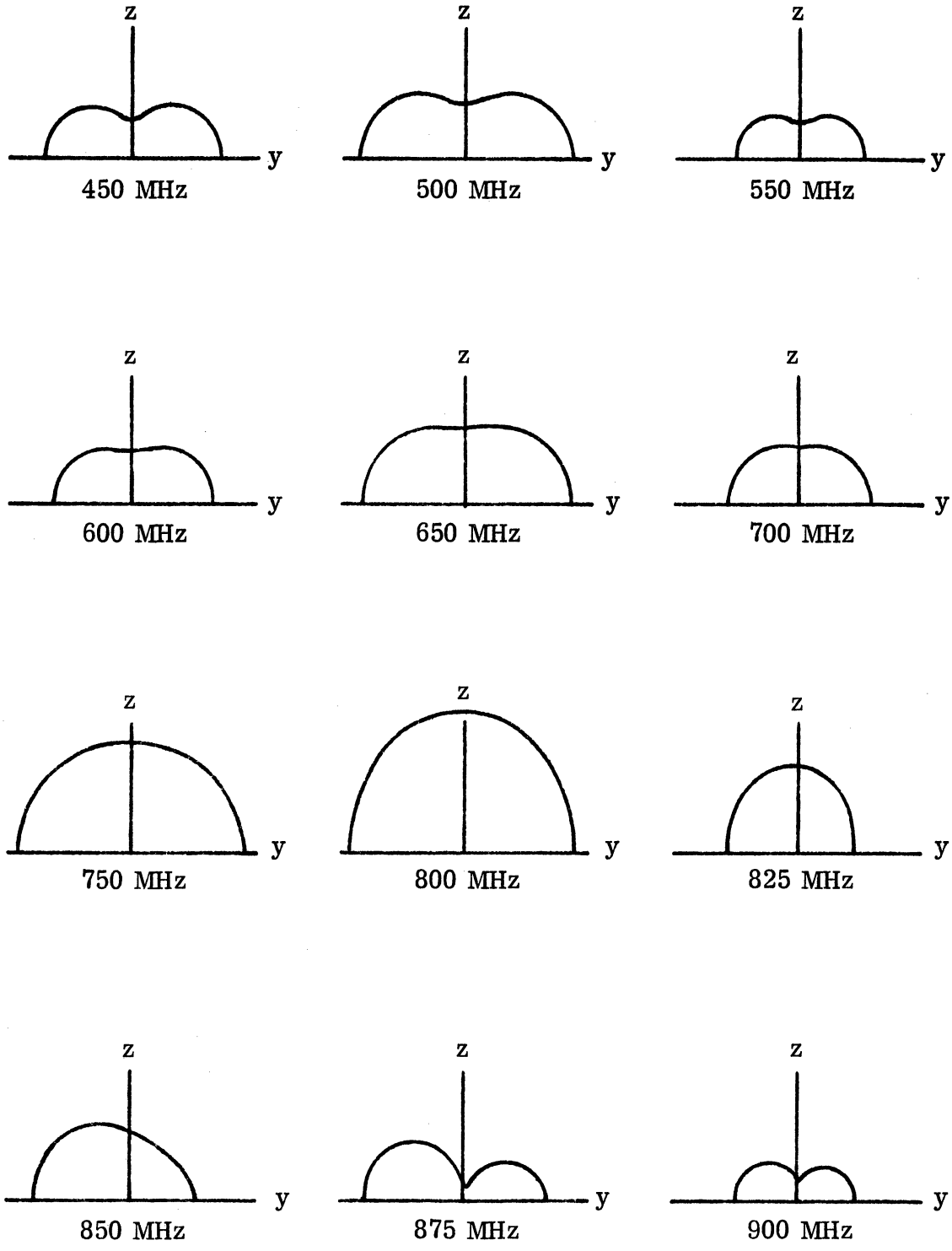

FIG. 3-27: E_θ PATTERNS IN y-z PLANE (d = 3.6 cm).

Chapter IV

EXPERIMENTAL RESULTS

4.1 Introduction

In this chapter, experimental results are presented for various models of the interdigital array. Whenever possible, a comparison is made between experiment and theory. Experiments have been performed to obtain the input impedance, the standing-wave ratio (VSWR), and antenna radiation patterns.

Each experimental model was constructed using a 10" x 15" sheet of copper for a ground plane. The thickness of the copper was 0.02". Lengths of wood 1 cm x 1 cm in cross-section were glued to the base and served as supports for the antenna elements. A three-element antenna is shown in Fig. 4-1.

The antenna elements were constructed from wire with a diameter of 0.08 cm. The ends of the parasitic elements which had to be grounded were passed through holes drilled in the ground plane. They were then bent to extend flush against the lower surface of the base. Conductive aluminum tape was used to bring the wires into firm contact with the lower surface of the ground plane. Compared to soldering, it was found that this method of construction provided a superior electrical ground.

The driven element was fed using a standard monopole mount, shown in Fig. 4-2. A hole was drilled in the copper base to allow the driven element to be inserted into the mount. In every experiment, the small ground plane of the model was attached to a larger ground plane with conductive tape. Thus, the monopole mount was designed to fit flush into the large ground plane to make the extended ground plane as flat as possible.

Experiments to measure the input impedance and VSWR were performed in the small anechoic chamber at North Campus. The chamber is a cube, measuring seven feet on a side. The experimental models were attached with

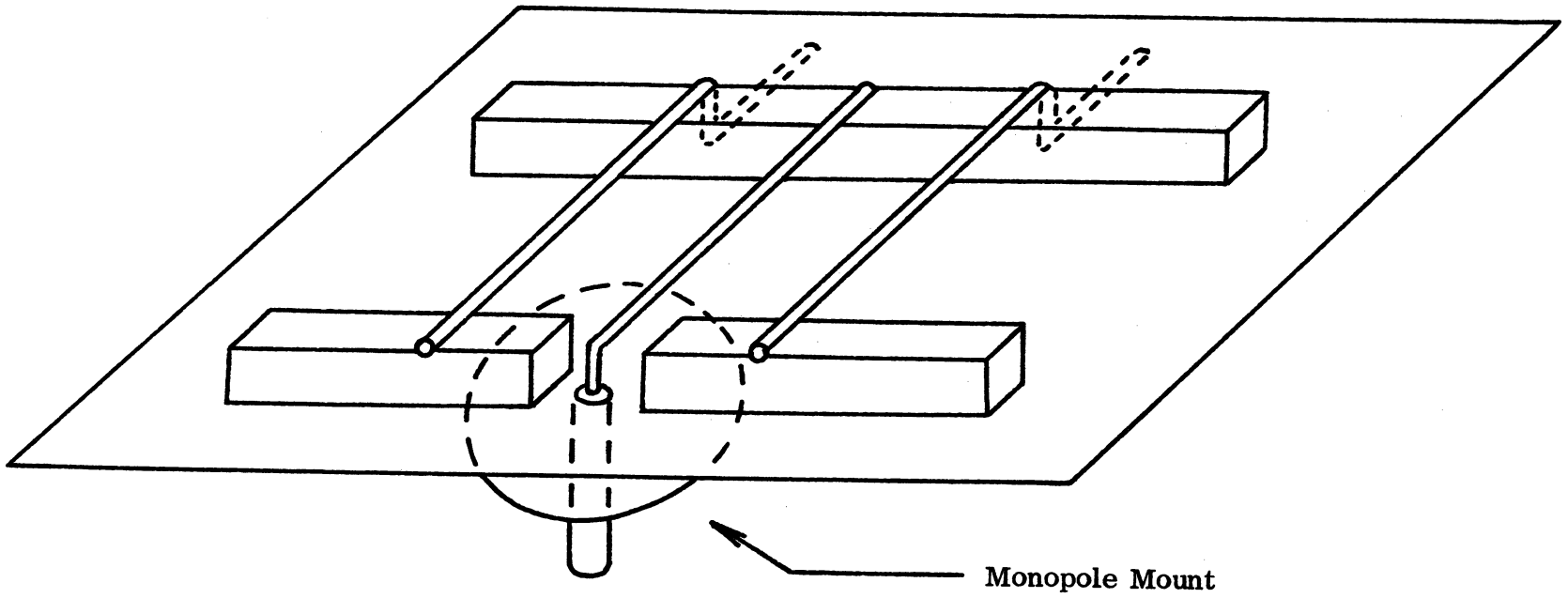

FIG. 4-1: EXPERIMENTAL MODEL OF A THREE-ELEMENT INTERDIGITAL ARRAY.

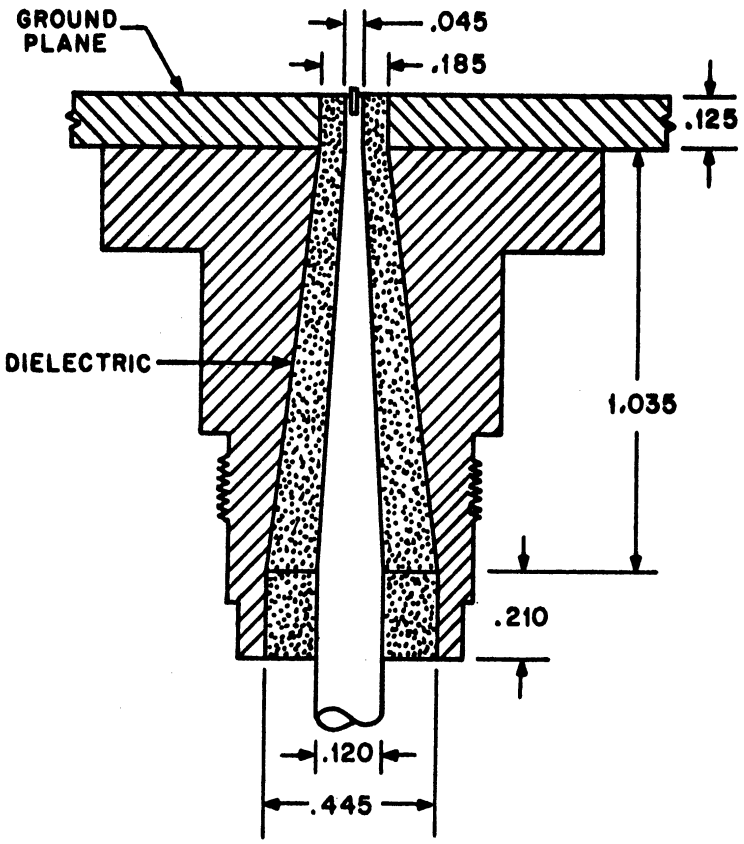

FIG. 4-2: MONOPOLE MOUNT (Dimensions in Inches).

conductive tape to a 5' x 5' ground plane, located in one wall of the chamber. Data were taken using a Hewlett-Packard 8405 A Vector Voltmeter. This instrument is used to measure the magnitude and angle of the reflection coefficient, ρ. With this information, the input impedance may be easily calculated:

$$R = \frac{Z_o (1 - |\rho|^2)}{1 - 2|\rho| \cos\theta + |\rho|^2} \tag{4.1}$$

$$X = \frac{2 Z_o |\rho| \sin\theta}{1 - 2|\rho| \cos\theta + |\rho|^2} \tag{4.2}$$

where R is the real part of the impedance, X is the imaginary part of the impedance, Z_o is the characteristic impedance of the cable used (50 Ω), and θ is the angle of ρ. For the VSWR, by definition:

$$VSWR = \frac{1 + |\rho|}{1 - |\rho|} \tag{4.3}$$

This information may also be obtained and displayed graphically on a Smith chart (Smith, 1939, 1944).

The radiation patterns were taken at the North Campus Antenna Range on the roof of the G.G. Brown Building. This is a 50' range, using a linearly-polarized log-tooth antenna for the transmitter. The experimental models were attached to a small (60" x 19-3/8") ground plane. Provision was made to ascertain the relative magnitudes of cross-polarized radiation components when they occurred.

4.2 The Driven Element

In this section, experimental data are presented for the driven element of the interdigital array. The experimental model had the following physical parameters: ℓ = 8.0 cm, h = 1.0 cm, and a = 0.04 cm, (see Fig. 2-1). These are the same parameters that were used in the theoretical study of the driven element in Chapter II. Thus, it is possible to make a direct comparison between theory and experiment.

The experimental and theoretical input impedance data are plotted on Smith charts in Figs. 4-3 and 4-4 respectively. Both charts are normalized to 50 Ω. Because of the use of image theory in Chapter II, the theoretical data have been divided by two to allow for the ground plane in the experimental model.

Both impedance plots have the same general shape. The impedance is capacitive for low frequencies, and becomes inductive at higher frequencies. However, the correspondence in frequency between theory and experiment is not one to one. The theoretical input impedance is slightly more capacitive.

The real part of the impedance is quite small in both plots, but it is somewhat larger in the experimental case. This is expected, for the experimental data include losses. In the theoretical model, the conductors are assumed to be perfect, and no losses are considered.

For further comparison, the experimental and theoretical input impedance data are plotted versus frequency. The real part is plotted in Fig. 4-5, and the imaginary part is plotted in Fig. 4-6.

For the real part, the experimental data are a few ohms greater than the theoretical values. The theoretical and experimental curves would be nearly parallel except for the peak in the experimental curve near 450 MHz. This peak actually may be due to a measurement inaccuracy. When an impedance is mainly reactive, a small error in measuring the magnitude of ρ will make a large error in the real part of the impedance.

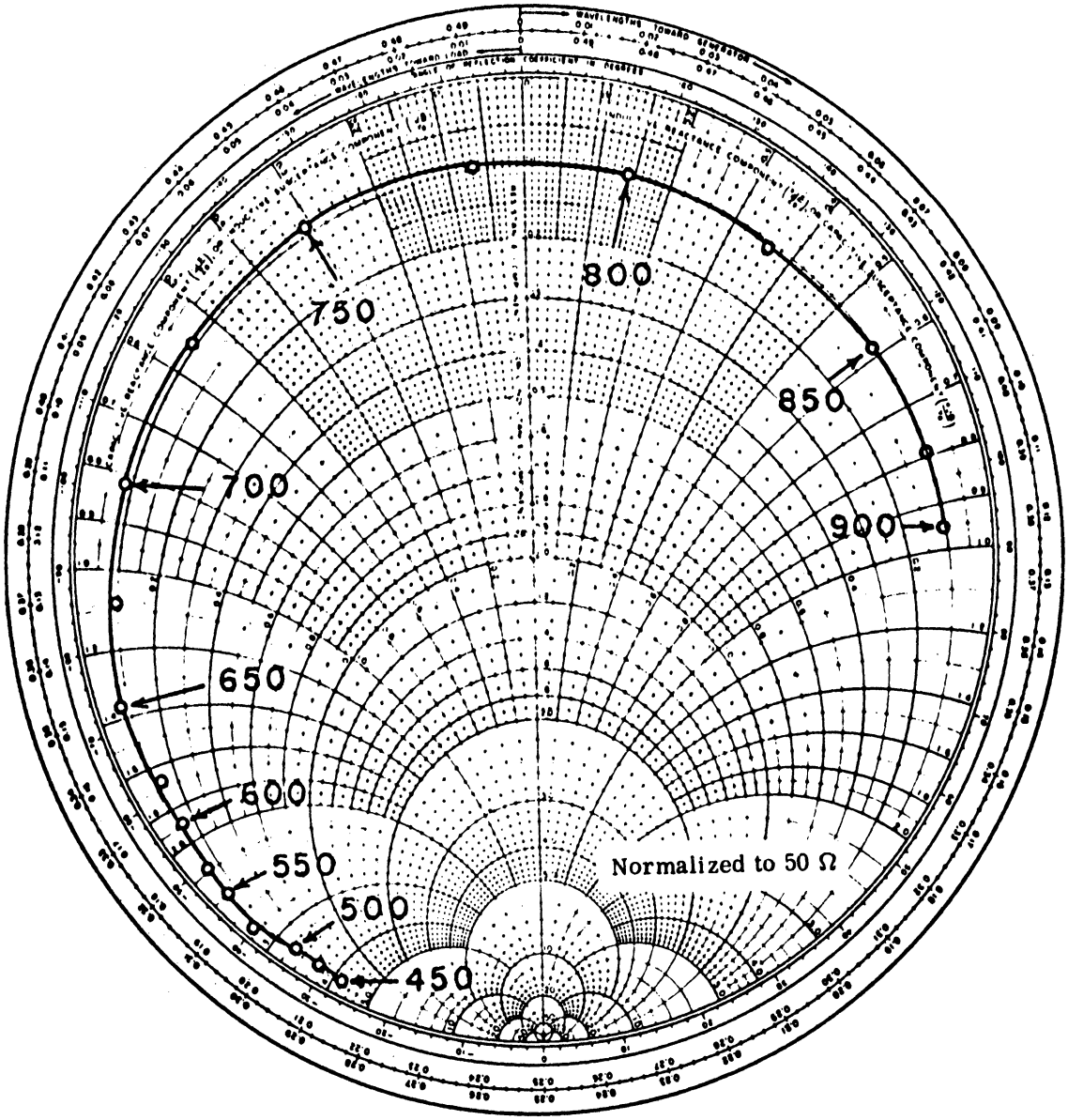

FIG. 4-3: INPUT IMPEDANCE OF DRIVEN ELEMENT (Experimental).

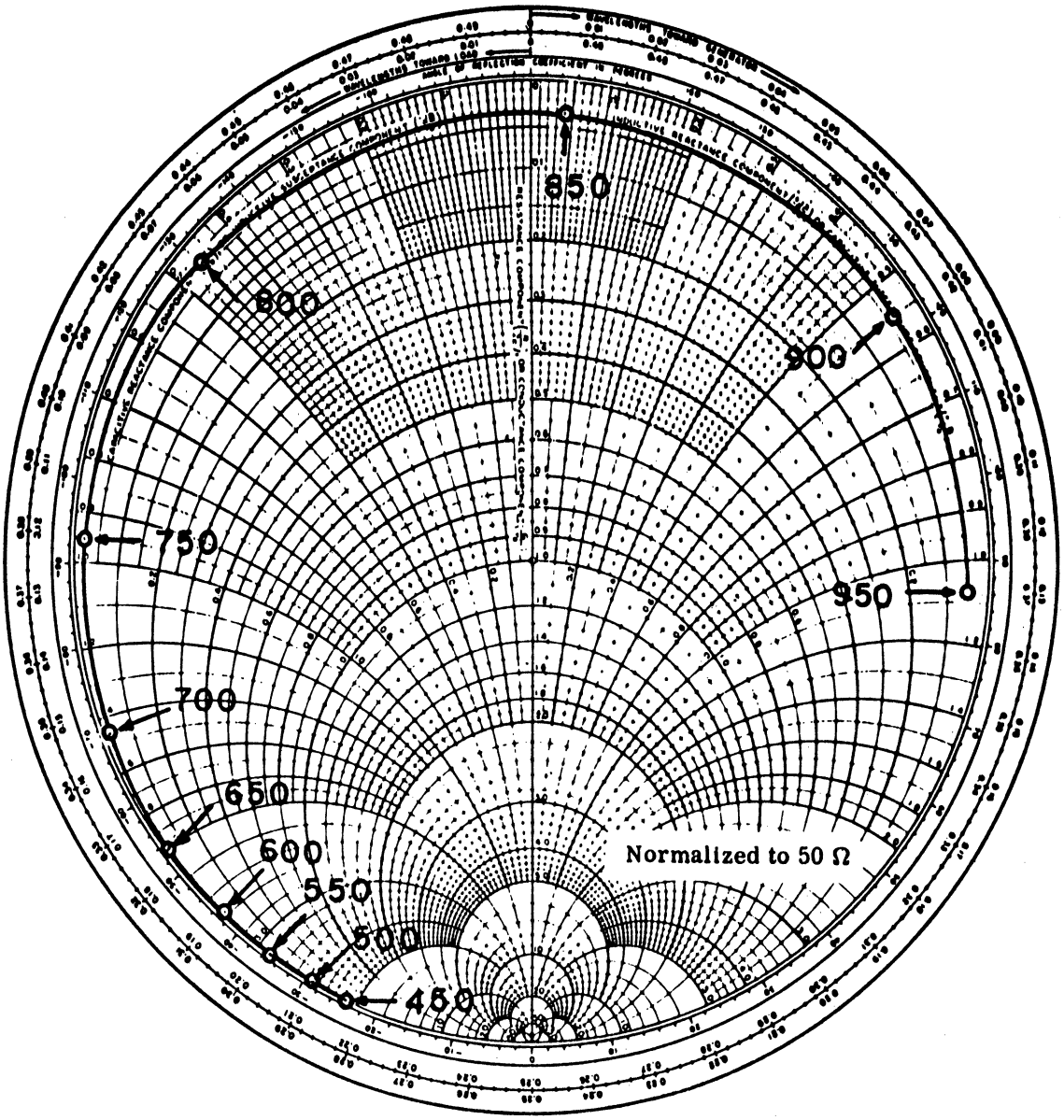

FIG. 4-4: INPUT IMPEDANCE OF DRIVEN ELEMENT (Theoretical).

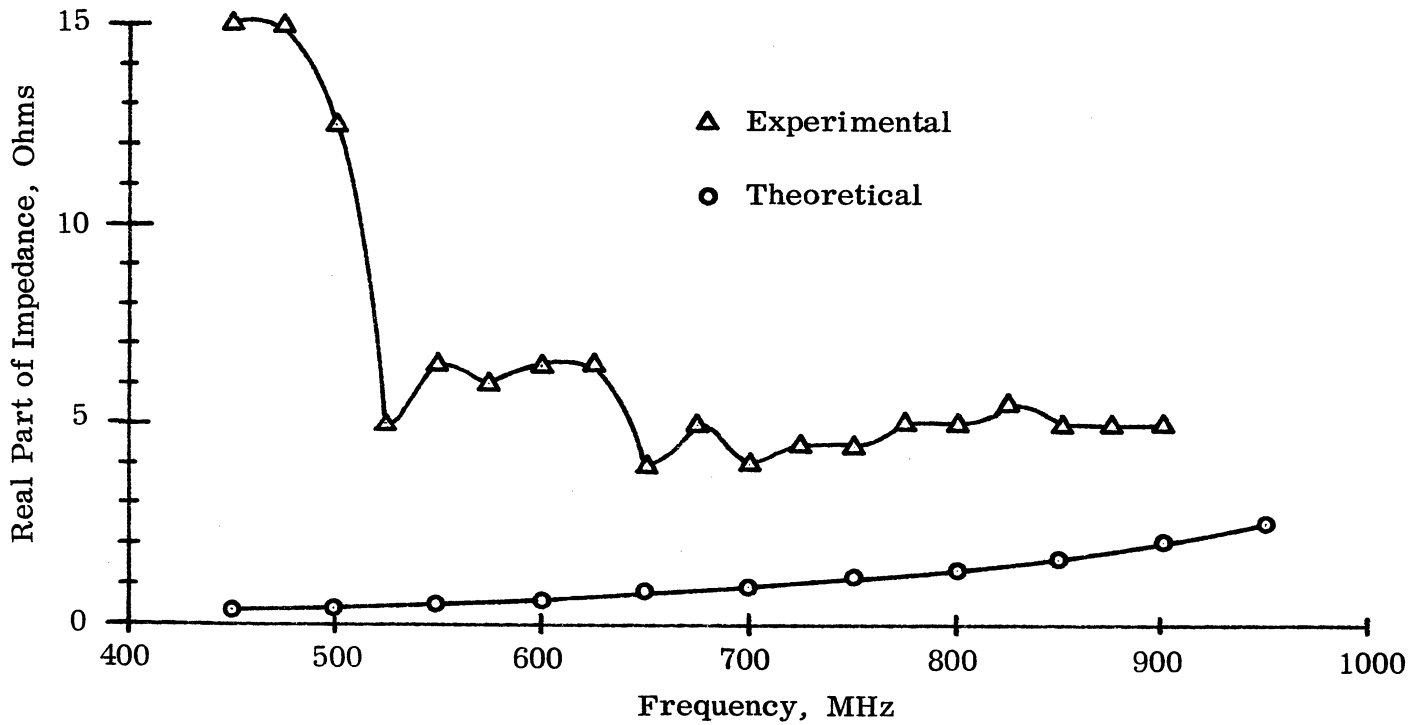

FIG. 4-5: INPUT IMPEDANCE OF DRIVEN ELEMENT (Real Part).

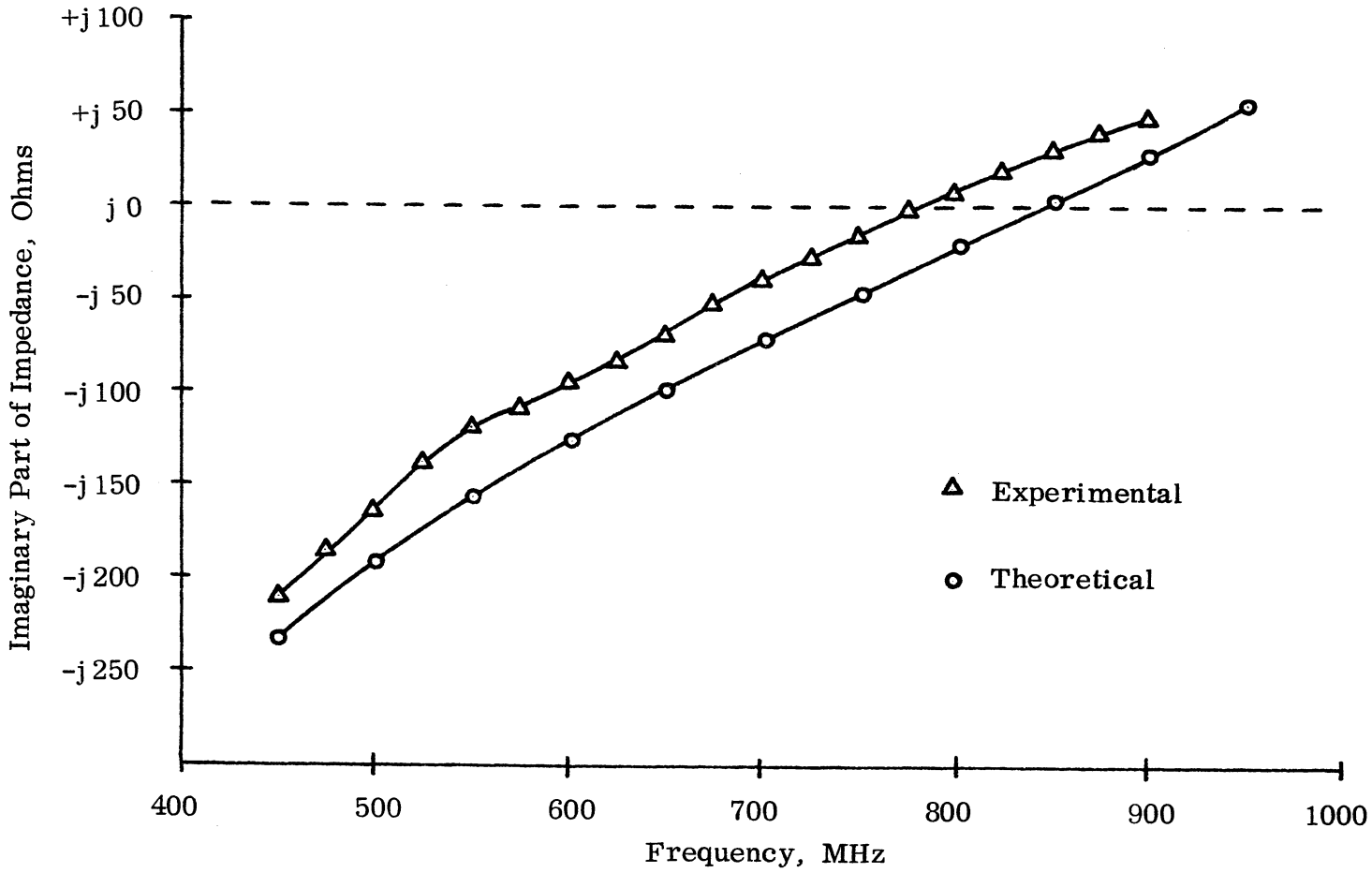

FIG. 4-6: INPUT IMPEDANCE OF DRIVEN ELEMENT (Imaginary Part).

For the imaginary part, the experimental and theoretical curves have almost exactly the same slope. The theoretical data are slightly more capacitive. This is considered excellent agreement.

The experimental and theoretical VSWR data are plotted in Fig. 4-7. Although the VSWR can never be less than one, the scale starts at zero for convenience. Since high VSWR values are rather meaningless, the graph is clipped at 50. This means that a VSWR of 50 or greater is plotted at 50.

The driven element is seen to have a high standing-wave ratio with respect to a 50 Ω cable. This is because the real part of the impedance is so low. Although the experimental VSWR is high, it is lower than the predicted VSWR. Naturally, this is because the real part of the experimental impedance is somewhat larger than the real part of the theoretical impedance.

Radiation patterns were obtained for the driven element every 50 MHz from 450 MHz to 900 MHz. The experimental model was mounted on a small ground plane at the North Campus Antenna Range. The effects of a small ground plane on radiation patterns are well known (Kraus, 1950). For example, consider a pattern which is supposed to have a maximum along an infinite ground plane. If the pattern is taken using a small ground plane, the maximum will be inclined at an angle above the ground plane. Thus, it is not very meaningful to take patterns in the plane of a small ground plane. Therefore, radiation patterns were obtained for the driven element only in the x - z and y - z planes. See Fig. 2-6 for the coordinate system.

Radiation patterns for six selected frequencies are shown in Figs. 4-8 through 4-13. Notice how the maximum of the E_θ patterns is inclined by the small ground plane. These patterns can be compared with the theoretical patterns in Figs. 2-8 through 2-17. Because the experimental patterns are actually power patterns (corresponding to E^2), they appear to be more pointed than the theoretical patterns.

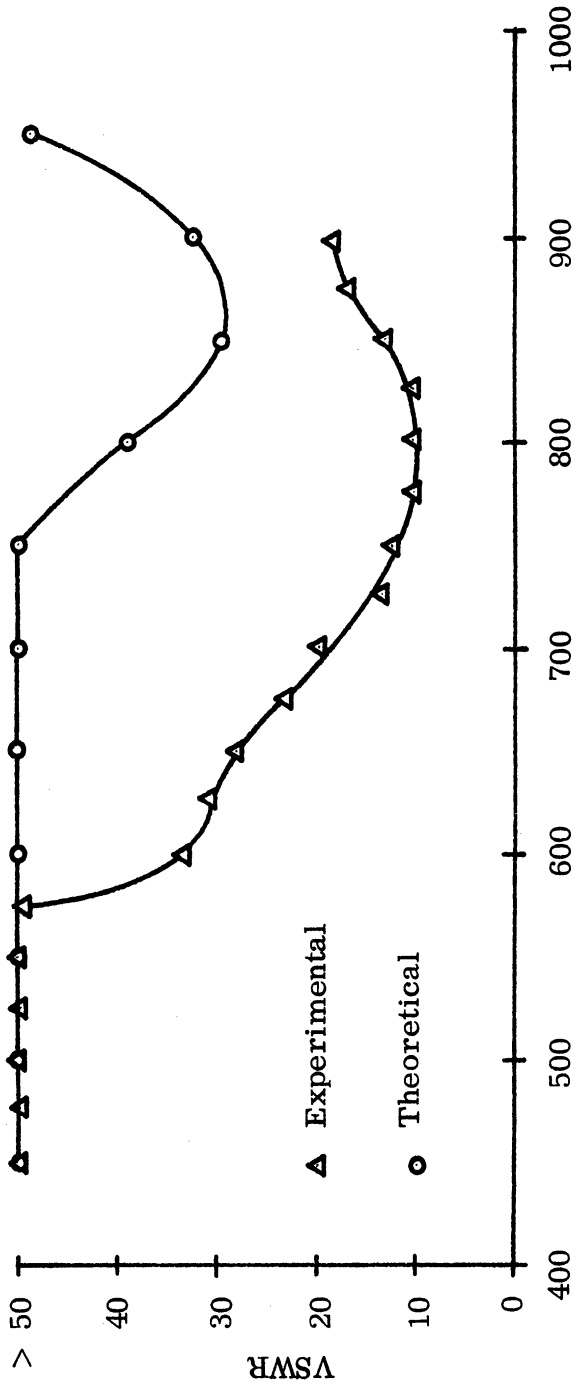

FIG. 4-7: VSWR OF THE DRIVEN ELEMENT.

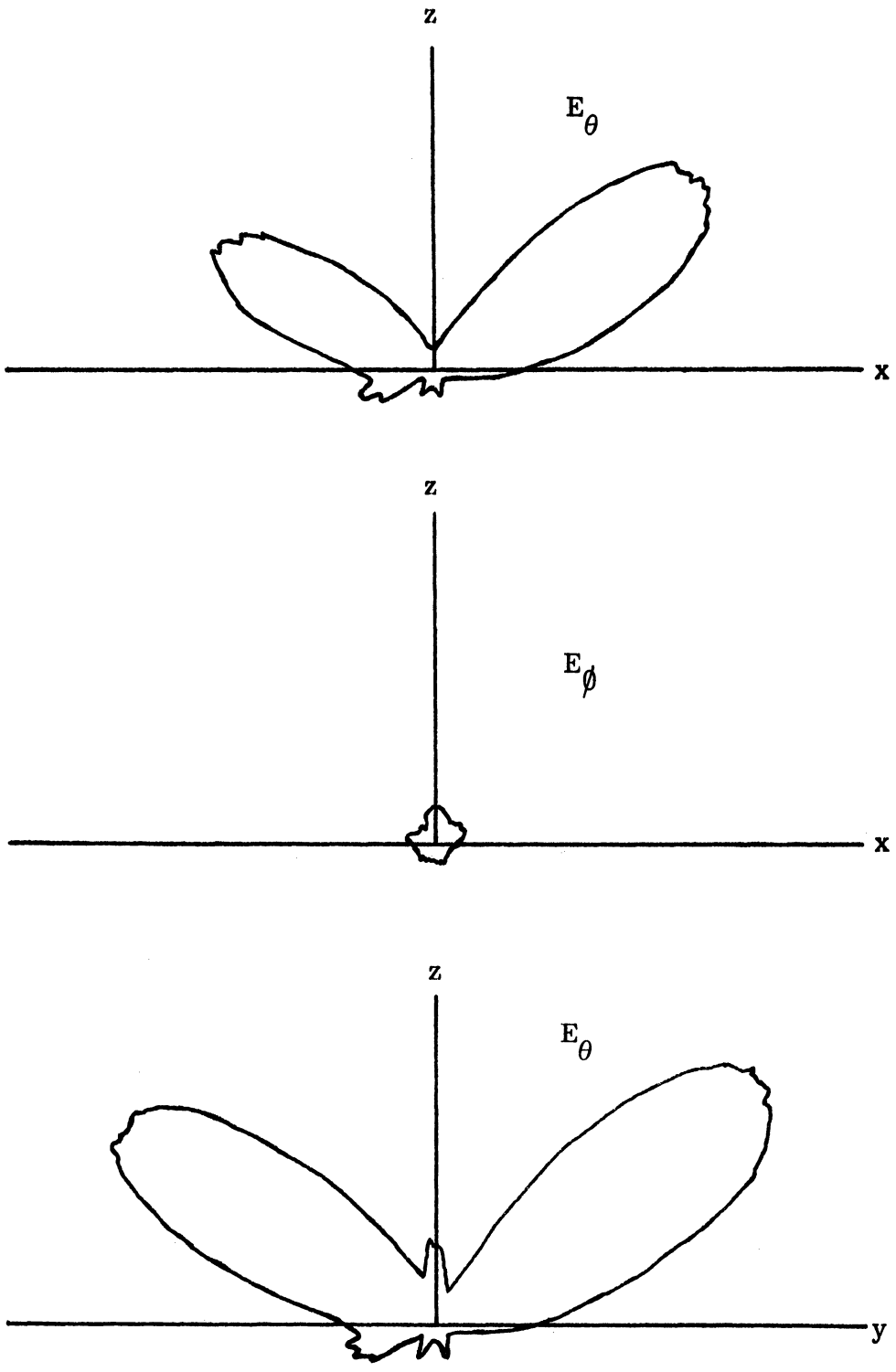

FIG. 4-8: DRIVEN ELEMENT (f = 450 MHz).

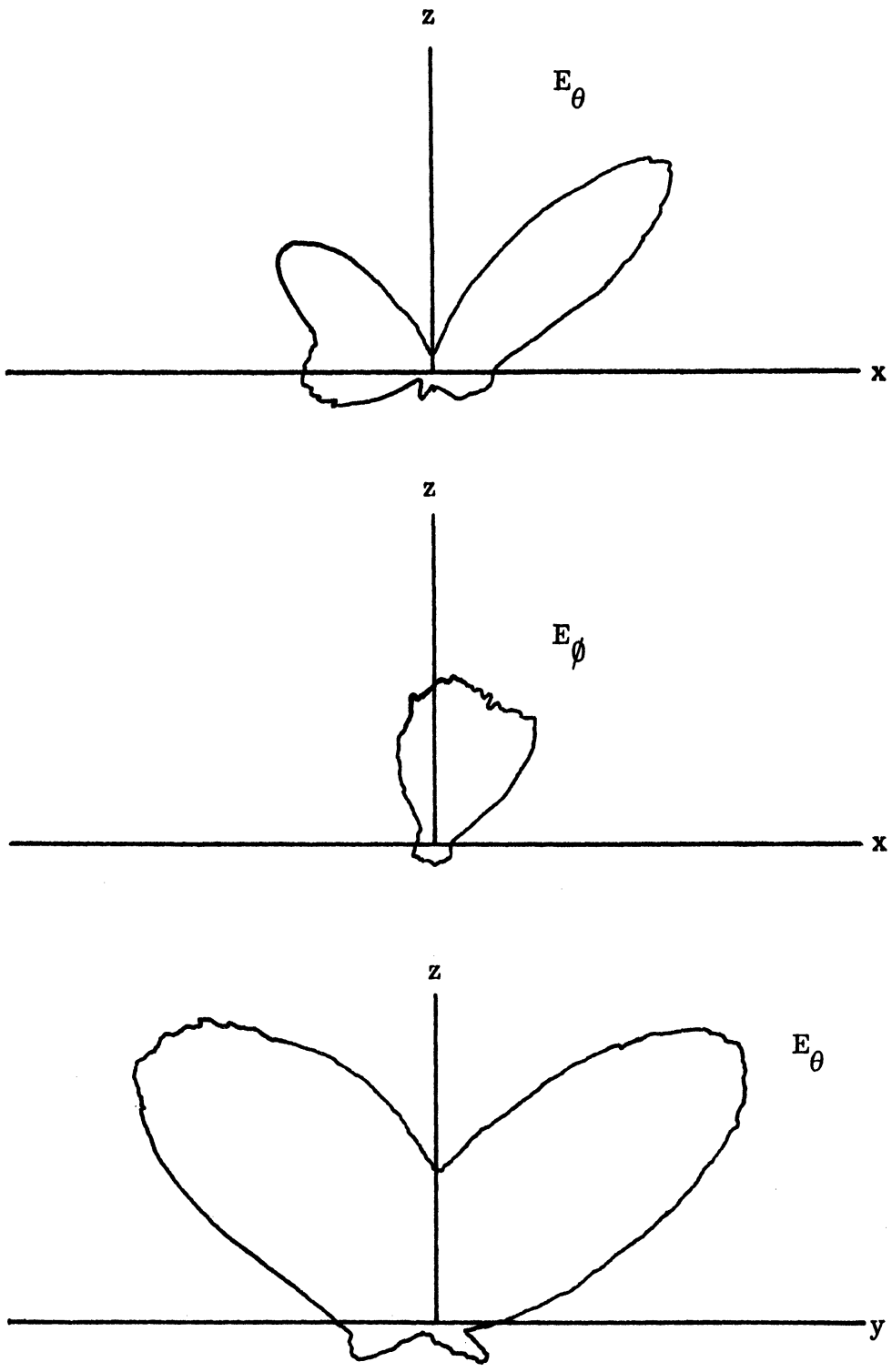

FIG. 4-9: DRIVEN ELEMENT (f = 600 MHz).

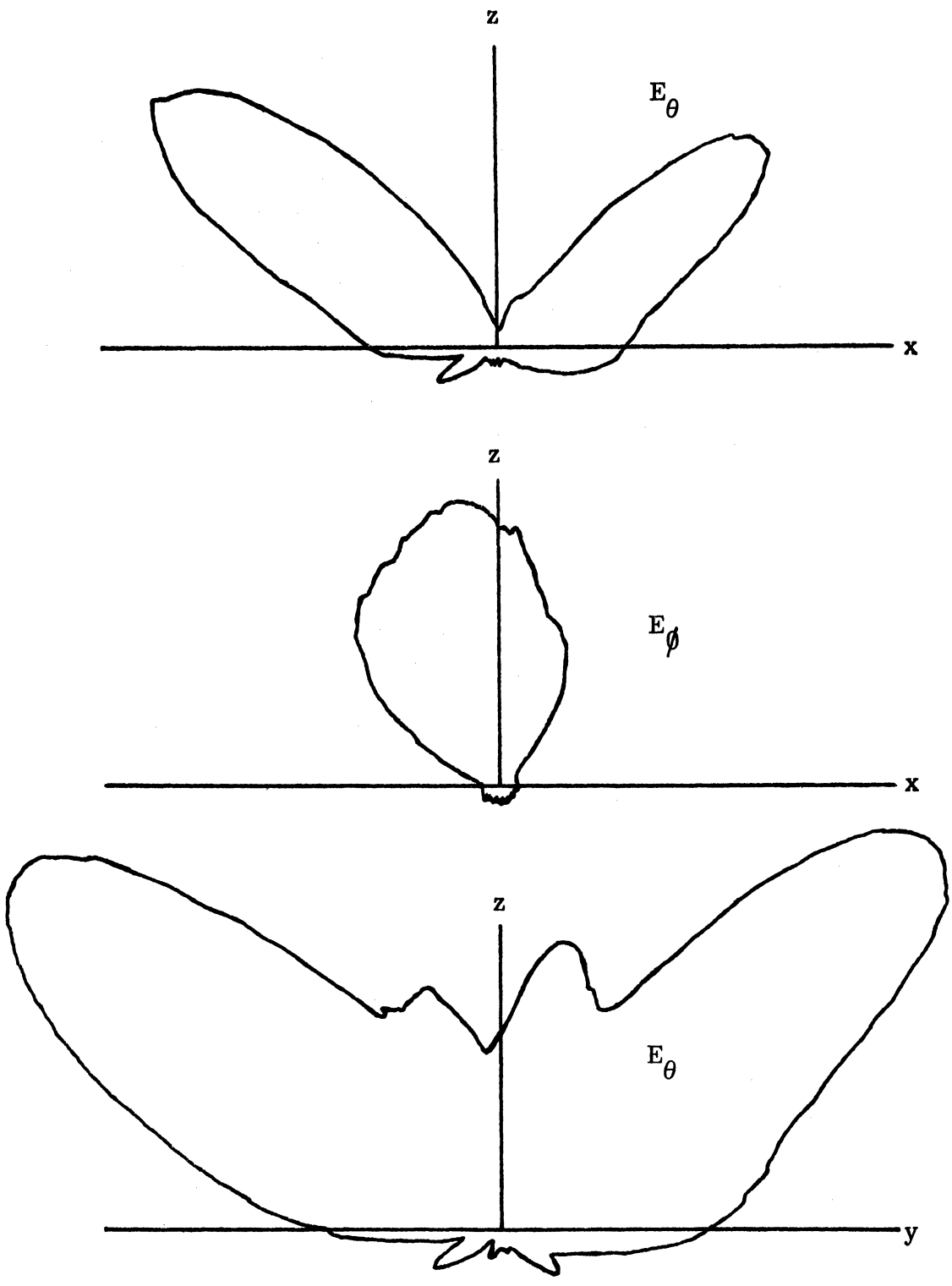

FIG. 4-10: DRIVEN ELEMENT (f = 700 MHz).

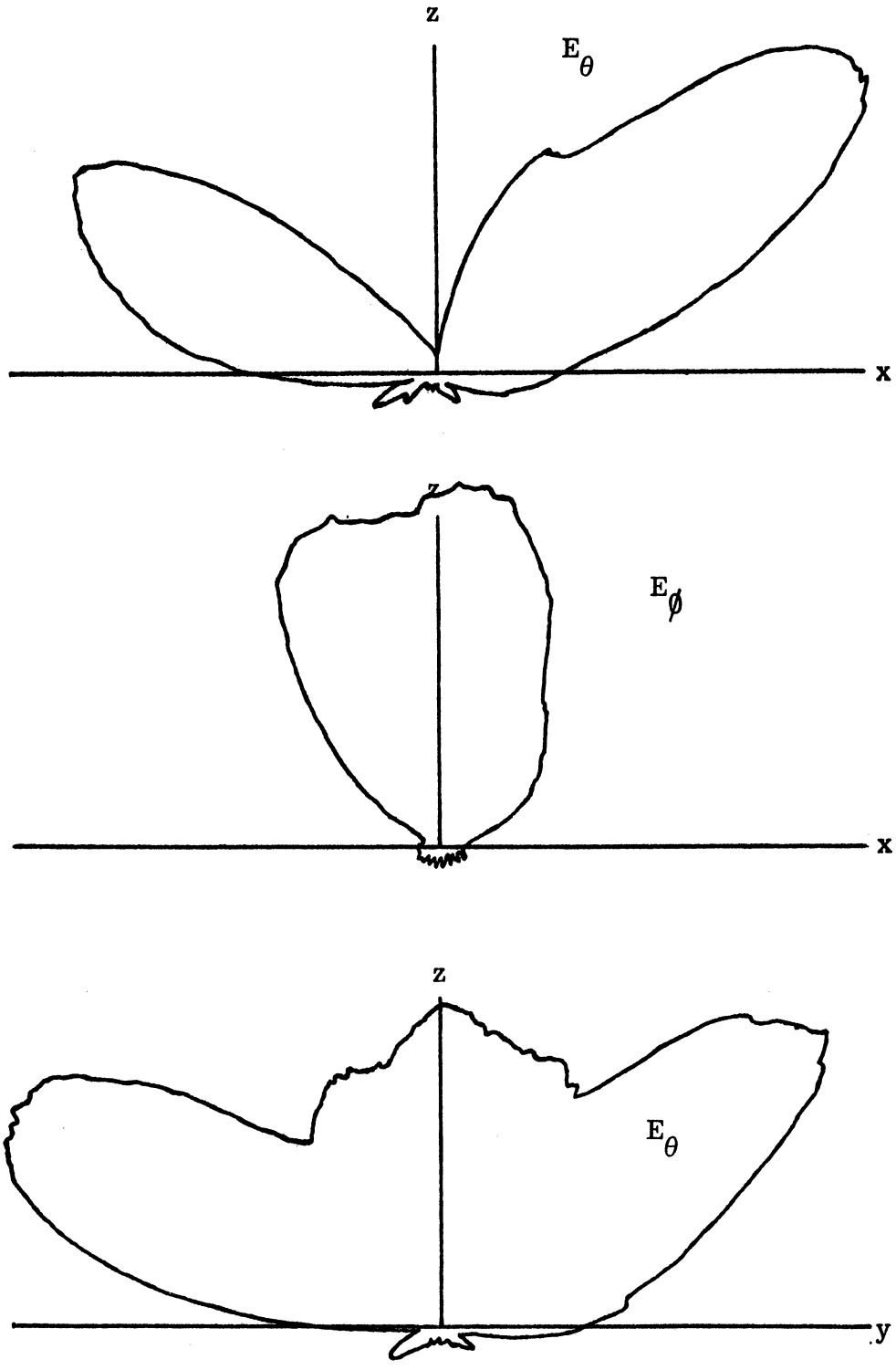

FIG. 4-11: DRIVEN ELEMENT (f = 800 MHz).

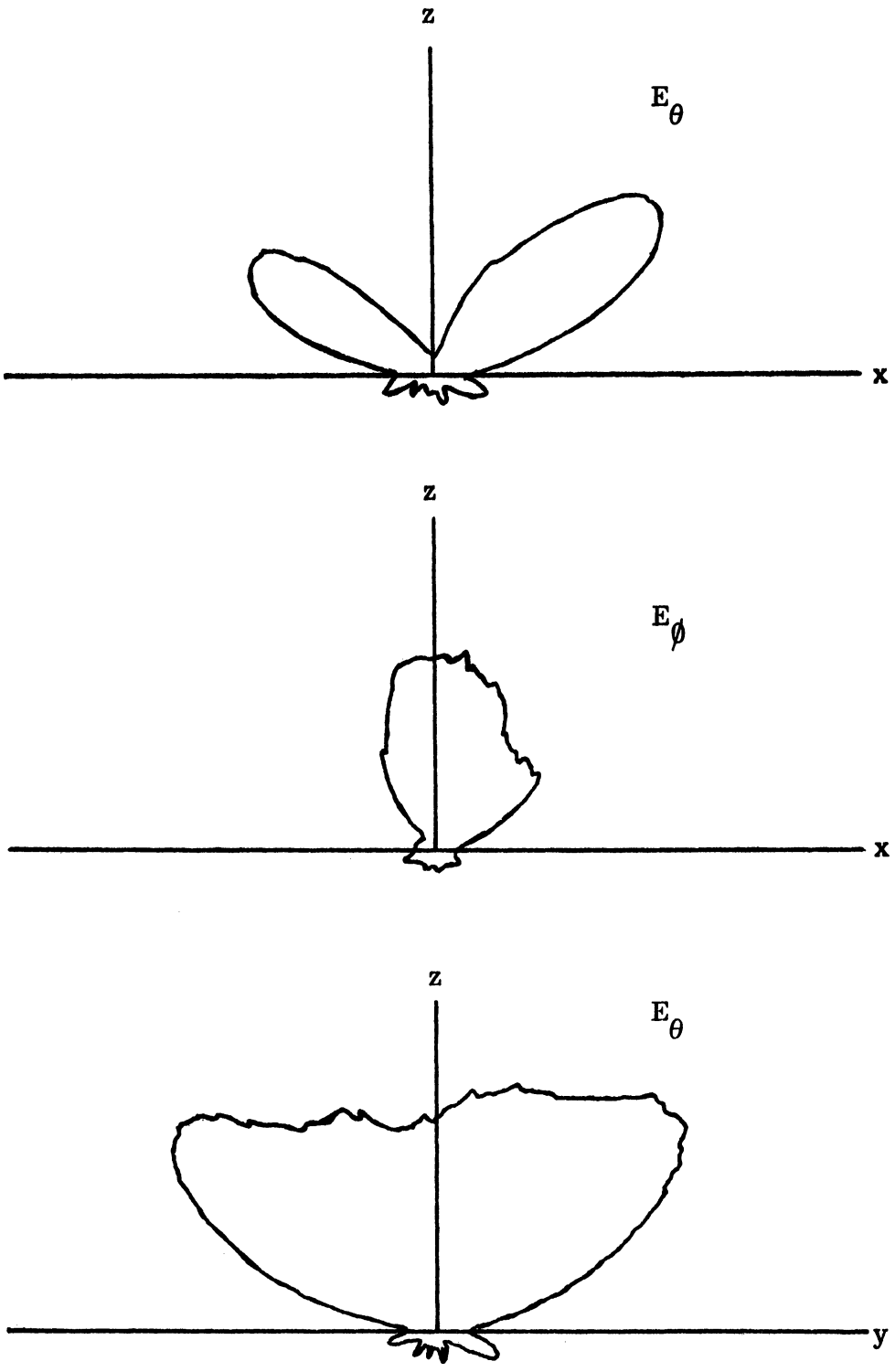

FIG. 4-12: DRIVEN ELEMENT (f = 850 MHz).

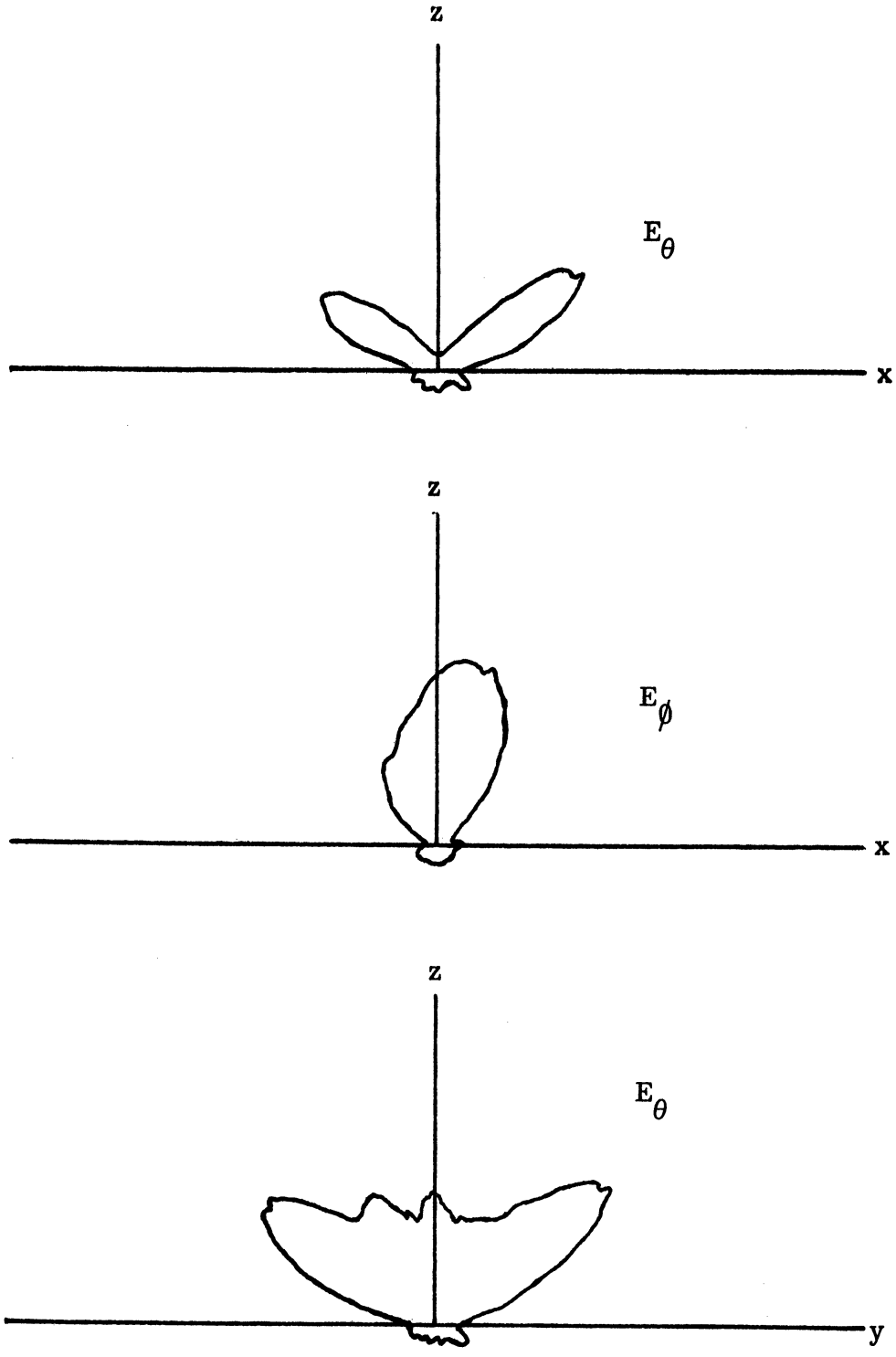

FIG. 4-13: DRIVEN ELEMENT (f = 900 MHz).

In the x - z plane, the experimental patterns confirm the cross-polarization which was predicted theoretically. The experimental E_ϕ pattern is broadside, and the experimental E_θ pattern is endfire. In Fig. 4-14 the experimental and theoretical power ratios of E_ϕ to E_θ are plotted versus frequency. The agreement is seen to be quite good.

In the y - z plane only the E_θ component exists. The experimental data confirm the prediction that the radiation pattern in this plane would approach a semicircle as the frequency was increased. Of course, the experimental pattern shape was modified near the y-axis because of the small ground plane.

The experimental data for the driven element of the interdigital array agree quite well with the theoretical data from Chapter II. The factors which contribute to the differences between theory and experiment will be discussed in Chapter V. It can be concluded that the driven element studied in this dissertation would not be a very good antenna by itself. The real part of the input impedance is too small, causing a high VSWR and a large mis-match with a 50 Ω feed.

4.3 Three-Element Arrays

In this section, experimental results are presented for four three-element interdigital arrays. These models had the following physical parameters in common: ℓ = 8.0 cm, h = 1.0 cm, and a = 0.04 cm. They differed in the spacing, d, between the elements (see Fig. 3-1). Values of d used were 0.6 cm, 1.2 cm, 2.4 cm, and 3.6 cm. The experimental models had the same dimensions as the four three-element antennas studied theoretically in Chapter III. Thus, a direct comparison is possible between theory and experiment.

Experiments were performed to measure the input impedance of each array in the frequency range from 450 MHz to 900 MHz. The experimental data are plotted on Smith charts in Figs. 4-15 through 4-18. The theoretical input impedances from Chapter III were divided by two to correct for the ground plane which was used in the experiments. The theoretical data are plotted on Smith charts in Figs. 4-19 through 4-22. All the Smith charts are normalized to 50 Ω.

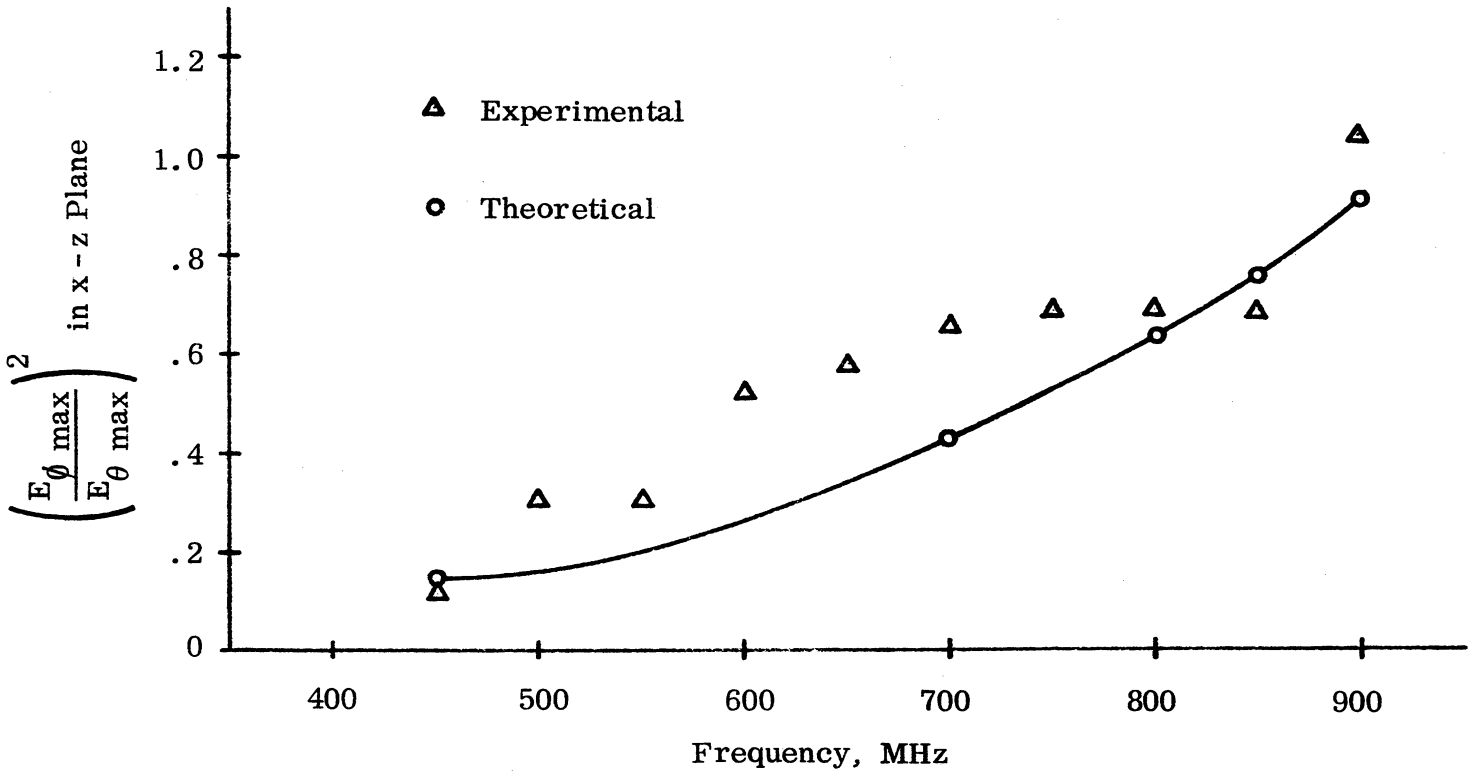

FIG. 4-14: POWER RATIO OF CROSS-POLARIZED COMPONENTS IN THE x-z PLANE.

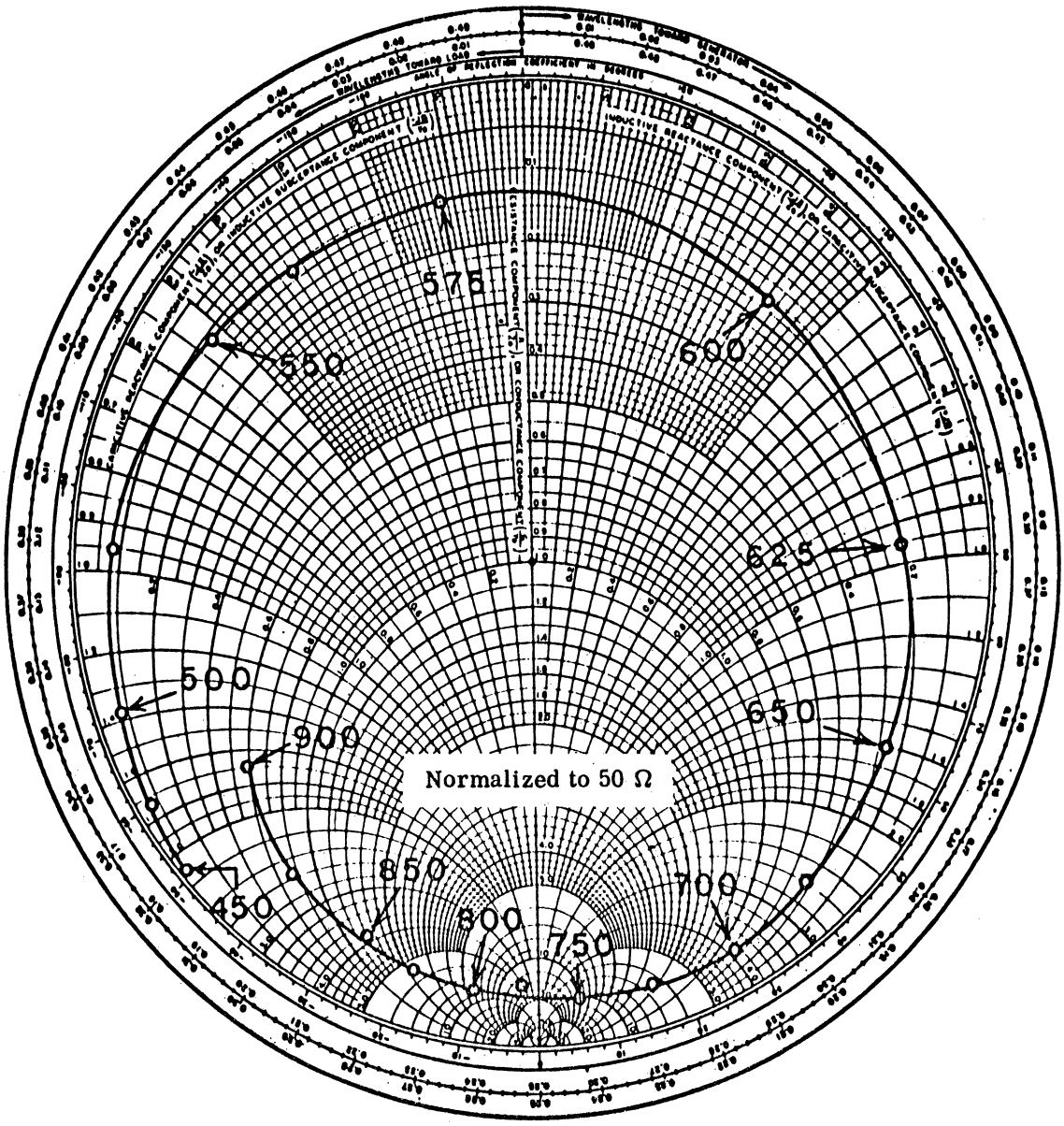

FIG. 4-15: INPUT IMPEDANCE WITH 3 ELEMENTS (d = 0.6 cm, Experimental).

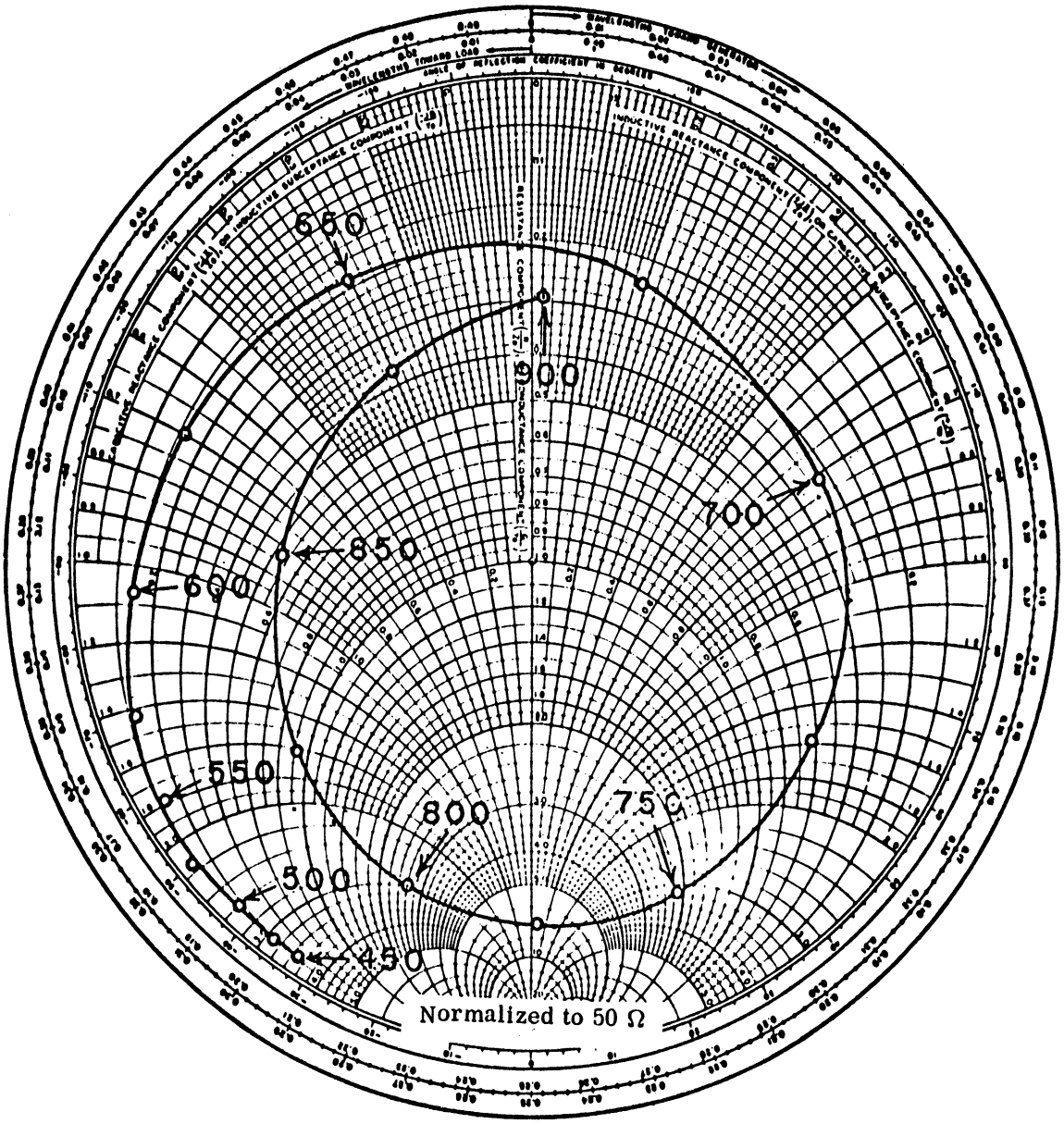

FIG. 4-16: INPUT IMPEDANCE WITH 3 ELEMENTS (d = 1.2 cm, Experimental).

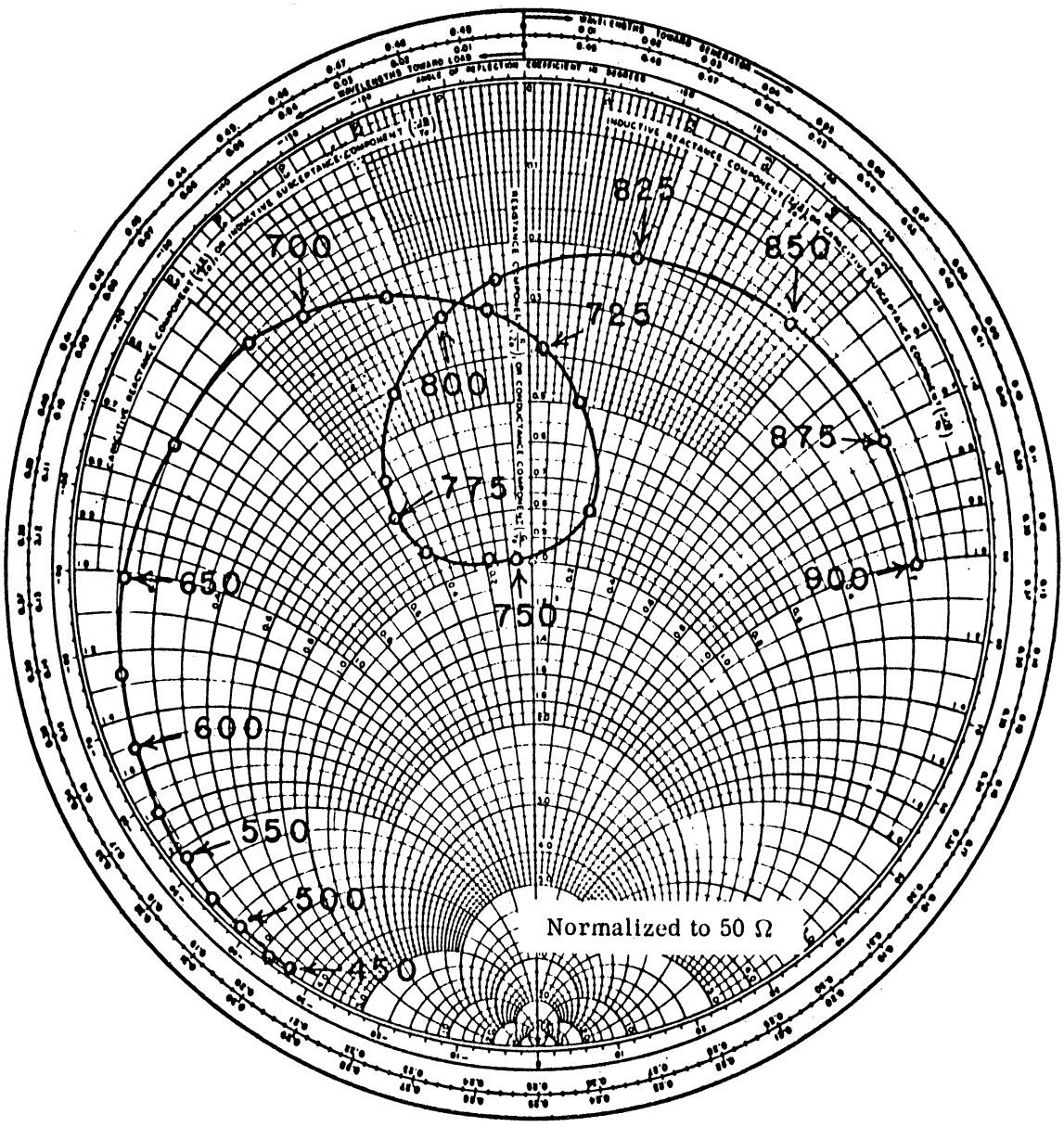

FIG. 4-17: INPUT IMPEDANCE WITH 3 ELEMENTS (d = 2.4 cm, Experimental).

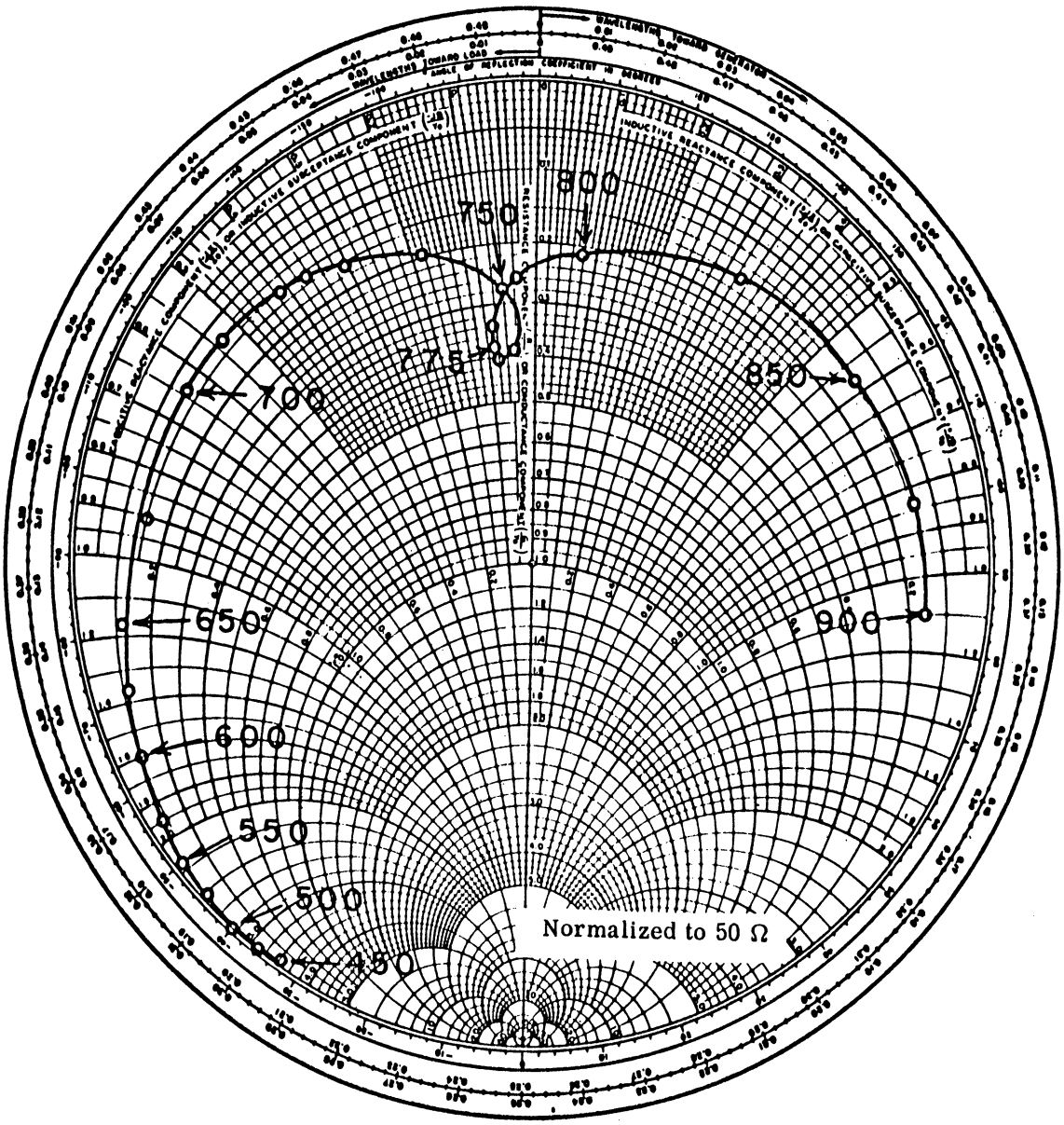

FIG. 4-18: INPUT IMPEDANCE WITH 3 ELEMENTS (d = 3.6 cm, Experimental).

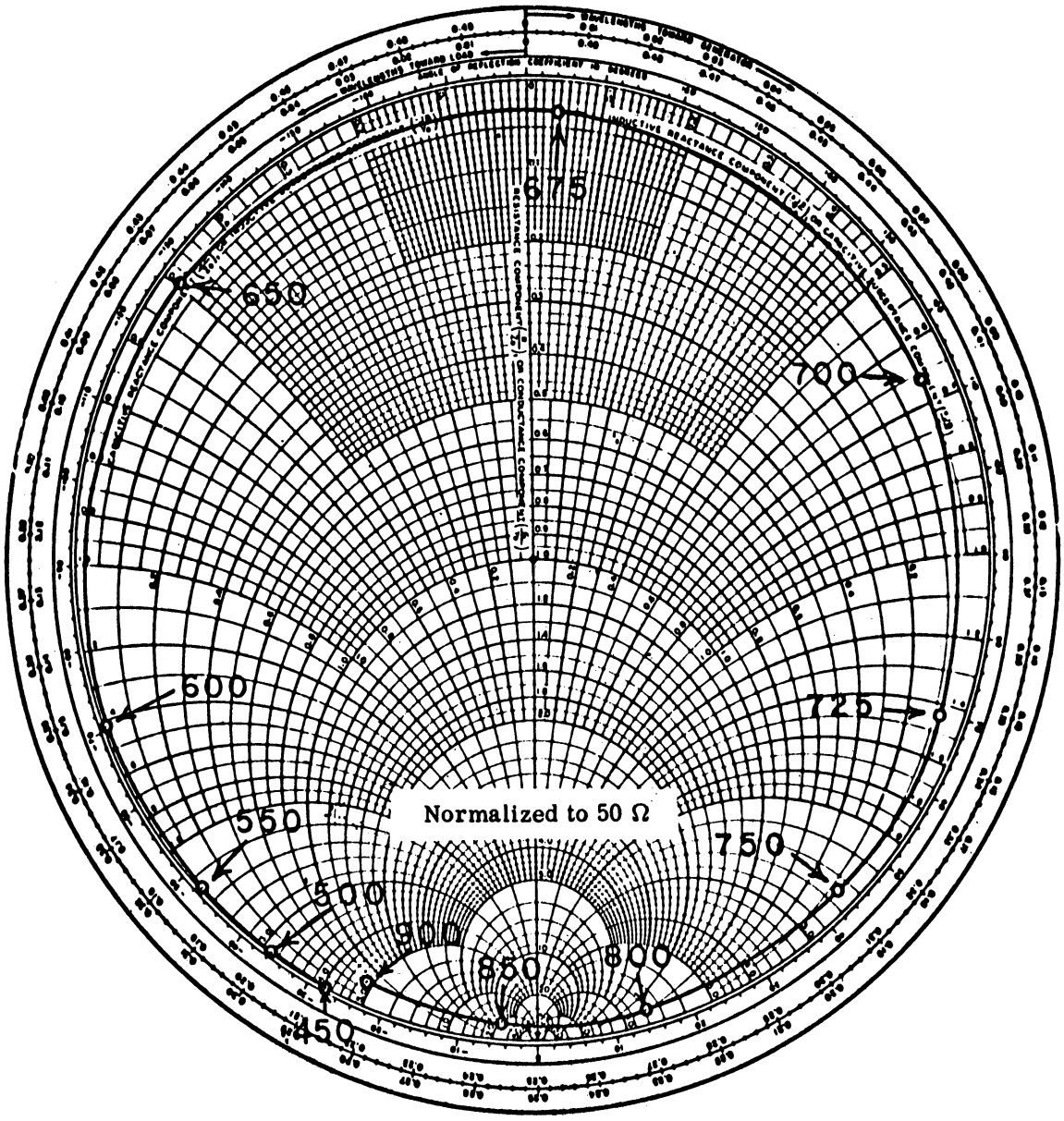

FIG. 4-19: INPUT IMPEDANCE WITH 3 ELEMENTS (d = 0.6 cm, Theoretical).

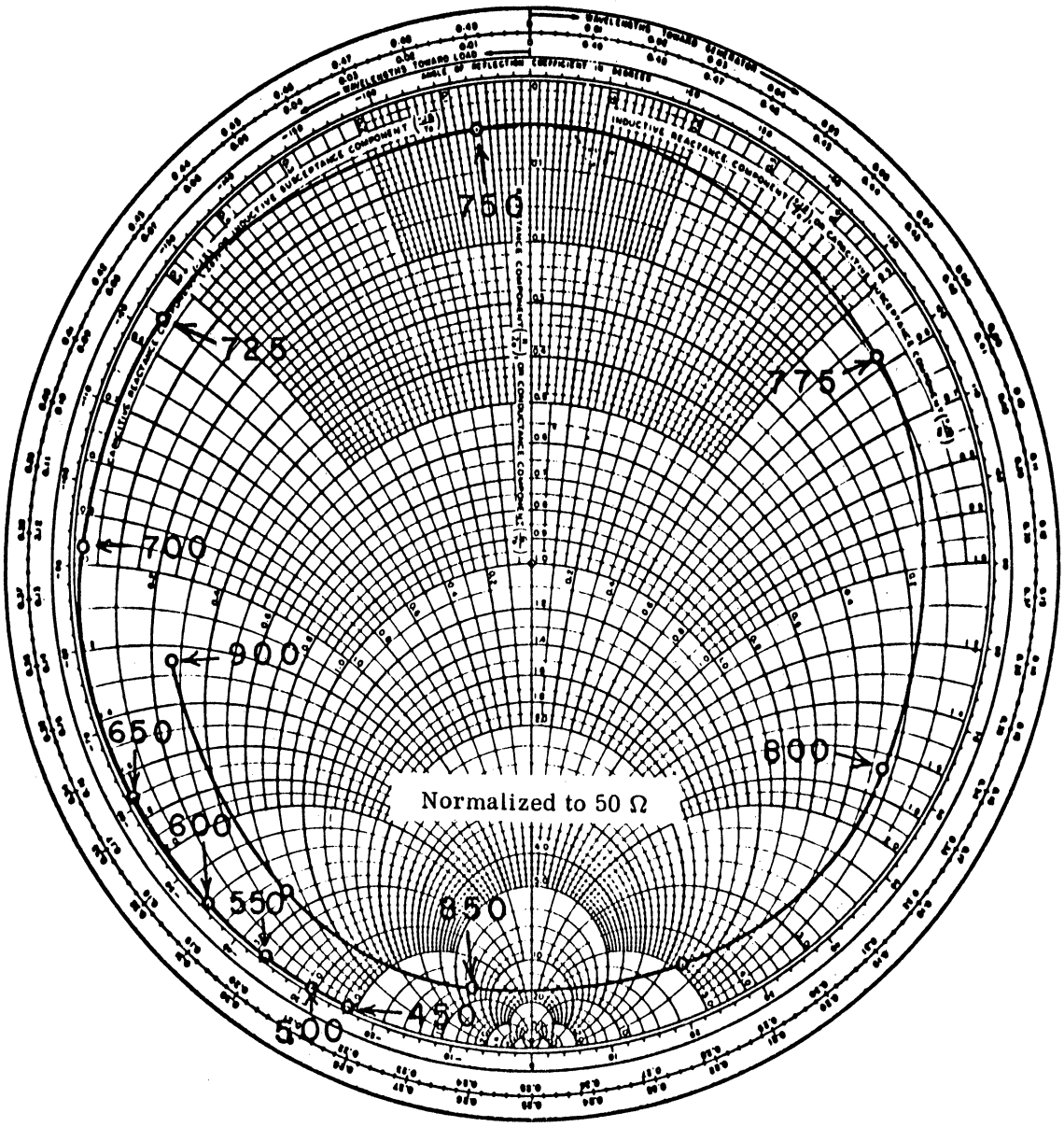

FIG. 4-20: INPUT IMPEDANCE WITH 3 ELEMENTS (d = 1.2 cm, Theoretical).

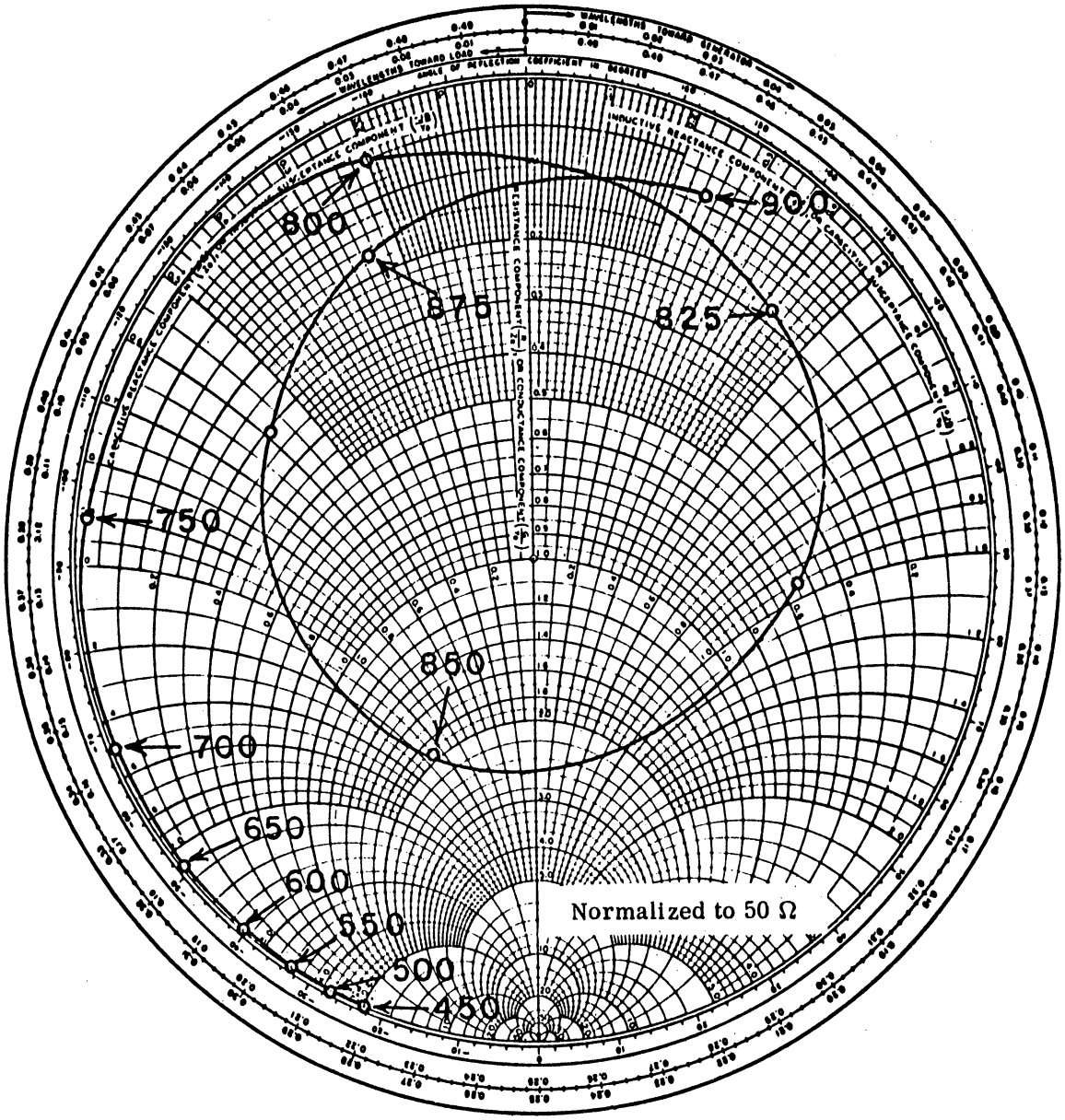

FIG. 4-21: INPUT IMPEDANCE WITH 3 ELEMENTS (d = 2.4 cm, Theoretical).

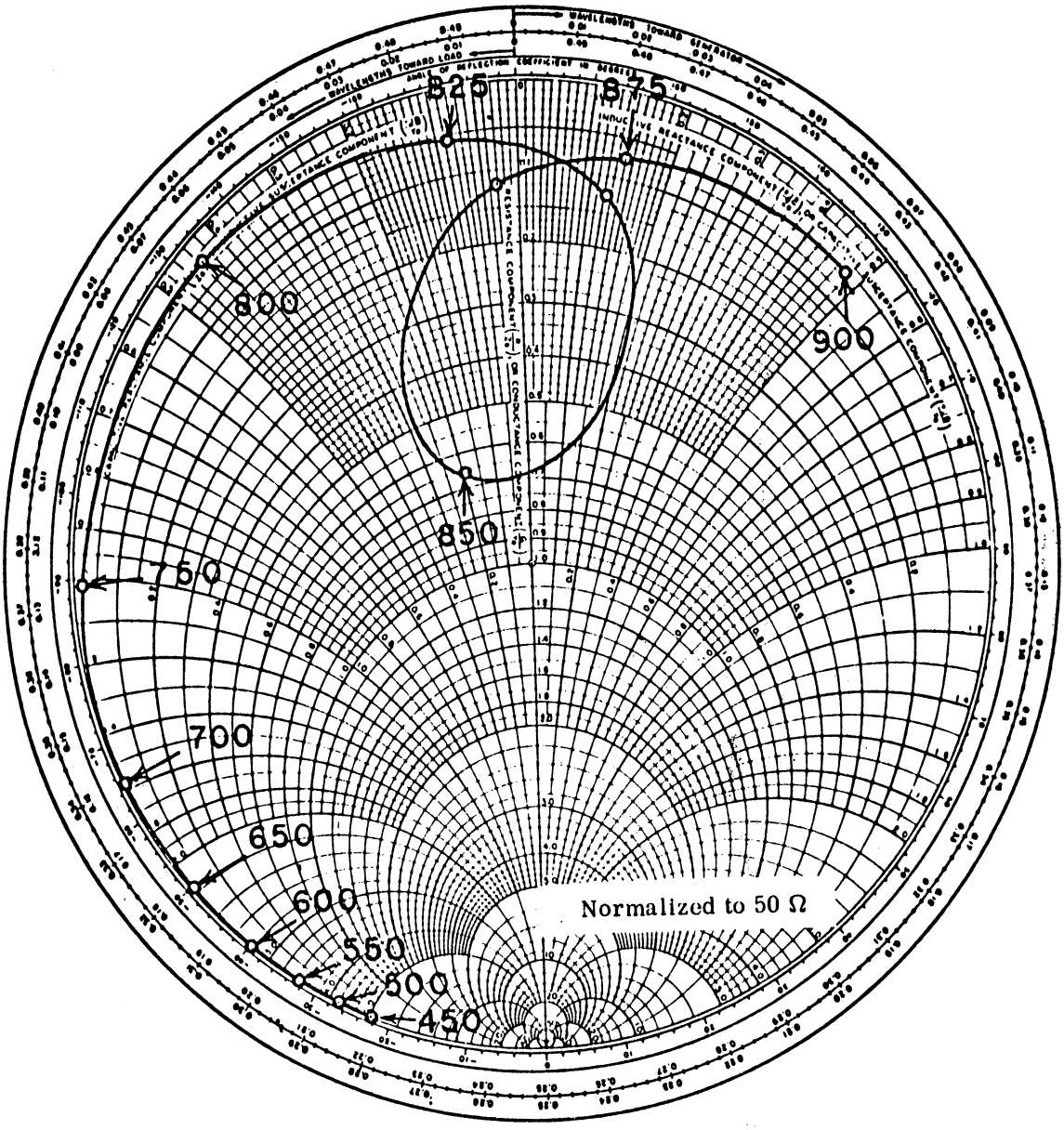

FIG. 4-22: INPUT IMPEDANCE WITH 3 ELEMENTS (d = 3.6 cm, Theoretical).

There is good agreement between theory and experiment in the general shape of the impedance curves. For d = 0.6 cm, the locus is approximately a circle. For d = 1.2 cm, the locus is beginning to form a loop. For d = 2.4 cm, a loop is formed, and for d = 3.6 cm, the loop is tighter. The variation in shape as d is increased is as expected, for the impedance curve must approach that of the driven element as d becomes large. In fact, if the loops are neglected in Figs. 4-18 and 4-22, the agreement between the experimental and theoretical curves with d = 3.6 cm and the experimental and theoretical curves of the driven element (Figs. 4-3 and 4-4) is already quite good.

Although there is good agreement between theory and experiment in the shape of the impedance curves, there are other differences. In general, the experimental impedance data points are closer to the center of the Smith chart than the theoretical data points for each antenna. This means that the experimental values for the magnitude of the reflection coefficient, ρ, are smaller than the theoretical values. This may be partially due to losses in the experimental setup.

It may be also noted that there is not a one to one correspondence in frequency between experiment and theory. Interestingly enough, points on the theoretical impedance curves are roughly 100 MHz higher in frequency than the corresponding points on the experimental impedance curves. The same type of difference between theory and experiment was also observed for the driven element in section 4.2. For the driven element, the theoretical data points were roughly 50 MHz higher in frequency than the corresponding experimental points.

The VSWR data for the four three-element interdigital arrays are presented in Figs. 4-23 through 4-26. Each figure contains experimental and theoretical data for one of the four antennas. Although the VSWR can never be less than one, the scales start at zero for convenience. The scales are also clipped at 50 (or 60) as explained in section 4.2.

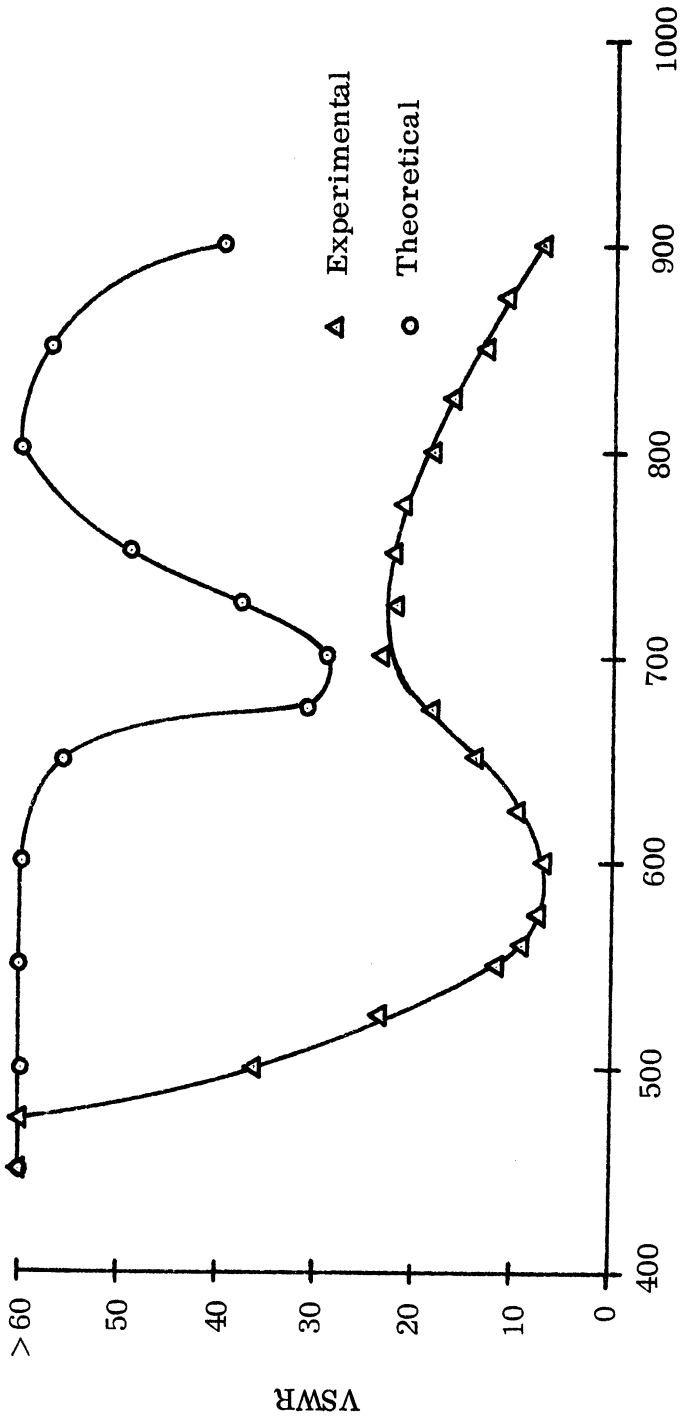

FIG. 4-23: VSWR WITH 3 ELEMENTS (d = 0.6 cm).

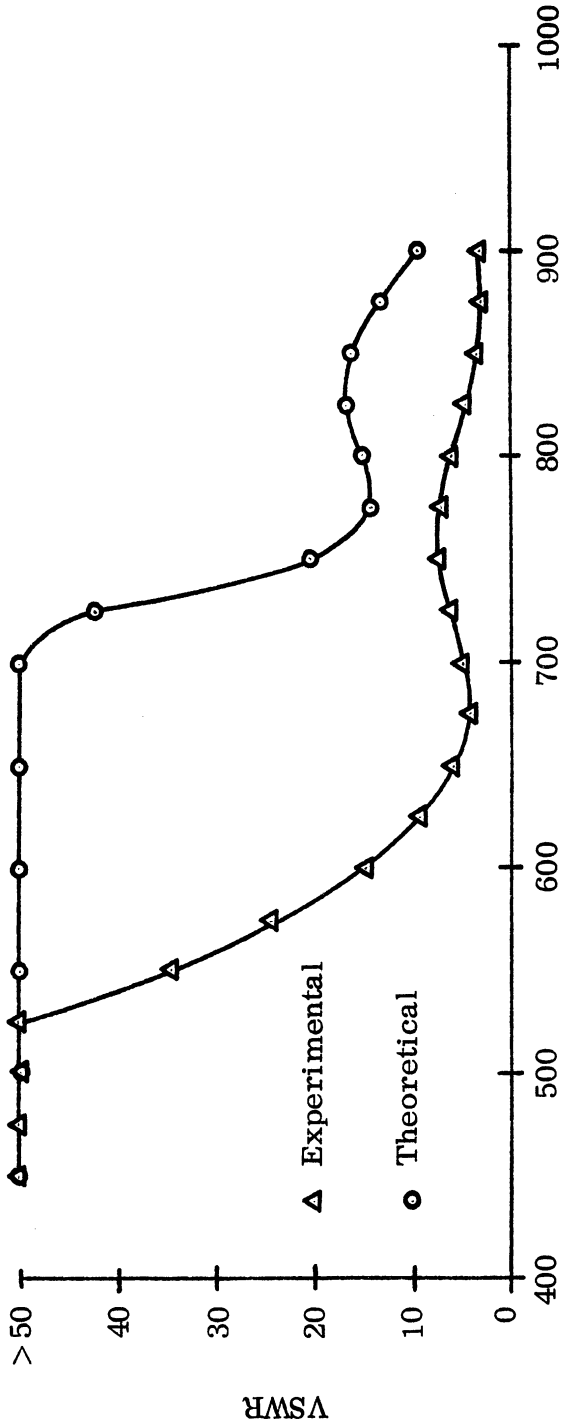

FIG. 4-24: VSWR WITH 3 ELEMENTS (d = 1.2 cm).

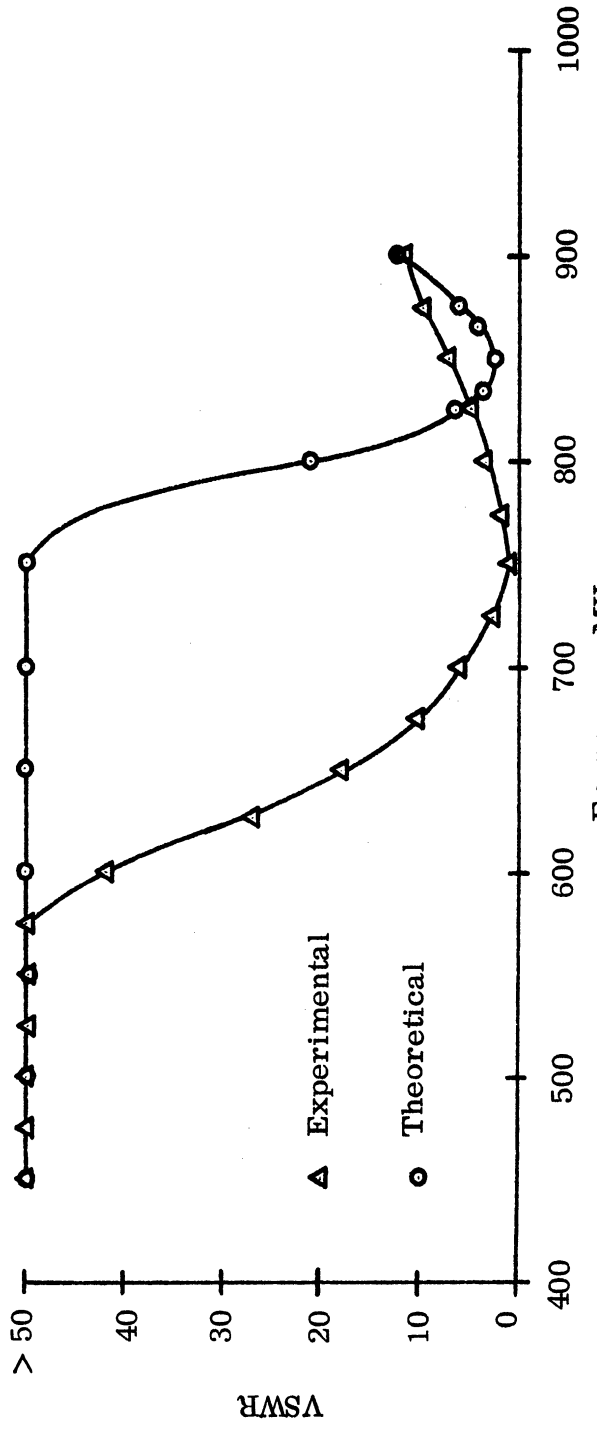

FIG. 4-25: VSWR WITH 3 ELEMENTS (d = 2.4 cm).

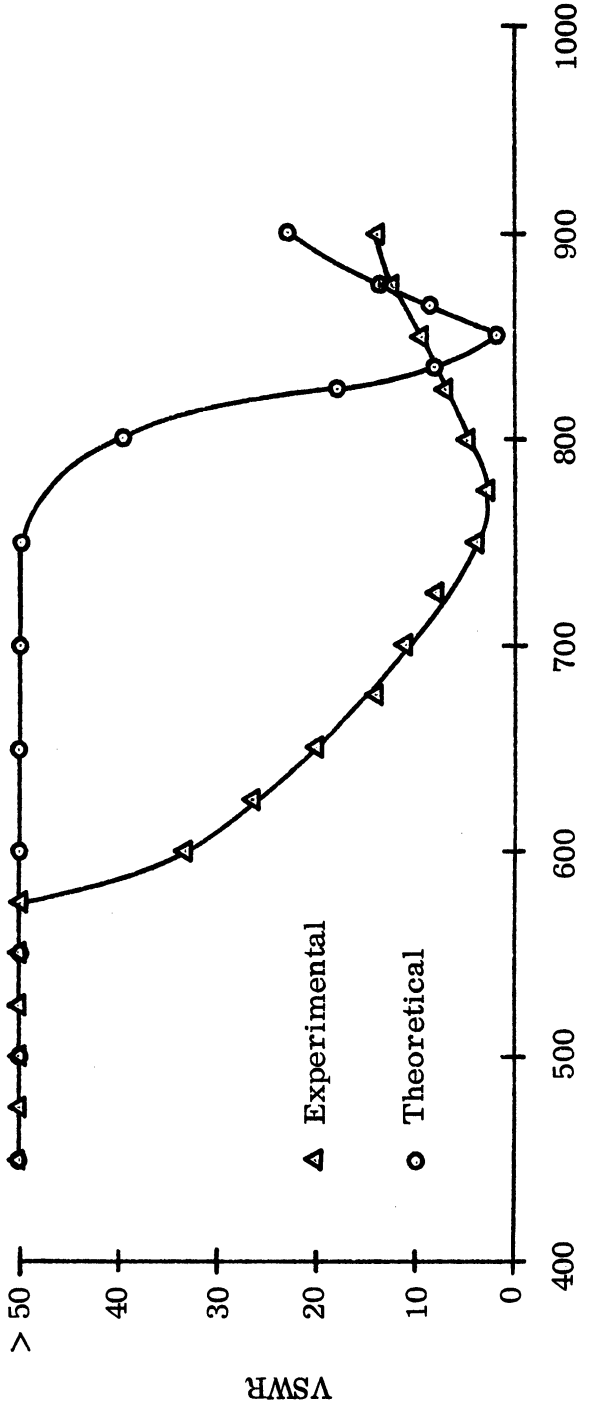

FIG. 4-26: VSWR WITH 3 ELEMENTS (d = 3.6 cm).

The experimental radiation patterns are presented in Figs. 4-27 through 4-42. Patterns at four frequencies have been selected for each antenna. These patterns can be compared with the theoretical patterns in the x-z and y-z planes in Figs. 3-20 through 3-27. Because the experimental patterns are actually power patterns (corresponding to E^2), they appear to be more pointed than the theoretical patterns. Notice how the maximum of the E_θ patterns is inclined by the small ground plane.

In the x - z plane, the experimental patterns confirm the cross-polarization which was predicted theoretically. Large ratios of E_ϕ/E_θ indeed do occur. For example in Fig. 4-27, E_ϕ is seen to completely dominate E_θ. The theoretical prediction in Chapter III was that the ratio of E_ϕ/E_θ first increases and then decreases as the frequency is increased for all four cases. Furthermore, as the spacing, d, is increased, it was predicted that the peak of the E_ϕ/E_θ ratio would occur at the higher frequency, but would last over a narrower bandwidth. The experimental patterns confirm these predictions very well. In Figs. 4-43 and 4-44 experimental and theoretical curves of the power ratio of $\left[E_\phi/E_\theta\right]^2$ in the x-z plane are plotted versus frequency. The two figures show the same type of behavior. The theoretical curves, however, do appear to have been shifted approximately 100 MHz higher in frequency relative to the experimental curves.

In the y - z plane, only the E_θ component exists. The experimental patterns in this plane agree quite well with the theoretical predictions. Of course the experimental pattern shape has been modified, especially near the y - axis, because of the small ground plane.

In general, the experimental data for the four three-element antennas agree quite well with the theoretical data from Chapter III. The factors which contribute to the differences between theory and experiment will be discussed in Chapter V. The addition of the two parasitic elements to the driven element has definitely improved the antenna. The spacing of d = 1.2 cm appears to be the best.

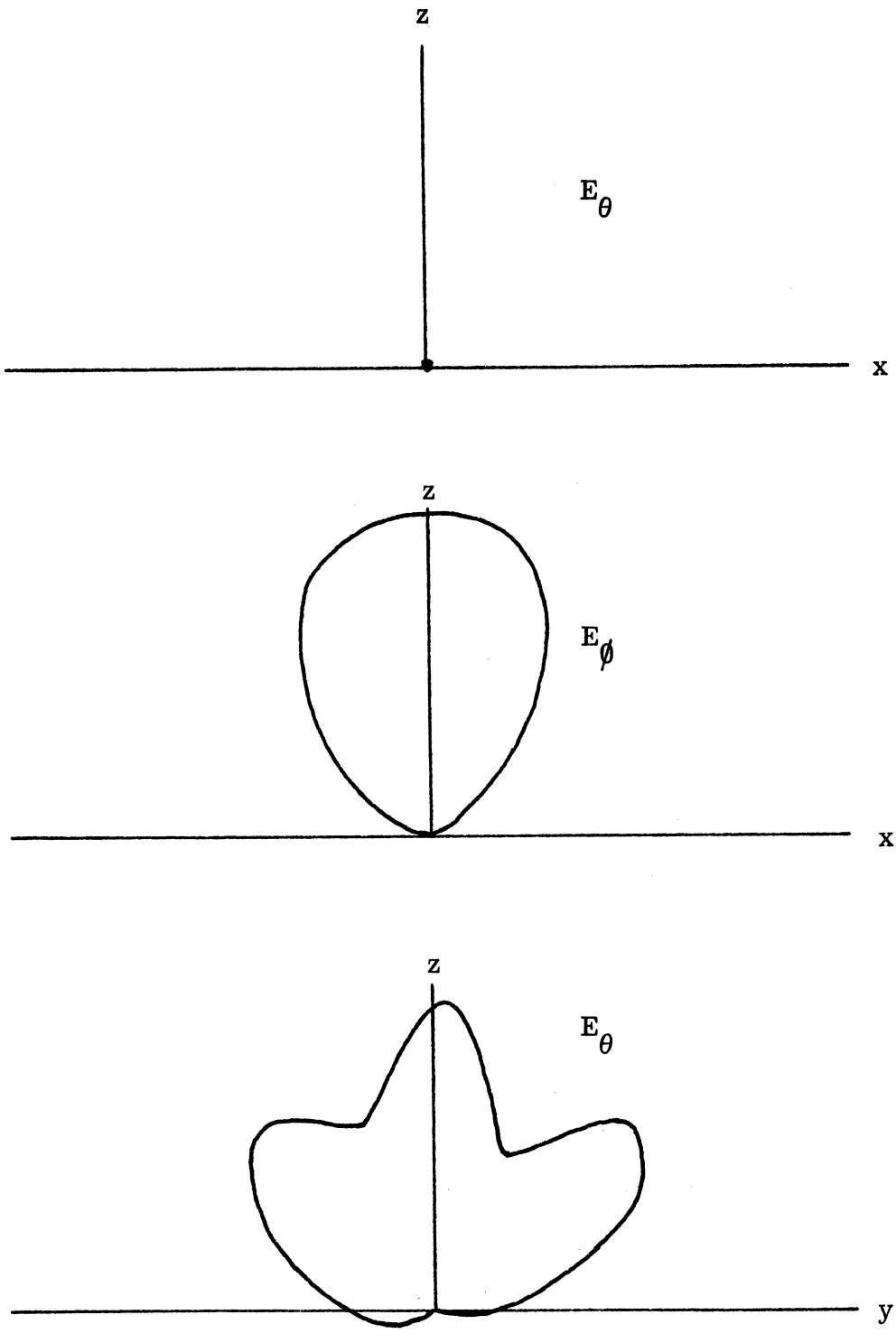

FIG. 4-27: 3 ELEMENTS (d = 0.6 cm, f = 500 MHz).

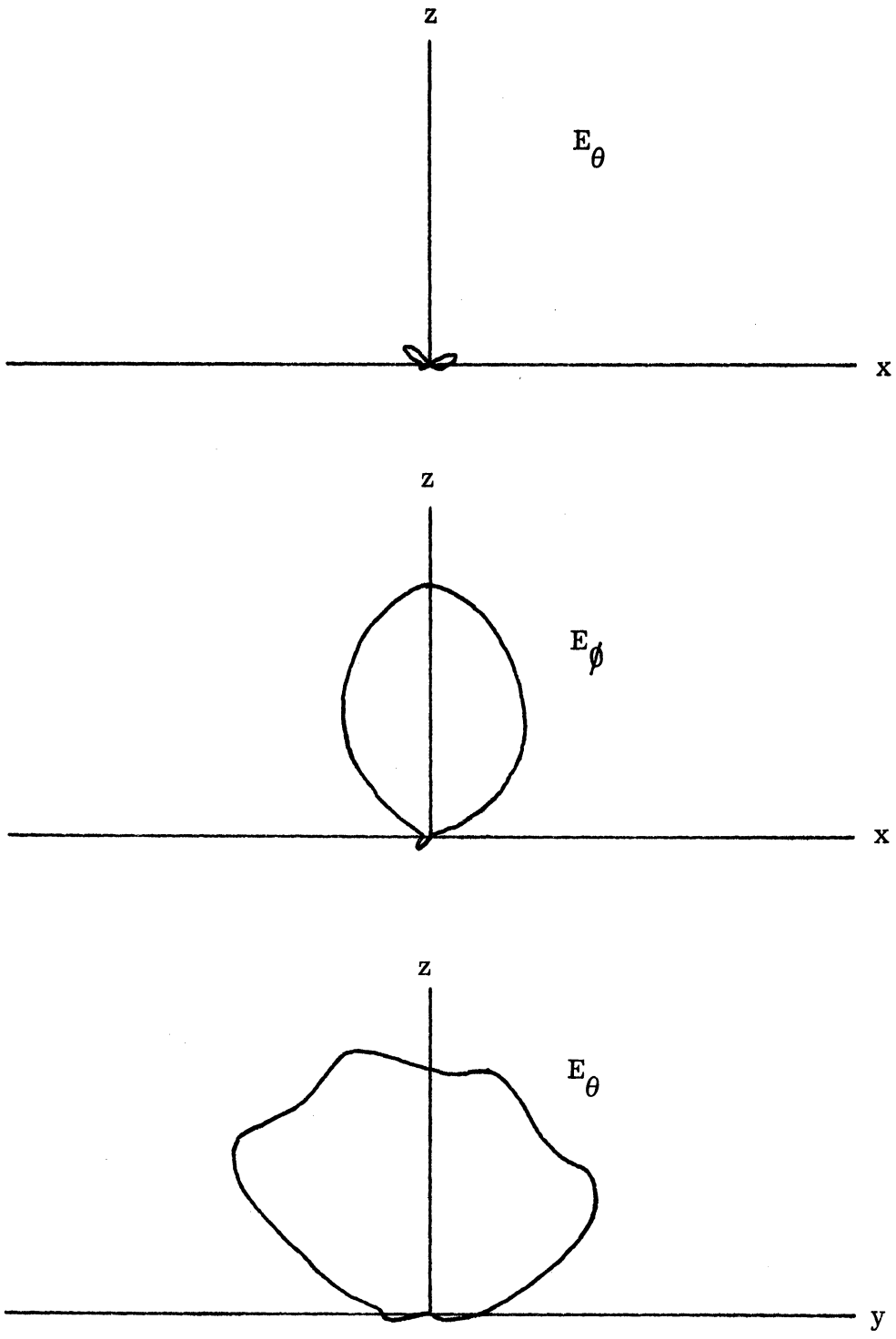

FIG. 4-28: 3 ELEMENTS (d = 0.6 cm, f = 650 MHz.)

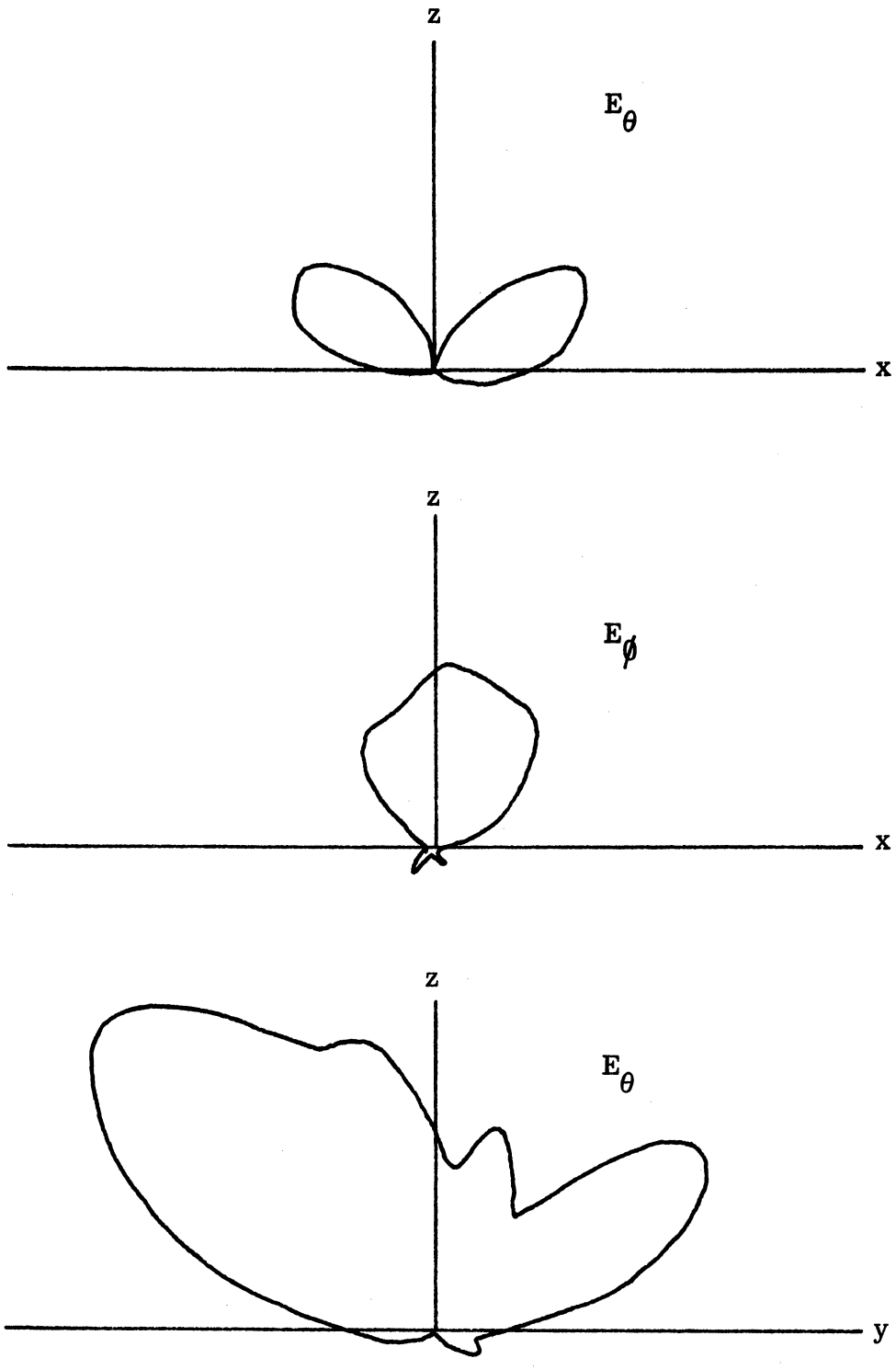

FIG. 4-29: 3 ELEMENTS (d = 0.6 cm, f = 750 MHz).

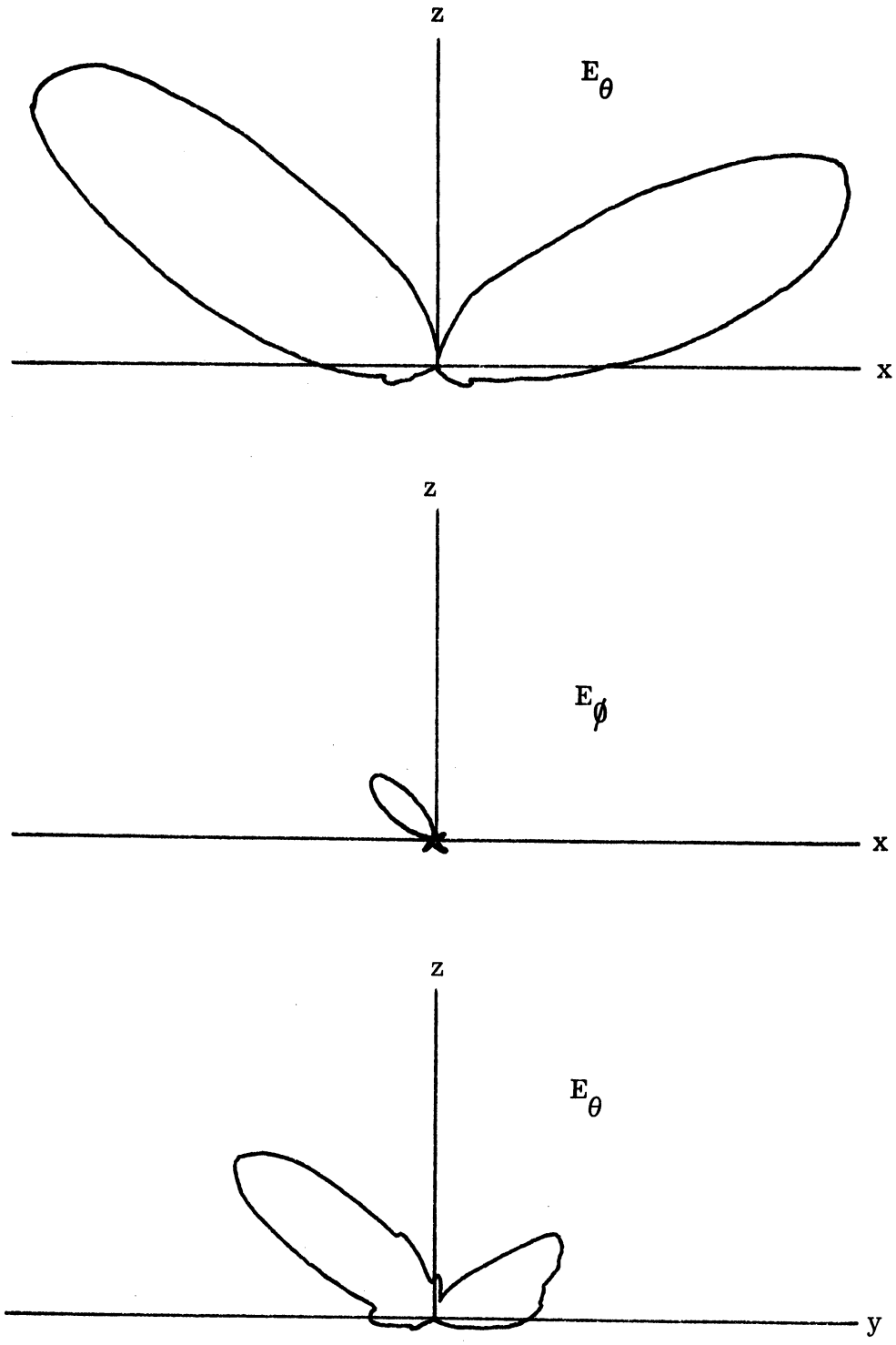

FIG. 4-30: 3 ELEMENTS (d = 0.6 cm, f = 900 MHz).

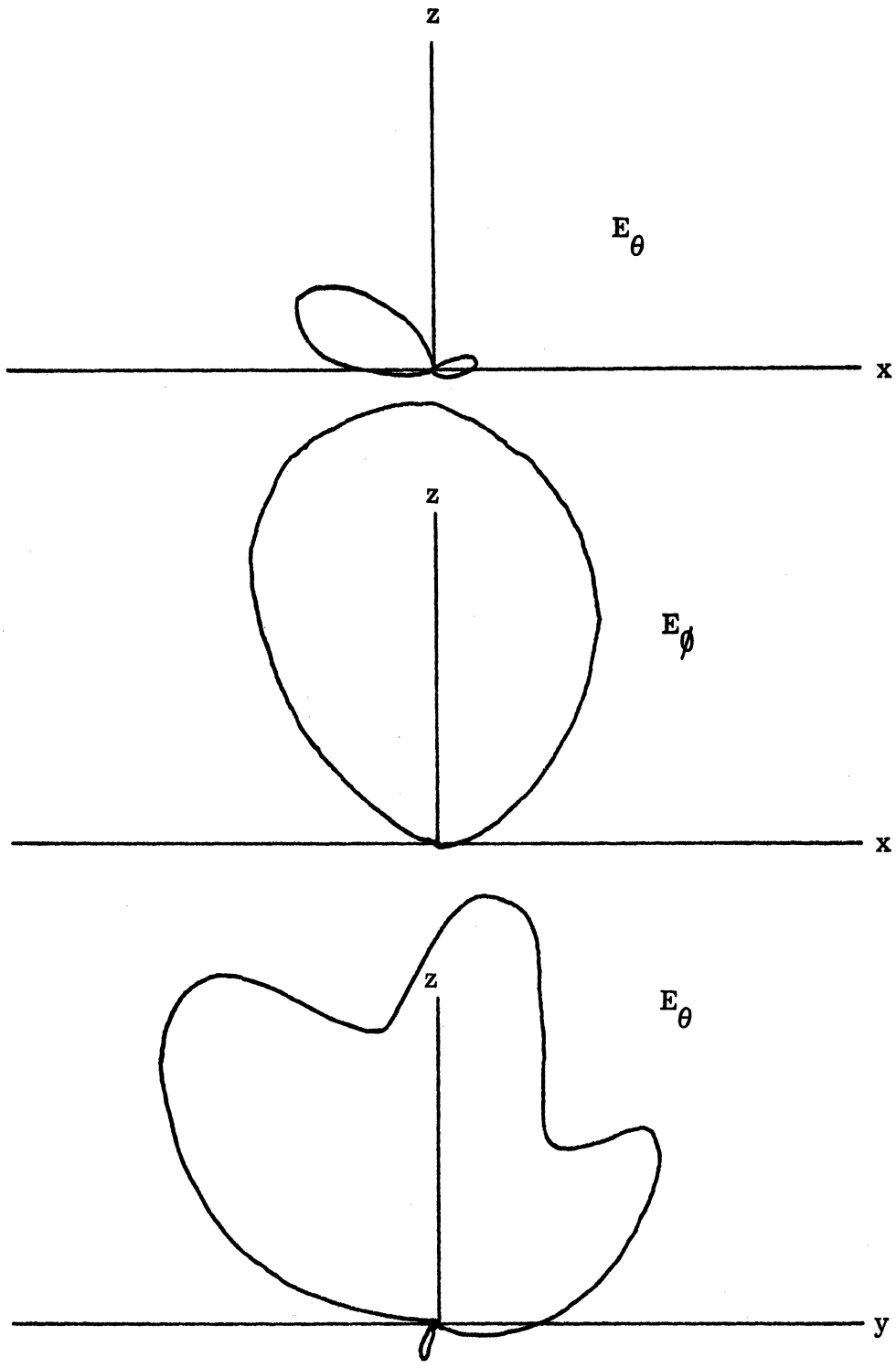

FIG. 4-31: 3 ELEMENTS (d = 1.2 cm, f = 500 MHz).

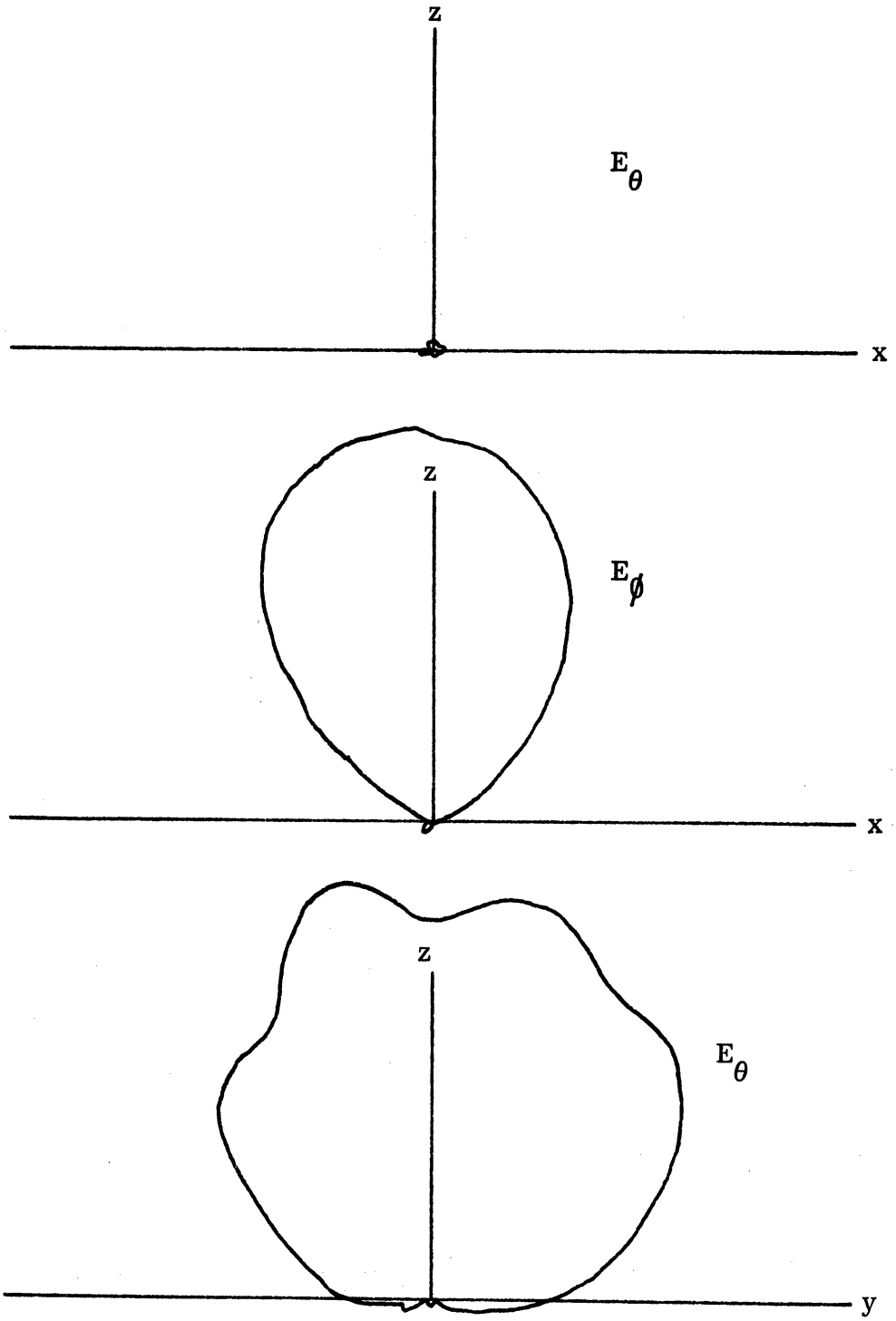

FIG. 4-32: 3 ELEMENTS (d = 1.2 cm, f = 600 MHz).

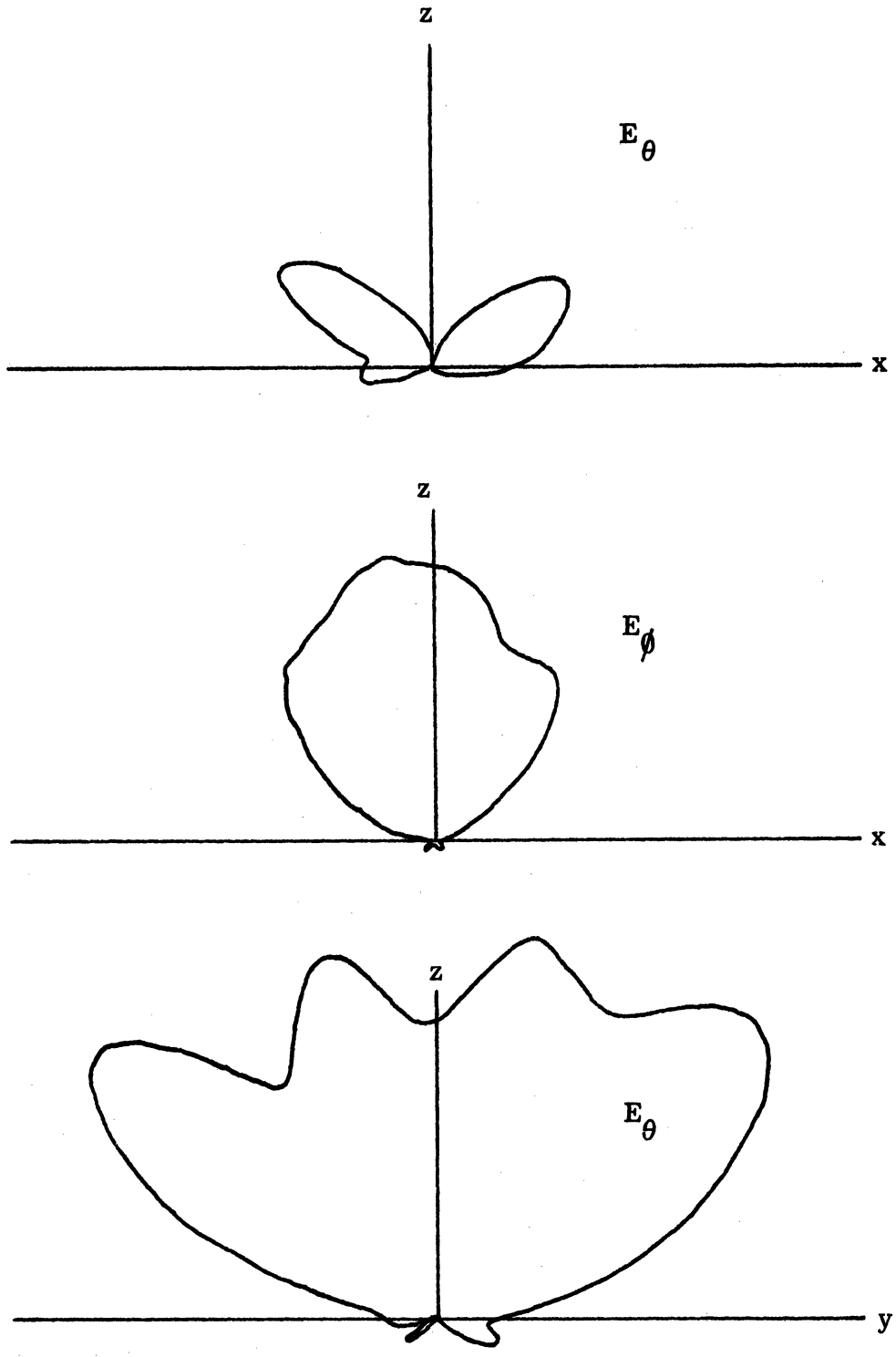

FIG. 4-33: 3 ELEMENTS (d = 1.2 cm, f = 750 MHz).

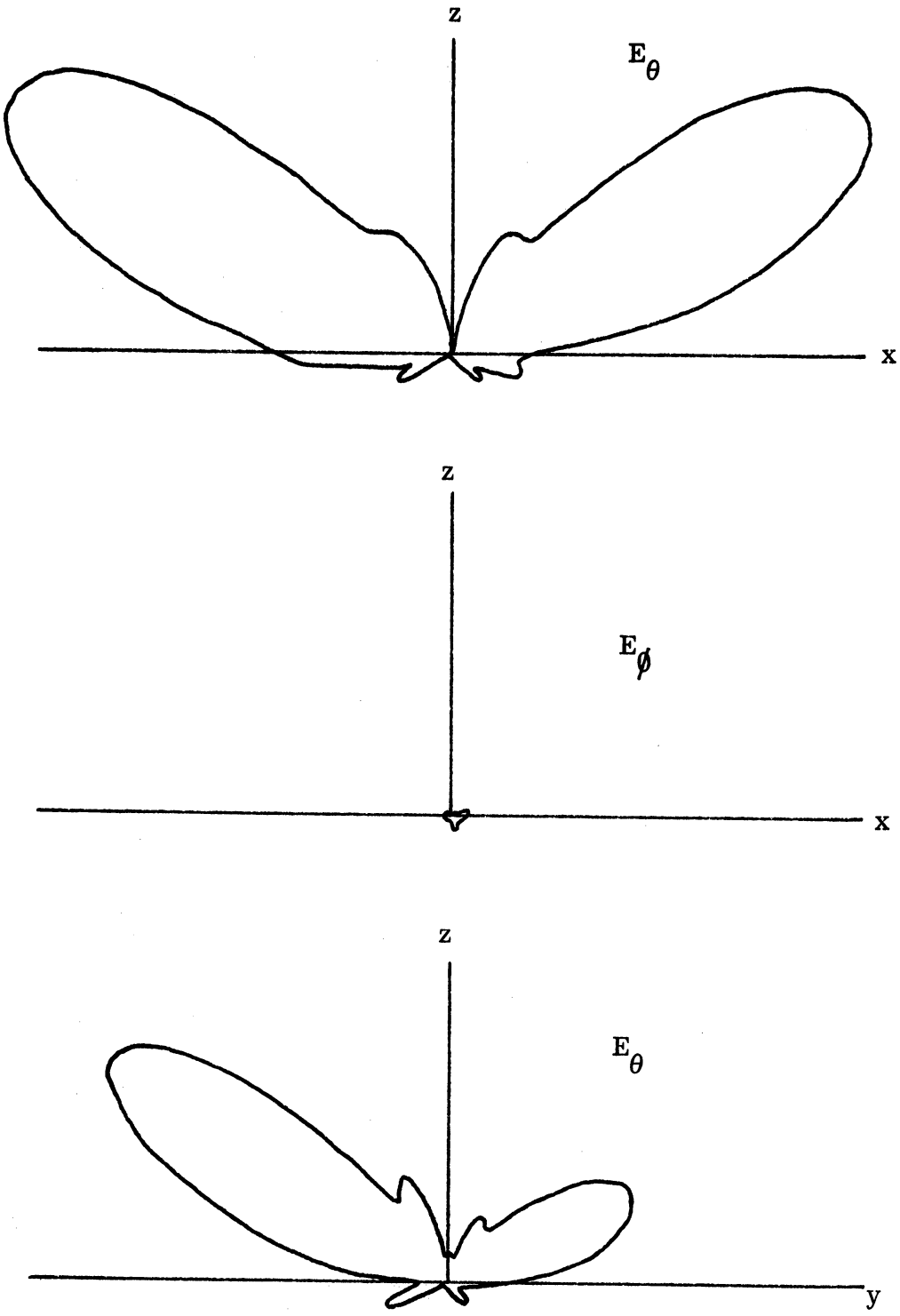

FIG. 4-34: 3 ELEMENTS (d= 1.2 cm, f = 900 MHz).

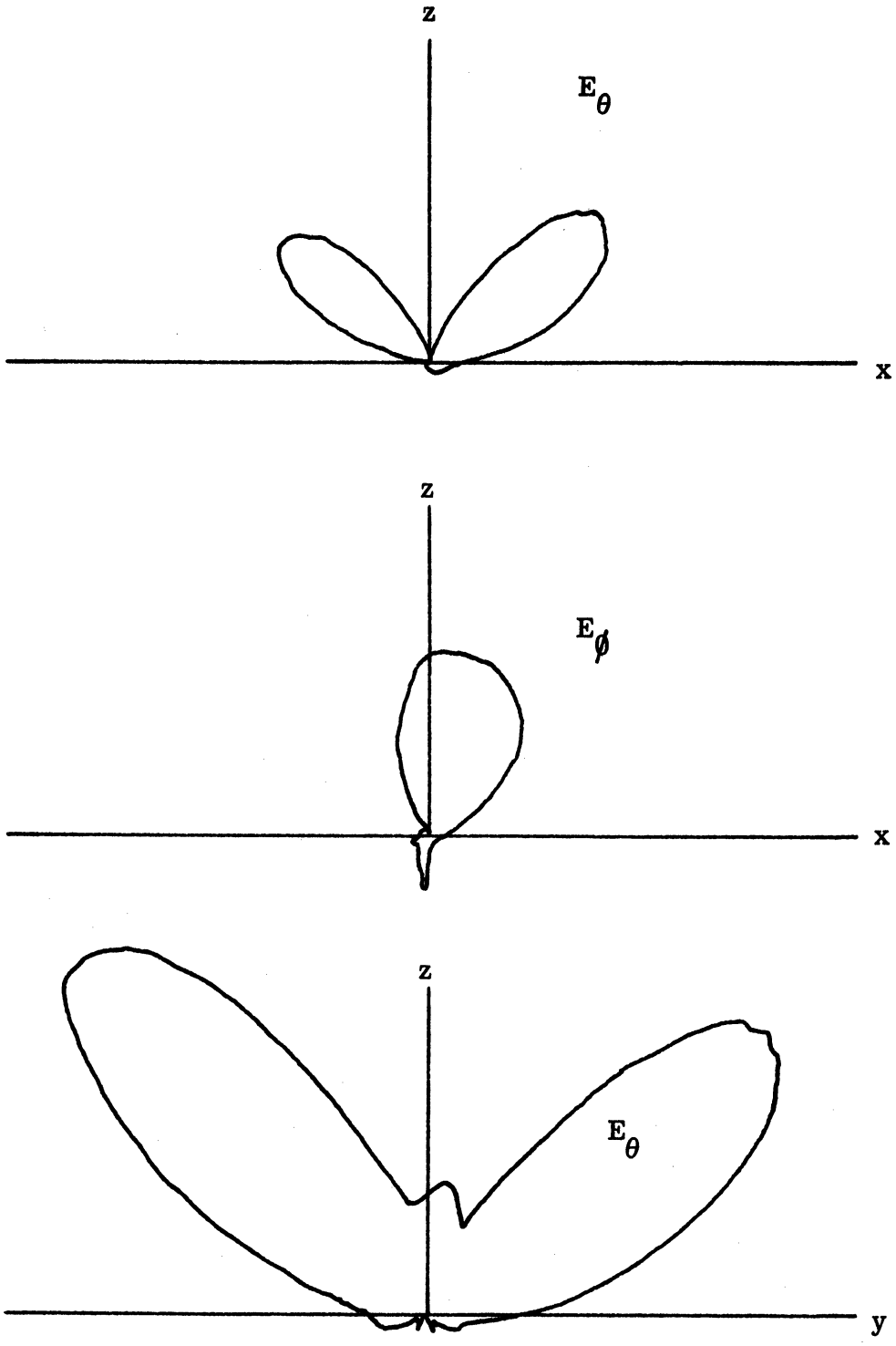

FIG. 4-35: 3 ELEMENTS (d = 2.4 cm, f = 450 MHz).

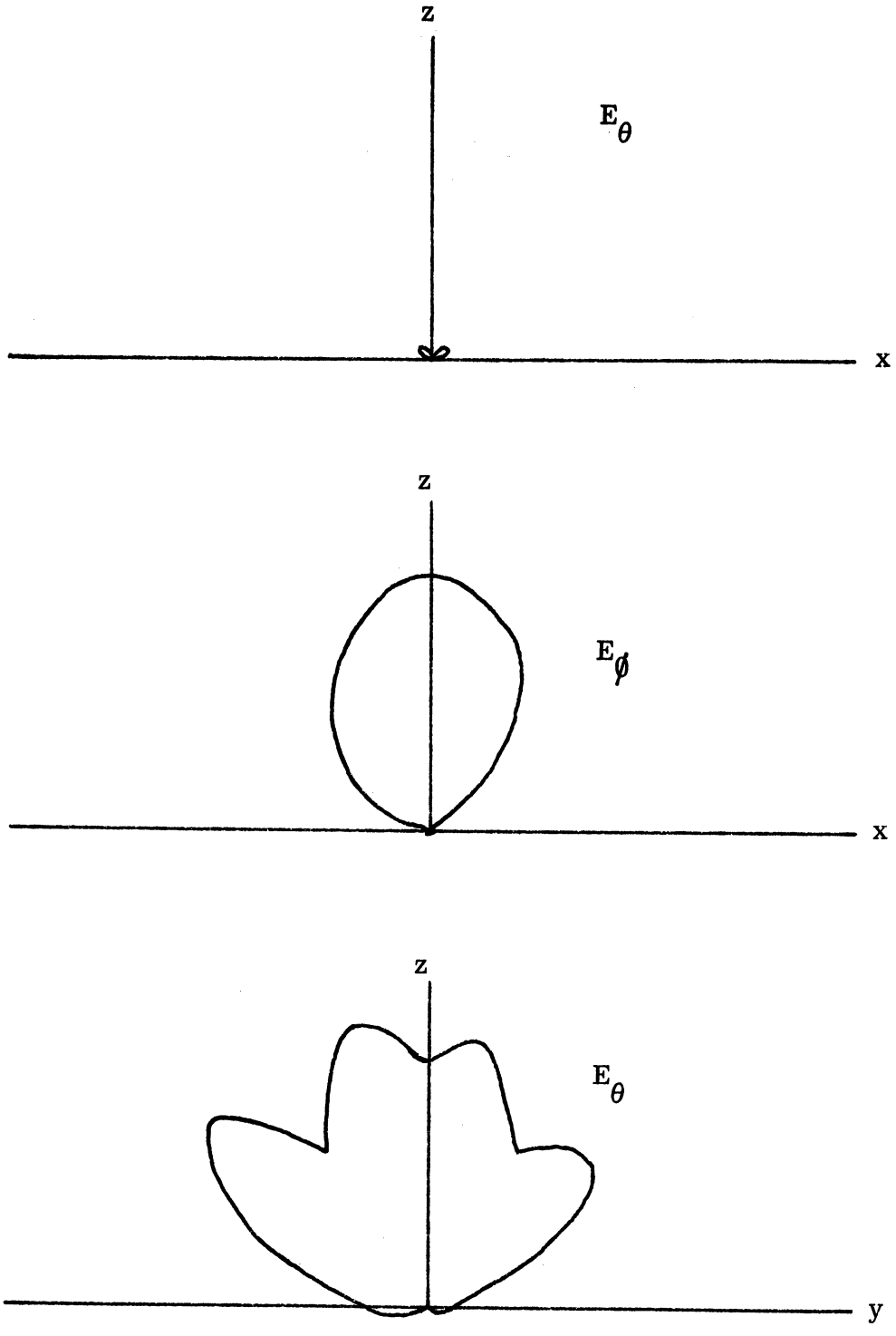

FIG. 4-36: 3 ELEMENTS (d = 2.4 cm, f = 650 MHz).

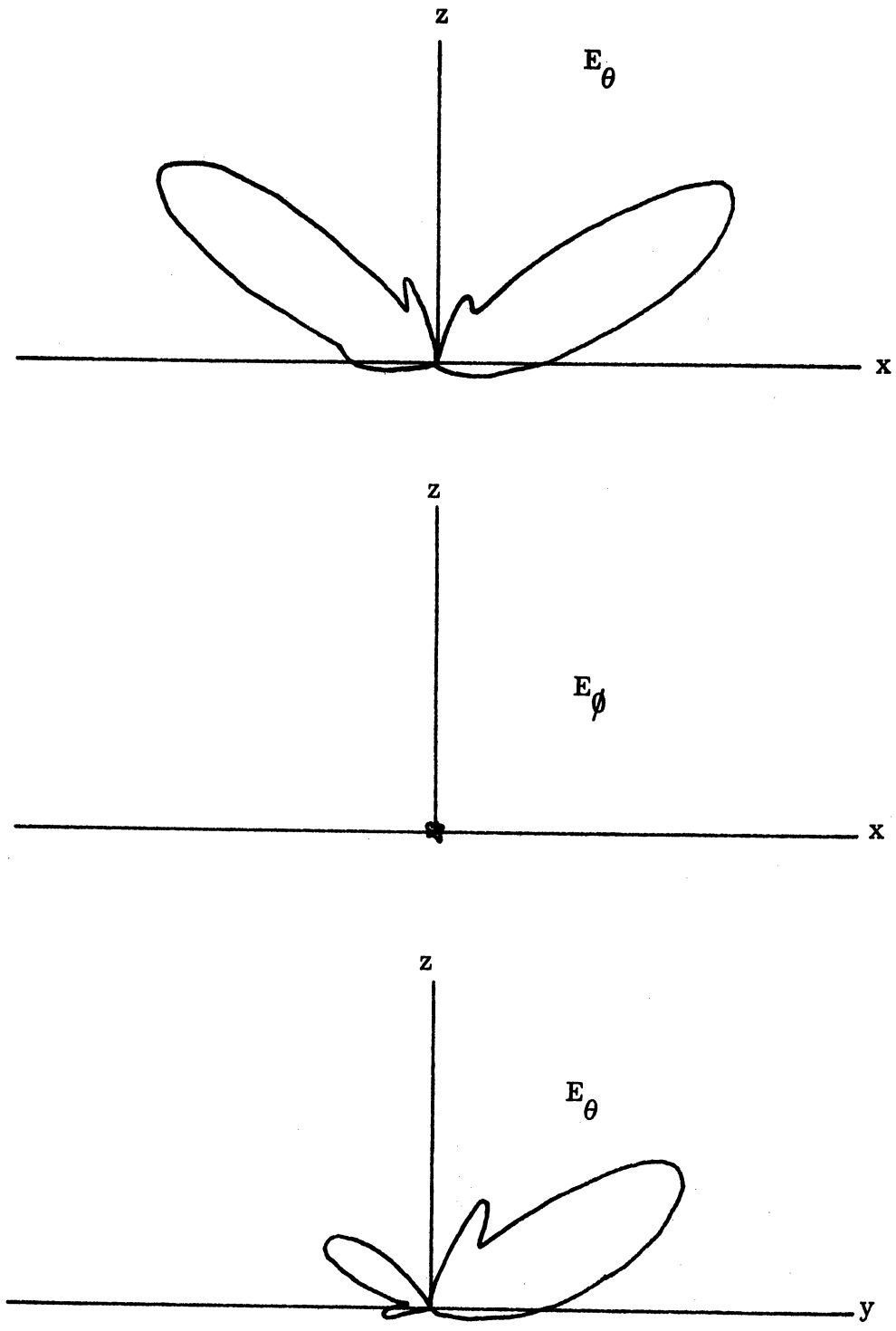

FIG. 4-37: 3 ELEMENTS (d = 2.4 cm, f = 800 MHz).

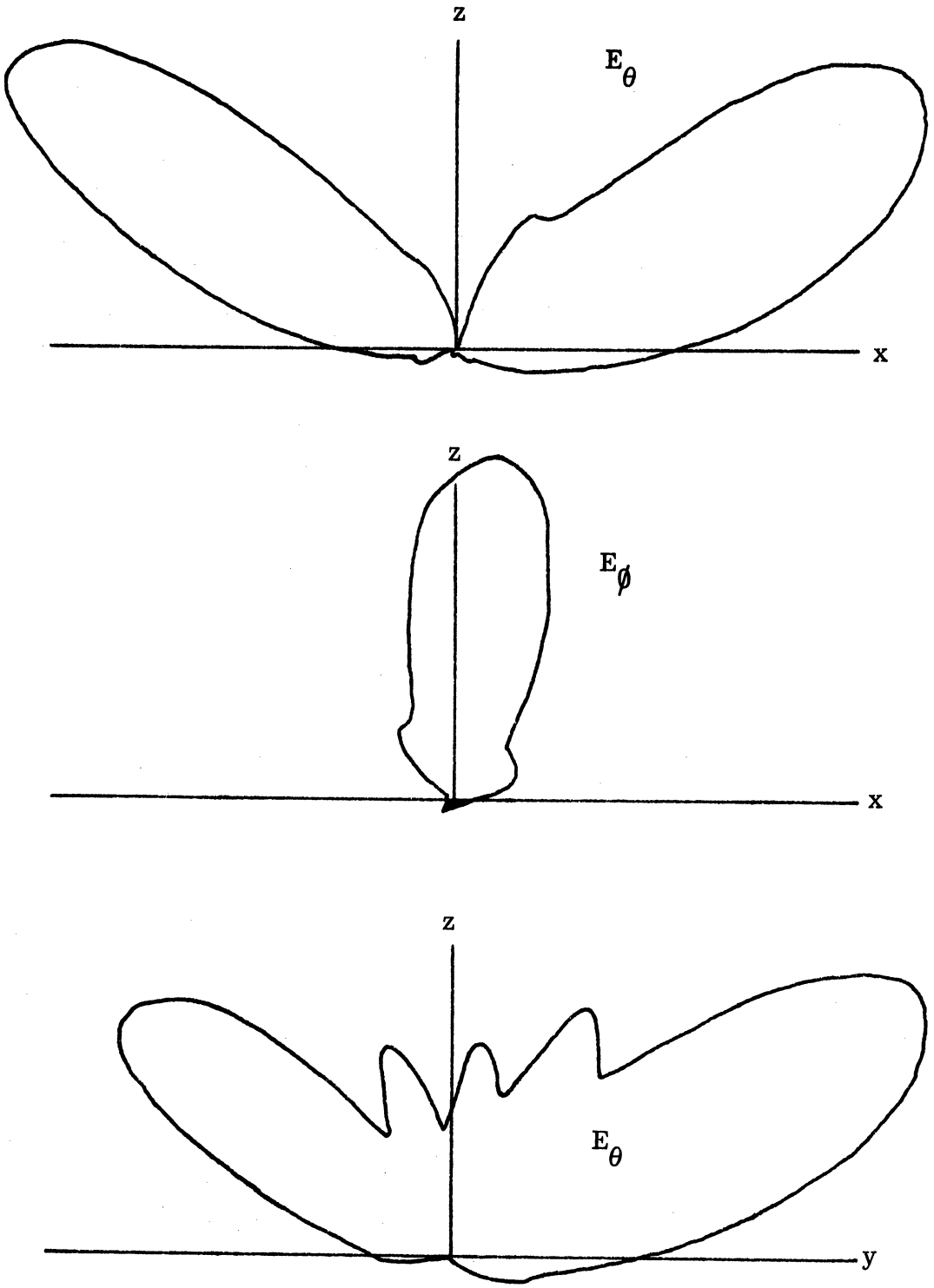

FIG. 4-38: 3 ELEMENTS (d = 2.4 cm, f = 900 MHz).

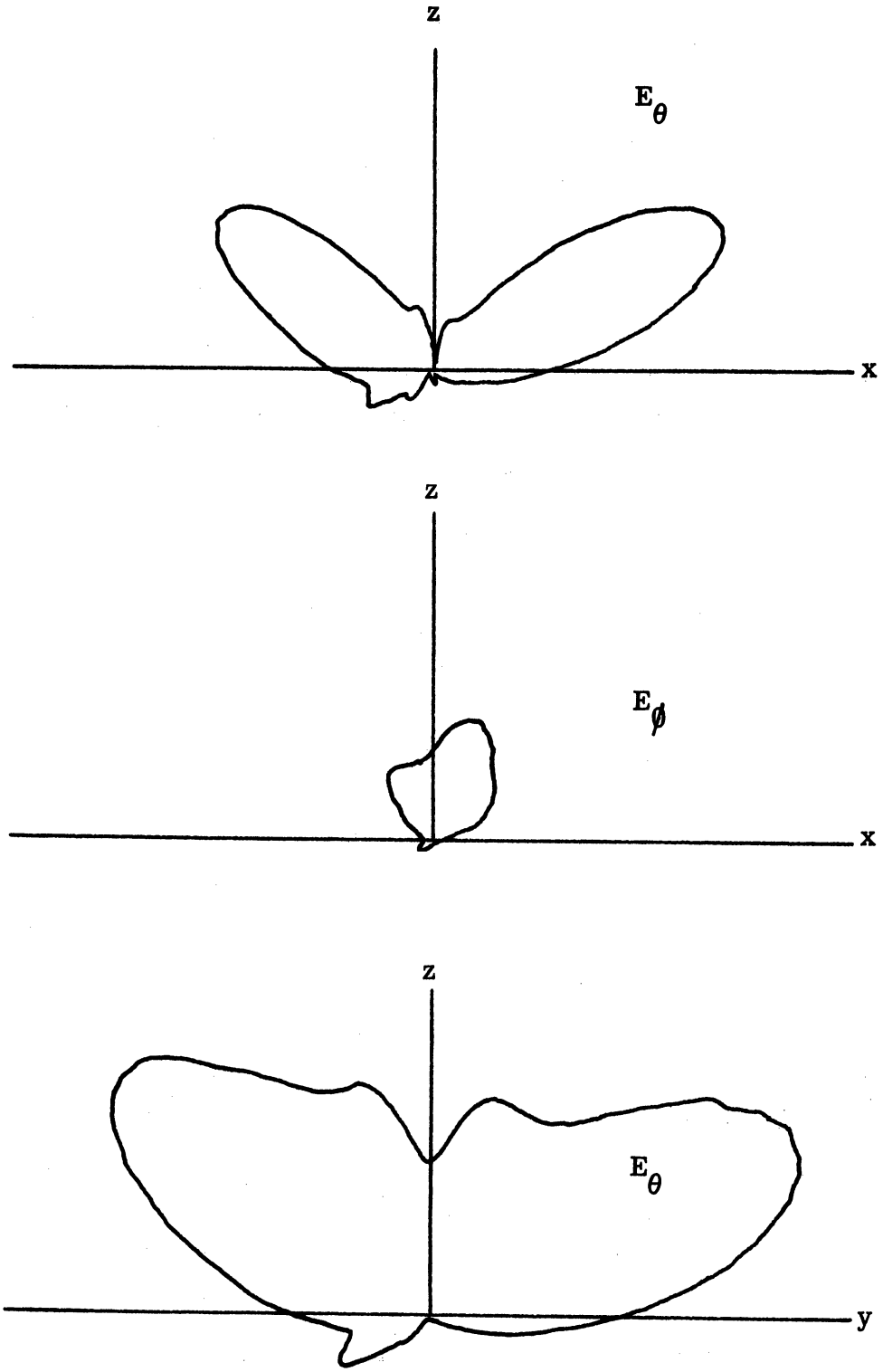

FIG. 4-39: 3 ELEMENTS (d = 3.6 cm, f = 550 MHz.)

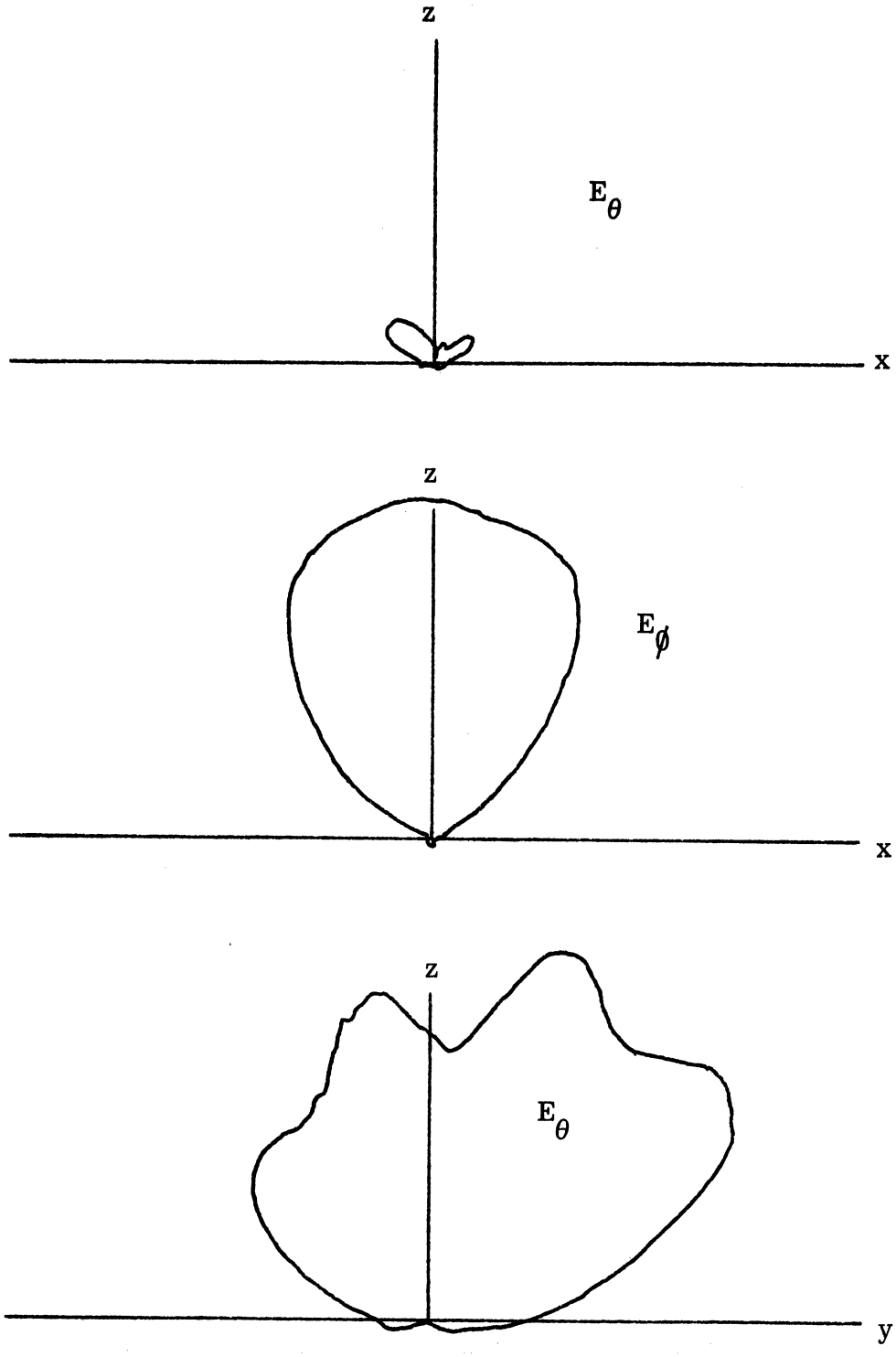

FIG. 4-40: 3 ELEMENTS (d = 3.6 cm, f = 700 MHz).

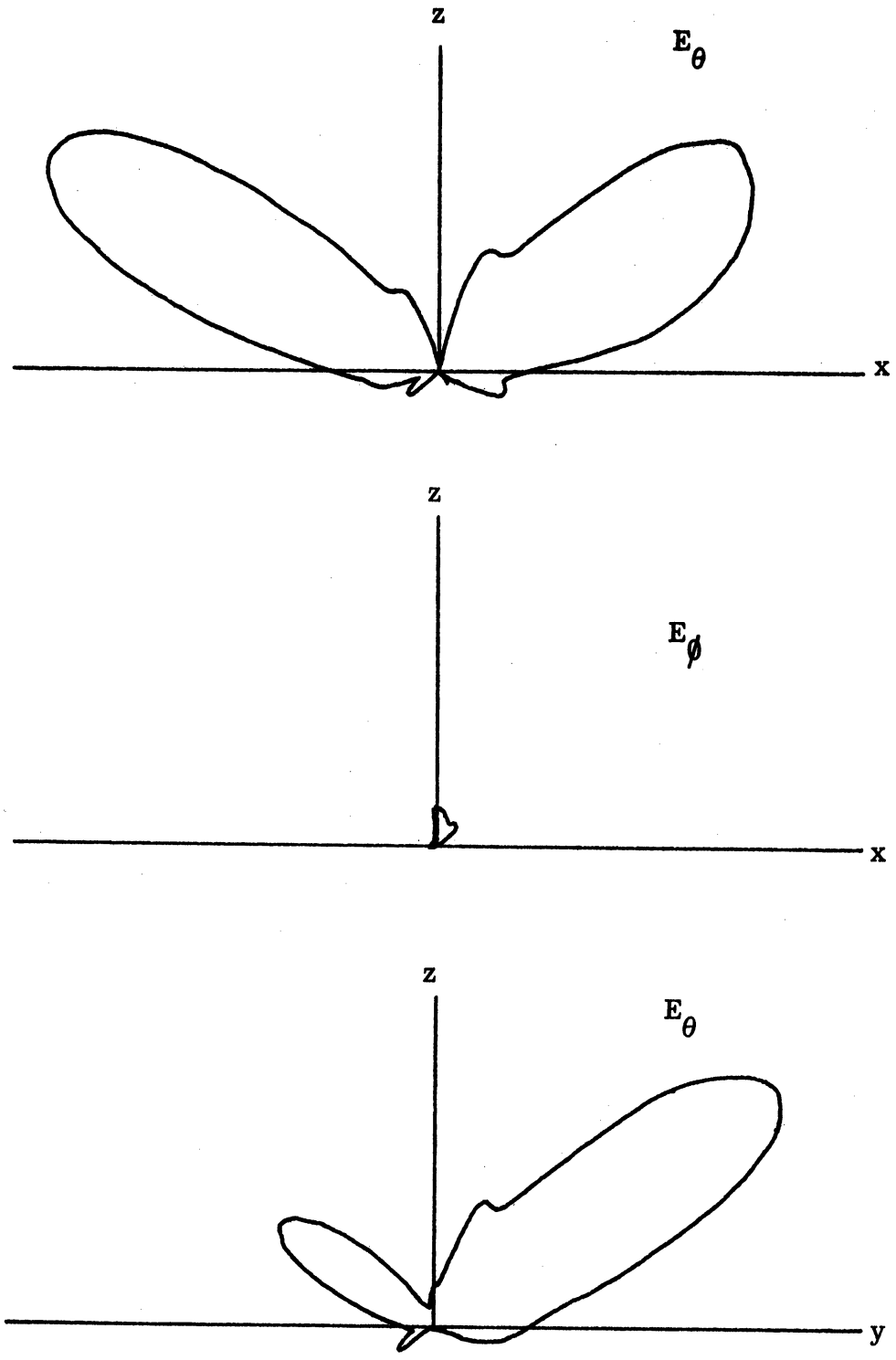

FIG. 4-41: 3 ELEMENTS (d = 3.6 cm, f = 800 MHz).

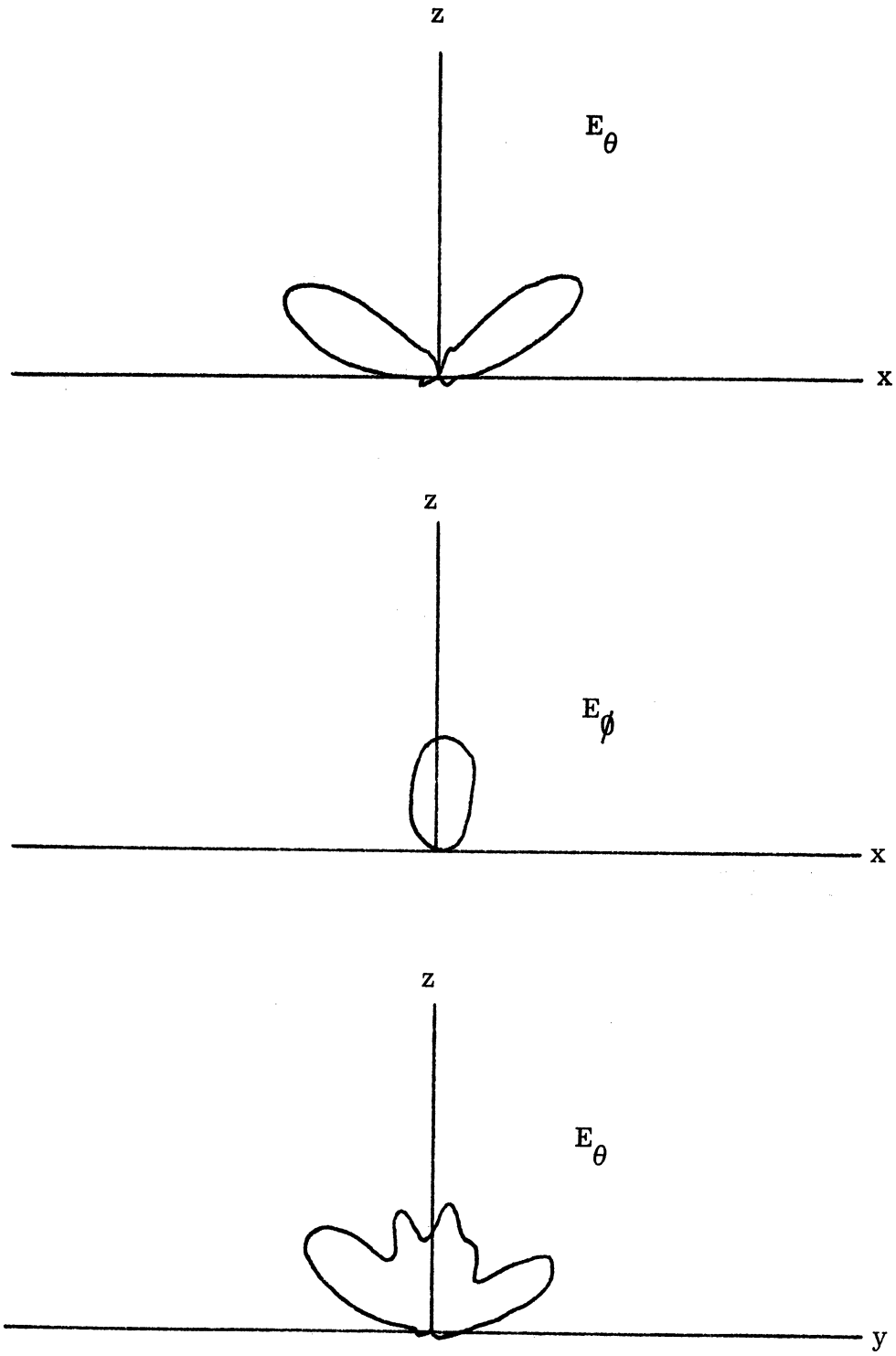

FIG. 4-42: 3 ELEMENTS (d = 3.6 cm, f = 900 MHz).

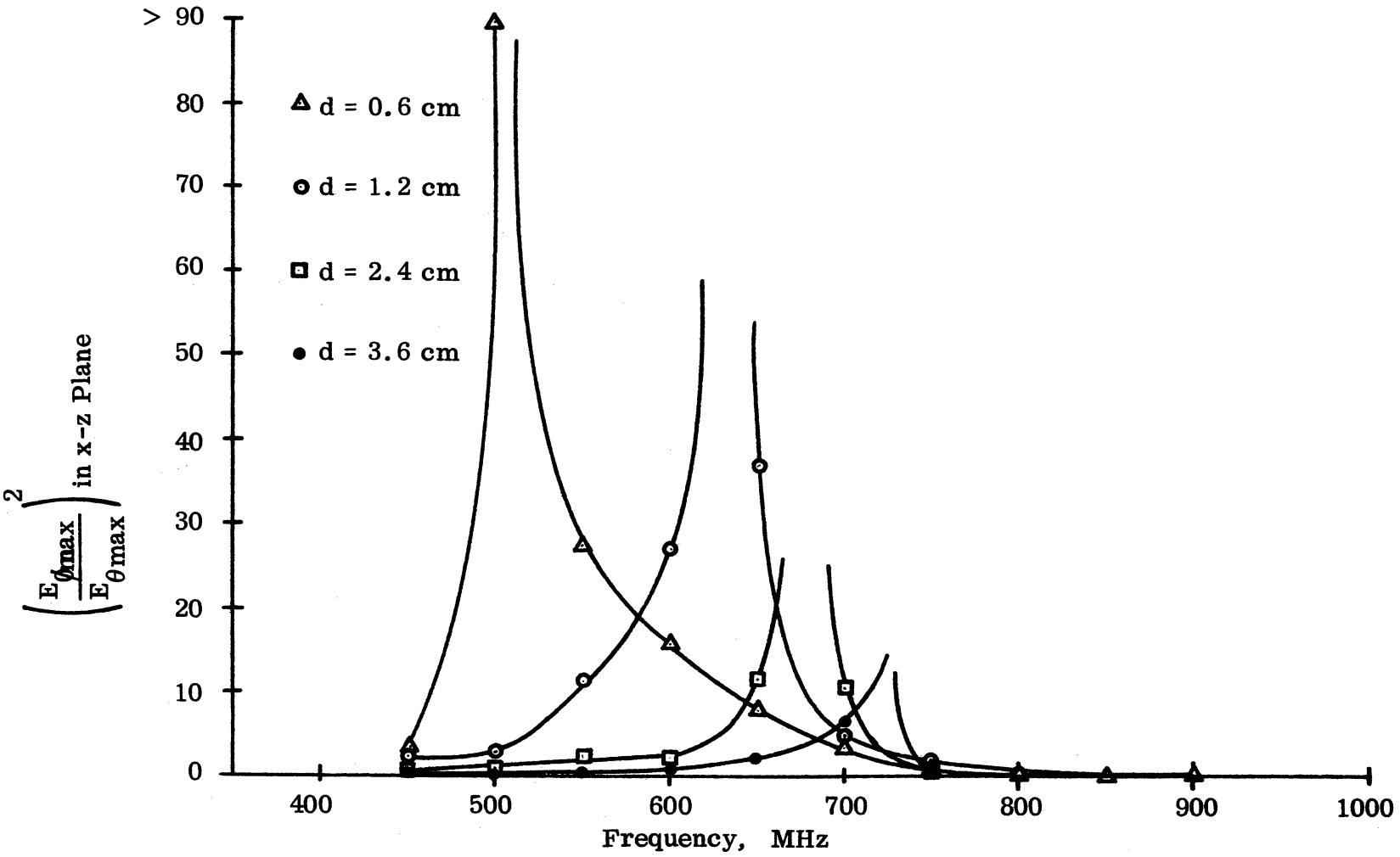

FIG. 4-43: POWER RATIO OF CROSS-POLARIZED COMPONENTS IN THE x-z PLANE (Three Elements, Experimental).

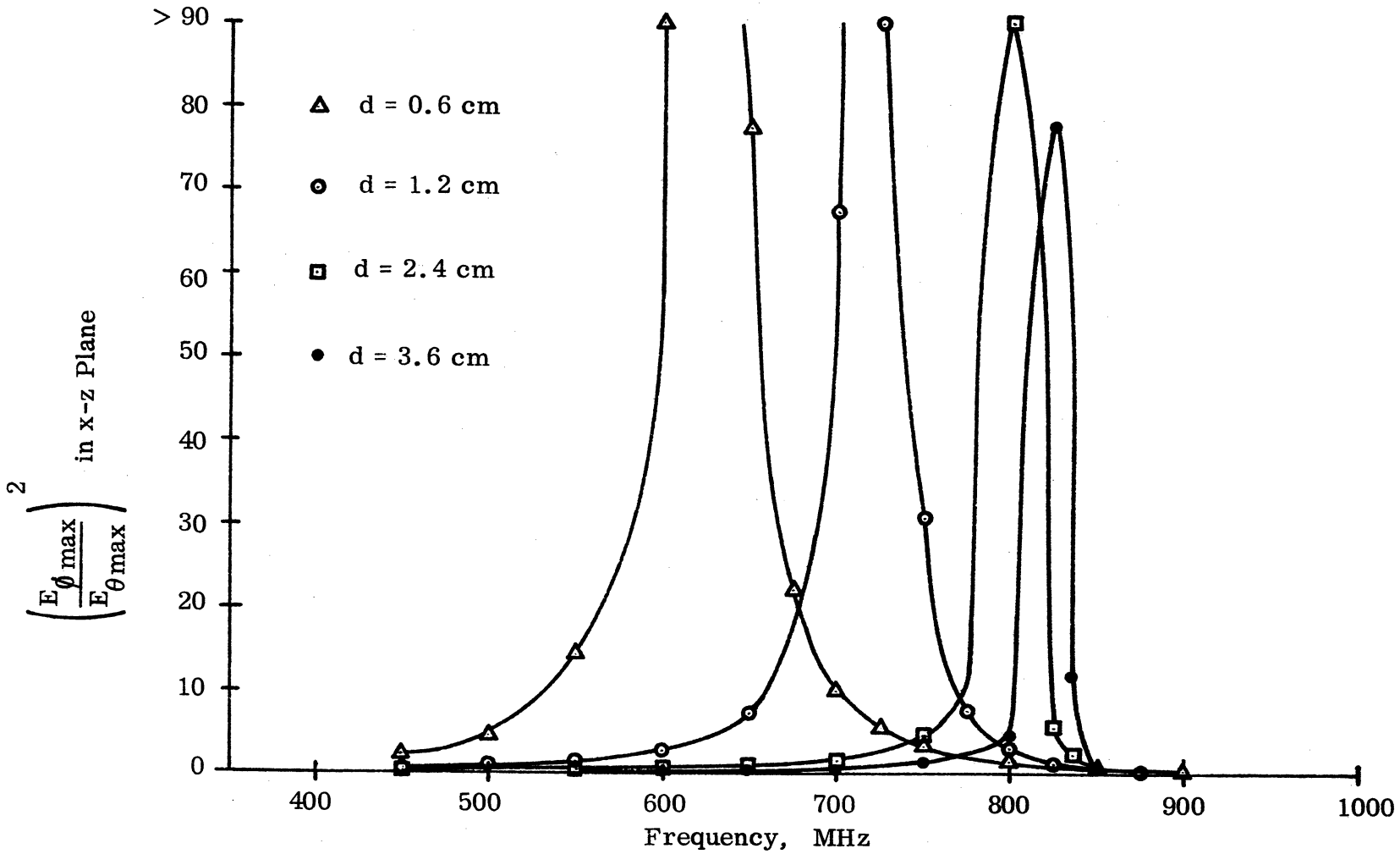

FIG. 4-44: POWER RATIO OF CROSS-POLARIZED COMPONENTS IN THE x - z PLANE (Three Elements, Theoretical).

4.4 Input Impedance Versus Number of Elements

An experimental study was conducted to learn how the input impedance of an interdigital array varied as parasitic elements were added to the antenna. The physical parameters were ℓ = 8.0 cm, h = 1.0 cm, a = 0.04 cm, and d = 1.2 cm. The experiment started with the driven element alone, and then pairs of parasitic elements were added to the antenna. The input impedance was measured in the frequency range from 450 MHz to 900 MHz after each addition. Data were obtained with 1, 3, 5, 7, 9, 11, and 13 elements.

The experimental input impedance data were normalized to 50 Ω and plotted on Smith charts. The Smith charts are shown in Figs. 4-45 through 4-51. Some interesting observations can be drawn from these figures.

First of all, consider what happens as the number of elements is increased. The input impedance curves contain more loops, and the impedance points gradually move toward the centers of the Smith charts. Thus, by increasing the number of parasitic elements, a better VSWR characteristic is obtained.

Eventually the addition of another pair of parasitic elements will not affect the input impedance plots very much. This is because the new pair of elements will be far enough away from the driven element so that they do not have much effect. It is apparent from this experiment, however, that the point of diminishing returns has not yet been reached with 13 elements. This is probably because the 6th pair of parasitic elements are less than $\lambda / 4$ from the driven element, even at the highest frequency, 900 MHz.

4.5 Thirteen-Element Arrays

In this section, experimental results are presented for two 13-element interdigital arrays. These antennas had the following physical parameters in common: ℓ = 8.0 cm, h = 1.0 cm, and a = 0.04 cm. The spacings between the elements were different; one had d = 0.6 cm, and the other had d = 1.2 cm. The antenna with d = 1.2 cm is identical to the 13-element antenna which was discussed in section 4.4.

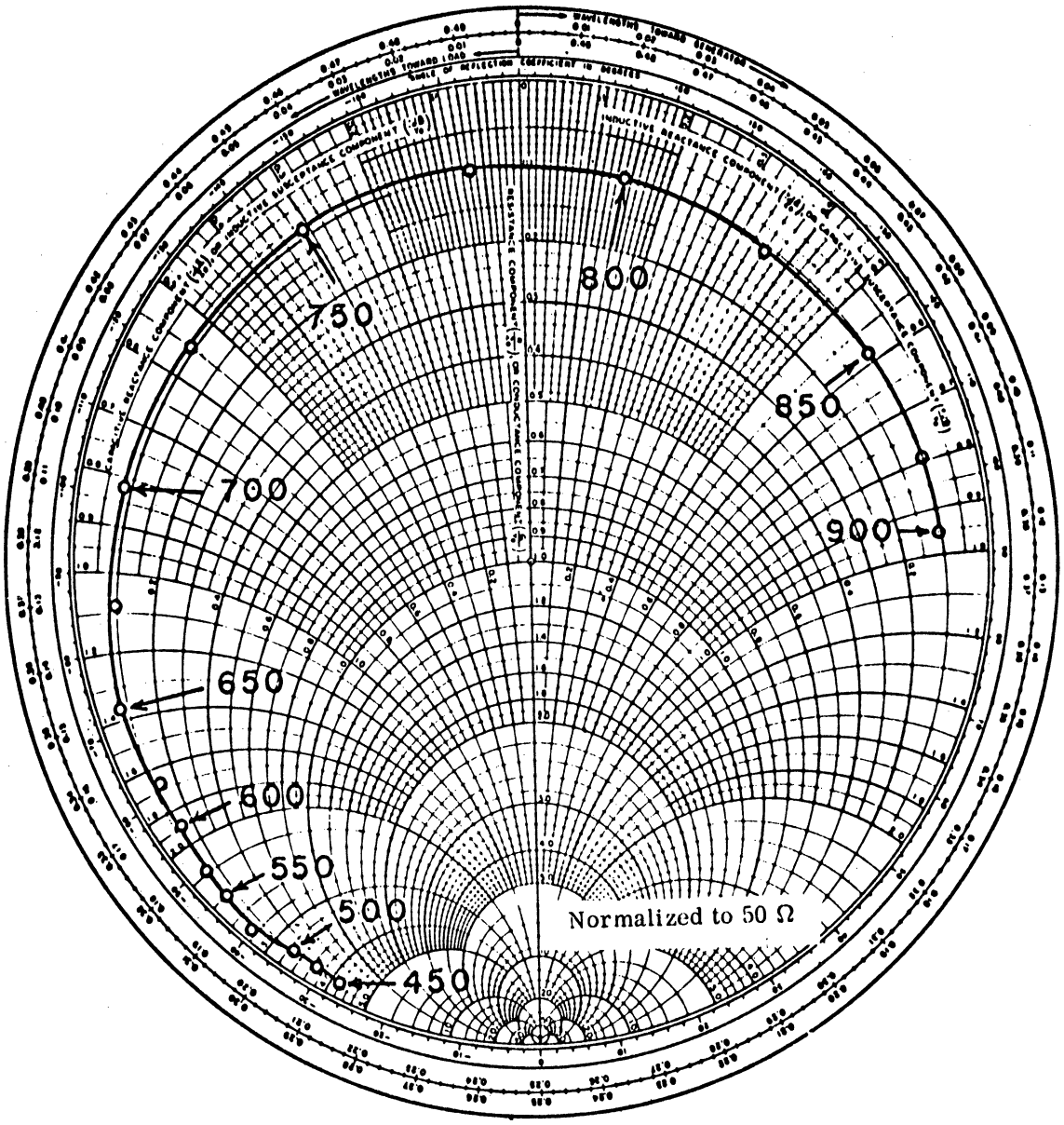

FIG. 4-45: INPUT IMPEDANCE (Driven Element).

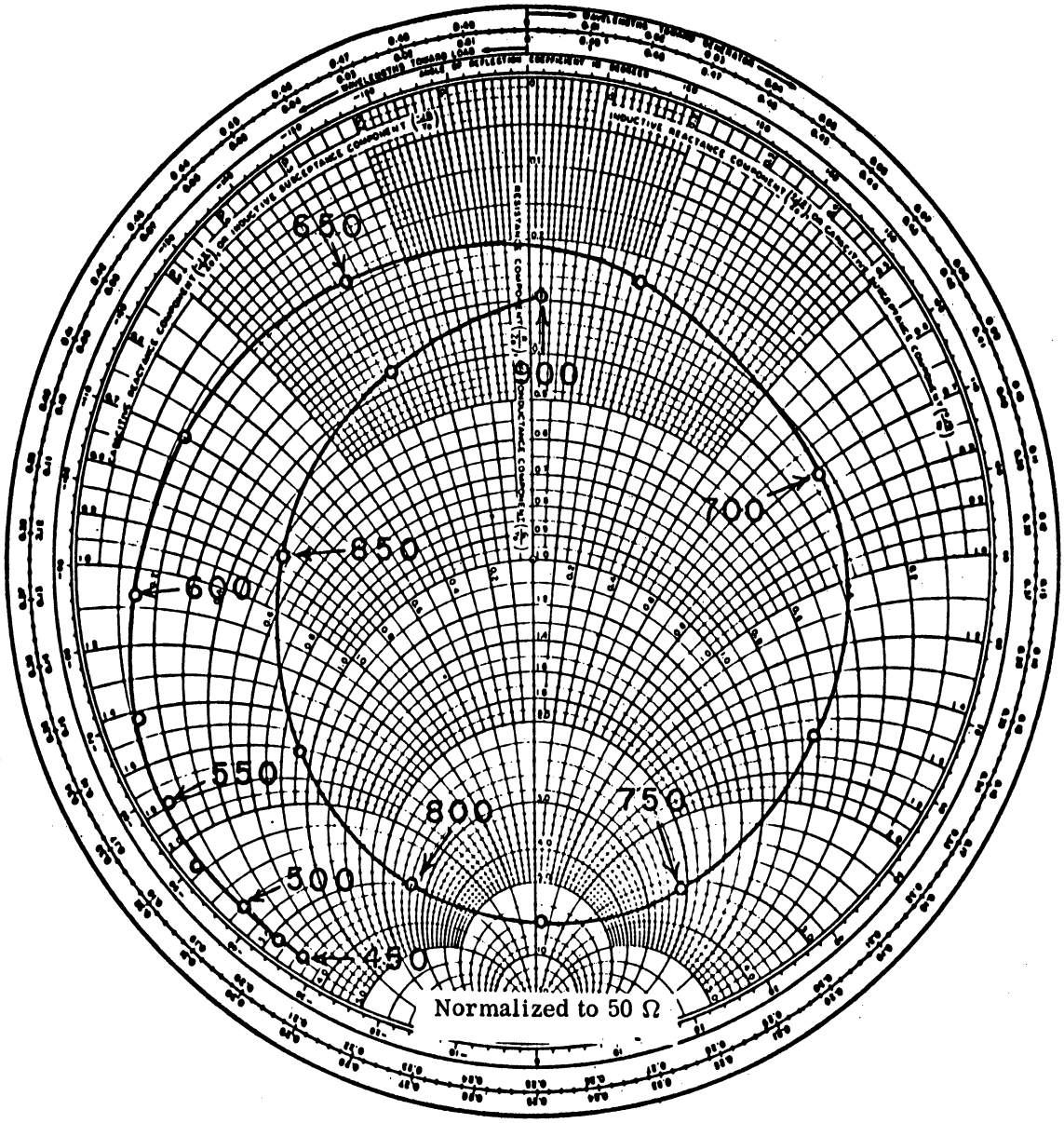

FIG. 4-46: INPUT IMPEDANCE (Three Elements).

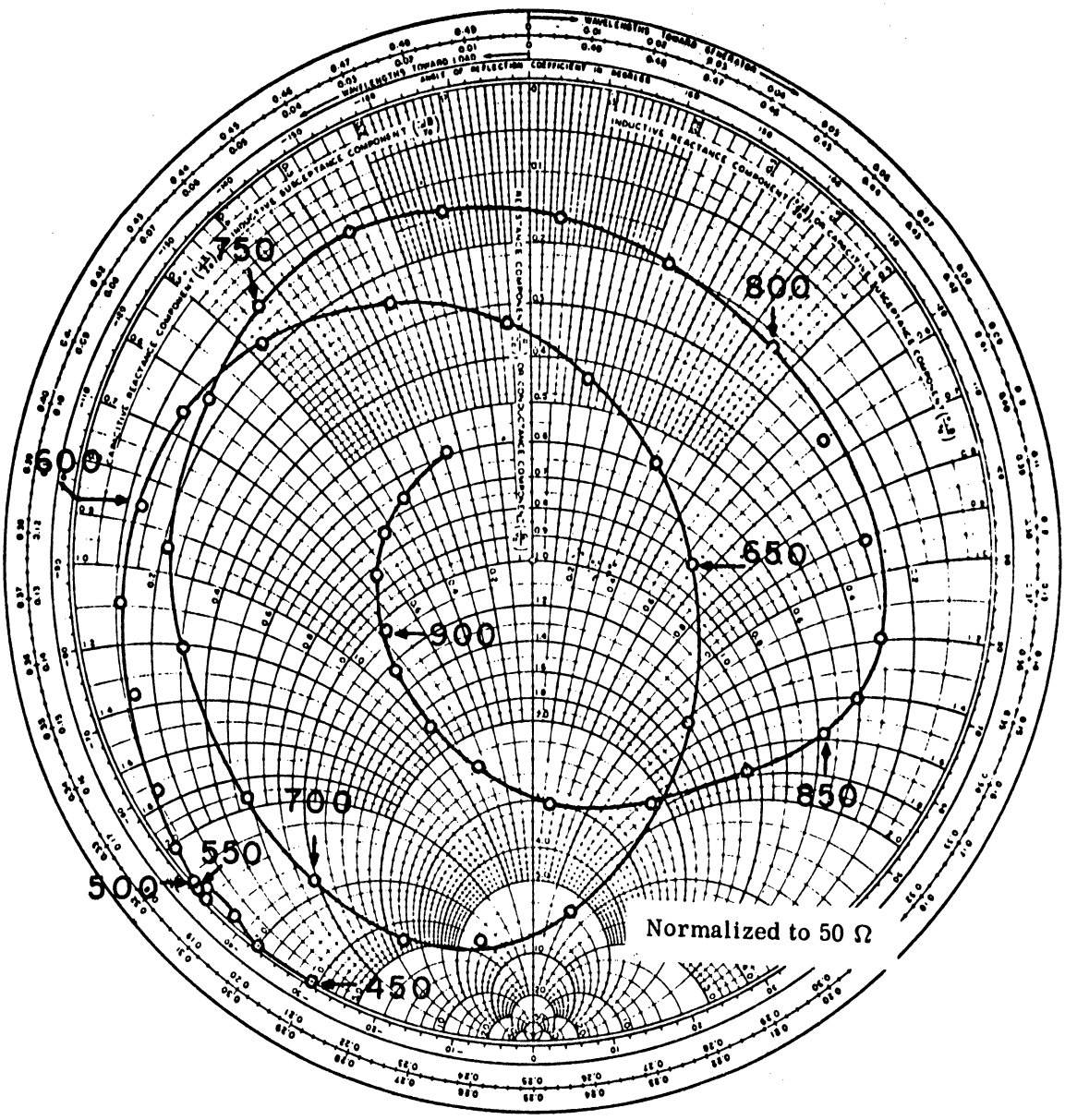

FIG. 4-47: INPUT IMPEDANCE (Five Elements).

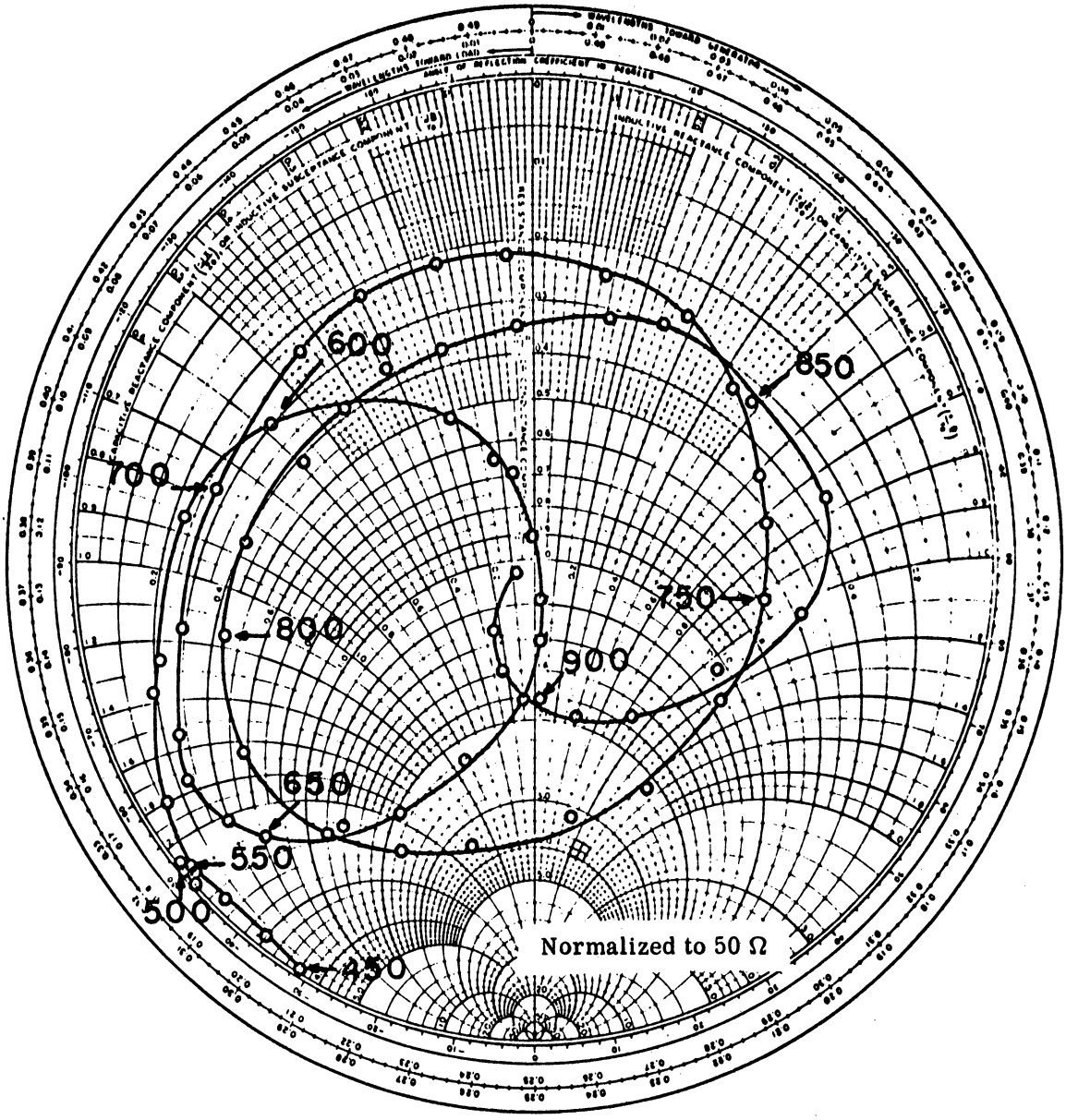

FIG. 4-48: INPUT IMPEDANCE (Seven Elements).

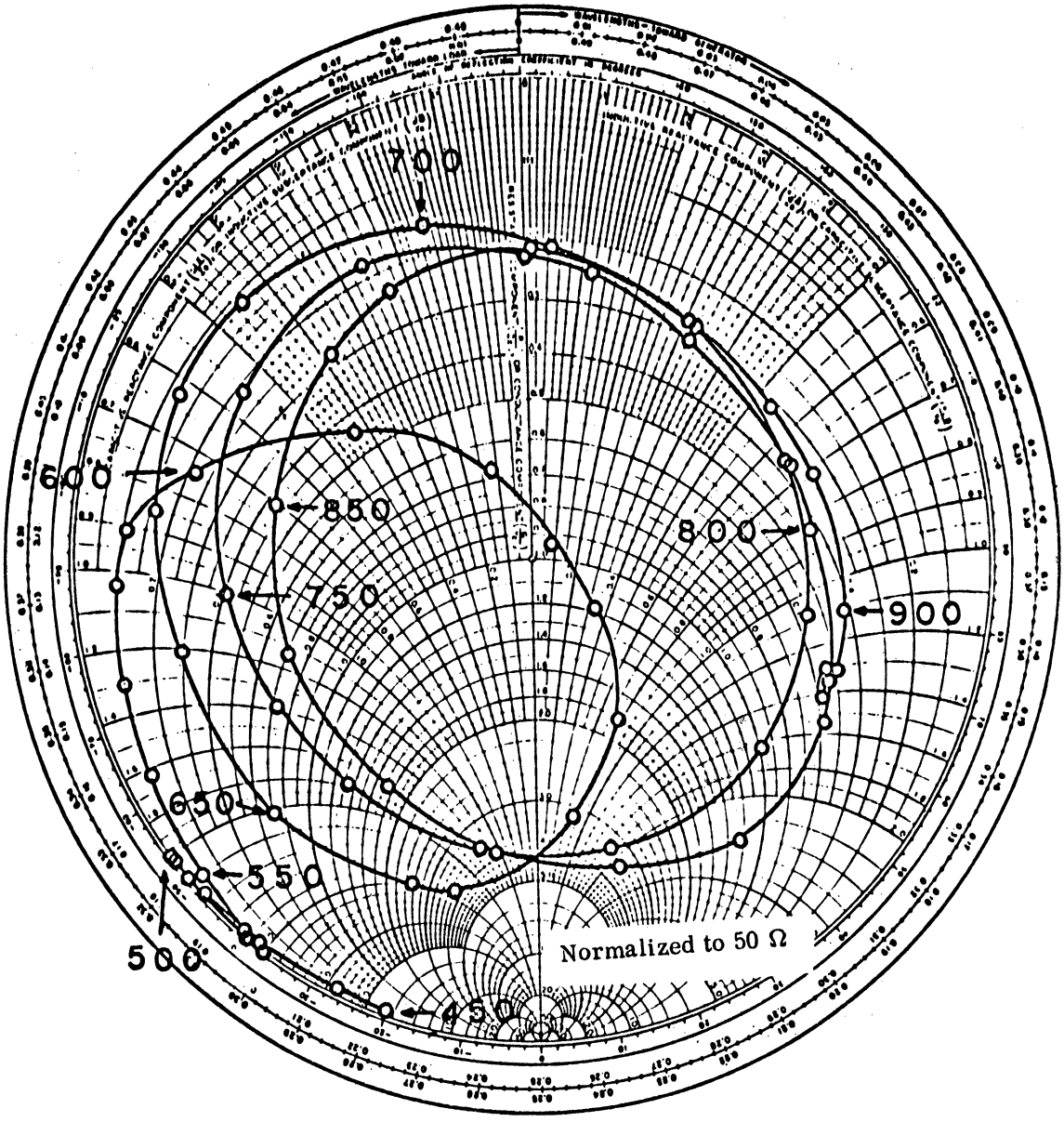

FIG. 4-49: INPUT IMPEDANCE (Nine Elements).

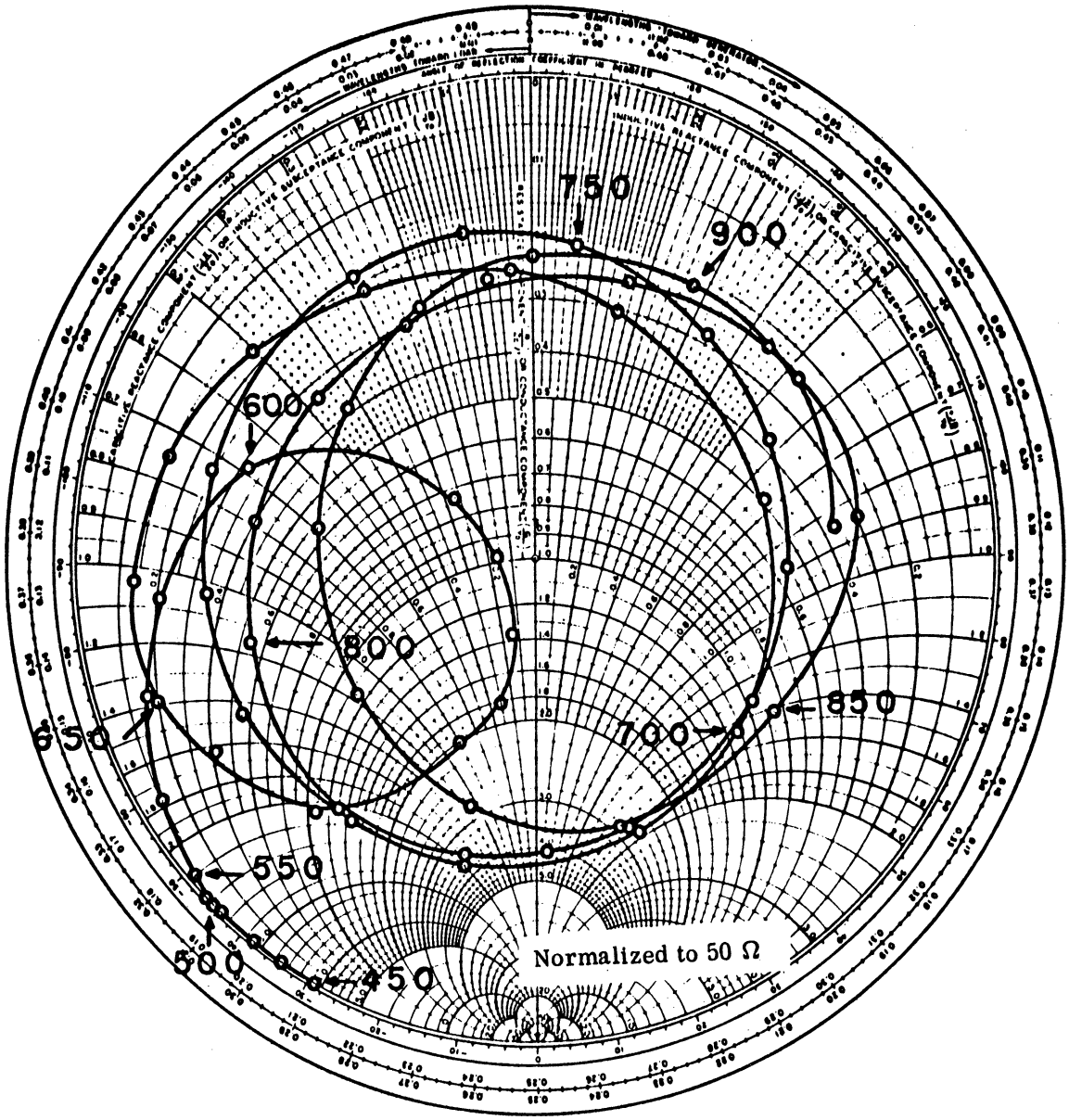

FIG. 4-50: INPUT IMPEDANCE (Eleven Elements).

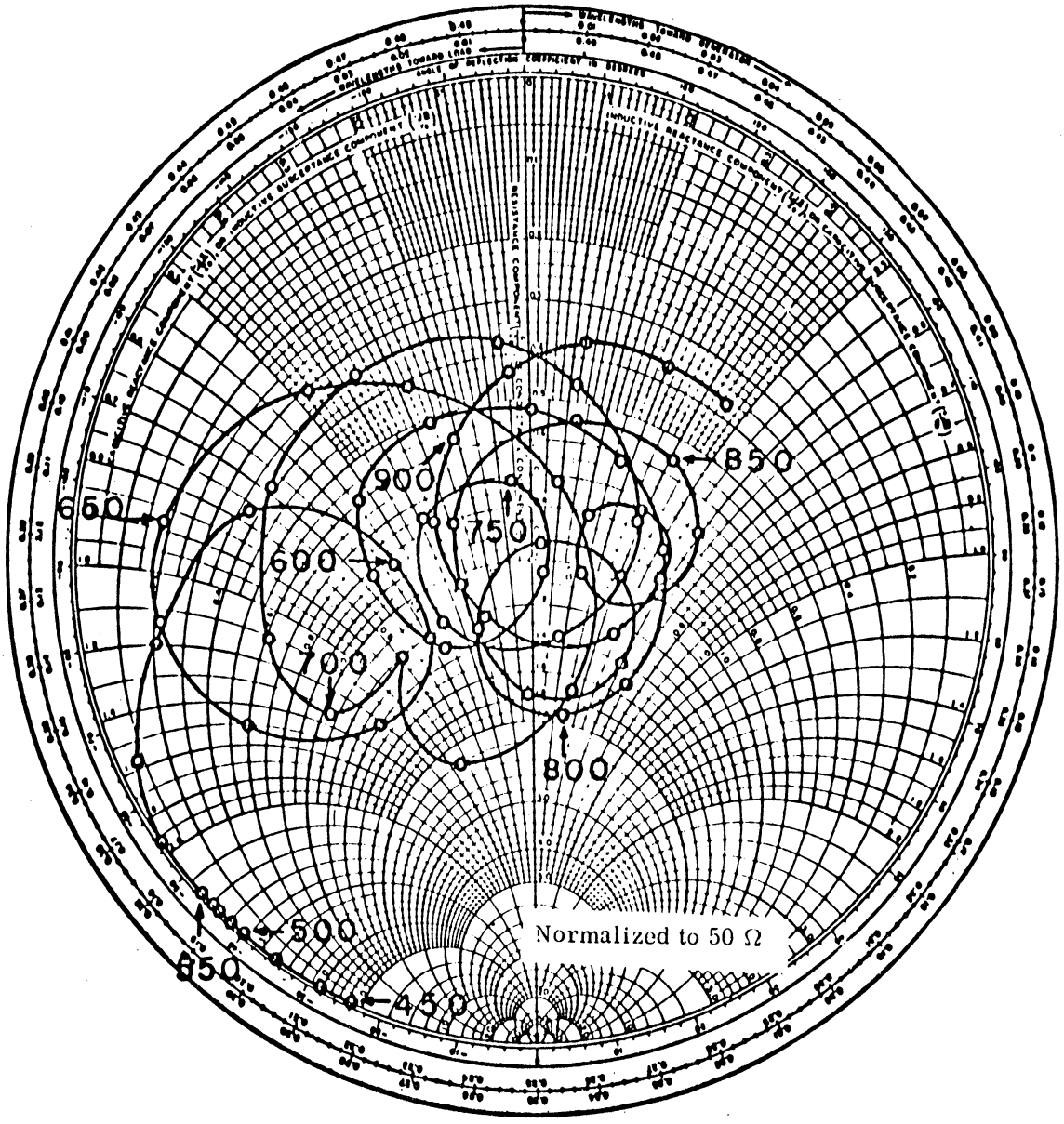

FIG. 4-51: INPUT IMPEDANCE (Thirteen Elements).

The input impedance was measured for each array in the frequency range from 450 MHz to 920 MHz. The experimental data are plotted on Smith charts in Figs. 4-52 and 4-53. Both charts are normalized to 50 Ω. Notice that the data points for the antenna with d = 1.2 cm are much closer to the center of the chart. This means that the VSWR characteristics are better for this antenna. This can be easily seen in the VSWR plots in Figs. 4-54 and 4-55. The antenna with d = 1.2 cm has a VSWR less than 3 from 720 MHz to 915 MHz. This is a bandwidth of nearly 200 MHz. It is interesting to compare the VSWR plots for the 13-element antennas with the VSWR plots for the appropriate three-element antennas in Figs. 4-23 and 4-24. The improvement obtained by adding more parasitic elements is obvious.

Radiation patterns were obtained for the two 13-element arrays from 450 MHz to 900 MHz. The patterns were taken in the x - z and the y - z planes at the North Campus antenna range. Because of the distortion caused by the small ground plane, patterns were not taken in the x - y plane.

The experimental radiation patterns are shown in Figs. 4-56 through 4-63. Patterns at four frequencies were selected for each antenna. Notice that the same kinds of patterns are obtained with 13-element arrays as were obtained with the three-element arrays. In the x - z plane, cross-polarization still exists. In Fig. 4-64, the power ratios of the cross-polarized components in the x - z plane are plotted versus frequency for both 13-element antennas. It is interesting to compare this figure with the corresponding figure for three-element antennas (Fig. 4-43). For the 13-element antenna with d = 0.6 cm, two peaks occur in the plot of $\left[E_{\phi\,\max}/E_{\theta\,\max}\right]^2$. For the three-element antenna with d = 0.6 cm, there is only one peak. For the 13-element and the three-element antennas with d = 1.2 cm, only one peak occurs in both cases.

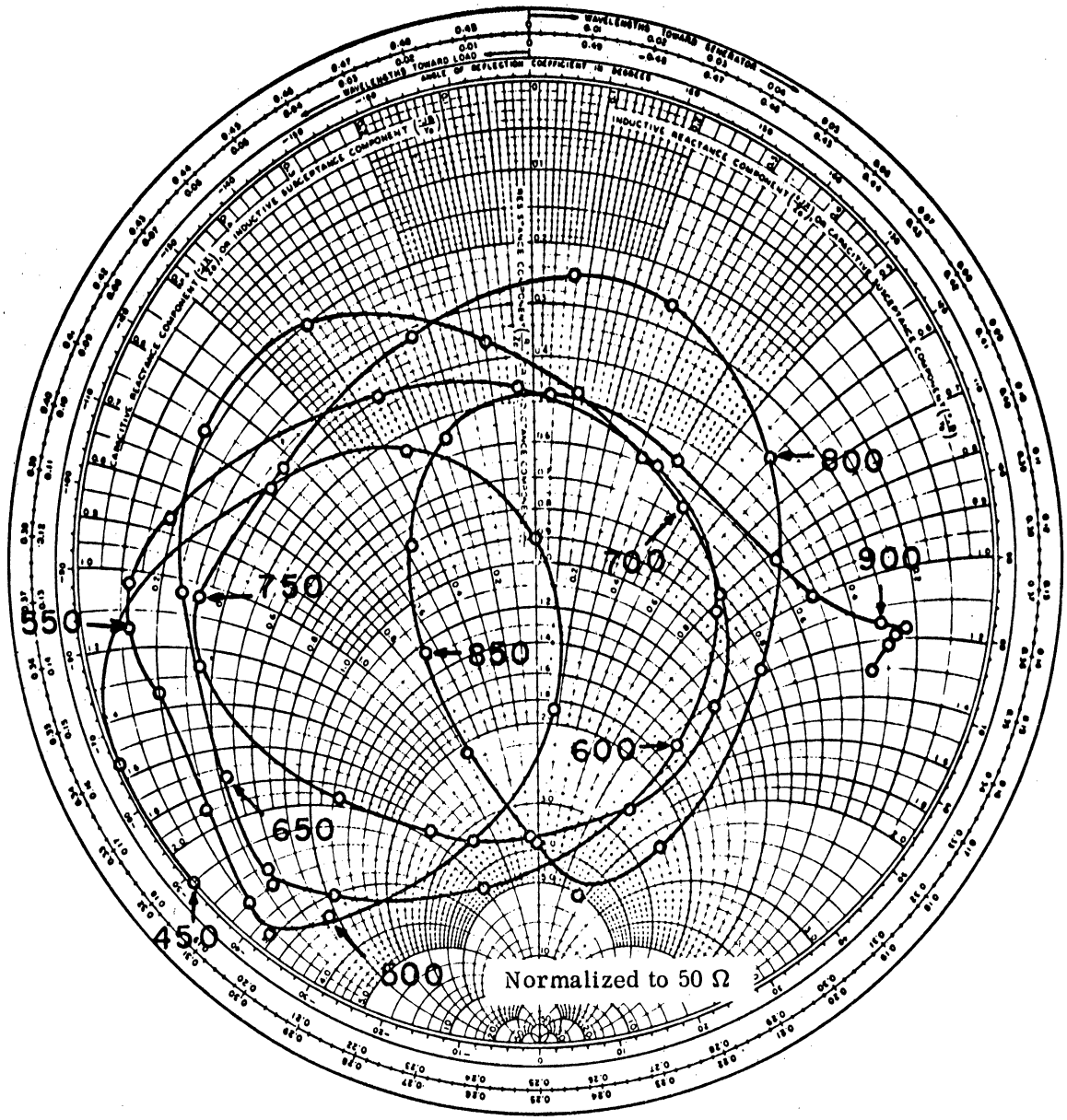

FIG. 4-52: INPUT IMPEDANCE WITH 13 ELEMENTS (d = 0.6 cm).

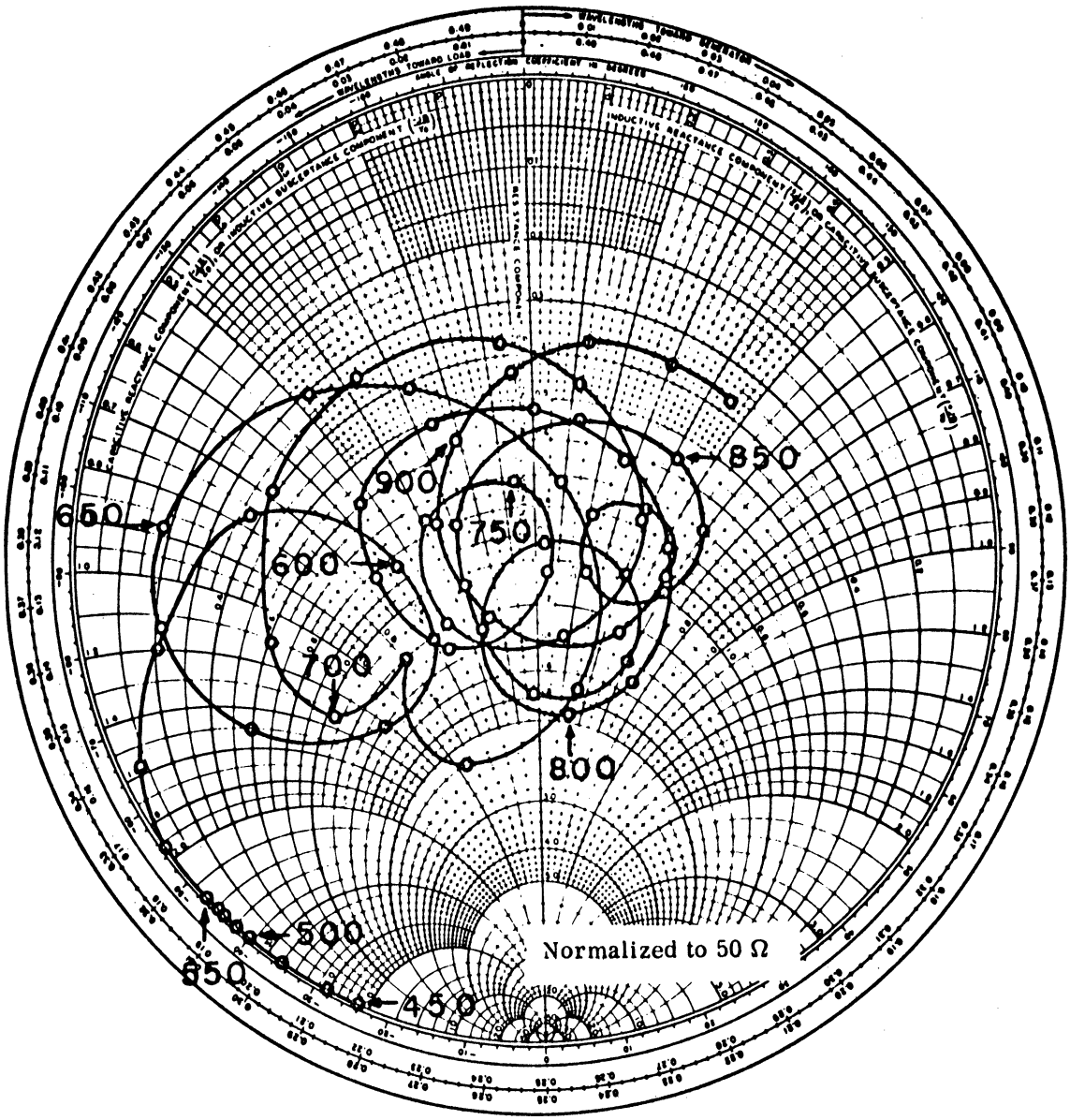

FIG. 4-53: INPUT IMPEDANCE WITH 13 ELEMENTS (d = 1.2 cm).

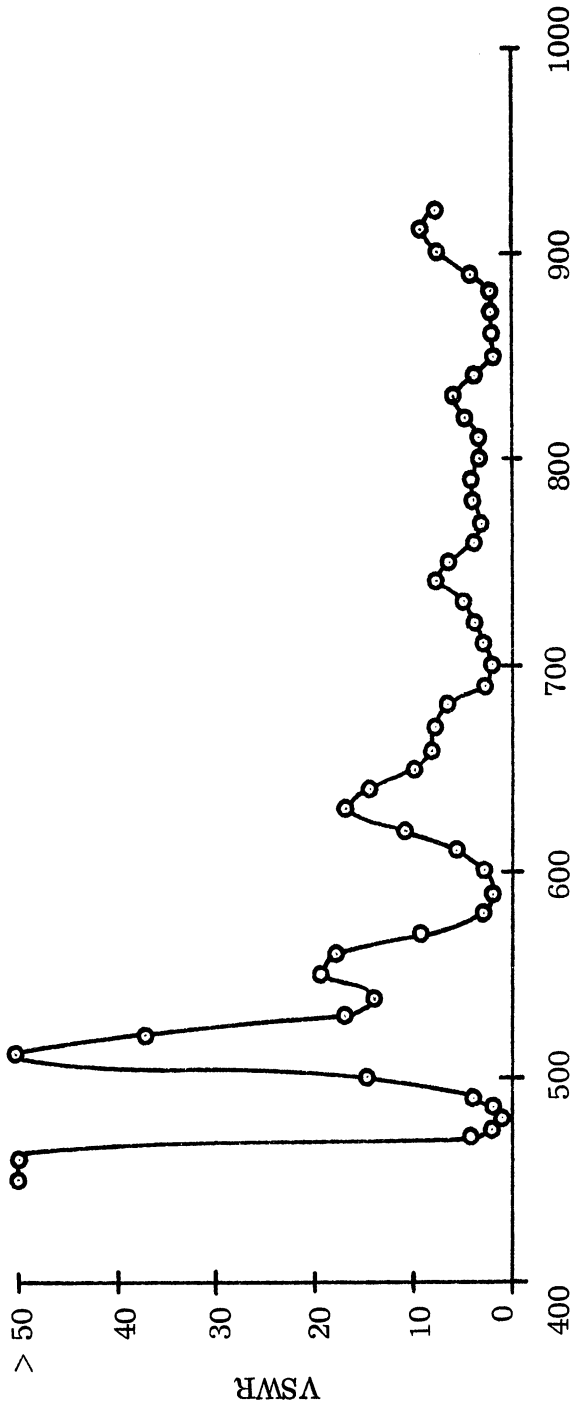

FIG. 4-54: EXPERIMENTAL VSWR WITH 13 ELEMENTS (d = 0.6 cm).

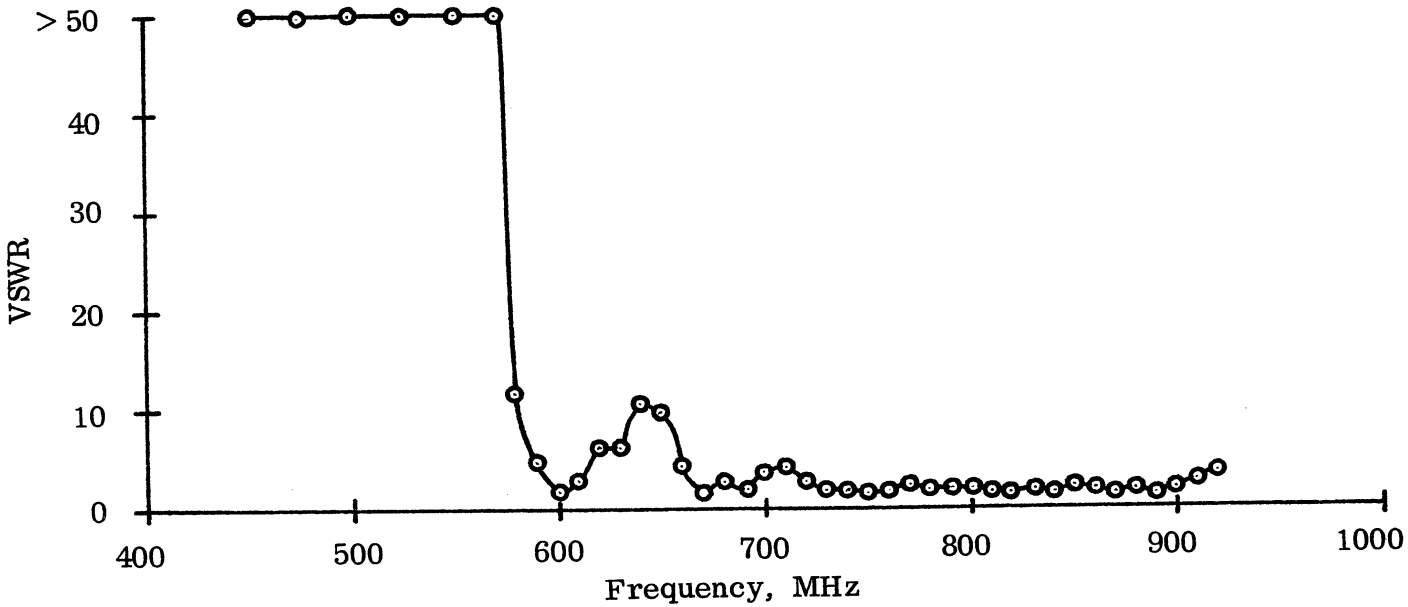

FIG. 4-55: EXPERIMENTAL VSWR WITH 13 ELEMENTS (d = 1.2 cm).

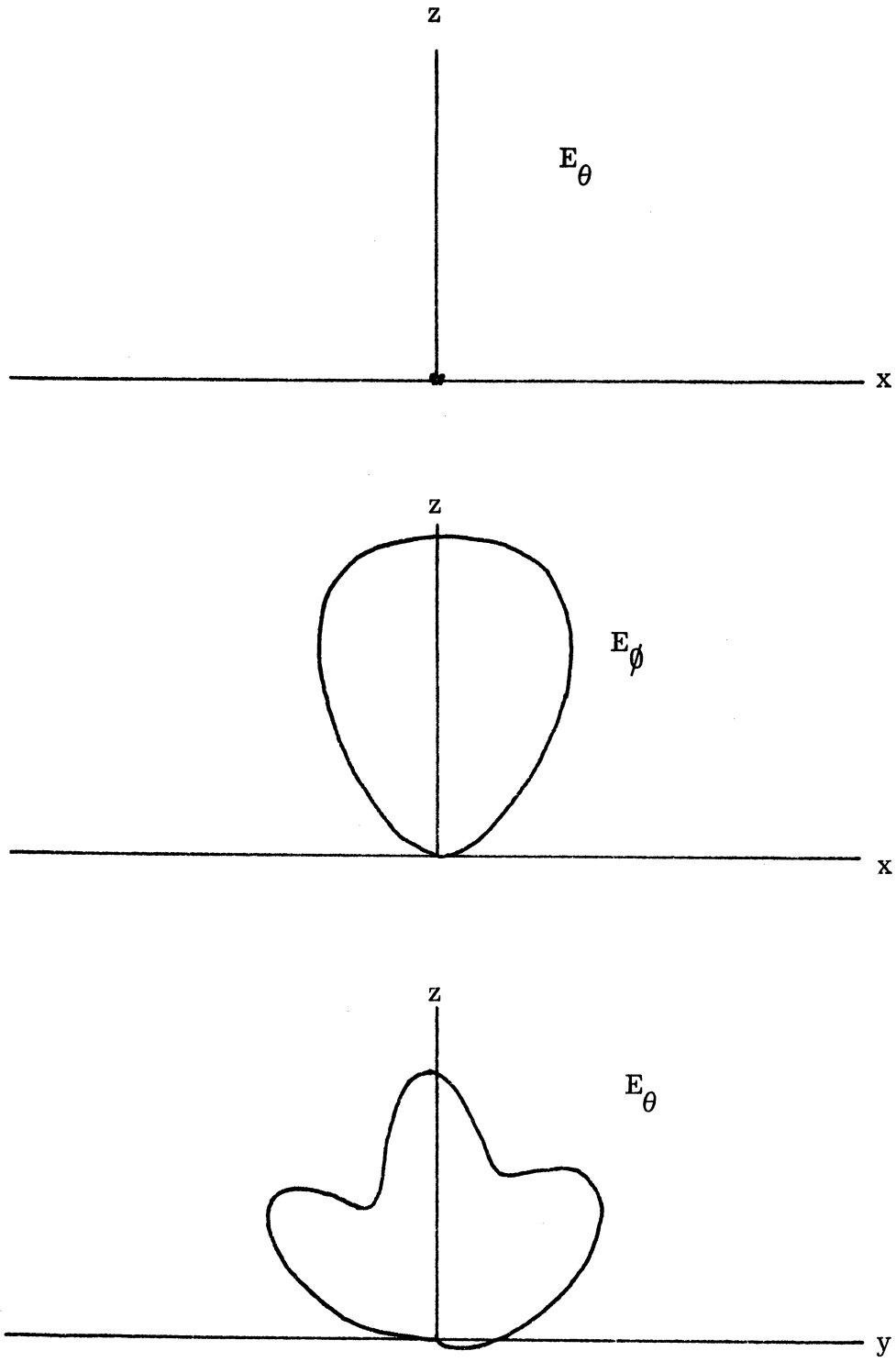

FIG. 4-56: 13 ELEMENTS (d = 0.6 cm, f = 500 MHz).

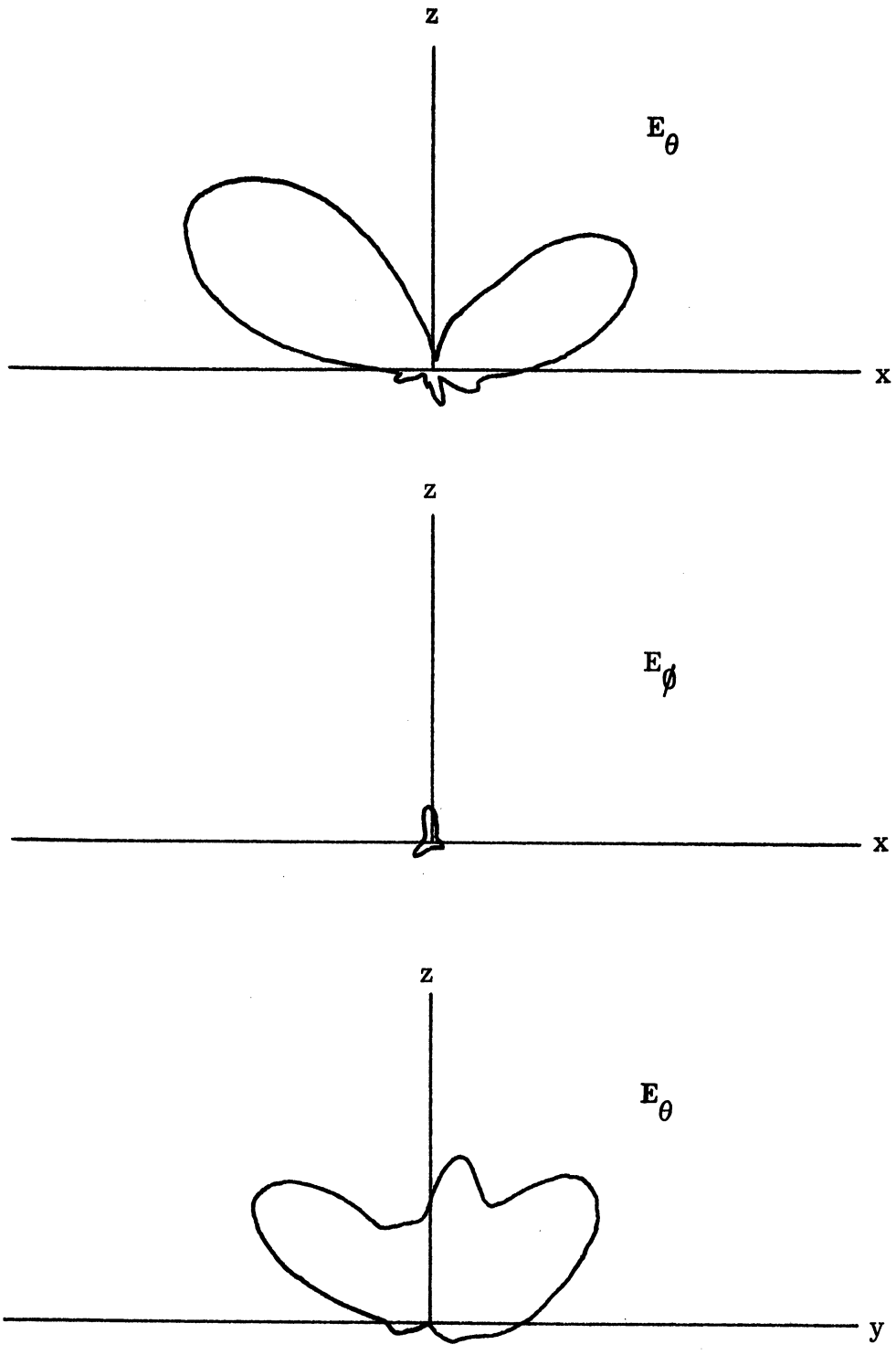

FIG. 4-57: 13 ELEMENTS (d = 0.6 cm, f = 650 MHz).

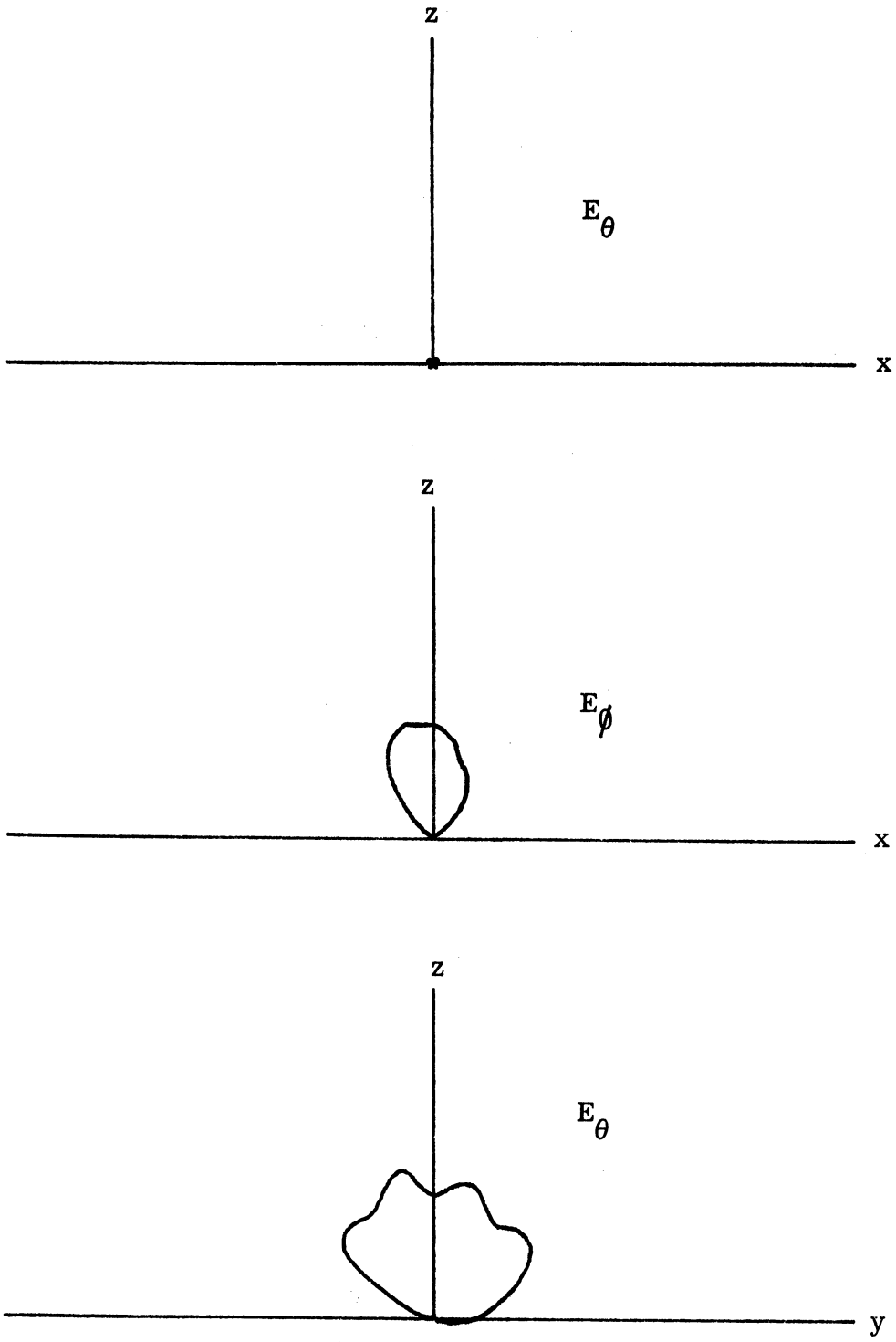

FIG. 4-58: 13 ELEMENTS (d = 0.6 cm, f = 750 MHz).

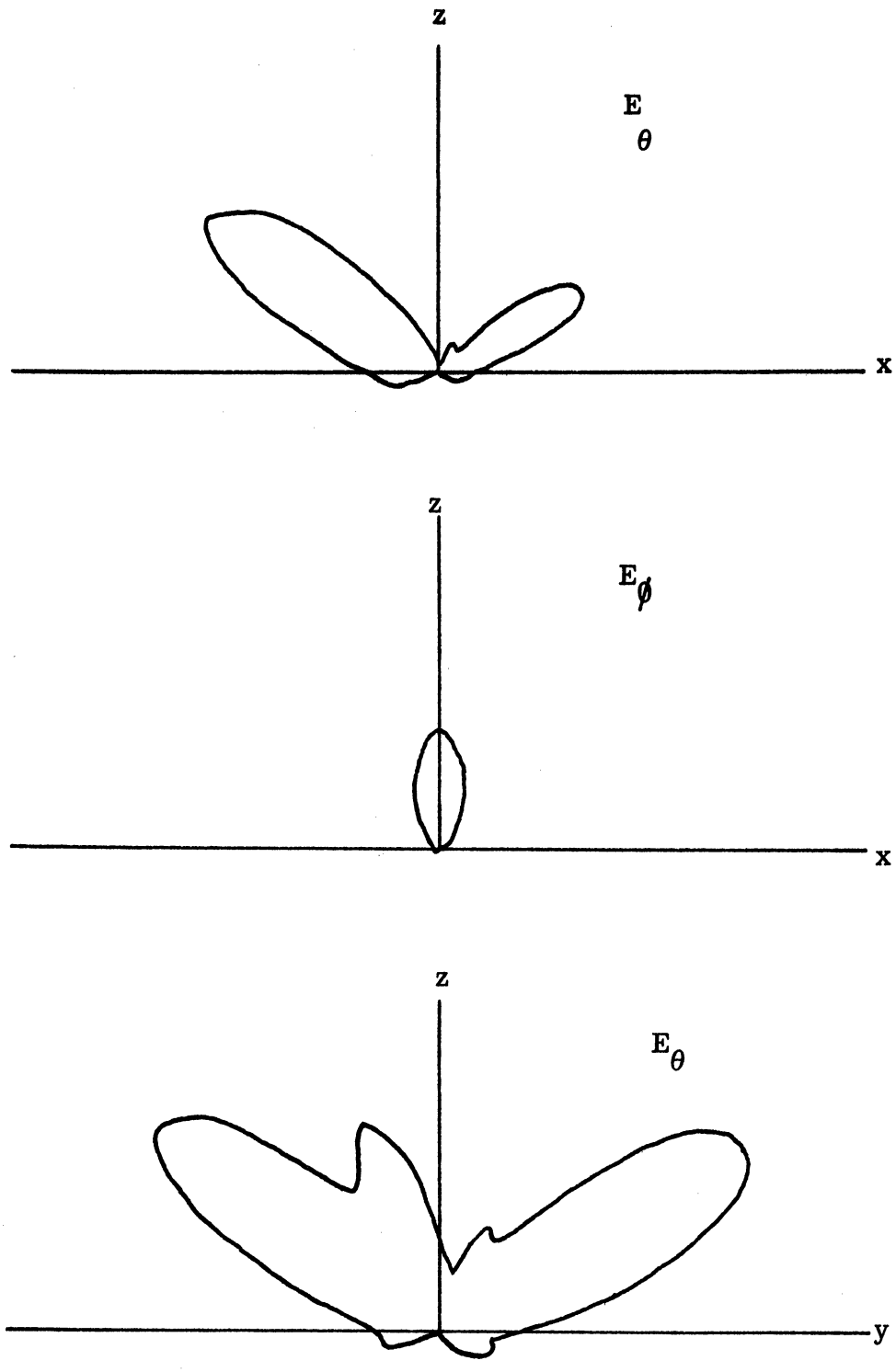

FIG. 4-59: 13 ELEMENTS (d = 0.6 cm, f = 850 MHz).

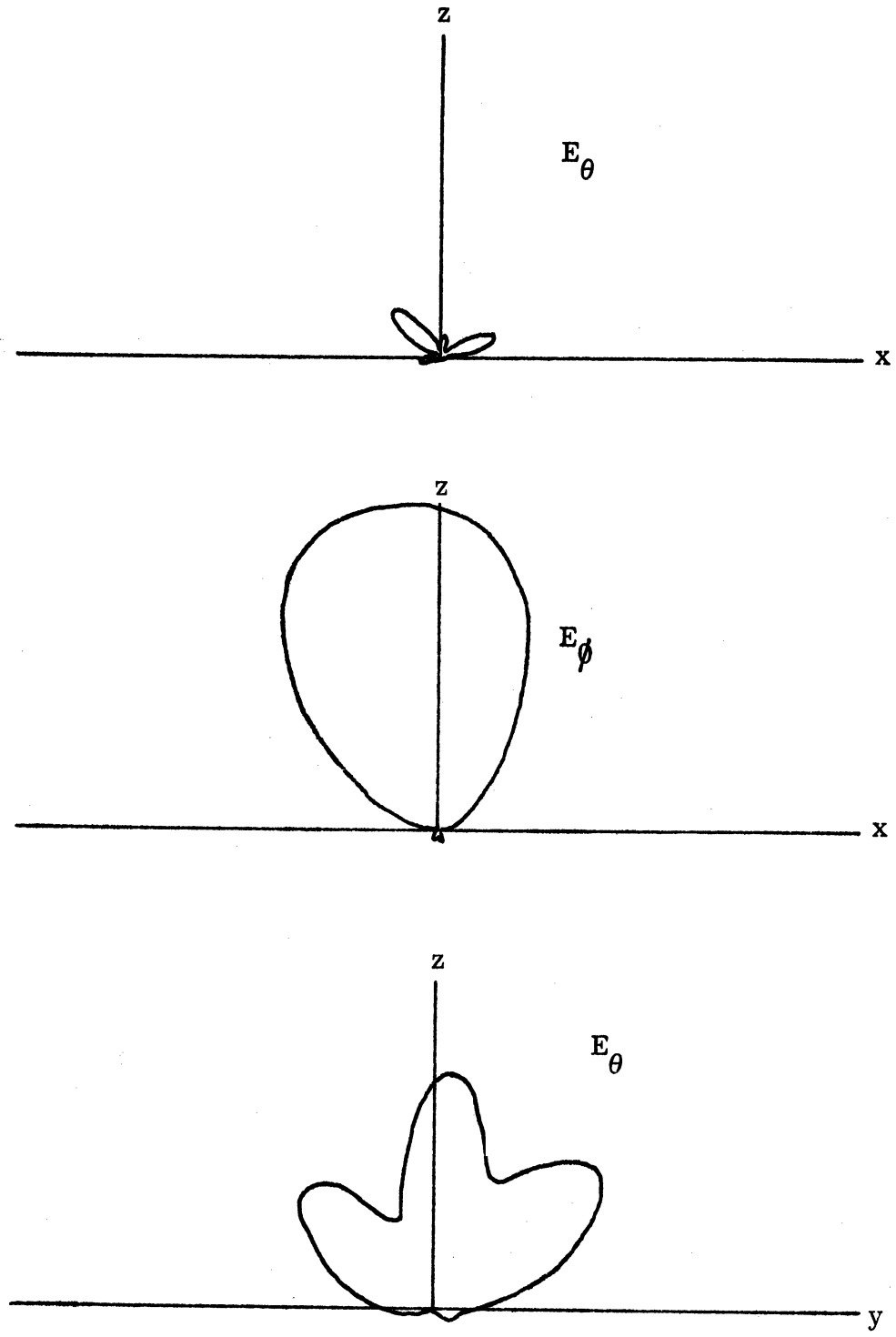

FIG. 4-60: 13 ELEMENTS (d = 1.2 cm, f = 450 MHz).

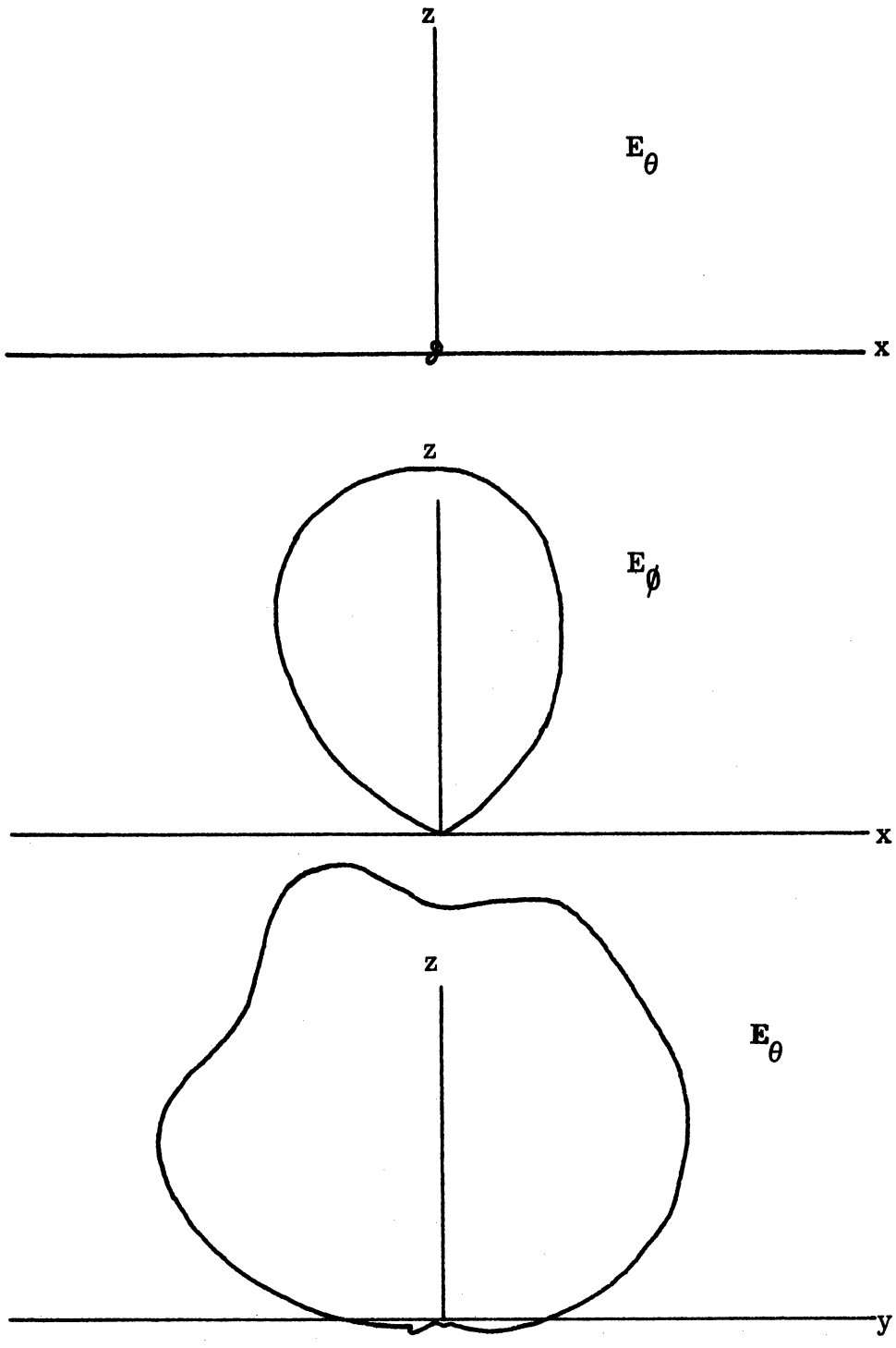

FIG. 4-61: 13 ELEMENTS (d = 1.2 cm, f = 600 MHz).

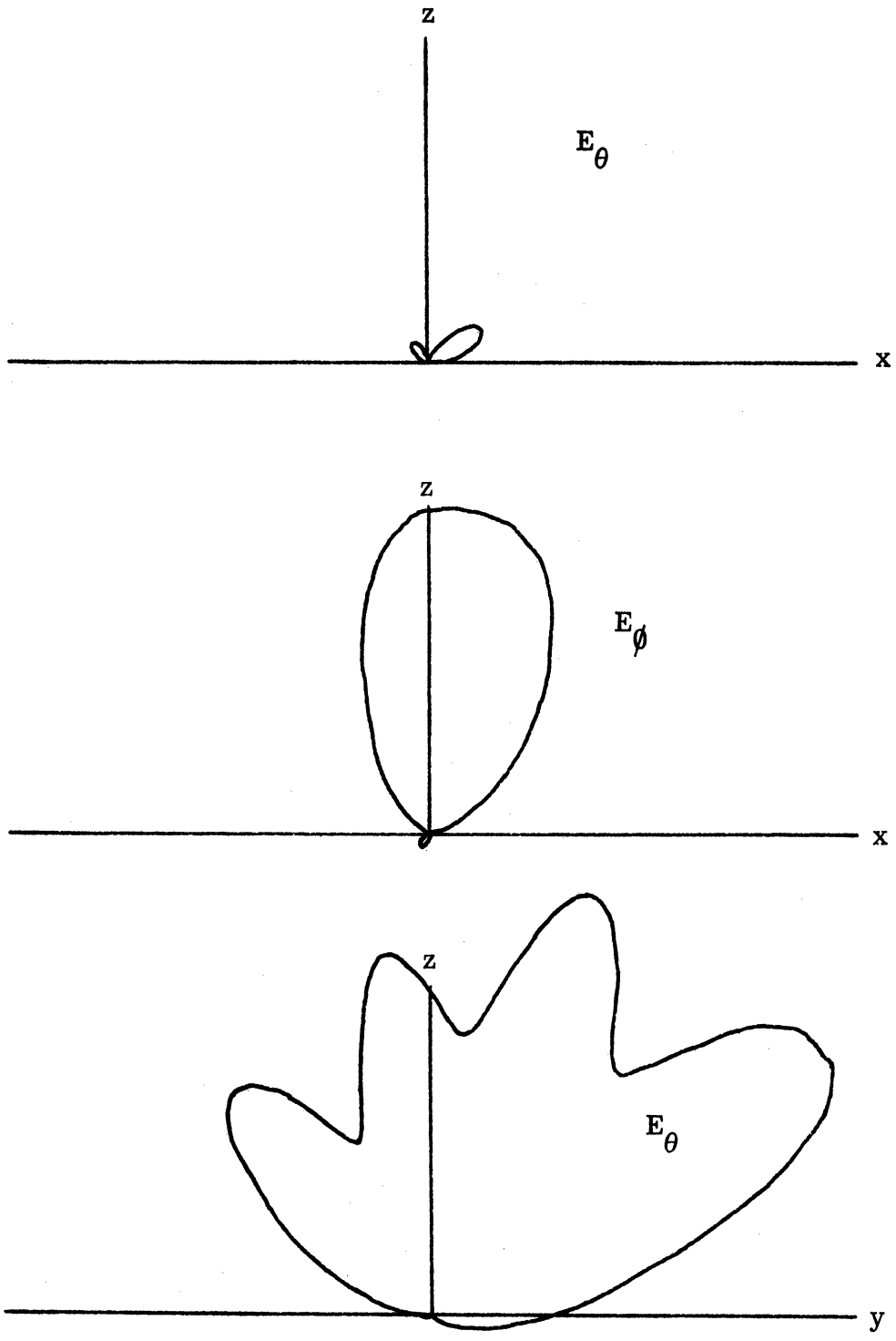

FIG. 4-62: 13 ELEMENTS (d = 1.2 cm, f = 700 MHz).

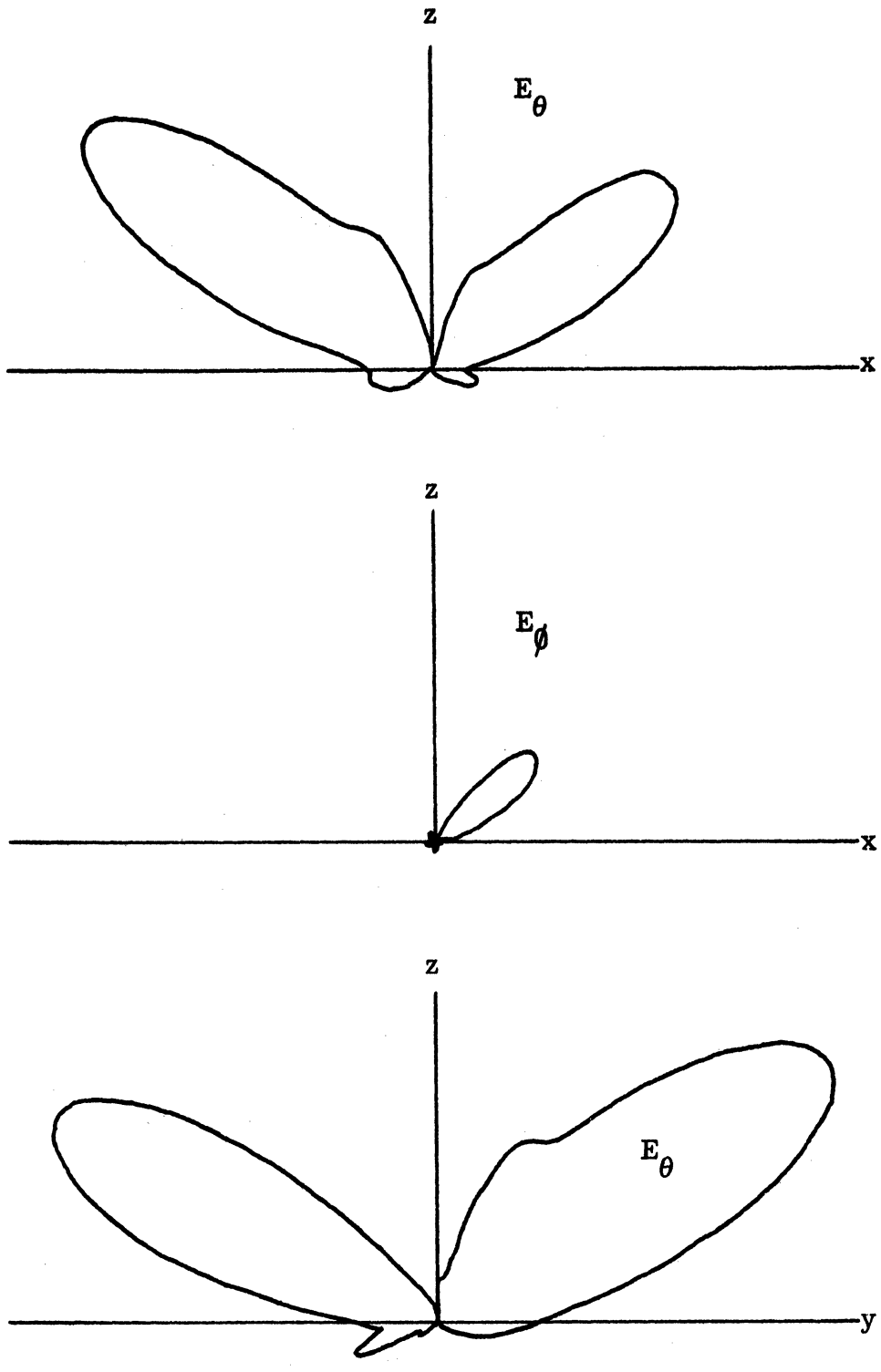

FIG. 4-63: 13 ELEMENTS (d = 1.2 cm, f = 800 MHz).

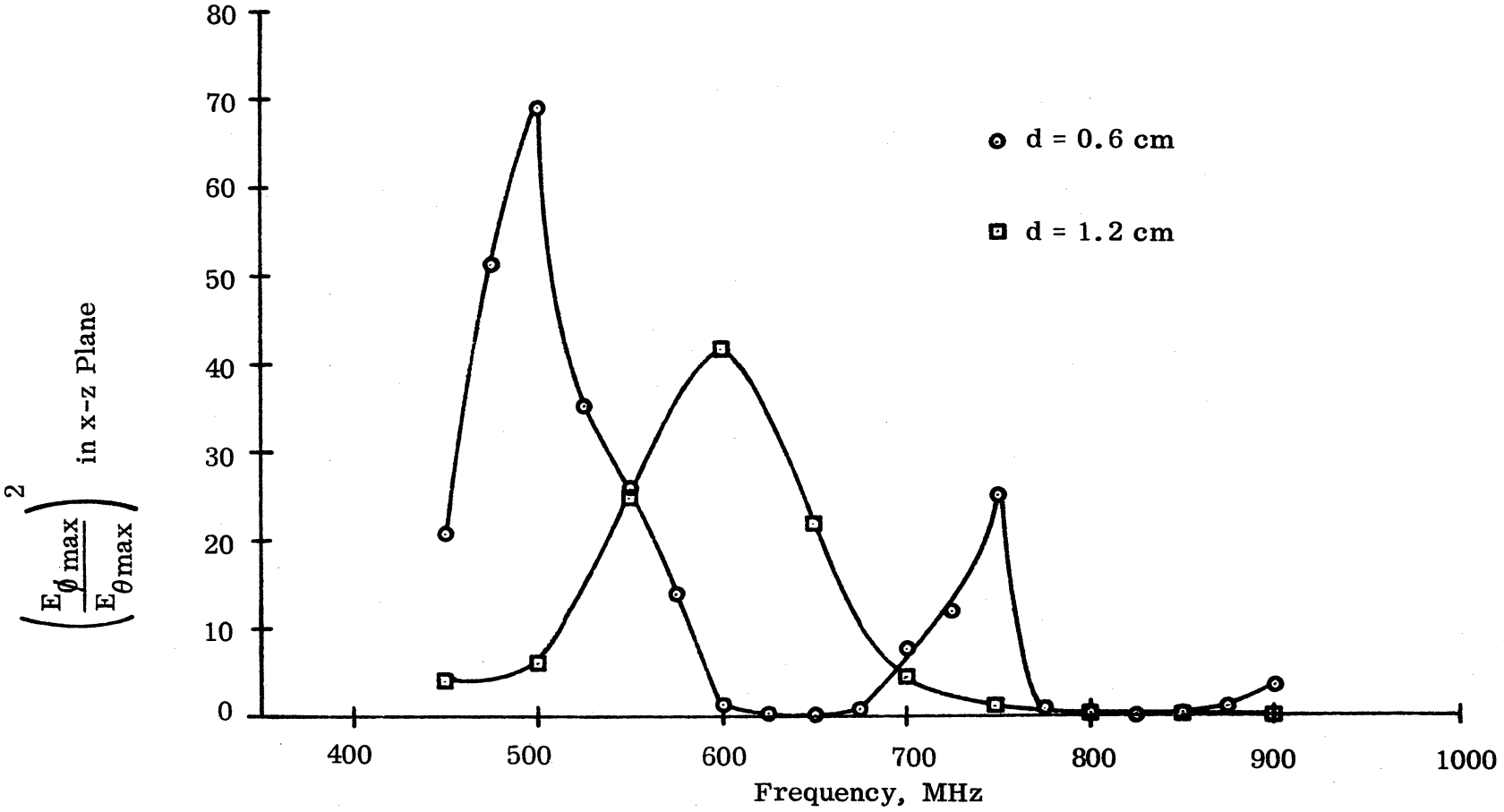

FIG. 4-64: POWER RATIO OF CROSS-POLARIZED COMPONENTS IN THE x - z PLANE (13 Element Antennas).

Chapter V

CONCLUSIONS AND FUTURE RECOMMENDATIONS

5.1 Conclusions

In this report, the theory has been developed for the finite center-fed interdigital array. This antenna has been analyzed as a boundary value problem. In Chapter II a system of integral equations was derived for the driven element of the array. Using a matrix method of solution, complex current distributions were obtained for this element from 450 MHz to 900 MHz. The input impedance, VSWR, and the radiation patterns were then calculated using the computed current distributions.

In Chapter III the theory was extended to a three-element interdigital array consisting of a driven element and two parasitic elements. Integral equations were derived for this case and the complex current distributions were obtained for the driven and parasitic elements. Data were obtained in the frequency range from 450 MHz to 900 MHz for four three-element antennas. The elements were all the same size in these antennas but the spacing between the elements was different. The input impedance, VSWR, and the radiation patterns were calculated theoretically for these four interdigital arrays.

Experimental results were presented in Chapter IV. Models were constructed having the same physical parameters as the antennas studied theoretically. In section 4.2 the experimental results for the driven element were compared with the theoretical data. In general, theory and experiment agreed quite well. However, the theoretical data appeared to be shifted higher in frequency by approximately 50 MHz. It was concluded that the driven element alone would not be a very effective antenna because the real part of the input impedance was too small.

In section 4.3 experimental results were presented for the four three-element arrays. There was good agreement between theory and experiment, except for a frequency shift of approximately 100 MHz. It was found that the

addition of the two parasitic elements to the driven element definitely improved the antenna. Furthermore, there is an optimum spacing for the elements. The best VSWR characteristics were obtained with d = 1.2 cm.

Although theory and experiment agreed in general, differences between them were observed. It is interesting to speculate on some of the factors which may have caused these differences. Some of the obvious factors have already been mentioned. For example, the theory is based on perfect conductors while the experimental models have some losses. There were also losses and mis-matches in the equipment used in the experiments. In the theoretical development, the ground plane was assumed to be infinite because image theory was used. Of course, a finite ground plane was used in the experiments. The effect of a small ground plane on the experimental radiation patterns has already been discussed.

The most interesting difference between theory and experiment is the apparent shift in frequency. When the theoretical and experimental data are plotted versus frequency, the theoretical curves appear to be translated to the right. The observed shift was approximately 100 MHz for the three-element arrays and 50 MHz for the driven element. This is too large a shift to be explained by dimensional errors in constructing the experimental models.

The shift in frequency is probably due to a combination of two factors. First, it is very difficult to model the feed of the driven element exactly. The theoretical model was fed by a discontinuity of the scalar potential in an infinitesimal gap, the so-called slice generator. Of course, this generator does not exist in practice (King, 1956). In the experimental models the driven element was inserted into a tapered monopole mount through a hole in the ground plane.

Second, there is some error involved in using the matrix method of solution of the integral equations. The accuracy of the solution obtained depends very strongly upon the fineness of the subdivisions used. In the solutions of the integral equations, fewer subdivisions were used for the three-element

arrays than were used for the driven element. This was because of increased cost. It is interesting that the discrepancy in frequency between theory and experiment was greater for the three-element antennas where the subdivisions were not as fine. To test this hypothesis, a computer run was made for the three-element case with more subdivisions (N = 11, M = 44). It was observed that the frequency discrepancy was somewhat reduced.

In section 4.4 an experimental study was described in which the input impedance was measured as a function of the number of parasitic elements. It was found that a better VSWR characteristic was obtained by increasing the number of parasitic elements. Since the addition of the last pair of parasitic elements to the antenna still produced significant changes in the input impedance, it is felt that improved performance might be obtained by further increasing the number of elements.

The interdigital array shows much promise as a broadband, low-profile antenna with small electrical size. Consider the 13-element interdigital array studied in section 4.5 with ℓ = 8.0 cm, h = 1.0 cm, a = 0.04 cm, and d = 1.2 cm. This antenna was found to have a VSWR of less than 3 (with respect to a 50 Ω line) from 720 MHz to 915 MHz. This is about a 25 per cent bandwidth. The array certainly has a low-profile, since it extends only 1.0 cm above the ground plane. At 900 MHz, this height is approximately $1/33\ \lambda$.

The interdigital array compares favorably with another parasitic array, the Yagi-Uda antenna. The interdigital array has a wider bandwidth, for the typical bandwidth for a Yagi-Uda antenna is about 2 per cent (Jasik, 1961). The interdigital antenna also has an inherent size advantage since it is excited at one quarter-wave length, while the Yagi-Uda array is excited at one half-wave length.

5.2 Future Recommendations

It would be interesting to extend the procedures presented herein to include interdigital arrays with more elements. A straightforward

extension of the method is possible, but this would prove to be costly. However, there are two possible ways to reduce the cost. Both ideas involve modifications in the method of solution of the integral equations.

The first approach is to attempt to simplify the matrix which represents the integral equations. The matrix elements are calculated by many different functions. Some of these functions could be reduced in complexity because they involve sums of terms where one term is dominant. It might even be possible to set certain matrix elements equal to zero without degrading the accuracy. This would reduce the computer time needed to fill and invert the matrix. Of course, these are basically problems in matrix theory and numerical analysis.

The second approach is to attempt to reduce the number of partitions necessary along the antenna elements to produce convergence in the currents. This would reduce the size of the matrix and would greatly lower the computer time needed to invert the matrix. In this dissertation the unknown current in each segment was assumed to be constant over the entire segment. Thus, the continuous current functions were replaced by segmented current functions.

Intuitively it seems that convergence could be obtained with fewer partitions if the unknown currents were allowed to assume a distribution over each interval. Possibly a triangular distribution could be tried. This would be an improvement, for there would be some control of the slope in each interval with the triangular distribution. If the unknown currents are assumed to be constants, then the slope in each interval is always zero.

REFERENCES

Bolljahn, J.T. and G.L. Matthaei, (March, 1962), "A Study of the Phase and Filter Properties of Arrays of Parallel Conductors Between Ground Planes," Proc. IRE, 50, pp. 299-311.

Collin, R.E., (1960), Field Theory of Guided Waves, McGraw-Hill, New York.

Fletcher, R.C., (August, 1952), "A Broadband Interdigital Circuit for Use in Traveling-Wave Type Amplifiers," Proc. IRE, 40, pp. 951-958.

Hallen, E., (November, 1938), "Theoretical Investigations into the Transmitting and Receiving Qualities of Antennae," Nova Acta Regiae Societatis Scientiarum Upsaliensis, Ser. IV, 11, No. 4, 1-44.

Harrington, R.F., (February, 1967), "Matrix Methods for Field Problems," Proc. IEEE, 55, pp. 136-149.

Harrington, R.F.,(1968), Field Computation by Moment Methods, Macmillan, New York.

Jasik, H.,(1961), Antenna Engineering Handbook, McGraw-Hill, New York.

King, R.W.P., (1956), The Theory of Linear Antennas, Harvard University Press, Cambridge, Massachusetts.

Kraus, J.D., (1950), Antennas, McGraw-Hill, New York.

Mei, K.K., (May, 1965), "On the Integral Equations of Thin Wire Antennas," Trans. IEEE, AP-13, pp. 374-378.

Ramo, S., J.R. Whinnery, and T. Van Duzer, (1965), Fields and Waves in Communication Electronics, John Wiley and Sons, New York.

Richmond, J.H., (August, 1965), "Digital Computer Solutions of the Rigorous Equations for Scattering Problems," Proc. IEEE, 53, pp. 796-804.

Smith, P.H., (January, 1939), "Transmission-Line Calculator," Electronics, 12, pp. 29-31.

Smith, P.H., (January, 1944), "An Improved Transmission-Line Calculator," Electronics, 17, p. 130.

Walter, C.H.,(1965), Traveling Wave Antennas, McGraw-Hill, New York.

Wu, P.R., (May, 1967), "A Study of an Interdigital Array Antenna," Ph.D. Dissertation, Department of Electrical Engineering, Radiation Laboratory University of Michigan, Ann Arbor, 5th Quarterly Report 7848-5-Q.

UNCLASSIFIED

Security Classification

DOCUMENT CONTROL DATA - R & D

(Security classification of title, body of abstract and indexing annotation must be entered when the overall report is classified)

1. ORIGINATING ACTIVITY *(Corporate author)* The University of Michigan Radiation Laboratory, Dept. of Electrical Engineering, 201 Catherine Street, Ann Arbor, Michigan 48108	2a. REPORT SECURITY CLASSIFICATION UNCLASSIFIED 2b. GROUP N/A

3. REPORT TITLE

The Interdigital Array as a Boundary Value Problem

4. DESCRIPTIVE NOTES *(Type of report and inclusive dates)*

Third Interim, Technical

5. AUTHOR(S) *(First name, middle initial, last name)*

William W. Parker

6. REPORT DATE	7a. TOTAL NO. OF PAGES	7b. NO. OF REFS
June 1970	190	16

8a. CONTRACT OR GRANT NO.	9a. ORIGINATOR'S REPORT NUMBER(S)
F33615-68-C-1381	
b. PROJECT NO. 6278	1770-3-T
c. Task 627801	9b. OTHER REPORT NO(S) *(Any other numbers that may be assigned this report)*
d.	AFAL-TR-70-94

10. DISTRIBUTION STATEMENT

This document is subject to special export control and each transmittal to foreign governments or foreign nationals may be made only with prior approval of AFAL (AVWE), Wright-Patterson Air Force Base, Ohio 45433

11. SUPPLEMENTARY NOTES	12. SPONSORING MILITARY ACTIVITY
	Air Force Avionics Laboratory Air Force Systems Command Wright-Patterson Air Force Base, Ohio 45433

13. ABSTRACT

In this report the center-fed interdigital array is analyzed as a boundary value problem. This antenna consists of an odd number of parallel conductors above a ground plane. Only the center element is driven and the other elements act as parasitics. Alternate ends of the parasitic elements are grounded, forming the interdigital boundary condition.

A system of integral equations is derived in which the unknowns are the line currents on the antenna elements. The equations are solved numerically using a matrix method of solution. The input impedance, standing-wave ratio, and the radiation patterns are calculated using the computed current distributions. Numerical data are obtained for the driven element alone and for four 3-element arrays.

Models were constructed and tested to confirm the theoretical data. Experiments were performed to obtain the input impedance, standing-wave ratio, and the radiation patterns for each model. There is good agreement between theory and experiment. The driven element alone is not an effective antenna but the addition of two parasitic elements markedly improves the performance.

In another experiment, the input impedance was measured as the number of parasitic elements was increased to a maximum of 13. It was found that the input impedance and standing-wave ratio improves as each pair of parasitic elements is added.

Two 13-element antennas with different element spacing were tested experimentally. Data are presented for the input impedance, standing-wave ratio, and the radiation patterns. The better of these two antennas has a VSWR of less than three (with respect to a 50 Ω line) over a 25-percent bandwidth.

DD FORM 1 NOV 65 1473

UNCLASSIFIED

Security Classification

14. KEY WORDS	LINK A		LINK B		LINK C	
	ROLE	WT	ROLE	WT	ROLE	WT
ANTENNAS						
PARASITIC ARRAYS						
INTERDIGITAL ARRAYS						
SIZE REDUCTION						
INTEGRAL EQUATIONS						